Development of West Nile virus candidate vaccines in *Nicotiana benthamiana*

By

Jennifer Wayland

Thesis presented for the degree of

DOCTOR OF PHILOSOPHY

In the Department of Molecular and Cell Biology,

Faculty of Science, University of Cape Town

November 2020

Supervisor: Dr Ann Meyers

Co-supervisors: Dr Aleyo Chabeda, Prof Ed Rybicki

Declaration

The work described in this thesis was conducted in the Biopharming Research Unit (Department of Molecular and Cell Biology, University of Cape Town) under the supervision of Dr Ann Meyers, Dr Aleyo Chabeda and Prof Ed Rybicki.

I, Jennifer Wayland, hereby declare that the work on which this thesis is based is my original work (except where acknowledgements indicate otherwise) and that neither the whole work nor any part of it has been or is being submitted for another degree in this or any other university. I authorise the university to reproduce for the purpose of research either the whole or any portion of the contents in any manner whatsoever.

Signed by candidate

Jennifer Wayland

Acknowledgements

They say it takes a village to raise a child, this is also true for completing a PhD.

- Philippians 4:13 – "I can do all things through Christ who strengthens me."

I would not be who I am or where I am today without the strength, love and guidance of my Saviour. I am humbled by His grace.

- To my Mother, thank you for all your love and support at all times. You taught me to never give up, even when things are not going my way. I am forever grateful for everything you have done and sacrificed for me to be where and who I am today. Ek is lief vir jou mamma.

- My loving husband, I couldn't do this without your continued support and words of encouragement. Thank you for always being patient during my times of breakdown and frustrated ramblings and thank you for celebrating with me during my times of success. Most of all thank you for believing in me and my abilities. Ek sal vir altyd lief wees vir jou my Gemmer ♥.

- My supervisor Dr Ann Meyers, thank you for taking me on as a student when I had no experience in protein expression, nevermind doing so in plants. If it wasn't for your open-door policy Ann, I wouldn't have learned as much as I have. You have been a beacon of support, guidance, knowledge and friendship. My co-supervisor and office-mate Dr Aleyo Chabeda, thank you for always listening to my chatter over coffee and keeping me sane. I appreciate all the advice and time you gave and truly miss having you around. My co-supervisor Prof Ed Rybicki, thank you for all your ideas and guidance. I have enjoyed every conversation shared with each of you and I am looking forward to continue learning from all of you.

- Thank you to all the BRU members especially Siphumelele Ndlovu, Ayesha Adams, Mélie Buyse, Dr Aleyo Chabeda (double love), Dr Megan Hendrikse, Dr Alta van Zyl, Dr Sandiswa Mbewana and Dr Sue Dennis for answering my many questions, laughing with me, sometimes crying with me and all the coffee breaks. Thank you all for accepting me into the BRU family.

- To all my friends and family that have supported me during this journey, thank you for all your love and support.

- Mohammed Jaffer at the Electron Microscope Unit, thank you for all the advice and assistance with the TEM, as well as all the jokes and chats shared.

- Thank you to Kayleen Baron and Phillip Venter at the Centre for Imaging Analysis, for your guidance with the ÄKTA FPLC system.

- Thank you to Rodney Lucas at the Research Animal Facility for performing the animal experiments.

- Thank you to Dr Marcel Prins for the *A. tumefaciens* LBA4404 strain carrying the pBIN-NSs silencing suppressor, Prof. Rainer Fischer for the pTRA vectors and Prof George Lomonossoff for the pEAQ-*HT* vector.

- Thank you to my funders, the Poliomyelitis Research Foundation, the Council for Scientific and Industrial Research and the Biopharming Research Unit for investing in my education and career.

Abstract

Development of West Nile virus candidate vaccines in *Nicotiana benthamiana*

By

Jennifer Wayland

Biopharming Research Unit

Department of Molecular and Cell Biology, Faculty of Science,

University of Cape Town, South Africa

West Nile virus (WNV) is a widely disseminated flavivirus, with a geographical range that now includes Africa, America, Europe, the Middle East, West Asia and Australia. The virus is vectored by *Culex* mosquitoes and is maintained in a bird-mosquito transmission cycle with hundreds of bird species acting as reservoir hosts. In humans, infections can develop into febrile illness and severe meningoencephalitis and to date, there is no treatment or vaccine available. In horses, approximately 20% of infections are symptomatic, of which 90% of cases involve neurological disease, with 30-40% fatality rates. Several veterinary vaccines specific to the lineage 1 WNV strains are commercially produced in America and Europe, however, these vaccines are not easily obtainable for low and middle-income countries (LMIC) due to their high cost and that associated with importation as well as the need for annual vaccination. Due to continuous global disease outbreaks in birds, humans and horse populations with no preventative measures for humans, WNV poses a major public health threat, especially in naïve populations. The development of a vaccine that contributes to the 'One Health' Initiative could be the answer to prevent the spread of the virus and control the disease.

Current veterinary vaccines are produced in expensive cell culture systems that require sterile conditions, high-level biosafety facilities and trained personnel for their preparation. Transient plant-based expression systems have proven to be a very cost-effective means of making complex proteins. Plants can produce and modify proteins in a similar manner to mammalian cells and production does not require sterile conditions or specialised facilities. We propose that plants could be a viable means of making feasible, low-cost reagents for WNV, specifically virus-like particles (VLPs) for use as vaccines in South Africa and other LMIC. In this study, we set out to develop two particulate candidate vaccines based on a virulent South African WNV strain using *Nicotiana benthamiana* as the expression platform.

We aimed to develop the first candidate vaccine by exploiting the virus's ability to form non-infectious VLPs by expressing only the WNV membrane (prM – precursor, M – matured) and envelope (E) proteins. Infiltration of these recombinant plasmids into plants yielded no protein expression unless co-expressed with the human chaperone protein calnexin (CNX), upon which expression of both M and E proteins were observed. We investigated the assembly of prM and E into VLPs by transmission electron microscopy (TEM), however, purification of these particles proved difficult with poor reproducibility and VLP yield.

This led to the development of an alternative candidate vaccine making use of the antigen-display technology based on the SpyTag (ST) and SpyCatcher (SC) peptides. The immunodominant epitope of the WNV E protein, domain III (EdIII), was selected for antigen display. Two constructs of the *EdIII* gene were generated, one with the SC peptide on the 5'-(SC-EdIII) and the other on the 3' end (EdIII-SC). Both SC-EdIII and EdIII-SC proteins were successfully expressed in the presence of the human chaperone protein calreticulin, and purified with yields of 9 mg/kg and 69 mg/kg fresh leaf weight (FLW), respectively.

The VLP core selected for the display of the SC-linked EdIII proteins comprised the coat protein of the bacteriophage AP205 with the ST peptide linked to its N-terminus (ST-AP205). Spytagged-VLPs were purified by density gradient ultracentrifugation at a yield of approximately 50 mg/kg FLW. The purified SC-linked EdIII proteins and ST-AP205 VLPs were coupled *in vitro*, but successful complex formation of AP205:EdIII was only observed between ST-AP205 and EdIII-SC and not when the SC peptide was located on the N-terminus of EdIII. We further demonstrated the successful complex formation of AP205:EdIII *in vivo* by co-infiltration of the EdIII-SC and ST-AP205 constructs, as well as by extracting leaves of plants infiltrated individually with either of the constructs. Due to the ease of purification and the high yields of AP205:EdIII achieved, the co-extraction process was optimised to obtain the best coupling yield possible by evaluating different FLW extraction ratios and the formation of VLPs was confirmed by TEM. The optimal co-extraction process was established at a FLW ratio of 1:2 ST-AP205 to EdIII-SC yielding approximately 23 mg/kg AP205:EdIII/FLW processed.

In this study, we describe the successful production of two particulate candidate vaccines. The first is based on the expression of the WNV *prM* and *E* genes in the presence of human CNX and the second is based on the ST/SC antigen-display technology. These outcomes exhibit the potential plants have of being used as biofactories for making significant pharmaceutical products for the 'One Health' Initiative and could be used to address the need for their local production in LMIC.

Abbreviations

ACNNV	Atlantic Cod nervous necrosis virus
ADE	Antibody-dependent enhancement
AHSV	African horse sickness virus
AP205	*Acinetobacter* bacteriophage
Arg	Arginine
Asp	Aspartic acid
Asn	Asparagine
BCIP	5-bromo-4-chloro-3-inodyl phosphate
BTV	Bluetongue virus
bp	Base pair(s)
BRU	Biopharming Research Unit
BSA	Bovine serum albumin
BSL	Biosafety level
C	Capsid / Coat protein
CaMV	Cauliflower mosaic virus
CnaB2	Collagen adhesion domain
CNS	Central nervous system
CNX	Calnexin
COVID-19	Coronavirus outbreak
CPMV	Cowpea mosaic virus
CRT	Calreticulin
CSF	Cerebrospinal fluid
DENV	Dengue virus
DIVA	Differentiate between infected and vaccinated animals
DNA	Deoxyribonucleic acid
dNTP	Deoxy-ribonucleoside triphosphates (dATP, dCTP, dTTP and dGTP)
dpi	Days post infiltration
E	Envelope protein
EdI	Envelope protein domain I
EdII	Envelope protein domain II
EdIII	Envelope protein domain III

EDTA	Ethylenediaminetetraacetic acid
EM	Electron microscopy
ER	Endoplasmic reticulum
EU	European Union
F	Fraction
FbaB	Fibronectin-binding protein
FLW	Fresh leaf weight
FMDV	Foot-and-mouth disease
g	Gram
g/cm^3	Gram per cubic centimeter
GFP	Green fluorescent protein
Glu	Glutamic acid
Gly	Glycine
h	Hour(s)
HBcAg	Hepatitis B core antigen
HCl	Hydrochloric acid
His	Histidine
HIV	Human immunodeficiency virus
HPV	Human papillomavirus
HT	Hypertranslational
iDNA	Infectious DNA
IFN	Interferon
Ig	Immunoglobulin
JEV	Japanese encephalitis virus
kb	Kilobase(s)
kDa	Kilodalton(s)
kg	Kilogram(s)
KH_2PO_4	Monopotassium phosphate
kPa	Kilopascal
L	Liter(s)

LAV	Live attenuated vaccine(s)
LB	Luria Bertani media
LBB	LB base media
LMIC	Low and middle-income countries
LPH	Murine mAB24 heavy chain
Lys	Lysine
LuS	*Aquifex aeolicus* lumazine synthase
M	Membrane protein / Molar
mA	Milli-amperes
mAbs	Monoclonal antibodies
MAC-ELISA	IgM antibody capture enzyme-linked immunosorbent assay
MES	2-N-morpholinoethanesulfonic acid
mg	Milligram(s)
$MgCl_2$	Magnesium chloride
min	Minute(s)
mL	Milliliter(s)
mM	Millimolar
mRNA	Messenger RNA
MW	Molecular weight marker
NAbs	Neutralising antibodies
NaCl	Sodium chloride
NaH_2PO	Monosodium phosphate
ng	Nanogram(s)
NIH	National Institute of Allergy and Infectious Disease
nm	Nanometer
NS	Non-structural protein(s)
NT	No template
NTB	Nitroblue tetrazolium
OD	Optical density
O/N	Overnight
ORF	Open reading frame
PAGE	Polyacrylamide gel electrophoresis
PBS	Phosphate buffer saline

PCR	Polymerase chain reaction
PCV	Porcine circovirus
PEG	Polyethylene glycol
PI	PBS with protease inhibitor
prM	Precursor of the membrane protein
PMF	Plant molecular farming
PRNT	Plaque-reduction neutralisation test
PTGS	Post-transcriptional gene silencing
PVX	Potato virus X
RBS	Receptor-binding domain
RC	Replication complex
RE	Restriction enzyme
RNA	Ribonucleic acid
RT	Room temperature
RT-qPCR	Quantitative real-time polymerase chain reaction
RVFV	Rift Valley fever virus
s	Second(s)
SAB	Sample application buffer
SARS-CoV	Severe acute respiratory syndrome coronavirus
SC	SpyCatcher peptide
SDS	Sodium dodecyl sulfate
Ser	Serine
siRNA	Small interfering RNA
SLEV	St. Louis encephalitis virus
SS	Signal sequence
ST	SpyTag peptide
Ta	Annealing temperature
TBSV	Tomato bushy stunt virus
T-DNA	Transfer-DNA
TEM	Transmission electron microscopy
TGN	Trans-Golgi network
TM	Transmembrane
tRNA	Transfer RNA
TSP	Total soluble protein

TSWV	Tomato spotted wilt virus
U	Unit(s)
UCT	University of Cape Town
USDA	U.S Department of Agriculture
UTR	Untranslated region
V	Volt(s)
VLP	Virus-like particle(s)
VPs	Vesicle packets
WND	WNV-associated neurological disease
WNF	West Nile fever
WNV	West Nile virus
w/v	Weight by volume
YFV	Yellow fever virus
ZIKV	Zika virus

Symbols

α	Alpha
β	Beta
γ	Gamma
Ω	Ohm(s)
µF	Microfarad(s)
µg	Microgram(s)
µL	Microlitre(s)
µM	Micromolar
°C	Degrees Celsius
%	Percentage

Table of Contents

Chapter 1:

Literature Review

1.1. Introduction

West Nile virus (WNV) is a member of the genus *Flavivirus* within the family *Flaviviridae* (Kuno *et al.*, 1998; Lindenbach *et al.*, 2007; Gray & Webb, 2014). WNV is a zoonotic mosquito-borne virus that was first isolated in 1937 from the blood of a local woman in the West Nile district of Uganda (Smithburn *et al.*, 1940). Since this first isolation, WNV has spread and become endemic in countries across Africa, America, the Middle East, West Asia and Australia (Castro-Jorge *et al.*, 2019). It is hypothesized that migratory birds, which are amplifier hosts, are responsible for the rapid dissemination of WNV (Mackenzie *et al.*, 2004; Bakonyi *et al.*, 2006; Reiter, 2010). Other factors that also contribute towards virus spread include urbanization, host-vector relationships, climate and wind patterns, and genetic changes in the virus (Mackenzie *et al.*, 2004).

In nature, WNV is maintained in a bird-mosquito transmission cycle and mammals are considered accidental dead-end hosts due to low viraemia levels (De Filette *et al.*, 2012). Serological data has shown that many species can be infected by WNV, with the highest incidence of infection observed in humans and horses (Marfin *et al.*, 2001). Infections in humans can result in febrile illness, and less commonly neuroinvasive disease with significant mortality and morbidity (Gray & Webb, 2014). To date, disease treatment is supportive with no antiviral treatment and no available human vaccine. Approximately 20% of infections in horses result in disease development of which 90% involve neurological symptoms, with 30-40% fatality rates (Ward *et al.*, 2006). As with humans, there is no antiviral treatment available for horses. However, several equine West Nile vaccines that are produced in the USA (Castro-Jorge *et al.*, 2019) and Europe (Rebollo *et al.*, 2018a) are licensed for use. These vaccines can be difficult and expensive to obtain in low and middle-income countries (LMIC), with regards to import permits, cost of the vaccines and the need for annual vaccination. Therefore, preventative strategies tend to rely on the low-tech prevention of mosquito bites (Sule *et al.*, 2018). The development of a vaccine that contributes to the 'One Health' Initiative could be the answer to overcoming this challenge. The 'One Health' Initiative is dedicated to improving the lives of all species, both human and animal, through the integration of human and veterinary medicine and environmental science.

WNV poses a major public health threat due to continuous disease outbreaks in both human and horse populations globally, no available treatment and little to no surveillance. As a result, the National Institute of Allergy and Infectious Disease (NIH) has deemed WNV a Category B pathogen, as it is moderately easy to spread, results in medium morbidity and low mortality rates and there is a necessity for the special development of diagnostics and enhanced disease surveillance protocols (NIH, 2018).

1.2. West Nile virus

1.2.1. Classification of WNV

WNV is one of the 70 viruses that make up the *Flavivirus* genus, which is the largest genus in the family *Flaviviridae* (Kuno *et al.*, 1998; Lindenbach *et al.*, 2007; Simmonds *et al.*, 2017). The genus can be divided into three clusters; mosquito-borne, tick-borne and vector-unknown viruses (Mukhopadhyay *et al.*, 2005). The mosquito-borne viruses can be further subdivided into two serogroups, namely the encephalitic group, more commonly known as the Japanese encephalitis virus (JEV) serocomplex, which includes JEV, WNV, and St. Louis encephalitis virus (SLEV); and the haemorrhagic fever group, which includes Zika virus (ZIKV), yellow fever virus (YFV) and dengue virus (DENV) (Castro-Jorge *et al.*, 2019).

The phylogenetic classification of WNV is dynamic with two main lineages described and three additional lineages suggested (Figure 1.1) (Bakonyi *et al.*, 2005; Bondre *et al.*, 2007). Strains from lineage 1 and 2 are the only West Nile viruses that have been associated with disease outbreaks in mammals (Petersen *et al.*, 2013). Lineage 1 WNV strains have a worldwide distribution and are the strains responsible for neuroinvasive diseases in humans, horses and birds (Chen, 2015). The lineage can be further divided into three sublineages; 1a, 1b and 1c. The most widely distributed WNV strains are from sublineage 1a, occurring in Africa, America, Europe and the Middle East (Burt *et al.*, 2002). Strains of the Kunjin virus, which is a subtype of WNV, represents sublineage 1b that occurs in Australia, South East Asia and Papua New Guinea (Hall *et al.*, 2001). Sublineage 1c WNV strains are only found in India, with recent evidence suggesting that these strains form a distinct lineage 5 (Bondre *et al.*, 2007).

Lineage 2 consisted of WNV strains predominantly from sub-Saharan Africa and Madagascar. However, in the mid-2000s WNV strains isolated in Hungary were ascribed to lineage 2 (Bakonyi *et al.*, 2006). Soon after, WNV strains associated with neurological disease in birds and humans were identified as lineage 2 strains in Russia (May *et al.*, 2011), Greece (Papa *et al.*, 2011) and Italy (Magurano *et al.*, 2012).

Lineage 3 is comprised of Rabensburg virus, a WNV strain named after the nearby Austrian town where the virus was isolated, and lineage 4 consists of a unique virus isolated from Caucasia. These viruses have been suggested to be a new species of the JEV serocomplex based on their genomic and antigenic diversity (Bakonyi *et al.*, 2005).

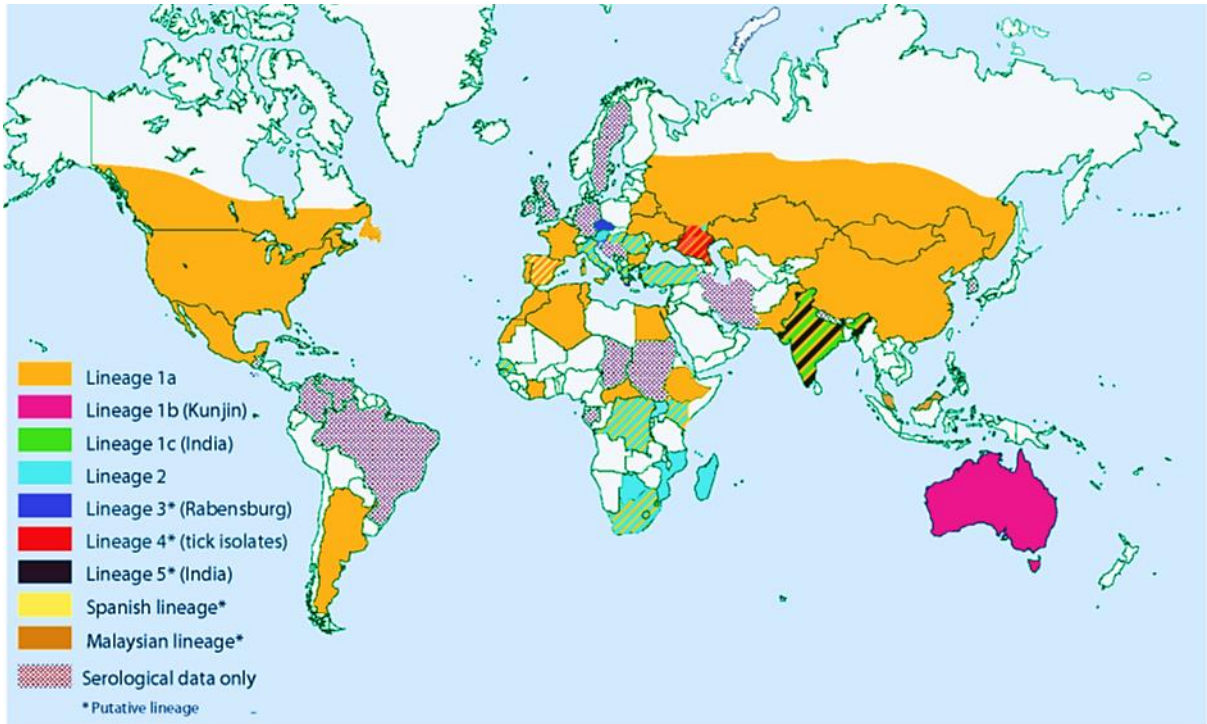

Figure 1.1. Worldwide distribution of West Nile virus. Reprinted with permission from *Viruses*; 9 December 2013:5. DOI: 10.3390/v5123021. (Ciota & Kramer, 2013)

1.2.2. Virus structure

The WNV genome is a positive-sense, single-stranded RNA of ~11 kb that contains one open reading frame (ORF) encoding a single polyprotein flanked by 5' and 3' untranslated regions (UTRs). The 5' UTR contains a type I m^7GpppAmp cap and the 3' UTR lacks a polyadenylated tail. The polyprotein is co- and post-translationally processed into three structural proteins; capsid (C), membrane (M, translated as prM, the precursor of the membrane protein) and envelope (E) proteins, and seven non-structural (NS) proteins: NS1, NS2A/B, NS3, NS4A/B and NS5 (Figure 1.2) (Chambers *et al.*, 1990; Lindenbach *et al.*, 2007). The C-prM, prM-E, E-NS1 and NS4A-NS4B proteins are cleaved by host signal peptidases located within the lumen of the endoplasmic reticulum (ER), whereas, the viral serine protease encoded by NS3 is responsible for the cleavage between the NS proteins (Figure 1.2B) (De Filette *et al.*, 2012).

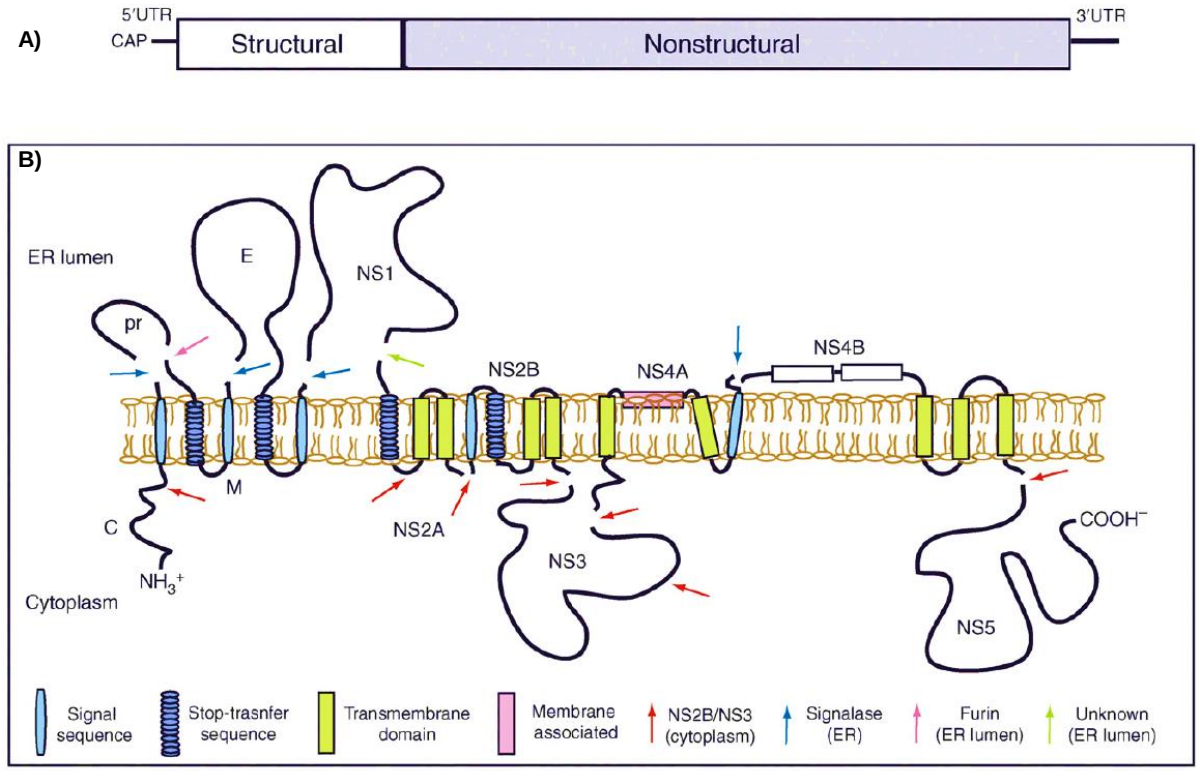

Figure 1.2. Schematic diagram of the flavivirus genome and polyprotein. **(A)** The genome is a positive sense RNA strand of ~11 kb and has a 5' cap but no 3' poly-(A) tail. **(B)** Membrane topology of the polyprotein. The viral RNA is translated as a polyprotein and processed by cellular and viral proteases (arrows). Reprinted from Current Opinion in Microbiology volume 11, Perera & Kuhn, Structural proteomics of dengue virus, p369-377, 2008, with permission from Elsevier. (Perera & Kuhn, 2008)

The roles of the structural and NS proteins have been extensively investigated for flaviviruses. The primary role of the C protein (12-14 kDa) in the flavivirus life cycle is the formation of the nucleocapsid and its association with viral RNA during virion assembly (Chambers *et al.*, 1990). Several critical roles have been proposed for the prM protein (19-25 kDa and 7-10 kDa for the M protein after furin cleavage): it might function as a chaperone for folding and assembly of the E protein (Lorenz *et al.*, 2002; Roby *et al.*, 2015); it could play a role in the pH-dependent conformational rearrangement of the prM-E heterodimers (Roby *et al.*, 2015); and it may conceal the E protein fusion loop to prevent premature fusion of the virion for exocytosis (Chambers *et al.*, 1990).

The E protein (~53 kDa) is the major virion surface protein and plays a role in virus entry. The protein consists of three structurally distinct β-barrel envelope domains, namely EdI, EdII and EdIII (Figure 1.3). The three domains are connected by flexible hinges that facilitate conformational changes during virus replication. EdI, is situated on the N-terminus but is spatially located in the middle of the E protein and therefore acts to stabilize the overall

orientation of the protein. On the one side, EdI is flanked by EdII that contains the fusion-loop peptide that is involved in pH-dependent virus-mediated membrane fusion during virus entry. EdIII is located on the opposite side of EdI and is the immunoglobulin-like domain that induces neutralising antibodies. EdIII is the immunodominant epitope that is highly variable among flaviviruses. It has also been suggested that it contains the cell receptor binding sites for infection (Mukhopadhyay *et al.*, 2005; Zhang *et al.*, 2017; Campos *et al.*, 2018).

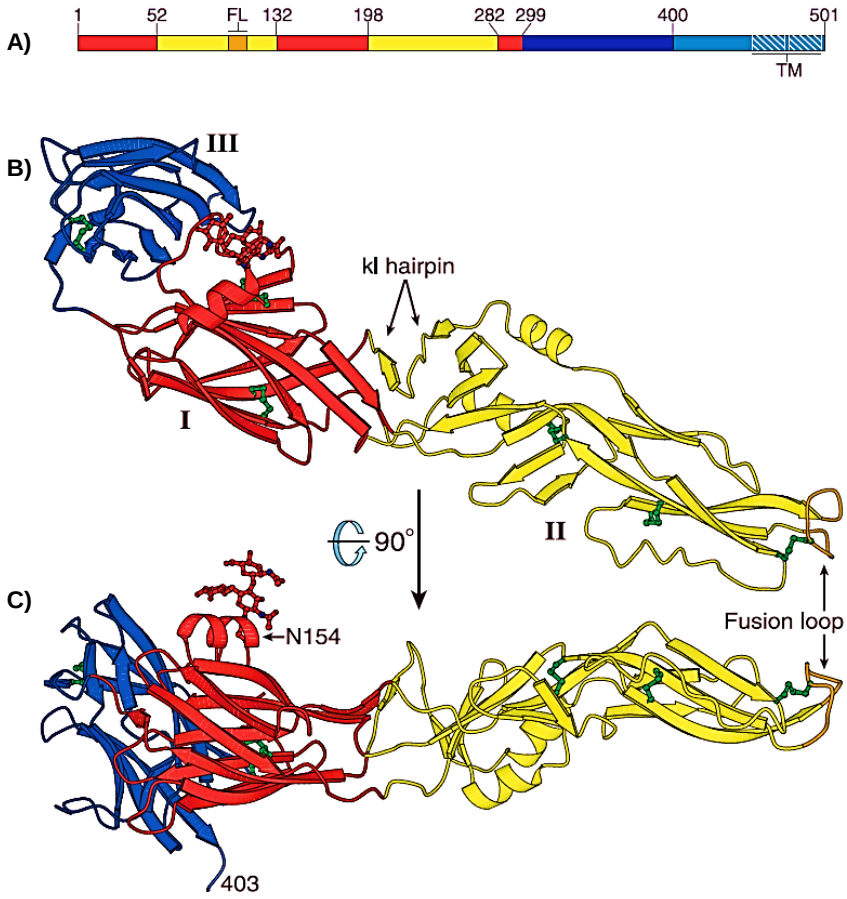

Figure 1.3. West Nile virus soluble E monomer structure. **(A)** The three E domains: domain I is red, domain II is yellow, and domain III is blue. The fusion loop is in orange. The ectodomain is linked to a two helix C-terminal transmembrane anchor (TM, white hatching) with a 53-residue 'stem' (cyan). **(B-C)** The West Nile virus soluble E monomer (residue 1-406), coloured as in panel A, viewed in two perpendicular orientations. The last ordered residue in the soluble E structure (Ser403) and the kI hairpin which forms the putative hydrophobic ligand-binding pocket, are labelled. The glycan at Asn154 (red) and the six disulfide bonds (green) are shown in ball and stick representation. Reprinted from Journal of Virology volume 80, Kanai *et al*., Crystal structure of West Nile virus envelope glycoprotein reveals viral surface epitopes, p11000-11008, with permission from American Society of Microbiology. (Kanai *et al.*, 2006)

The viral NS proteins play various roles during transcription, translation and replication. NS1 (~46 kDa) acts as an essential co-factor for virus RNA replication. NS2A (~22 kDa) is a multi-functional protein that also plays a role in virus replication, as well as virion assembly. In addition, NS2A inhibits the interferon-β (IFN-β) response through the inhibition of IFN-β transcription. NS2B (~14 kDa) acts as a co-factor for the virus-derived protease, NS3 (~70 kDa). NS2B and NS3 form a heterodimeric complex (NS2B-3) that is responsible for the post-translational cleavage of the virus proteins. However, NS3 also contains helicase, nucleoside triphosphatase and RNA triphosphatase domains. Therefore, together with the NS5 (103 kDa) polymerase, it plays an important role in virus replication. It has been proposed that NS4A (16 kDa) plays the role of 'organiser' of the replication complex (RC) of flaviviruses and also acts as a co-factor for NS3 helicase activity. NS4B (27 kDa) together with NS4A and NS2A plays a role in the inhibition of the host IFN-β response. Lastly, NS5 functions as a methyltransferase, RNA-dependent RNA polymerase (Lindenbach & Rice, 2003; De Filette *et al.*, 2012; Valiakos *et al.*, 2013) and major IFN antagonist (Best, 2017).

West Nile virions are enveloped spherical particles of approximately 50 nm in diameter with a buoyant density of ~1.2 g/cm^3 (Brinton, 2002; Ohtaki *et al.*, 2010). The RNA genome is packaged in a spherical nucleocapsid consisting of multiple copies of the C protein within a host-derived lipid bilayer with an outer glycoprotein shell. This shell consists of 180 copies each of the virus E and M proteins that are anchored in the host lipid bilayer (Figure 1.4) (Lindenbach & Rice, 2003; Mukhopadhyay *et al.*, 2003). In the absence of the viral genome and C protein, the M and E proteins remain capable of assembling into particles of approximately 20-30 nm. These particles are non-infectious and are termed virus-like particles (VLPs) (Chambers *et al.*, 1990; Takahashi *et al.*, 2009).

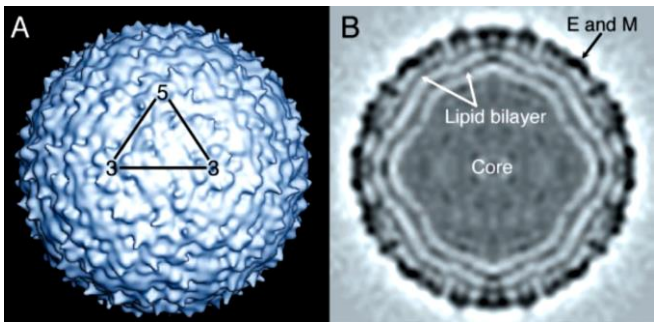

Figure 1.4. Structure of West Nile virus determined by cryo-EM. **(A)** A surface shaded view of the virion, with one asymmetric unit of the icosahedron shown by the triangle. The 5-fold and 3-fold icosahedral symmetry axes are labelled. **(B)** A central cross-section showing the concentric layers of density. Virion core, lipid bilayer, E and M proteins are indicated. Reprinted with permission from Science, 10 October 2003:248. DOI:10.1126/science.1089316. (Mukhopadhyay *et al.*, 2003)

1.2.3. Virus replication

The replication cycle of WNV is a well-regulated process (Figure 1.5) (Roby *et al.*, 2015). During viral entry, the E protein interacts with one or more host cell receptors binding the virus to the cell. After binding, the virus enters the cell via clathrin-mediated endocytosis (Figure 1.5i) (Chu & Ng, 2004). The low pH of the endosome induces a conformational change of the E protein which results in the fusion of the viral envelope with the endosome (Gollins & Porterfield, 1986). The nucleocapsid is released into the cytoplasm of the cell, disassembles and releases the viral RNA (Figure 1.5ii). The positive-sense RNA is translated into a single polyprotein that is co- and post-translationally processed by viral and host proteases. RCs form within the ER-derived vesicle packets (VPs) with subsequent replication of the genomic RNA (Figure 1.5iii) (Valiakos *et al.*, 2013; Roby *et al.*, 2015). The C proteins bind and wrap around the progeny RNA to form an icosahedral shell that is enclosed by an ER-derived cellular membrane. The evagination into the ER lumen creates the viral envelope embedded with 90 homodimers of the prM-E proteins that extend as 60 heterotrimeric spikes from the envelope surface (Figure 1.5iv and 1.6A). The immature virions are transported in individual vesicles to the trans-Golgi network (TGN) for glycan maturation (Figure 1.5v). The low pH (~5.8-6.0) in the TGN induces the conformational rearrangement of prM-E, with the disassociation of the heterotrimeric spike-like conformation to form 90 antiparallel homodimers that lie flat against the viral surface (Figure 1.5vi and 1.6B). These conformational changes drive the cleavage of the pr peptide from the M protein by furin-like proteases to generate mature infectious virions (Figure 1.5vi and 1.6C-D). However, the furin processing of prM is rather inefficient, resulting in the secretion of a mixture of mature and immature virions from the cell (Figure 1.5vii) (Mukhopadhyay *et al.*, 2005; Perera & Kuhn, 2008; Valiakos *et al.*, 2013; Roby *et al.*, 2015; Campos *et al.*, 2018).

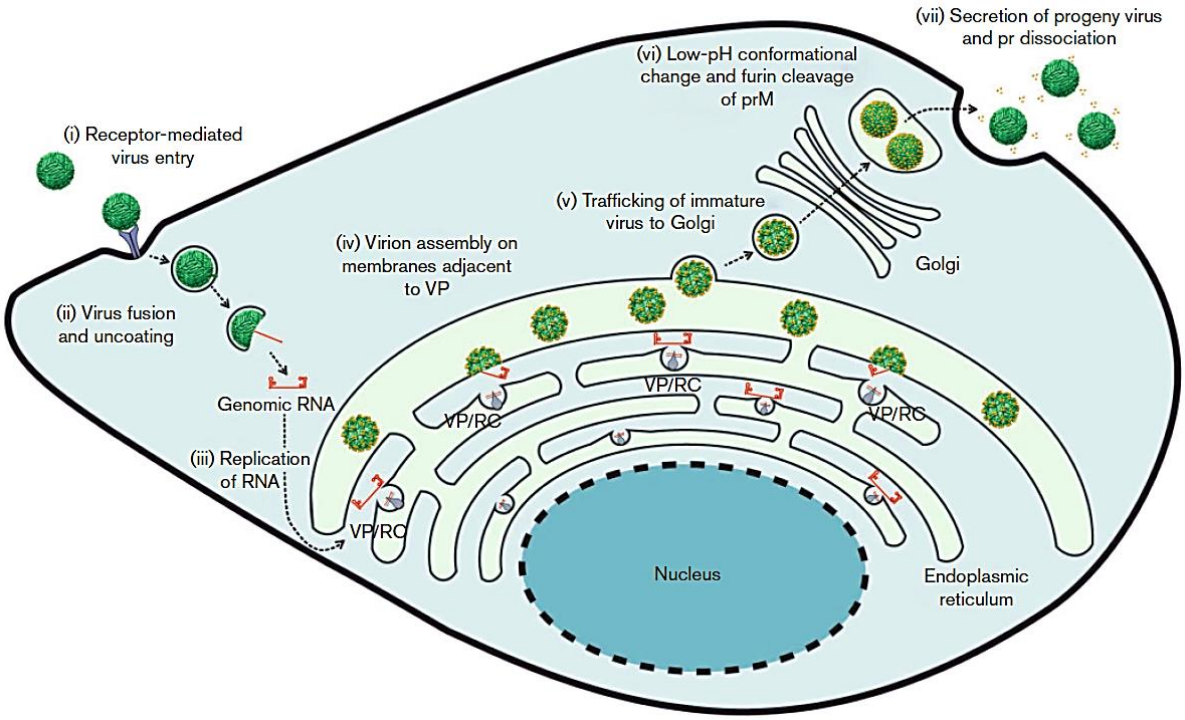

Figure 1.5. West Nile virus replication cycle. **(i)** receptor-mediated endocytosis of virus; **(ii)** low-pH induced fusion of the viral envelope with the endosome and release of viral RNA into the cytoplasm; **(iii)** formation of replication complex (RC) within the ER-derived vesicle packets (VPs) and subsequent replication of RNA; **(iv)** the capsid protein binds and wraps around the progeny RNA and evagination into the ER lumen creates the viral envelope embedded with prM and E proteins assembled in heterotrimeric spikes; this process also occurs independently of the capsid protein and viral RNA to produce empty prM-E particles (VLPs); **(v)** immature virions and VLPs are transported in individual vesicles to the TGN for glycan maturation; **(vi)** the low pH within the TGN induces conformational rearrangement of prM-E heterodimers and the cleavage of the pr peptide from M by host furin; **(vii)** mature virions and VLPs are secreted by exocytosis from the cell and the pr peptide is released. Republished with permission of Microbiology Society, from Post-translational regulation and modifications of flavivirus structural proteins, Roby *et al*., 96, 2015; permission conveyed through Copyright Clearance Center, Inc. (Roby *et al.*, 2015)

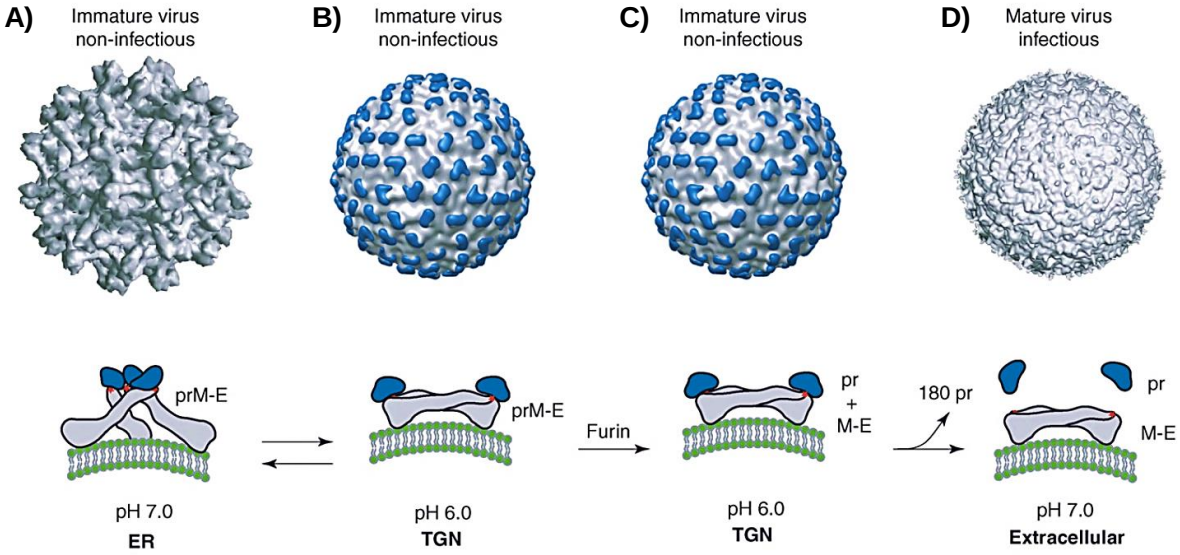

Figure 1.6. Structure of the dengue virion during maturation. **(A)** Cryo-EM of the immature virion at a neutral pH, where prM-E exists as 60 heterotrimeric spikes that extend away from the virion surface. The conformation of the E (grey) protein and 'pr' peptide (blue) protecting the fusion peptide of E (red) are shown below the virion. **(B)** Cryo-EM reconstruction of the immature virion at a low pH encountered in the TGN. The prM-E heterodimers disassociate from their trimeric spike-like conformation and form 90 dimers that lie flat against the virion surface resulting in a 'smooth' morphology. **(C)** Within the TGN, the prM protein is cleaved into its 'pr' peptide and M protein by host furin. The cleaved 'pr' peptide remains in position as a 'cap' for the fusion peptide for the E protein. The M protein (not shown) lies embedded in the viral membrane beneath the E protein shell. **(D)** Cryo-EM reconstruction of the mature virion. Following furin cleavage, the mature virion is released into the neutral pH of the extracellular environment and the 'pr' peptide disassociates. Reprinted from Current Opinion in Microbiology volume 11, Perera & Kuhn, Structural proteomics of dengue virus, p369-377, 2008, with permission from Elsevier. (Perera & Kuhn, 2008)

1.3. West Nile disease

1.3.1. Ecology

WNV is maintained in the environment within a bird-mosquito transmission cycle. Mosquito vectors take up WNV when they feed on infected birds. Following a short period of virus replication in the mosquito, it is spread to a reservoir or dead-end host after mosquito feeding. More than 60 species of ornithophilic mosquitoes have been implicated in the transmission of WNV, however, the principal vector species belongs to the *Culex* genus (Ciota & Kramer, 2013; Castro-Jorge *et al.*, 2019). WNV is transmitted by different species of *Culex* mosquitoes based on their prevalence in a particular geographic region (Figure 1.7) (Farajollahi *et al.*,

2011). *Cx. univittatus* and *Cx. pipiens* are the principal vectors in Africa, Europe and North America, whereas *Cx. vishnui* is the principal species in India (Hayes, 1989b). Another vector considered to play a minor role in WNV transmission are hard and soft ticks since they can become infected with WNV (Hubalek & Halouzka, 1999).

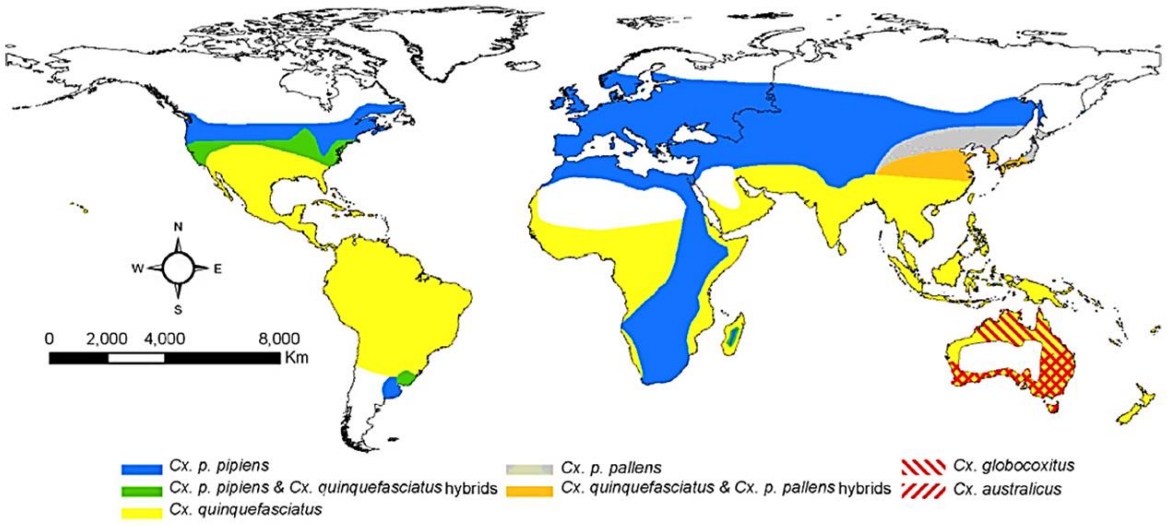

Figure 1.7. Global distribution of *Cx. pipiens* complex mosquitoes. Reprinted from Infection, Genetics and Evolution volume 11, Farajollahi *et al*., ‘‘Bird biting’’ mosquitoes and human disease: A review of the role of *Culex pipiens* complex mosquitoes in epidemiology, p1577-1585, 2011, with permission from Elsevier. (Farajollahi *et al.*, 2011)

Wild birds are the predominant amplifying hosts of WNV due to the high level of viraemia observed during infection (Sule *et al.*, 2018). The degree and the duration of viraemia varies across bird species but has proven sufficient to infect feeding mosquitoes (Brinton, 2002). Bird orders prone to disease include the Passeriformes, Charadriiformes and Falconiformes, whereas infections in birds from the Galliformes order are subclinical (Castro-Jorge *et al.*, 2019).

In addition to birds, WNV can also infect reptiles and amphibians with high enough viraemia levels to infect feeding mosquitoes (Hayes, 2005). To a lesser extent, WNV also infects mammals which are considered to be accidental dead-end hosts due to short-lived viraemia with insufficient levels for contagion (Brinton, 2002). Humans and horses are the predominant mammals affected by WNV, although only ~20% of infections result in disease development (Venter *et al.*, 2017). In humans, there is more than one route of WNV infection. The main route of infection is through the bite of an infected mosquito, yet, infection has also been shown to occur from organ transplants and blood transfusions (Hayes, 2005).

With an influx in vector numbers, an influx of infection in reservoir and dead-end hosts are expected (Sule *et al.*, 2018), since WNV infections are seasonal as based on mosquito populations.

1.3.2. Clinical signs

In humans, approximately 80% of infections are subclinical. In the instance of disease development, patients usually experience symptoms after a 3 to 15 day incubation period. When symptomatic, most patients present with West Nile fever (WNF), which is characterised by an abrupt onset of fever, headache, malaise, fatigue, loss of appetite, nausea, muscle pain, and weakness. In about half of symptomatic cases, a maculopapular rash will occur on the extremities, palms, soles, and torso of individuals. In rare instances, hepatitis, myocarditis, pancreatitis, orchitis and ocular manifestations can occur. Generally, WNF is a mild illness that only persists for a few days, but in some cases the illness has persisted for weeks, causing a debilitating illness (Mackenzie *et al.*, 2004; Hayes *et al.*, 2005; Sule *et al.*, 2018; Castro-Jorge *et al.*, 2019).

In less than 1% of infected cases, patients will develop a neurological disease such as meningitis, encephalitis or paralysis. WNV-associated neurological disease (WND) clinical severity can range from mild disorientation to death, with mortality rates of about 10%. The risk of contracting WND is greater for the elderly and immunocompromised (Mackenzie *et al.*, 2004; Hayes *et al.*, 2005; Sejvar, 2014).

Horses are the most prominently infected animal of WNV. Similar to human cases, ~20% of infected cases are symptomatic, of which 90% will involve neurological disease with a 30 to 40% fatality rate. Horses with WND may present with ataxia, rear limb paresis, muscle tremors of the face and neck, and recumbency (Ward *et al.*, 2006; Venter *et al.*, 2017; Sule *et al.*, 2018).

1.3.3. Distribution and outbreaks

WNV was first isolated in 1937 from a woman presenting with a febrile illness in Uganda (Smithburn *et al.*, 1940). Data from a serosurvey conducted during 1939-1940 showed widespread human seropositivity for WNV in Uganda, Sudan, Kenya and the current Democratic Republic of Congo (Chancey *et al.*, 2015). However, it was not until the 1950s that WNV was associated with evident disease and epidemics. In 1951 WNV was isolated from apparently healthy children in Egypt (Melnick *et al.*, 1951); however, throughout the 1950s-

1980s WNV was associated with several outbreaks in humans of WNF, and in Israel some cases with encephalitis (Bernkopf *et al.*, 1953; Marberg *et al.*, 1956). Between 1998 and 2000 WNV was isolated from migratory birds and domestic geese in Israel, and high morbidity in goose flocks was associated with clinical signs in goose farmers (Bin *et al.*, 2001).

In the early 1950s and 1960s, seropositivity was found in humans throughout India (Rao, 1971), with the first paediatric fatalities of neurological disease reported in 1981 (George *et al.*, 1984). Since then, WNF and WN-associated encephalitis have been reported in India throughout the 1990s, early 2000s and as recently as in 2014 (David & Abraham, 2016).

In 1954, seropositivity in humans, monkeys, domestic animals and birds was demonstrated in South Africa, with no clinical manifestations (Kokernot *et al.*, 1956). However, in 1974, the largest ever WNV epidemic with tens of thousands of humans presenting with WNF was recorded in the Karoo (McIntosh *et al.*, 1976). Another epizootic with more than usual human cases was also recorded in 1984 (Jupp *et al.*, 1986). Several human cases of WND were recorded in 2008 (Zaayman & Venter, 2012) and seropositivity was confirmed in veterinarians in 2011 and 2012 (van Eeden *et al.*, 2014). During an eight-year surveillance program, from 2008-2015, several neurological disorders in horses were found to be associated with WNV with approximately 34% fatality rates (Venter *et al.*, 2017).

The first case of WNV detection in Europe was in 1958 in Albania, with the discovery of WNV neutralising antibodies (NAbs) in human sera (Chancey *et al.*, 2015). This was followed by several cases of WNF and encephalitis in humans recorded in France from 1962-1964. Neurological disorders in horses were also reported with a fatality rate of 25-30%. However, since 1965 there has been no real evidence of WNV infection in France (Hayes, 1989a; Murgue *et al.*, 2001).

In Kenya, a serological survey conducted from 1966-1968 presented the presence of WNV in the human population (Geser *et al.*, 1970). Since then WNV has been continuously detected in humans (Mease *et al.*, 2011; Sutherland *et al.*, 2011; Tigoi *et al.*, 2015; Inziani *et al.*, 2020) and mosquito populations (Miller *et al.*, 2000; LaBeaud *et al.*, 2011).

WNV was isolated in the 1970s in Hungary from rodents, cattle and humans with no incidence of disease (Bakonyi *et al.*, 2005). In 2003, the first clinical signs of WNV infection were observed in a Hungarian goose flock that presented with encephalitis, which resulted in 16% fatalities. In the same study, a single incidence of neurological disease in a goshawk fledgling that resulted in death was recorded in 2004 (Bakonyi *et al.*, 2006). A yearly average of 6 WND cases were diagnosed between 2003 and 2007 (Krisztalovics *et al.*, 2008). A large outbreak of neuroinvasive disease across Hungary was diagnosed in 2008 with 25 bird, 12 horse and

22 human cases (Kutasi *et al.*, 2011; Bakonyi *et al.*, 2013). In 2017 and 2018, human and equine WNV infections were recorded (Zana *et al.*, 2020).

In the early 1970s, WNV antibodies were detected in healthy humans in Austria (Gresikova *et al.*, 1973). The first cases of WNV disease were retrospectively identified from patients in 2009 and 2010, two with neurological disease and one with WNF (Stiasny *et al.*, 2013). Since then WNV disease cases have been diagnosed yearly, except during 2011-2013, up until 2018 (Aberle *et al.*, 2018). Besides humans, WNV has also been detected in birds of prey since 2008 (Wodak *et al.*, 2011; Kolodziejek *et al.*, 2018). The first case of WND in horses was recorded in 2016 and resulted in death (Kolodziejek *et al.*, 2018).

Several serosurveys conducted in animals in 1980 in Greece detected WNV antibodies in sheep, goats, horses, cattle, pigs and birds, and from 2001 to 2004, 4% of tested horses were positive for WNV (Papa *et al.*, 2010a). WNV antibodies were first detected in healthy farmers, woodcutters and shepherds in the 1980s (Antoniadis *et al.*, 1990), and again in 2007 from residents in selected urban areas (Papa *et al.*, 2010b). In 2010, the first cases of WND were confirmed in 197 patients with 33 fatalities (Papa *et al.*, 2010a; Danis *et al.*, 2011). Since then, WNV cases have been reported every year except for 2015 and 2016 (Papagiannis *et al.*, 2020).

Seroprevalence studies performed by Omilabu and colleagues in Nigeria in 1990 found WNV-specific-antibodies in both humans and domestic animals that included camels, goats, cattle and sheep (Omilabu *et al.*, 1990). WNV antibodies were also detected in 2008 in patients presenting with febrile illness (Baba *et al.*, 2013). A seroprevalence study conducted on asymptomatic horses during 2011-2012, reported WNV seroconversion (Sule *et al.*, 2015).

In Algeria, an epidemic occurred in 1994, where 50 cases presented with WNF and neurological symptoms. Among them, 20 were clinical cases of encephalitis of whom 8 died (Le Guenno *et al.*, 1996). A fatal clinical case of WND was reported in 2012, and two clinical cases were reported between 2013 and 2014. A seroprevalence study in equids conducted in 2014 highlighted the presence of WNV (Lafri *et al.*, 2019). Medrouh *et al*. conducted a serosurvey in wild birds during 2014-2015 and published the first report of WNV circulation in birds in Algeria (Medrouh *et al.*, 2020).

In 1996, WNV infection in 94 equines in Morocco was recorded, of which 42 died (Murgue *et al.*, 2001). Dozens of confirmed equine cases followed in 2003 and 2010. During a seroprevalence study in humans, WNV NAbs were detected in 2012 (El Rhaffouli *et al.*, 2013). In 2018, WNV was detected in *Cx. pipiens* mosquitoes for the first time in Morocco, together with high seroprevalence in horses (Assaid *et al.*, 2020).

In Romania in 1996, 393 positive WNV infections were recorded in humans presenting with encephalitis, meningitis and meningoencephalitis, with 17 deaths (Tsai *et al.*, 1998). Subsequent WNV infections associated with both WNF and WND was reported in 2010 (Sirbu *et al.*, 2011) and 2011 to 2013 (Dinu *et al.*, 2015).

In 1997, 111 patients hospitalised with meningitis or meningoencephalitis in Tunisia tested positive for WNV, of which 5 cases were fatal. These patients were predominantly over 50 years of age (Murgue *et al.*, 2001).

WNV was identified in 14 horses, of which 6 died, in Italy in 1998 (Murgue *et al.*, 2001). During 2008 and 2009 several WNV cases in horses and WND cases in humans were recorded (Macini *et al.*, 2008; Rossini *et al.*, 2008; Barzon *et al.*, 2009; Rizzo *et al.*, 2009). This was followed by a single incidence of WNF recorded from a male in his late 50s in 2011 (Bagnarelli *et al.*, 2011). Most recently in 2018, 440 human cases of WNV infection were recorded, of which 81 were neurological and 304 febrile (Sinigaglia *et al.*, 2019), indicating the persistence of WNV in Italy.

In 1999, a major epidemic was recorded in Russia. Eight hundred and twenty-six patients presented with either febrile or neurological disease and serological assays confirmed 183 WNV positive cases, with 40 recorded fatalities (Platonov *et al.*, 2001).

WNV is now endemic in the United States, with recurring outbreaks since 1999. The first outbreak was in New York and included 59 cases of WND, which resulted in 7 deaths (Mostashari *et al.*, 2001). A serosurvey on birds in the same year recorded WNV NAbs in 9 species (Komar *et al.*, 2001). By 2000, WNV had spread to New Jersey and Connecticut with 19 cases of neurological disease and 2 deaths (Centers for Disease Control and Prevention, 2001). By 2001, WNV was found in 10 states with 64 cases of neurological disease and 9 deaths, and by 2002, 4 156 WNV human cases were reported across 40 states. From these, 2 946 cases were neurological with 284 deaths (Chancey *et al.*, 2015). A total of 1 698 equine WNV cases were also confirmed in 2002, with 1 381 cases presenting with neurological disease (Ward *et al.*, 2006). In 2003, 9 862 WNV cases were reported with 2 866 represented by neurological disease, and by 2004 WNV was detected in all 48 contiguous states. In 2006, 4 260 cases of WNV were confirmed of which 1 495 presented with neurological disease and 177 deaths. Less cases were observed in 2007 and in 2011, a total of 712 WNV cases were reported. In 2012 however, there was a large outbreak with 2 873 cases of WND. During the time period from 1999-2013, a total of 39 557 cases of WNV were reported, of which 17 381 were neurological diseases resulting in 1 667 deaths in the U.S. (Chancey *et al.*, 2015).

The first detection of WNV in Canada was in 128 dead birds and 9 mosquito pools in 2001 (Sockett, 2005), and was followed by the first human cases in 2002. Since then the annual

occurrence of WNV infection has been recorded, with the largest outbreak in 2007 of 2 215 human cases. Since 2013, the average percentage of WND cases in humans has been 49.8%, with 13 cases in 2019. Annual WNF infection in horses has also been recorded with 6 cases in 2019 (Government of Canada, 2019).

The first detection of WNV in Spain was also in 2001, with 12 human samples positive for WNV IgG (Bofill *et al.*, 2006). The first clinical case was identified in 2004 in a 21-year-old male presenting with meningitis (Kaptoul *et al.*, 2007). A seroconversion study on partially migratory birds displayed evidence for the circulation of WNV during 2004-2005 (Figuerola *et al.*, 2007). NAbs for WNV were detected in healthy horses in southern Spain in 2005 (Jiménez-Clavero *et al.*, 2007), with the first clinical case in 2010 (García-Bocanegra *et al.*, 2011). Since then, WNV has become endemic in southern Spain in both horse and human populations (López-Ruiz *et al.*, 2018).

In Columbia, WNV was first detected in horses in 2004 (Mattar *et al.*, 2005). In a serosurvey conducted from 2005-2008, healthy horses tested positive for WNV (Góez-Rivillas *et al.*, 2010). Another study in 2008, tested for WNV in 18 species of healthy captive birds from the Santa Fe zoo collection in Medellin and flamingoes were the only species that tested positive (Osorio *et al.*, 2012).

WNV was detected for the first time in humans in Guinea (Jentes *et al.*, 2010), Ghana (Wang *et al.*, 2009) and Gabon (Mandji *et al.*, 2009), and in encephalitic brain samples of diseased horses in Argentina (Morales *et al.*, 2006) in 2006. However, Diaz and colleagues retrospectively identified WNV in several bird samples from 2005, suggesting that WNV might have been introduced into Argentina as early as 2004 (Diaz *et al.*, 2008).

WNV was detected in healthy horses by two independent studies conducted in Brazil in 2009 (Pauvolid-Corrêa *et al.*, 2011; Silva *et al.*, 2013). In 2014, the first human case of WNV encephalitis was recorded in a 52-year-old man (Vieira *et al.*, 2015). More recently, WNV was detected in central nervous system (CNS) fragments of 4 encephalitic equids in 2018 (Silva *et al.*, 2019).

In Zambia, WNV antibodies were detected in 10.3% of persons tested, in a serosurvey conducted in 2015 (Mweene-Ndumba *et al.*, 2015). In 2016, WNV was isolated for the first time from mosquitoes. The WNV strains isolated from *Cx. quinquefasciatus* mosquitoes were closely related to the neuroinvasive lineage 2 WNV strain from South Africa (Orba *et al.*, 2018).

Throughout the past few decades, WNV has spread expansively across the globe and has caused disease in humans, equines and birds. Based on the data presented above regarding the rapid and continuous spread of the virus, the few countries still naïve to WNV are at risk of exposure in the coming years.

1.3.4. Disease surveillance and diagnosis

The use of sentinel birds for the surveillance of arboviruses is decades old. Since birds act as a reservoir for maintenance of WNV, they are appropriate for use as sentinels for monitoring WNV prevalence. It is assumed that WNV infections in birds occur more frequently and earlier than WNV disease in humans and horses. Therefore, these sentinels allow for the quantification of infection rates that in turn are used for recommendations of disease prevention in animal and public health systems (Komar, 2001). Besides birds, horses have also been shown to be appropriate sentinels for WNV, especially for detecting new strains present in a specific geographical region (Venter *et al.*, 2011). Continuous surveillance regimes of sentinel animals together with entomological surveillance of the primary mosquito vectors are pertinent for the early identification of WNV circulation (Castro-Jorge *et al.*, 2019).

WNV disease cannot be diagnosed by clinical symptoms alone since flavivirus infections share their most common symptoms which are similar to influenza symptoms. Consequently, laboratory methods are required for the diagnosis of WNV disease. Detection of WNV-specific immunoglobulin (Ig) M in serum or cerebrospinal fluid (CSF), 5 or 8 days after the onset of symptoms, respectively, using the IgM antibody capture enzyme-linked immunosorbent assay (MAC-ELISA) is the principal test for WNV diagnosis in most clinical settings. The presence of WNV IgM in CSF confirms CNS infection as IgM cannot cross the blood-brain-barrier (Petersen *et al.*, 2013). Validation of MAC-ELISA results are commonly done by plaque-reduction neutralisation tests (PRNT) since cross-reactivity with other flaviviruses could occur. This assay is based on the ability of serum antibodies to neutralise live virus and requires BSL-3 facilities and therefore is usually only available in reference laboratories (David & Abraham, 2016).

WNV disease can also be diagnosed by the detection of virus in serum or CSF by virus isolation or nucleic acid-based tests. Following the isolation of WNV in cell culture or suckling mice, the virus can be detected by indirect immunofluorescence assays using WNV-specific monoclonal antibodies (Hayes *et al.*, 2005; David & Abraham, 2016). Alternatively, virus can be detected by quantitative Real-Time Polymerase Chain Reaction (RT-qPCR) amplification during the viraemic phase of infection; however, due to short-lived viraemia, this is not common practice (Castro-Jorge *et al.*, 2019).

The detection of WNV RNA by molecular methods is predominantly used in the screening of blood donors and organ donations in areas where WNV is endemic. For these screenings, tests of great sensitivity are required to screen both healthy and asymptomatic donors. Currently, there are two commercial nucleic acid amplification tests available, a PCR platform

from Roche Diagnostics (Mannheim, Germany) and a transcription-mediated amplification test from Novartis Diagnostics (Siena, Italy) (David & Abraham, 2016).

1.3.5. Disease treatment and prevention

To date, there are no licensed therapies for treating WNV infection in humans and animals. Treatment is supportive based on patient symptoms; namely, pain control for headaches, hydration for nausea and vomiting, monitoring of intracranial pressure and containment of seizures if present (David & Abraham, 2016). The development of WNV antiviral therapies is challenging due to the short-lived viraemic period and the clearing of the infection shortly after the onset of symptoms (Castro-Jorge *et al.*, 2019). Candidate antiviral therapies include ribavirin, interferon α (IFN-α) and WNV-specific immunoglobulins.

Ribavirin is a broad-spectrum guanosine analogue with antiviral activity against many RNA and DNA viruses. Ribavirin inhibits host-cell inosine monophosphate dehydrogenase, depleting the intracellular guanosine pools. In cell culture, ribavirin inhibited WNV replication and its cytopathic effect (Jordan *et al.*, 2000), but in hamsters it resulted in increased mortality (Morrey *et al.*, 2004). Even though ribavirin inhibited WNV in cell culture, *in vivo* it exhibited an immunosuppressive effect and therefore is not considered an appropriate therapy for the treatment of WNV.

IFNs are naturally occurring immunoregulatory glycopeptides vital in the innate host response to viral infections. In primate cell culture, the inhibitory effect of IFN-α2b for WNV infection was demonstrated as both therapeutic and protective (Anderson & Rahal, 2002). IFN-α has also been used successfully in the treatment of 2 WNV encephalitis patients (Kalil *et al.*, 2005). However, since IFN cannot penetrate the blood-brain barrier into the CSF, the response in these encephalitic cases remain unexplained (Gray & Webb, 2014). Moreover, the effect of IFN is attenuated once the virus starts replicating due to the antagonising effect NS proteins have on the IFN signalling pathway (Lai *et al.*, 2010; Best, 2017).

WNV-specific immunoglobulins such as monoclonal antibodies (mAbs) are another potential therapeutic for the treatment of WNV infection. It has been suggested that neurotropic viruses such as WNV are more sensitive to antibody-mediated immunity than cell-mediated immunity, as clearance of these viruses is not dependent on cytolytic T cell activity (Agrawal & Petersen, 2003). Flavivirus NAbs predominantly recognise the E protein. Several studies have identified candidate therapeutic mouse and human neutralising mAbs that localise to the E protein (Beasley & Barrett, 2002; Oliphant *et al.*, 2005; Goo *et al.*, 2019). In a recent study by Goo and colleagues, mice survived WNV infection when treated with the humanised mAb E16 or

the human mAb WNV-86. Reduced viral load was observed in both the spinal cord and brain of mice treated with WNV-86 post WNV infection (Goo *et al.*, 2019), highlighting the potential of neutralising mAbs as possible therapeutics for WNV infection.

WNV disease prevention strategies are focused on avoiding human exposure to WNV-infected mosquitos by vector control and personal protection due to the lack of a human WNV vaccine. Mosquito-control strategies include the elimination of breeding sites, larviciding and the control of adult mosquito populations (Petersen *et al.*, 2013). Personal protection strategies include the use of insect repellent on skin and clothes, avoiding the outdoors during peak mosquito active times such as dawn and dusk, and using bed nets and mosquito traps. Breeding sites can also be reduced around living quarters by emptying water from flowerpots, bird-baths, buckets, barrels, cans, swimming pool covers and other receptacles likely to collect water (Sule *et al.*, 2018).

With no specific antiviral treatment for WNV, there is a desperate need for the development of a safe, effective and affordable prophylactic vaccine. To date, there is no human WNV vaccine available, but several candidate vaccines have been published and evaluated in clinical trials (Kaiser & Barrett, 2019). However, in the case of horses, there are four licensed vaccines (Rebollo *et al.*, 2018a; Castro-Jorge *et al.*, 2019).

1.4. West Nile vaccines

The expanding epidemics of WNV across the world illustrate the need for the development of affordable and effective vaccines. Currently, four USDA-licensed veterinary vaccines that confer immunity for at least a year are available (Kaiser & Barrett, 2019), and three European-licensed veterinary vaccines identical to three of the USDA-licensed vaccines (but licensed under different names (Table 1)) are available (Rebollo *et al.*, 2018a). Although there is no licensed human WNV vaccine available, several different types of candidate vaccines are under development (Martina *et al.*, 2008; Ohtaki *et al.*, 2010; Spohn *et al.*, 2010; Cielens *et al.*, 2014; He *et al.*, 2014; Lai *et al.*, 2018; Quintel *et al.*, 2019). Ideally, vaccines against WNV should confer protection against all WNV serotypes, induce a robust neutralising immune response, not play a role in antibody-dependent enhancement (ADE), and should be DIVA compliant (able to differentiate between infected and vaccinated animals).

Live attenuated vaccines (LAV) or inactivated whole virus vaccines are not regarded as DIVA-compliant since they induce antibody responses similar to those induced by wild-type infections. The goal of DIVA strategies is to facilitate the detection of specific antibodies induced by natural infection rather than by vaccination, therefore, enabling mass vaccination

without compromising serological identification of natural infection. This would ensure the safe trade of products from immunised animals (Liu *et al.*, 2013). Therefore, recent focus has shifted to the development of recombinant vaccines rather than conventional inactivated and live attenuated whole virus vaccines to achieve this.

ADE is the phenomenon whereby the presence of specific virus antibodies enhance and facilitate the entry of a different virus strain through the interaction of the Fc receptor and/or complement system into monocytes/macrophages and granulocytes with subsequent replication of the secondary virus. Thus, a mild infection can become life-threatening due to the inability of pre-existing antibodies to neutralise the virus. Consequently, numerous studies have been conducted to identify epitopes that are associated with ADE for the development of vaccines with minimum or no ADE activity (Tirado & Yoon, 2003). In the instance of WNV, ADE may occur between WNV and other flaviviruses such as DENV and ZIKV due to their genetic similarity and co-circulation. Thus, WNV vaccines constructed on conserved flavivirus epitopes will have the potential of inducing cross-reactive epitopes that can result in the augmentation of virus entry and replication of other flaviviruses (Lai *et al.*, 2018). For WNV, the E protein is the principal target of virus NAbs as it predominantly makes up the virion surface and therefore has two roles during cell entry; binding to cell receptors and membrane fusion (Mukhopadhyay *et al.*, 2003; Heinz & Stiasny, 2012; Lai *et al.*, 2018). Several studies have been conducted on NAbs that bind different epitopes across the three E protein domains (EdI, EdII and EdIII) (Beasley & Barrett, 2002; Nybakken *et al.*, 2005; Oliphant *et al.*, 2005; Oliphant *et al.*, 2006; Goo *et al.*, 2019), but data from murine mAbs suggests that EdIII has the highest neutralising potency (Heinz & Stiasny, 2012). Data has also shown that EdIII does not play a similar role in ADE in comparison to EdI and EdII when inside cells expressing Fc γ receptors (Oliphant *et al.*, 2006; Brandler & Tangy, 2013). Consequently, for the development of recombinant vaccines, EdIII is the favoured target epitope.

Table 1. Overview of currently commercialised West Nile vaccines.

Name	Antigen	Licensed	Reference
WNV-Innovator (Zoetis)	Whole inactivated WNV	US	(Zoetis, 2020c)
Vetera™ WNV (Boehringer Ingelheim)		US	(Boehringer Ingelheim, 2019)
Equip® WNV (Duvaxyn WNV) (Zoetis)		EU	(Zoetis, 2020b; Zoetis, 2020a)
Prestige® WNV (Merck)	Inactivated WNV prM-E in a YF17D backbone	US	(Merck, 2019)
Prevenile (Intervet)	Live WNV prM-E in a YF17D backbone	US (recalled)	(Seino *et al.*, 2007; American Veterinary Medical Association, 2010)
Equilis® West Nile (Merial)		EU	(Rebollo *et al.*, 2018a; Merial, 2020)
Recombitek™ equine WNV (Merial)	WNV prM-E in a canarypox backbone	US	(Minke *et al.*, 2004)
Proteq® WNV (Merial)		EU	(Minke *et al.*, 2004; Rebollo *et al.*, 2018a)

1.4.1. Inactivated vaccines

Three inactivated whole WNV vaccines have been approved for veterinary use. The first WNV vaccine was developed in 2001: WNV-Innovator® (Zoetis, 2020c) is a formalin-inactivated vaccine based on the highly virulent WNV NY99 strain. The same vaccine is licensed in Europe as Equip WNV® (Zoetis, 2020b) and as Duvaxyn® WNV for use in South Africa (Zoetis, 2020a). In a horse challenge model with severe WNV encephalitis, vaccination with WNV-Innovator® resulted in 100% survival illustrating the efficacy of this vaccine (Seino *et al.*, 2007).

The second licensed vaccine, Vetera® WNV (Boehringer Ingelheim, 2019), was developed in 2009. This vaccine is similar to WNV-Innovator® except that it is based on the WNV WN02 strain. WNV WN02 arose during 2002-2003 in America during the peak of WNV human infections, suggesting the displacement of NY99 as the most virulent WNV strain in America. In comparison to NY99, WN02 has a substitution in the E protein at residue 159 from a valine to alanine, a substitution found in many Old World strains (Davis *et al.*, 2005; Chisenhall & Mores, 2009). The third inactivated WNV vaccine licensed is a killed flavivirus chimaera that

consists of a yellow fever backbone with WNV prM and E genes commercialised as Prestige® WNV (Sterner *et al.*, 2012; Merck, 2019).

Although the listed inactivated vaccines are effective, the drawback of using inactivated vaccines is that a single dose only results in transient levels of induced antibodies that don't generate long-lasting immunity; therefore, these vaccines require a second dose in addition to an annual booster dose (Kaiser & Barrett, 2019). The requirement of additional booster doses significantly increases the cost of these vaccines. Other drawbacks of inactivated vaccines are the requirement of large-scale production of the infectious pathogen which requires specialised facilities and trained staff, and the risk of incomplete inactivation of the pathogen (Minke *et al.*, 2004; Chen & Lai, 2013). Additionally, inactivated vaccines run the risk of inducing antibodies that can result in ADE, which in turn can augment the entry of related flaviviruses into cells presenting the Fc γ receptor (Lai *et al.*, 2018).

1.4.2. Non-replicating single-cycle vaccines

Non-replicating single-cycle vaccines are under development, such as RepliVAX WN that is based on the expression of a WNV strain with a deleted C gene. Consequently, the viral infection cycle can be initiated producing prM-E containing VLPs in a special mammalian cell line expressing the WNV C protein in *trans* producing non-infectious progeny (Widman *et al.*, 2008). A single immunisation with RepliVAX WN in mice and hamsters, induced strong NAbs and protected all vaccinated animals against lethal WNV challenge (Widman *et al.*, 2008; Widman *et al.*, 2009). RepliVAX WN also elicited a protective immune response in rhesus macaques (Widman *et al.*, 2010).

Another replication-incompetent vaccine under development is that of the complex adenovirus (Ad)-based multiantigen WNV vaccine candidate. The vaccine consists of a WNV lineage 2 strain C, prM, E and NS1 proteins expressed by adenovirus vector: CAdVAX-WNII. Immunisation in mice induced WNV-specific humoral and cellular responses and showed broad neutralisation of both WNV lineage 1 and 2 strains (Schepp-Berglind *et al.*, 2007).

1.4.3. Recombinant vaccines

The disadvantages of inactivated vaccines have led to the development and in some cases commercialisation of recombinant WNV vaccines. Currently, there are two recombinant WNV vaccines licensed for veterinary use: these are Recombitek™ equine WNV/Proteq® WNV (Merial) and Equilis® West Nile (Merial). Several other candidate recombinant vaccines have

been investigated to meet the requirements of an effective and affordable WNV vaccine. The advantages of using recombinant vaccines include the limitation of risks associated with inactivated vaccines such as ADE, lower production costs, single-dose vaccinations, and the possibility of DIVA compliance.

1.4.3.1. Viral vector vaccines

Recombitek™ equine WNV/Proteq® WNV (Merial) (Minke *et al.*, 2004; Rebollo *et al.*, 2018a) is a viral vector vaccine licensed for use in the US and EU, respectively, and is based on the canarypox vector (ALVAC®) technology. These vectors undergo an abortive replication cycle during which the transgene is expressed, stimulating both the humoral and cell-mediated immune responses. The prM and E genes of the NY99 WNV lineage 1 strain were inserted into the canarypox vector backbone to generate this vaccine which has been shown to induce strong NAbs in horses (Seino *et al.*, 2007; El Garch *et al.*, 2008), and protected horses against a WNV lineage 2 strain challenge (Minke *et al.*, 2011). Interestingly, cats and dogs immunised with this vaccine induced NAbs that protected against WNV challenge. Illustrating the possibility of using this vaccine for the prevention of WNV infection in domestic animals such as cats and dogs (Karaca *et al.*, 2005).

1.4.3.2. Chimaeric live attenuated vaccines

Equilis® West Nile (Merial, 2020) is licensed for use in the EU and Prevenile (Intervet) (Seino *et al.*, 2007) was licensed in the US in 2006, but in 2010 the vaccine was recalled due to serious side effects observed in vaccinated horses (American Veterinary Medical Association, 2010; Brandler & Tangy, 2013). This chimaeric LAV was developed based on the ChimeriVax technology which makes use of yellow fever (YF) 17D vaccine capsid and non-structural genes for the delivery of other flaviviral structural prM and E genes, in this instance, WNV ChimeriVax-WN01 (Arroyo *et al.*, 2004). Only a single dose of vaccination was required to elicit strong NAbs in horses that protected against WNV challenge (Seino *et al.*, 2007). Additionally, the ChimeriVax-WN02 vaccine was developed from the ChimeriVax-WN01 vaccine with the addition of three mutations in the E gene (Arroyo *et al.*, 2004) and has been evaluated for safety and efficacy in phase I and phase II clinical trials in healthy adult humans. In phase I clinical trials, no differential adverse effects were observed between patients who received the vaccine versus the placebo, and high titres of NAbs were detected in vaccinated patients after only a single dose (Monath *et al.*, 2006). The safety, tolerability, viraemia and immunogenicity of ChimeriVax-WN02 was evaluated in a phase II clinical trial that included

elderly patients (≥40 years). As in the phase I trial high seroconversion was observed and antibody titres remained the highest at 12 months in patients aged ≥65 years. Reported adverse effects post-vaccination primarily included fatigue, headache and myalgia, suggesting the vaccine was well tolerated and safe (Biedenbender *et al.*, 2011). A second phase II clinical trial in healthy adults ≥50 years was conducted. Three different doses of the ChimeriVax-WN02 vaccine or placebo was administered to a total of 473 participants. Seroconversion was achieved on day 28 by an average of 93.6% of subjects; these results are consistent with the two previous clinical trials. In addition, strong and durable NAbs were elicited. As with the previous phase II clinical trial, the ChimeriVax-WN02 vaccine was found to be well tolerated with no increase in incidence of adverse effects compared between the vaccine and placebo recipients (Dayan *et al.*, 2012). However, the sporadic and unpredictable nature of WNV activity, along with the relative low incidence has made the demonstration of field efficacy difficult. Therefore, the epidemiology of WNV impedes a classical licensure pathway, which has made the continuation to a phase III clinical trial difficult (Dayan *et al.*, 2013).

Another chimaeric LAV candidate that has been developed using recombinant DNA technology is WN/DEN4Δ30. The vaccine is based on the DENV type 4 backbone with a 30-nucleotide deletion in its 3' non-coding region and the replacement of DENV4 prM and E proteins with that of WNV. Vaccination in mice induced high titres of NAbs and protection against lethal WNV challenge (Pletnev *et al.*, 2002). Upon evaluation in non-human primates, WN/DEN4Δ30 did not cause detectable viraemia even after WNV challenge and induced a moderate titre of NAbs (Pletnev *et al.*, 2003). Further evaluation of WN/DEN4Δ30, demonstrated that it was non-neuroinvasive in severe combined immunodeficient mice, indicating its high restrictiveness to access the CNS, and immunisation of non-human primates induced high levels of serum NAbs (Pletnev *et al.*, 2006). Two phase I clinical trials were performed first in healthy participants 19-50 years old followed by participants 60-65 years old. In the first trial, 75% of subjects seroconverted after a single dose vaccination, and 89% of subjects that received two doses 6 months apart seroconverted. The vaccine was considered well tolerated since no WNV-like or DENV-like illness was observed, and no adverse effects in comparison to the placebo group were observed (Durbin *et al.*, 2013). For the second phase I clinical trial healthy adults 50-65 years old were vaccinated with two doses WN/DEN4Δ30 6 months apart. Following the first dose, 90% of vaccinated subjects had seroconverted by day 90 and had high levels of NAbs. The authors concluded that a second dose may not be required to obtain proper immunisation in an older population (Pierce *et al.*, 2016).

1.4.3.3. DNA vaccines

Some progress has also been made on the development of WNV DNA vaccines. Davis and colleagues constructed a recombinant WNV plasmid, pCBWN, that expressed the WNV prM and E genes (Davis *et al.*, 2001). Transient transformation of COS-1 cells with pCBWN DNA resulted in the secretion of the prM and E proteins into the culture medium and the production of extracellular VLPs. NAbs were induced in both mice and horses vaccinated with the pCBWN DNA. In addition, vaccinated mice and horses were protected against WNV challenge. The vaccine was approved by the USDA for use in horses in 2006 but has not been commercially available. The pCBWN DNA vaccine was also evaluated in a phase I clinical trial in 15 healthy adult humans. No significant adverse effects were observed and the vaccine induced NAbs in subjects that completed a 3 dose vaccination schedule (Martin *et al.*, 2007). In another phase I clinical trial in healthy subjects of 2 age groups (15-50 years and 51-65 years), the pCBWN DNA vaccine with a modified cytomegalovirus promoter to include the 'R' region derived from human T-cell leukemia virus type 1, induced both T-cell and NAb responses in the majority of subjects (Ledgerwood *et al.*, 2011). These results illustrate the potential of a DNA vaccine for human use since they are safe and can induce both T-cell and antibody responses.

In addition to the development of a conventional DNA vaccine, some work has been carried out on the design of a chimaeric infectious DNA vaccine (iDNA) by inserting the virulent NY99 WNV strain prM and E genes into a highly attenuated fast-growing WNV strain (Borisevich *et al.*, 2006; Yamshchikov, 2015). Additionally, the glycosylation site on the E gene was mutated from a NYS→SYS which entirely eliminated the virulence of the virus isolate W1806. In comparison to the iDNA vaccine without the glycosylation site mutation, W1806 was found to have high immunogenicity in mice. Further attenuation of W1806 was investigated with the introduction of 10 mutations in the E gene, similar to those found in the JEV vaccine SA14-14-2. However, the introduction of the 10 substitutions in the E gene of W1806 resulted in the complete loss of infectivity in mammalian cells and low immunogenicity in mice. Thus, W1806 became over-attenuated and no single reversion could restore infectivity (Yamshchikov *et al.*, 2016). Following this observation, the authors investigated the influence of a subset of mutations on the attenuation level of W1806. They identified a subset of four mutations in the E gene: E138K, K279M, K439R and G447D. These fulfilled the safety requirements while maintaining the immunogenicity of the vaccine. However, genetic instability was observed to be an issue and the authors propose further investigation on the effects of these mutations (Yamshchikov *et al.*, 2017).

1.4.3.4. Subunit vaccines

Several WNV candidate subunit vaccines based on the E protein have been developed (Wang *et al.*, 2001; Ledizet *et al.*, 2005; Watts *et al.*, 2007). Lieberman and colleagues developed a recombinant candidate vaccine by truncating the C terminus of the E protein and produced the recombinant protein in a *Drosophila melanogaster* expression system. Upon challenge in rhesus monkeys, the recombinant protein protected all vaccinated monkeys (Lieberman *et al.*, 2009). In another study, a candidate vaccine was developed from amino acid residues 1-404 of the E ectodomain and immunogenicity evaluated in mice with the saponin-based adjuvant Matrix-M™. The authors observed an increased IgG1 and IgG2 response for the adjuvanted E protein in comparison to those without. Notably, the cellular and humoral immune responses were maintained for more than 200 days when adjuvanted with Matrix-M™ and protected mice against lethal challenge (Magnusson *et al.*, 2014).

Other studies have been focused on the EdIII protein of WNV as it encompasses the cellular receptor-binding motifs and the neutralising epitopes that induce a potent immune response with a low probability of ADE. WNV EdIII protein produced in bacteria (Martina *et al.*, 2008) and insect larvae (Alonso-Padilla *et al.*, 2011) protected mice against WNV NY99 challenge and elicited high NAb titers. Similarly, a plant produced EdIII induced potent NAbs in mice and protected them from a lethal challenge of WNV infection. Additionally, the authors illustrated the safety of EdIII as a subunit vaccine when no ADE was observed for ZIKV and DENV (He *et al.*, 2014; Lai *et al.*, 2018). The drawback of these vaccines are that multiple injections and/or strong adjuvants for the induction of NAbs are required (Martina *et al.*, 2008; Alonso-Padilla *et al.*, 2011; He *et al.*, 2014; Lai *et al.*, 2018). This could be ascribed to the possibility that these antigens do not display the immunogenic epitopes in their native conformation (Chen & Lai, 2013). Moreover, the WNV EdIII antigen is a small peptide that is susceptible to proteolytic degradation thus limiting the extent of the immune response stimulated (Thrane *et al.*, 2016).

1.4.3.5. Virus-like particles (VLPs)

VLPs are composed of single or multiple recombinant proteins, that spontaneously assemble into organized particulate structures that mimic native virions in shape and size. These structures are non-infectious and are therefore regarded as safe, and the absence of viral genomic material in VLPs makes them promising candidates as DIVA compliant vaccines (Liu *et al.*, 2013). The size of VLPs (20-200 nm) mediates optimal uptake by antigen-presenting cells and their dense repetitive surface structures enable complement fixation and B cell

receptor clustering (Chen & Lai, 2013; Thrane *et al.*, 2016). These characteristics are responsible for the activation of the innate immune system and antibody production, combining the best attributes of whole-virus and subunit vaccines (Chen & Lai, 2013; Thrane *et al.*, 2016). Due to these characteristics, several candidate WNV VLP-based vaccines have been developed in recent years.

The development of candidate vaccines based on VLPs has proven promising for several flaviviruses that include JEV, DENV, ZIKV and YFV (Krol *et al.*, 2019; Wong *et al.*, 2019; Garg *et al.*, 2020). Flavivirus VLPs form when the prM and E proteins are co-expressed in eukaryotic cells and assemble and bud. As seen with the viral vector vaccines, particles containing these proteins induce strong viral NAbs. In the instance of WNV, Takahashi and colleagues generated VLPs approximately 30 nm in size from the co-expression of the prM and E proteins in human 293T cells (Takahashi *et al.*, 2009). The immunogenicity of these particles was evaluated in mice and NAb titers for mice immunised with a lower dose of VLPs were substantial (1:320) compared to those immunised with inactivated WNV (1:1280). When the same construct, with the addition of a blasticidin S resistant gene, was expressed in Chinese hamster CHO-K1 cells, purified VLPs exhibited protection against WNV challenge in mice (Ohtaki *et al.*, 2010).

Another approach for the development of VLP-based vaccines is focused on the conjugation or linking of relevant antigens to VLPs. This display-based approach has become popular in recent years due to the ease of molecular and biotechnological techniques in the present decade. Several VLP cores have been identified for use including the hepatitis B core antigen (HBcAg) (Gregson *et al.*, 2008; Ding *et al.*, 2009; Chu *et al.*, 2016; Yang *et al.*, 2017) and the *Acinetobacter* bacteriophage AP205 coat (C) protein (Tissot *et al.*, 2010; Hu *et al.*, 2017). Upon expression, these proteins self-assemble into VLPs at high concentrations, usually regardless of the expression system used, making them ideal cores for the basis of display technology. Additionally, it has been proposed that these particles have adjuvanting effects since they are able to induce high antibody titres when used as an immunogen. In the instance of AP205, a high titre of antibodies were detected following immunisation in mice of the AP205 VLP on its own (Tissot *et al.*, 2010). A similar antibody response was observed when the authors immunised mice with AP205 VLPs that displayed the N-terminal ectodomain of *Influenza A* M2 protein. The mice were also protected following lethal influenza challenge. Besides influenza, the authors demonstrated similar results for other antigens with high antibody titres reached by day 14 following immunisation, illustrating the rapid antibody response elicited when immunising with AP205 particles. This is specifically promising in the instance of a pandemic, where a rapid and strong immune response needs to be mounted.

Chen and colleagues developed a candidate WNV VLP vaccine by fusing the immunodominant WNV EdIII gene to the 3' end of the HBcAg gene. Following expression in *Nicotiana benthamiana*, assembly of these chimaeric VLPs was confirmed at high expression levels and they induced potent EdIII specific B and T cell responses in mice (Chen *et al.*, 2011).

In contrast, Spohn *et al*. post-translationally linked purified WNV EdIII protein to AP205 VLPs. Upon immunization, the EdIII-AP205 conjugate vaccine induced virus NAbs and protected mice from WNV challenge (Spohn *et al.*, 2010). Another group linked the EdIII gene to the 5' end of the AP205 C gene to create an AP205-WNV-EdIII cassette in a bacterial expression vector. EdIII-display AP205 VLPs were observed by electron microscopy after expression in and purification from *Escherichia coli* and EdIII-specific NAbs were induced in mice. It is noteworthy that AP205-display derivatives can induce IgG2 antibodies as a result of the activation of the Th1 pathway. In this study, the authors showed the induction of IgG2a antibodies by the AP205-WNV-EdIII vaccine without adjuvants; however, when the EdIII protein was used as an immunogen on its own without adjuvants it was unable to switch antibody production from the IgM to the IgG isotype (Cielens *et al.*, 2014).

Recently, interest in the use of protein nanocages as VLP core substitutes has been investigated for antigen-display technology. An example of this is the mi3 nanocage which was computationally designed using the i301 nanocage which is based on the 2-keto-3-deoxy-phoshogluconate aldolase from the Enter-Doudoroff pathway from the hyperthermophilic bacterium *Thermotoga maritima* (Bruun *et al.*, 2018; Tan *et al.*, 2020).

1.5. SpyTag/SpyCatcher technology

Several antigen-display technologies have been developed and employed for various applications e.g. protein cyclisation, creation of multi-component architectures such as hydrogels (Reddington & Howarth, 2015), vaccine development (Liu *et al.*, 2014) and protein stabilization such as enzymes (Röder *et al.*, 2017). Of interest for this study is the split-intein conjugation system named SpyTag/SpyCatcher (ST/SC). This technology is based on the formation of spontaneous irreversible isopeptide bonds between complementary peptides, in this instance the ST and SC peptides. The ST and SC peptides originate from the Gram-positive bacterium *Streptococcus pyogenes*. The immunoglobulin-like collagen adhesion domain (CnaB2) of the fibronectin-binding protein (FbaB), of this bacterium inherently contains an isopeptide bond between the amine of Lys31 and carbonyl carbon of Asp117. The amine of Lys31 nucleophilically attacks the carbonyl carbon of Asp117, which is catalysed by the

neighbouring Glu77 for bond formation. Consequently, the CnaB2 domain was split into two peptides: a 13 amino acid ST peptide containing the Asp117 residue and its complimentary SC peptide of 116 amino acids containing the Lys31 residue (Figure 1.8). The coupling of ST and SC by the formation of an amide bond has been demonstrated to occur at a range of temperatures (4-37°C), pH values (5-8), buffers and in the presence of non-ionic detergents (Zakeri *et al.*, 2012).

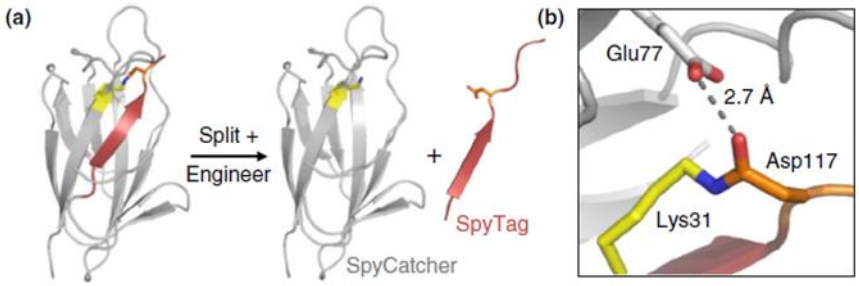

Figure 1.8. Generation of SpyTag/SpyCatcher. **(A)** Schematic of CnaB2 splitting into ST (red) and SC (grey). **(B)** The environment of the isopeptide bond between Asp117 (carbons orange) and Lys31 (carbons yellow), facilitated by Glu77 (carbons grey). Article open access. (Reddington & Howarth, 2015).

Thrane and colleagues used the ST/SC technology to develop a Spy-VLP platform. This was achieved by the genetic incorporation of the ST and SC peptides at the N-terminus of the C gene of the AP205 bacteriophage, yielding particles of approximately 36 nm and 43 nm, respectively, that display 180 peptide-binding motifs on the surface (Figure 1.9) (Thrane *et al.*, 2016). They evaluated the versatility of this platform by expressing 11 diverse vaccine candidate antigens genetically fused to either ST or SC in *E. coli*. These antigens included proteins from malaria, *Mycobacterium tuberculosis* and mouse proteins involved in cancer and cardiovascular disease. The authors successfully expressed and coupled the Spy-antigens to the Spy-AP205 VLPs *in vitro* and observed a mean display capacity of 65%. Immunogenicity of the coupled products were evaluated in mice; robust IgG responses were elicited and they observed a significant positive effect on the avidity of the humoral response against two malaria displayed proteins. They postulated that the higher observed avidity might be due to the ability of VLP-display to break B cell peripheral self-tolerance and activate anergic B cells. Overall, the ability of the Spy-VLP platform to display whole antigens enables the induction of polyclonal antibody responses that might mitigate the need for the addition of external adjuvants. This technology has since been used to develop candidate vaccines for *Plasmodium* for the improvement of antibody responses (Yenkoidiok-Douti *et al.*, 2019;

Harmsen *et al.*, 2020). These studies have illustrated the promise of this system for the development of VLP-based vaccines. This technology presents the possibility of ease of candidate vaccine production in the instance of disease outbreaks as well as the opportunity for the development of multivalent vaccines. Therefore, the Spy-VLP system could be most favourable for candidate vaccine production for flaviviruses such as WNV due to the potential of using EdIII as the display epitope.

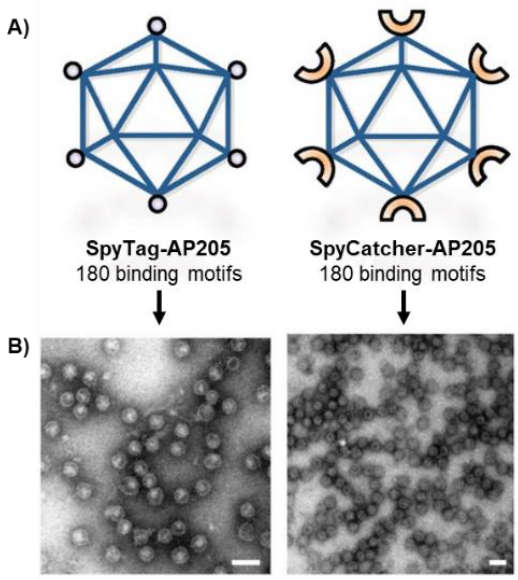

Figure 1.9. The Spy-VLP antigen display platform. **(A)** ST-AP205 VLP and SC-AP205 VLP schematic diagrams. **(B)** Electron micrographs of ST-AP205 and SC-AP205 VLPs. Scale bar = 50 nm. Article open access. (Thrane *et al.*, 2016).

1.6. Plant expression systems

Plant molecular farming (PMF) – the production of recombinant proteins in plants – is appealing due to the lower cost involved in biomass production and the infrastructure required in comparison to cell-based expression systems (Twyman *et al.*, 2003; Rybicki, 2009; Egelkrout *et al.*, 2012; Martinez *et al.*, 2012; Schillberg *et al.*, 2019; Fischer & Buyel, 2020). In the past two decades, plant expression systems have gained increased popularity for use as biofactories for the large-scale production of recombinant proteins. Plants allow for post-translational modifications similar to their mammalian counterparts such as proper folding and glycosylation, with the additional advantage of abolishing the risk of viral, prion and bacterial endotoxin contamination (Ma *et al.*, 2003; Moustafa *et al.*, 2016; Tschofen *et al.*, 2016; Margolin *et al.*, 2018). These unique qualities of PMF are particularly attractive for developing

countries where there is a high burden of preventable diseases and limited to no resources for pharmaceutical production (Hefferon, 2013; Rybicki *et al.*, 2013; Cardona-Ospina *et al.*, 2016; Tsekoa *et al.*, 2020).

There are various platforms used in PMF: whole plants, *in vitro* cultured plant cells and aquatic plants, each of which has its own strengths and weaknesses (Xu *et al.*, 2012; Moustafa *et al.*, 2016). Of focus in this study is whole plant expression systems and more specifically transient expression. Transient expression is based on the induction of foreign protein expression without the integration of the transgene into the host genome that is mediated by recombinant viral vector or *Agrobacterium* infiltration-based systems. The promise of this system is due to its speed, scalability and high protein yields (Rybicki, 2010; Xu *et al.*, 2012; Schillberg *et al.*, 2019; Fischer & Buyel, 2020).

Agroinfiltration occurs when the plant leaf intercellular spaces are flooded with *Agrobacterium* containing a recombinant plant binary vector either by syringe or vacuum infiltration (Sainsbury & Lomonossoff, 2014; Moustafa *et al.*, 2016). Following infiltration, the gene of interest within the transfer-DNA (T-DNA) is transferred into the plant cells for protein transcription and translation (Tzfira & Citovsky, 2006); this is initiated within 24 hours of infiltration and continues for several days (Xu *et al.*, 2012), with peak protein expression usually observed within 7 days (Loh *et al.*, 2017). Several plant binary vectors have been constructed for transient *Agrobacterium*-mediated protein expression in plants that include the pTRA vector series (Maclean *et al.*, 2007), the pEAQ-*HT* vector (Sainsbury *et al.*, 2009), the pRIC vector (Regnard *et al.*, 2010), the pCamGate vector series (Pereira *et al.*, 2014), the pHREAC vector (Peyret *et al.*, 2019), and many others (Nakamura *et al.*, 2010; Chen *et al.*, 2011; Murai, 2013; Nada, 2016; Pasin *et al.*, 2017).

Nicotiana species are well-established hosts for plant expression with the advantages of high biomass yield, prolific seed production, rapid scalability, and versatility in hosting a wide range of plant viruses for replication (Marsian & Lomonossoff, 2016). The predominant species used for transient expression is *N. benthamiana* – a wild relative of Australian tobacco. *N. benthamiana* is preferred due to its amenability to infiltration, more rapid growth rate and what appears to be a defective RNA silencing system (Lomonossoff & D'Aoust, 2016). These attributes together with the fact that tobacco is a non-food crop, have made tobacco the principal candidate for large-scale pharmaceutical production (Twyman *et al.*, 2003; Fischer *et al.*, 2004).

Several types of recombinant proteins have been successfully produced in *Nicotiana* that include vaccine antigens, antibodies, therapeutic enzymes, industrial enzymes and biopolymers (Xu *et al.*, 2012; Tschofen *et al.*, 2016; Loh *et al.*, 2017). An example of successful

protein expression as a candidate vaccine antigen is that of porcine circovirus type 2 (PCV-2), a single protein VLP. The C protein of PCV-2 was transiently expressed in *N. benthamiana* and VLPs purified by density centrifugation. The authors also demonstrated that PCV-2 VLPs elicited strong PCV-2 specific serum immune responses in mice (Gunter *et al.*, 2019). Maclean and colleagues produced human papillomavirus type 16 (HPV-16) VLPs in *N. tabacum* by transiently expressing the L1 protein (Maclean *et al.*, 2007). The plant-produced HPV-16 VLPs induced both HPV-16 VLP-specific antibodies and NAbs in mice.

Other studies have illustrated the success of producing VLPs made up of different proteins in the plant expression system. Van Zyl *et al*. transiently co-expressed the VP2, VP3, VP5 and VP7 of bluetongue virus serotype 8 (BTV-8) in *N. benthamiana* to form VLPs (van Zyl *et al.*, 2016). Similarly, the transient co-expression of VP2, VP3, VP5 and VP7 of African horse sickness virus serotype 5 (AHSV-5) in *N. benthamiana* resulted in the assembly of VLPs. NAbs were induced in both guinea pigs (Dennis *et al.*, 2018a) and horses (Dennis *et al.*, 2018b) administered with the purified AHSV-5 VLPs. These examples of VLPs produced in tobacco from the expression of single or multiple proteins illustrate the potential of PMF for the production of pharmaceuticals for LMIC.

As with mammalian, insect and bacterial-based expression systems, plant expression systems also have limitations. These limitations include potential low protein yield, possibly due to poor protein stability and downstream processing difficulties that result in inconsistent quality (Fischer *et al.*, 2004). Several advances have been made towards addressing protein yield. There are two main factors that influence protein accumulation namely the rate of synthesis and degradation. The rate of transcription and translation affects protein synthesis and can be addressed with the use of strong plant promotors such as the constitutive Cauliflower mosaic virus 35s (CaMV35S) promoter for dicotyledonous species (Egelkrout *et al.*, 2012). The vulnerability of a protein to breakdown determines the rate of degradation, which is influenced by the location of the protein. Selection of the appropriate cellular compartment for protein expression will therefore directly affect protein yield (Egelkrout *et al.*, 2012). To address this, proteins can be targeted to specific cellular compartments such as the cytosol, apoplast, chloroplast and ER using specific peptide tags to determine the appropriate location for optimal protein expression and processing (Maclean *et al.*, 2007; Pereira *et al.*, 2014; Tschofen *et al.*, 2016; Marques *et al.*, 2019). Protein yield is also affected by the plant host defences – for example small interfering RNAs (siRNAs). siRNAs play a role in the degradation of viral messenger RNAs, known as RNA silencing. This can be overcome with the co-expression of a plant binary vector that encodes for an RNA silencing suppressor protein (Takeda *et al.*, 2002; Sainsbury *et al.*, 2009). Another approach to increase protein yield is the optimisation of codon usage of the gene of interest to that of the expression host.

Different species have different codon preferences that in turn correlate to their available tRNAs (Egelkrout *et al.*, 2012). Codon optimisation can therefore circumvent the rapid saturation of preferred tRNAs during translation.

Techno-economic modelling of plant-based expression has also been investigated to determine the requirements, constraints and cost drivers for the production of a target product. With regard to emerging biomanufacturing industries, this is particularly important to provide the tools to help companies assess the economic feasibility of their proposed processes (Nandi *et al.*, 2016; Alam *et al.*, 2018; McNulty *et al.*, 2019; Mir-Artigues *et al.*, 2019). Nandi and colleagues developed an online model called The Base Case SuperPro Designer® to assist companies in their techno-economic analyses of new products. This model considers the total capital investment (CAPEX, US dollars, USD), total annual operating costs (OPEX, USD/year) and the unit production costs in cost of goods sold (COGS, USD/g product). These parameters are influenced by the product expression level (g product/kg FLW) and the facility production capacity (kg product/year) (Nandi *et al.*, 2016). This model has been used to evaluate the techno-economic modelling of plant-produced Griffithsin for use as HIV microbicides (Alam *et al.*, 2018) and antimicrobial proteins as biotic sanitisers for food safety (McNulty *et al.*, 2019). These studies provide evidence of the lower manufacturing cost of specific products in plants in comparison to their production in mammalian cell systems. Based on these advances in PMF it is hoped that plants will pave the way toward the development of human and veterinary pharmaceuticals that are safe, effective and affordable for developing countries.

1.7. Concluding remarks

The global distribution of WNV, its association with severe neurological disease in its avian reservoir hosts and dead-end mammalian hosts, lack of antiviral treatment and in the case of humans a licensed vaccine, demands for the development of an affordable and effective vaccine. The fact that there is little to no infrastructure for the development of these therapeutics in developing countries, the high costs associated with the importation of these products and the difficulty associated with the regulatory procedures for the procurement of permits, further necessitates the local development of these products. It is consequently highly desirable to develop a WNV candidate vaccine that is DIVA compliant. The development and production of such a vaccine using *N. benthamiana* as a platform for local production would be most appropriate for working towards the ‘One Health’ Initiative – one vaccine for both humans and horses.

1.8. Project aims

The overall aim of this project was to develop VLP-based candidate vaccines for WNV by *Agrobacterium*-mediated transient expression in *N. benthamiana.* Specifically, this project was focused on developing two candidate WNV vaccine types based on a virulent South African strain. One approach was to develop a 'native' VLP vaccine candidate using the virus prM and E proteins, and the second was to develop an antigen-display based VLP vaccine candidate using the EdIII protein and the ST/SC platform.

The specific objectives to achieve the aims were to:

- Clone and optimise protein expression of prM and E genes (from a South African WNV strain) in *N. benthamiana*.
- Purify proteins and putative VLPs and characterise VLP formation.
- Clone and express Spy-EdIII and Spy-AP205 coat protein in *N. benthamiana.*
- Characterise Spy-AP205 particles and couple them to EdIII to make EdIII-display VLPs.

Chapter 2:

Design and transient expression of WNV *prM* and *E* genes in *Nicotiana benthamiana*

2.1. Introduction

WNV is responsible for causing disease in birds, humans and horses worldwide, that range from febrile illness to severe neurological disease (Castro-Jorge *et al.*, 2019). The spread of disease can be prevented by vaccination against WNV; however, current vaccines are only licensed for use in horses (Rebollo *et al.*, 2018a; Castro-Jorge *et al.*, 2019). With WNV endemic in most of sub-Saharan Africa (Sule *et al.*, 2018), there is a need for the local production of an inexpensive and efficient WNV vaccine.

Expression of the prM and E proteins of WNV in mammalian cells successfully form VLPs (Takahashi *et al.*, 2009; Ohtaki *et al.*, 2010). However, the cost associated with the production of VLPs in this system is significantly higher than other systems (Chen & Lai, 2013). In recent years, researchers have begun focussing on the transient production of recombinant proteins and their assembly into VLPs in plants due to the affordability, scalability and safety of this expression platform (Rybicki, 2009; Schillberg *et al.*, 2019; Fischer & Buyel, 2020). Additionally, plants allow for post-translational modifications such as proper folding and glycosylation of proteins (Ma *et al.*, 2003) which is necessary for the proper assembly of VLPs. There are currently numerous published examples of transiently produced VLPs in plants targeting a variety of viral diseases, suggesting that the generation of WNV VLPs in plants by co-expression of the prM and E glycoproteins may be a possibility (examples in section 1.6).

Transient production is mainly carried out by *Agrobacterium*-mediated gene transfer and there are several binary plant expression vectors available which have been developed for transient expression such as pEAQ-*HT*, a Cowpea mosaic virus (CPMV)-based hypertranslatable expression vector (Sainsbury *et al.*, 2009), and the pTRA vector series that have signal peptides for localisation to different subcellular compartments (Maclean *et al.*, 2007).

The plant secretory pathway plays an important role in protein folding and glycosylation and subsequent VLP assembly; it is therefore critical to target recombinant glycoproteins to their appropriate subcellular compartments (Margolin *et al.*, 2018). This can be achieved by using the appropriate signal peptides for translocation such as the virus's native gene signal peptides or heterologous signal peptides such as LPH – a plant-codon optimised murine

mAB24 heavy chain signal sequence that targets proteins to the ER (Vaquero *et al.*, 1999) or rbsc1-cTP – a chloroplast-transit peptide sequence of the potato Rubisco small subunit gene (Maclean *et al.*, 2007). Interestingly for WNV, Takahashi *et al*. observed that the number of amino acids around the NS2B-3 cleavage site (Figure 1.2B) that is located 5' to the native signal peptide of prM, was important for the efficient processing and assembly of the E protein when expressed in mammalian cells (Takahashi *et al.*, 2009), thereby proving the critical role signal peptides play in protein expression.

In the ER folding pathway, misfolded glycoproteins will either cycle through the pathway until correct folding is achieved or they will be degraded. It is speculated that the poor expression levels associated with viral glycoproteins in plants are due to the incompatibility of these proteins with the endogenous plant chaperone machinery involved in protein folding within this pathway (Margolin *et al.*, 2018). Recently Margolin and colleagues provided evidence of the difference in sequence homology between plant and human chaperone proteins (Margolin *et al.*, 2020). They found that the co-expression of the human chaperone proteins, calnexin (CNX) and calreticulin (CRT) improved expression of several different glycoproteins in *N. benthamiana* with HIV gp140 expression increasing by 13-fold when co-expressed with human CRT. In addition, they demonstrated the reduction in ER stress upon co-expression with human CRT presented as a reduction in levels of misfolded protein. In summary, the co-expression of these human homologues of plant chaperones have shown to assist in correct viral glycoprotein folding and thus increased protein yield as well as the reduction in ER stress *in planta*.

Another process that takes place in plants that can negatively affect protein yield is post-transcriptional gene silencing (PTGS), which leads to the degradation of mRNA transcripts thereby reducing the expression of heterologous genes. PTGS can be overcome by the co-expression of silencing suppressors such as p19 of tomato bushy stunt virus (TBSV) or NSs from tomato spotted wilt virus (TSWV) (Takeda *et al.*, 2002). These are often included in transient expression vectors themselves such as that of pEAQ-*HT* (p19) (Sainsbury *et al.*, 2009) or constructs encoding them are co-expressed with vectors encoding the genes of interest. Expression of these silencing suppressor proteins can prolong and amplify transient expression of foreign proteins in *N. benthamiana* (Maclean *et al.*, 2007; van Zyl *et al.*, 2016).

This chapter describes the cloning and expression of the membrane (*prM*) and envelope (*E*) genes of a virulent South African WNV strain in *N. benthamiana.* Two strategies were employed to achieve this: i) the cloning and expression of the prM-E polyprotein since plant cells are known to undergo similar protease activities which are required for the cleavage of prM-E to M and E, and ii) the individual cloning of the *prM* and *E* genes and their co-expression. Since prM and E are glycoproteins they need to be targeted to the ER for post-

translational processing, thus the WNV native signal sequence with or without eight amino acid residues of the *C* gene (Takahashi *et al.*, 2009) and the well-established LPH signal peptide were evaluated.

Two versions of the E protein, with and without a 6x histidine tag, were expressed with and without the human chaperone proteins, CNX and CRT, and the NSs silencing suppressor protein to determine the optimal expression conditions for maximisation of protein yield. Four permutations of the prM protein regarding its signal peptide were established in the pEAQ-*HT*, pTRAc and pTRAkc-ERH plant expression vectors, and co-expression of each with the envelope protein was evaluated.

2.2. Materials and Methods

2.2.1. Selection of a South African WNV strain for gene synthesis

Three South African WNV strains associated with WND were compared at the amino acid level using BioEdit (Hall, 1999) for the *prM* and *E* genes. WNV strain SPU116/89 (GenBank accession EF429197) was isolated from a patient with fatal hepatitis, strain SA93/01 (GenBank accession EF429198) was isolated from a patient with non-fatal encephalitis and the third strain HS101/08 (GenBank accession JN393308) was isolated from a horse with fatal neurological disease. Due to the high level of amino acid identity between the three strains (Appendix A: Figure 1), SPU116/89 *prM* and *E* gene sequences were selected for gene synthesis.

A construct encoding the *prM-E* polyprotein gene codon optimised for *N. benthamiana* was synthesised by GenScript (GenScript Biotechnologies, Piscataway, NJ, US) (Figure 2.1A). However, since Takahashi *et al.* (2009) implied that the region upstream of the *prM* gene may influence its expression, a second construct codon optimised for *N. benthamiana* encoding the *prM* gene was subsequently synthesised by GenScript which included its native signal sequence (SS) and 8 amino acids of the C protein (C_8) situated upstream of the native SS (Figure 2.1B).

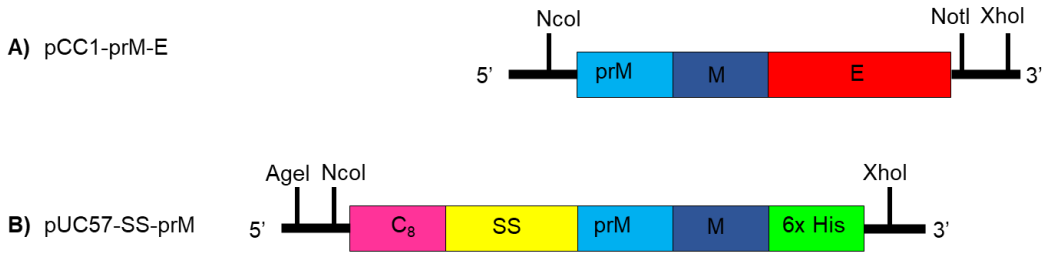

Figure 2.1. Schematic representation of synthesised WNV genes. **(A)** The polyprotein *prM-E* was synthesised with 5' *Nco*I and 3' *Not*I and *Xho*I restriction enzyme sites for cloning into plant expression vectors. The gene was constructed in the pCC1 vector. **(B)** The C_8-SS-prM fragment included a C terminal 6x histidine tag. The 5' terminus included *Age*I and *Nco*I and the 3' terminus the *Xho*I restriction enzyme sites for subsequent cloning into plant expression vectors.

2.2.2. PCR amplification of WNV *prM* and *E* genes

Modification of the *E* gene by PCR amplification of pCC1-prM-E to add appropriate restriction enzyme (RE) sites on the 5' and 3' termini to facilitate: i) directional cloning into the plant

expression vector, pTRAkc-ERH (Figure 2.2C) and ii) to generate a 6x histidine (His) tagged version of *E* was performed to allow for co-expression with *prM*. The influence of the His tag on particle formation was unknown, therefore expression was evaluated with and without the tag. In addition, during the preparation of the constructs, E-specific antiserum was not available and the presence of a His tag would allow for protein detection by anti-His antiserum.

Similarly, the *prM* gene was further modified by PCR amplification of pUC57-SS-prM to add appropriate RE sites on the 5' and 3' termini to facilitate: i) directional cloning into 3 different plant expression vectors (pEAQ-*HT*, pTRAc and pTRAkc-ERH) (Figure 2.2) and ii) the removal of the native SS or just the C_8 5' to the SS. The influence of the ER-targeting signal peptide used (LPH vs WNV native SS), and the effect of the number of amino acids 5' to the NS2B-3 cleavage site of WNV native SS was evaluated.

PCR amplification reactions consisted of 10 ng template DNA, 0.16 mM dNTPs (Kapa Biosystems), 0.2 µM forward and reverse primer each (Table 2.1, Appendix B: Table 2), 10x Ampliqon Ammonium Buffer, 2.5 U AccuPOL DNA polymerase (AMPLIQON) and dH_2O to a total volume of 50 µL. The PCR cycling conditions were carried out as per manufacturer's instructions with specific annealing temperatures for each primer pair described in Table 2.1.

Table 2.1. Primers used to generate prM- and E encoding-DNA fragments.

Gene	Primers	Ta (°C)	Size (kb)	Signal peptide	Construct
E	E-NcoI-F32 E-XhoI-R	60	~1.5	LPH	pJet-E
E	LPH-AgeI-F E-HIS-XhoI-R	58	~1.6	LPH	pJet-E-HIS
C_8-SS-prM	LPH-AgeI-F XhoI-prM-R	61	~0.6	LPH	pJet-prM
C_8-SS-prM	AgeI-NcoI-prM-F XhoI-prM-R	64	~0.6	C_8 + native SS	pJet-C_8-SS-prM
C_8-SS-prM	Age-NcoI-SS-F XhoI-prM-R	60	~0.6	Native SS	pJet-SS-prM

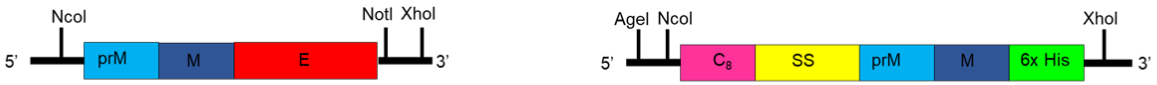

PCR modification of *prM* and *E* genes

Cloning into pJET1.2/blunt vector

Excision of *prM* and *E* genes from pJET1.2/blunt constructs for directional cloning into pEAQ-*HT* and/or pTRA vector

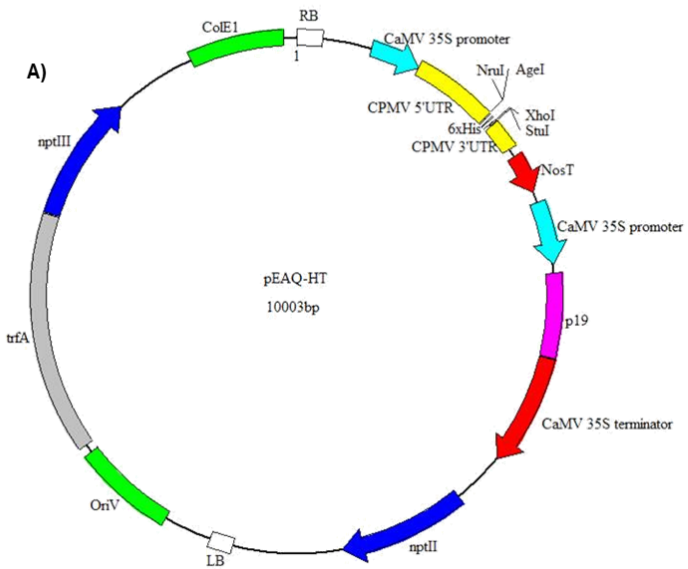

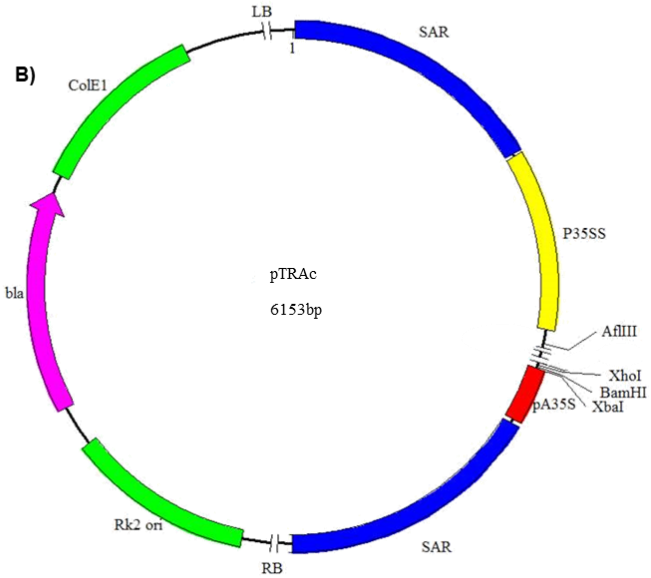

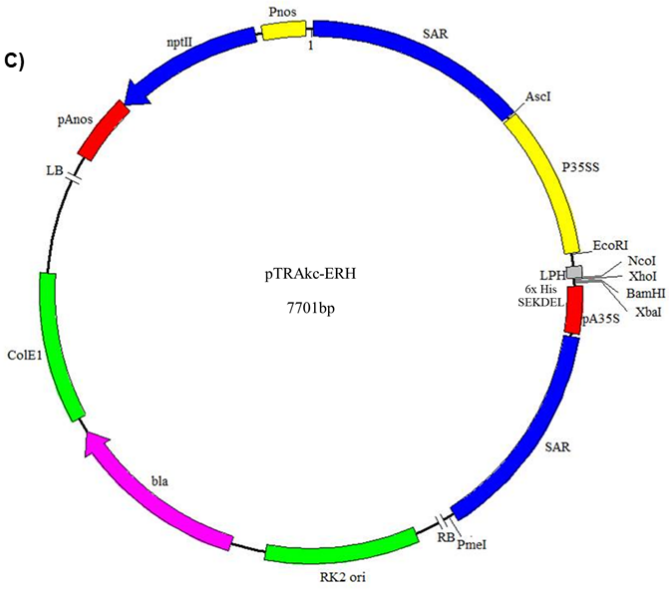

Figure 2.2. *From the previous page.* Flow diagram depicting the cloning strategy employed for WNV *prM* and *E* genes. Following gene modification by PCR amplification, the amplified products were cloned into the pJET1.2/blunt vector and subsequently excised and cloned into the plant expression vectors: (A) pEAQ-*HT*, (B) pTRAc, and (C) pTRAkc-ERH. The vector elements are illustrated in the figure. **(A)** pEAQ-*HT* is a CPMV-based hypertranslatable expression vector: RB and LB; right and left borders for T-DNA integration, CaMV 35S promoter, 5' UTR; modified 5' UTR from CPMV RNA-2, 3' UTR from CPMV RNA-2, NosT; nopaline synthase terminator, p19; TBSV silencing suppressor gene, 35S terminator from CaMV, *npt*II; kanamycin resistance gene, OriV; pRK2 origin of replication for *Agrobacterium*, TrfA; replication locus, and ColEI; the pBR322 *E. coli* origin of replication (Sainsbury *et al.*, 2009). **(B-C)** pTRAc is a cytoplasmic expression vector and pTRAkc-ERH is an ER targeting vector: RB and LB; right and left borders for T-DNA integration, P35SS; CaMV 35S promoter with a duplicated transcriptional enhancer, CHS; chalcone synthase 59 UTR, pA35S; CaMV 35S polyadenylation signal, SAR; scaffold attachment region of the tobacco Rb7 gene, ColEI; origin of replication for *E. coli*, RK2ori; origin of replication for *Agrobacterium*, *bla*; gene for ampicillin/carbenicillin resistance, (C) contains a signal peptide sequence from the murine mAB24 heavy chain gene (LPH), SEKDEL; ER-retention signal sequence, *npt*II; kanamycin resistance gene, and pNos/pAnos; promoter and polyadenylation signal of the nopaline synthase gene (Maclean *et al.*, 2007).

2.2.3. Cloning of amplified *prM* and *E* fragments into the interim vector pJET1.2/blunt

Amplified fragments were purified from agarose gels using the QIAquick® Gel Extraction kit (Qiagen) following the manufacturer's instructions. The purified DNA was ligated into the pJET1.2/blunt vector (Thermo Scientific) according to the manufacturer's instructions and incubated overnight (O/N) at 4 °C.

The ligated constructs were transformed into chemically competent DH5α *E. coli* cells (E. cloni™, Lucigen) as follows: 2.5 µL ligation reaction was added to 15 µL cells, incubated on ice for 30 min then heat-shocked at 42°C for 40 s. Following heat-shock, the cells were cooled on ice for 2 min and 800 µL of Luria Bertani (LB) broth was added to the transformation reaction and incubated at 37°C with agitation for 1 h. The transformed cells were selected on LB agar supplemented with 100 µg/mL ampicillin and incubated at 37°C O/N.

Colonies were screened for recombination by colony PCR using Taq 2x Master Mix (AMPLIQON) as per manufacturer's instructions, using specific annealing temperatures in Table 2.1.

Positive recombinant colonies were inoculated into 10 mL LB broth supplemented with 100 µg/mL ampicillin and were incubated with agitation at 37°C O/N. Plasmids were isolated using the QIAprep® Spin Miniprep kit (Qiagen) as per manufacturer's instructions and stored at -20°C for further use.

2.2.4. Sub-cloning of *prM* and *E* genes into plant expression vectors

The prM-E polyprotein and prM and E-encoding DNA fragments were subcloned into either pEAQ-*HT*, pTRAc or pTRAkc-ERH (Figure 2.2, Table 2.2). A total of six constructs (Figure 2.3) were generated.

Table 2.2. Restriction enzymes and pJET1.2/blunt templates used for the subcloning of the prM and E DNA fragments into pEAQ-*HT*, pTRAc and pTRAkc-ERH.

Template	Destination vector	5' Enzyme site	3' Enzyme site	Signal peptide	Construct
pCC1-prM-E	pTRAkc-ERH	*Nco*I	*Xho*I	LPH	-
pJet-E	pTRAkc-ERH	*Nco*I	*Xho*I	LPH	pTRAkc-E
pJet-E-HIS	pTRAkc-ERH	*Nco*I	*Xho*I	LPH	pTRAkc-E-HIS
pJet-prM	pTRAkc-ERH	*Nco*I	*Xho*I	LPH	pTRAkc-prM
pJet-C_8-SS-prM	pEAQ-*HT*	*Age*I	*Xho*I	C_8 + native SS	pEAQ- C_8-SS-prM
pJet-C_8-SS-prM	pTRAc	*Nco*I/*Afl*III	*Xho*I	C_8 + native SS	pTRAc- C_8-SS-prM
pJet-SS-prM	pTRAc	*Nco*I/*Afl*III	*Xho*I	Native SS	pTRAc-SS-prM

The prM-E polyprotein fragment was excised from the pCC1 backbone and the modified prM and E fragments were excised from the pJET1.2/blunt backbone by using the appropriate 5' and 3'-flanking RE sites to facilitate cloning into each respective plant expression vector (Table 2.2). Double digestions were performed for pCC1 and all pJET1.2/blunt constructs with *Nco*I and *Xho*I except for subcloning into pEAQ-*HT*, where *Age*I and *Xho*I were used. All digestions were performed using RE from Fermentas (Thermo Scientific) as per manufacturer's instructions. Digested products were excised and gel purified using the QIAquick® Gel Extraction kit (Qiagen) following the manufacturer's instructions.

The pEAQ-*HT* vector was linearised with *Age*I and *Xho*I (Figure 2.2A), the pTRAc vector was linearised with *Afl*III and *Xho*I (Figure 2.2B) and the pTRAkc-ERH vector was linearised with *Nco*I and *Xho*I (Figure 2.2C). Linearised vector DNA was purified as described above.

Purified prM-E, prM and E DNA fragments were sub-cloned into linearised vectors to yield the constructs listed in Figure 2.3. Ligation reactions were transformed as described in section 2.2.3 and transformed cells were selected on LB agar supplemented with either 100 µg/mL ampicillin (pTRA vectors) or 30 µg/mL kanamycin (pEAQ-*HT*) incubated at 37°C O/N. Colonies were screened for recombination by colony PCR using vector-specific primers (Appendix B: Table 1) and recombinant plasmids isolated as described in section 2.2.3.

All constructs were verified by sequencing.

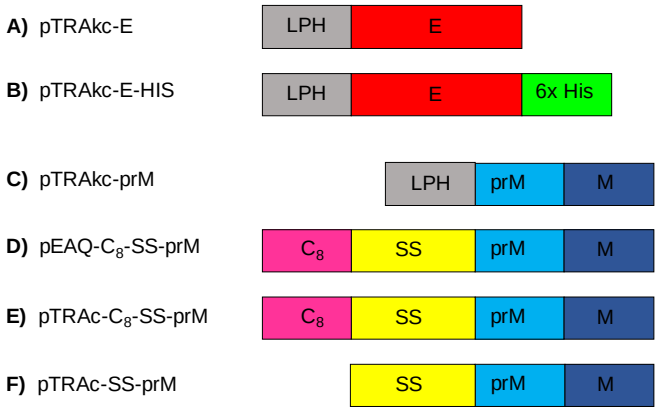

Figure 2.3. Schematic representation of WNV *prM* and *E* gene constructs in plant expression vectors. **(A)** pTRAkc-E: *E* gene with ER-targeting LPH signal peptide. **(B)** pTRAkc-E-HIS: the same construct as pTRAkc-E with the addition of a C terminal 6x His tag. **(C)** pTRAkc-prM: *prM* gene with ER-targeting LPH signal peptide. **(D)** pEAQ-C_8-SS-prM: *prM* gene including eight amino acids of the *C* gene and WNV native signal peptide. **(E)** pTRAc-C_8-SS-prM: the same construct as pEAQ-C_8-SS-prM but in the pTRAc vector. **(F)** pTRAc-SS-prM: *prM* gene with WNV native signal peptide.

2.2.5. Transformation of Agrobacterium tumefaciens

A. tumefaciens LBA4404 and *A. tumefaciens* GV3101::pMP90RK cells were made electrocompetent using the method described by Shen and Forde (1989). Two-hundred to 400 ng recombinant pEAQ-*HT* and pTRA plasmids were electroporated into *A. tumefaciens* LBA4404 and *A. tumefaciens* GV3101::pMP90RK cells, respectively, as described by Maclean *et al*. 2007.

Recombinant cells were selected on LB agar containing 30 µg/mL kanamycin and 50 µg/mL rifampicin for pEAQ-*HT* constructs with the addition of 50 µg/mL carbenicillin for pTRA constructs and incubated at 27°C for 2-3 days. Colonies were screened for recombination by colony PCR using vector-specific primers (Appendix B: Table 1) as described in section 2.2.3.

2.2.6. *Agrobacterium tumefaciens*-mediated transient expression

Ten milliliter cultures of recombinant *A. tumefaciens* of pEAQ-*HT*, pTRA, pBIN-NSs and pEAQ-CNX or pEAQ-CRT (kindly provided by Dr Emmanuel Margolin (IDM, UCT)) were supplemented with the relevant antibiotics (Appendix C: Table 4) and grown O/N at 27°C. The cultures were scaled up to 500 mL in LB base (LBB) medium [2.5 g/L tryptone, 12.5 g/L yeast extract, 5 g/L NaCl, 10 mM 2-N-morpholinoethanesulfonic acid (MES) (pH 5.6)], with 20 µM acetosyringone supplemented during the final culture step. After cultivation, the cells were

diluted to the required optical density (OD_{600}) (Appendix D: Table 5) in infiltration medium [10 mM $MgCl_2$, 10 mM MES (pH 5.6)].

Two six-week-old *N. benthamiana* plants were submerged, upside-down, in a beaker of the bacterial culture for each co-infiltration (Appendix D: Table 5) and placed inside a vacuum chamber. A vacuum of ~100 kPa was applied to the chamber for infiltration of the leaves. As a negative control, pTRAkc-ERH vector lacking any gene cloned into the multiple cloning site (empty vector) was infiltrated at an OD_{600} of 0.25. The agroinfiltrated plants were returned to the plant growth room (temperature = 22°C, light:dark photoperiod = 16:8 h, relative humidity = 55%) until harvest.

2.2.7. Small scale protein extraction

2.2.7.1. Co-expression of E and human chaperones

Two grams of plant material was homogenised in 2 volumes 100 mM Tris.HCl (pH 7.4) using an IKA® T-25 ULTRA-TURRAX® (Sigma-Aldrich) homogeniser. The plant homogenate was incubated at 4°C for 30 min with gentle shaking and clarified by centrifugation at 15 000 *x* g for 10 min. The pellet and supernatant were separated and the pellet resuspended in the same volume of buffer used for extraction. Both pellet and supernatant solutions were incubated at room temperature (RT) with gentle shaking O/N. Following maturation, pellet and supernatant crude extracts were evaluated for protein expression.

2.2.7.2. Co-expression of prM and E

Two grams of plant material was homogenised in 2 volumes 1x phosphate buffer saline (PBS) (pH 6.0) using an IKA® T-25 ULTRA-TURRAX® (Sigma-Aldrich) homogeniser. The plant homogenate was incubated at 4°C for 30 min with gentle shaking and clarified by centrifugation at 15 000 *x* g for 20 min. The pellet and supernatant were separated and the pellet resuspended in the same volume and buffer used for extraction. Both pellet and supernatant extracts were incubated at RT with gentle shaking O/N. Following maturation, pellet and supernatant crude extracts were evaluated for protein expression

2.2.8. Protein analysis

The amount of total soluble protein (TSP) was calculated for both pellet and supernatant extracts using the *DC* Protein Assay (BioRad) according to manufacturer's instructions.

For western blot analysis, the pellet and supernatant crude extracts were diluted in extraction buffer to equal amounts of TSP and denatured at 95°C for 10 min in 5x sample application buffer (SAB) [940 µL 10% sodium dodecyl sulfate (SDS), 470 µL 1 M Tris.HCl (pH7.5), 95 µL 100 mM Ethylenediaminetetraacetic acid (EDTA), 205 µL β-mercaptoethanol, 2.45 mL 100% glycerol, 0.2 mg bromophenol blue, 545 µL dH_2O]. Equal amounts of TSP of the pellet and supernatant were loaded in each well and separated on either 10% or 15% SDS polyacrylamide gels (PAGE). After electrophoresis, the proteins were transferred by semi-dry blotting onto nitrocellulose membranes at 15 volts (V) for 1 h 30 min using a Trans-blot®SD semi-dry transfer cell (BioRad). Following the transfer, the membranes were blocked in blocking buffer [1x PBS (pH 7.4), 0.1% Tween-20, 5% fat-free milk]. After blocking, the membranes were probed with the appropriate antiserum diluted in blocking buffer (Appendix E: Table 6) either at 4°C O/N or 37°C for 1 h with agitation. The membranes were washed three times with blocking buffer for 10 min and subsequently incubated with 1:10 000 dilution of alkaline phosphatase-conjugated polyclonal goat anti-rabbit antibody (Biocom Africa) for 1 h at 37°C or O/N at 4°C with agitation. The membranes were then washed three times in 1x PBST [1x PBS, 0.1% Tween-20 (pH 7.4)]. Detection was performed using 5-bromo-4-chloro-3-inodyl phosphate (BCIP) and nitroblue tetrazolium (NTB) phosphatase substrate (BCIP/NBT 1-component, KPL).

Protein expression, extraction and western blot analysis was repeated at least three times to confirm the expression of WNV glycoproteins.

2.3. Results

2.3.1. Verification of pJET1.2/blunt clones

Amplified prM and E DNA fragments were subcloned into pJET1.2/blunt to generate stable constructs for downstream processing. Cloning into pJET1.2/blunt also acted as a control for RE digestion, since RE digestion from amplified products yield indistinguishable products between digested and undigested fragments.

The WNV *prM* and *E* genes were successfully amplified with the primers listed in Table 2.1 and cloned into the pJET1.2/blunt vector. Clones were verified by PCR amplification of the genes with the different primer sets listed in Table 2.1 to yield the following fragments: E; ~1.5 kb, E-HIS; ~1.6 kb, prM; ~0.6 kb, C_8-SS-prM, ~0.6 kb, and SS-prM; ~0.6 kb (Figure 2.4).

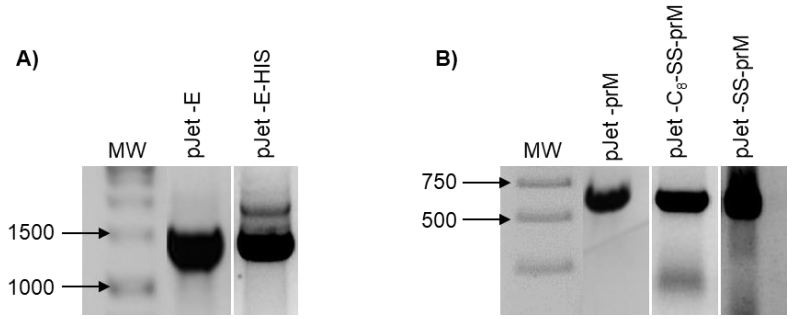

Figure 2.4. PCR amplification of *prM* and *E* genes from pJET1.2/blunt clones visualised on agarose gels stained with ethidium bromide. **(A)** pJET1.2/blunt clones containing the *E* gene permutations. **(B)** pJET1.2/blunt clones containing the *prM* gene permutations. Label: MW, the molecular weight marker.

2.3.2. Sub-cloning of *prM* and *E* genes into plant expression vectors

The plant expression vectors selected as destination plasmids included pTRAkc-ERH, pTRAc and pEAQ-*HT*. Since the prM and E proteins are glycoproteins they need to be targeted to the ER for post-translational processing. Therefore, the pTRAkc-ERH vector that contains the ER-targeting LPH signal peptide was used for the cloning of the *prM-E*, *E* (Figure 2.2A-B) and *prM* (Figure 2.2C) genes. pTRAc and pEAQ-*HT* are cytoplasmic vectors that contain no signal peptides and for this reason they were selected for the cloning of the *prM* gene with its native SS with (Figure 2.2D-E) or without (Figure 2.2F) the C_8. Several attempts at cloning the

prM-E polyprotein gene into pTRAkc-ERH proved unsuccessful and therefore this approach towards protein expression was discontinued.

The *prM* and *E* gene permutations were excised from the pJET1.2/blunt backbone using construct-specific REs listed in Table 2.2 and subsequently ligated into either pEAQ-*HT* or pTRA plant expression vectors. Ligated DNA was transformed into *E. coli* and recombinant cells were evaluated by colony PCR using vector-specific primers (Appendix B: Table 1). Amplified bands of the expected size were observed for each construct: E; ~1.7 kb, E-HIS; ~1.8 kb, prM; ~0.8 kb, C_8-SS-prM, ~0.8 kb, and SS-prM; ~0.8 kb (Figure 2.5).

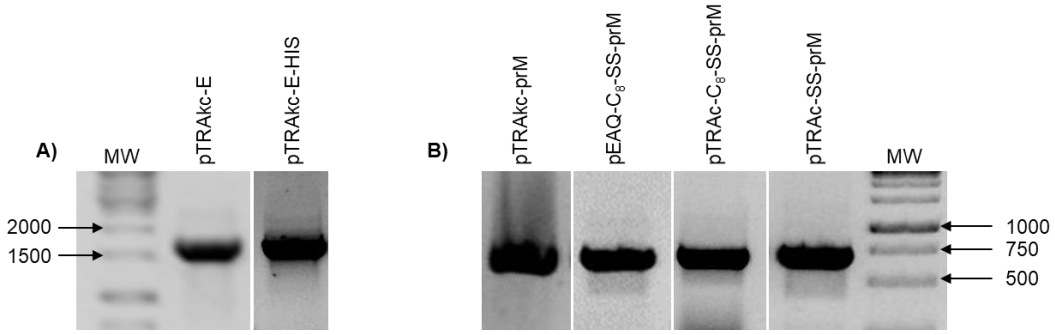

Figure 2.5. PCR amplification of *prM* and *E* gene permutations from pEAQ-*HT* and pTRA clones in *E. coli* visualised on agarose gels stained with ethidium bromide. **(A)** The pTRAkc-ERH clones containing the *E* gene permutations. **(B)** The pEAQ-*HT*, pTRAc and pTRAkc-ERH clones containing the *prM* gene permutations. Label: MW, the molecular weight marker.

2.3.3. Confirmation of successful *A. tumefaciens* transformation

The recombinant pEAQ-*HT* construct was transformed into *A. tumefaciens* LBA4404 and the recombinant pTRA constructs were transformed into *A. tumefaciens* GV3101::pMP90RK. Successful transformation was confirmed by colony PCR using vector-specific primers (Appendix B: Table 1). Amplified fragments of expected sizes were observed as described in section 2.3.2 confirming successful transformation into *Agrobacterium* strains (data not shown).

2.3.4. Transient expression of WNV proteins in *N. benthamiana*

2.3.4.1. Co-expression of E and human chaperones

The influence of human chaperone proteins CNX and CRT and the NSs silencing suppressor on the expression of the E protein (His-tagged) was investigated. The His-tagged E construct was used for infiltration while the E-specific antiserum was being produced, so that anti-His sera could be used for protein detection. However, by the time of protein analysis the E-specific antiserum was available for use.

The CNX, CRT and NSs proteins were co-expressed with the E protein either alone or as a combination (Appendix D: Table 5). Leaves were harvested 3, 4 and 5 dpi and proteins extracted with 100 mM Tris.HCl (pH 7.4). Thirty micrograms of crude pellet (insoluble) and supernatant (soluble) E protein extracts were evaluated by western blot using polyclonal rabbit anti-WNV-EdIII antiserum for detection of the E protein; ~53 kDa.

The optimal expression day for maximum expression levels was determined for the E protein when expressed alone (Figure 2.6 – black arrow). No protein was detected 3 dpi in either the insoluble or soluble fractions. At 4 dpi E protein was only detected in the soluble fraction and at 5 dpi in both the insoluble and soluble fractions. Based on the band intensities, more protein was observed in both the insoluble and soluble fractions at 5 dpi in comparison to the soluble fraction at 4 dpi. Thus, the optimal expression day for the E protein was determined to be 5 dpi. Interestingly, in the insoluble fraction at 5 dpi a protein doublet could be observed which suggests the presence of different E protein glycoforms; this was also observed in the insoluble fractions when E was co-expressed with CNX, CRT and NSs (Figure 2.7B).

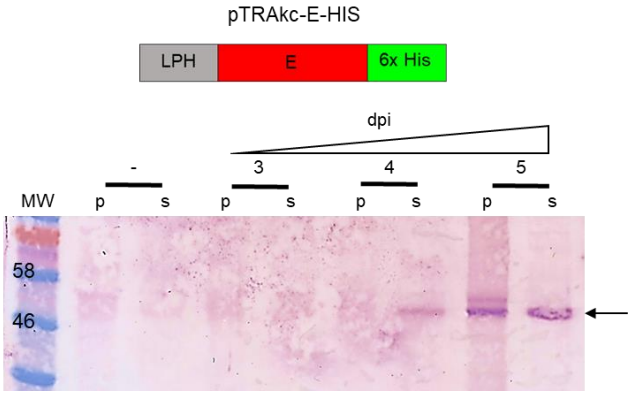

Figure 2.6. Expression of the E protein with a 6x His tag for optimal harvest day determination. Proteins were isolated 3, 4 and 5 dpi and 30 µg of TSP of pellet (p) and supernatant (s) was loaded into each lane – black arrow indicates ~ 53 kDa E protein. The negative controls (-) are crude leaf extracts of plants infiltrated with pTRAkc-ERH empty vector. Proteins were detected with anti-WNV-EdIII antiserum (1:20 000). Label: MW, the molecular weight marker.

When expressed alone or in the presence of NSs, the E protein was predominantly present in the insoluble fraction as suggested by the darker band intensities (Figure 2.7B – black arrow). However, when co-expressed with either chaperone protein (E+CNX or E+CRT), with both chaperone proteins (E+CNX+CRT) or in combination with the chaperone proteins and NSs (E+CNX+NSs or E+CRT+NSs), more protein was observed in the soluble fraction in comparison to when E was expressed alone or only with NSs (Figure 2.7A – black arrow). These observations were made qualitatively based on the intensity of the protein bands since equal amounts of TSP was loaded in each lane. The effect on E protein yield was augmented when co-expressed with either of the human chaperone proteins. A slightly more intense band was observed in the soluble fraction when E was co-expressed with CNX (E+CNX) in comparison to co-expression with CRT (E+CRT), and in comparison to the combination co-expressions (E+CNX+NSs, E+CRT+NSs and E+CNX+CRT) a similar band intensity was observed (Figure 2.7A). From these observations, it was decided to select the pEAQ-CNX construct for future co-infiltrations.

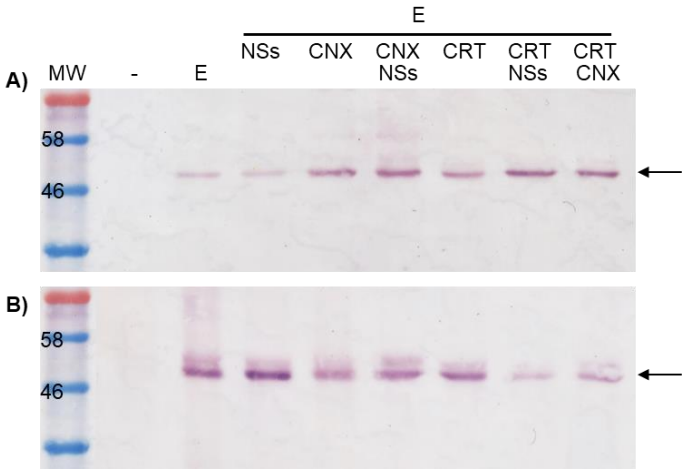

Figure 2.7. Co-expression of the E protein with NSs, CNX, CRT or in combination as indicated above the lanes. Proteins were isolated 5 dpi and 30 µg of TSP was loaded into each lane for both the soluble **(A)** and insoluble fractions **(B)** – black arrow indicates ~ 53 kDa E protein. The negative controls (-) are crude leaf extracts of plants infiltrated with pTRAkc-ERH empty vector in *Agrobacterium*. Proteins were detected with anti-WNV-EdIII antiserum (1:20 000). Label: MW, the molecular weight marker.

2.3.4.2. Co-expression of prM and E

When the constructs containing the *prM* gene were expressed on their own, little or no protein was detected by western blot; in addition where protein was detected it was insoluble (Appendix F: Figure 2). Therefore, the prM constructs were co-expressed with the E protein (Figure 2.8). The two constructs (prM and E) were co-infiltrated at an OD_{600} of 0.5 each and leaves harvested 4, 5 and 6 dpi. Protein was extracted using 1x PBS (pH 6.0) and crude extracts containing equal amounts of TSP were evaluated by western blotting for M, prM and E protein expression. Polyclonal rabbit anti-WNV-EdIII and anti-WNV-M antiserum (both produced specifically for this study) were used for the detection of the E (~53 kDa – green arrow), prM (19-25 kDa – blue arrow) and M (7-10 kDa – pink arrow) proteins, respectively. From the co-expression of the prM and E proteins, both the M and E proteins could be detected in all prM construct permutations. In the soluble fraction at 4 dpi for E expressed with pEAQ-C_8-SS-prM there was a faint band of approximately 25 kDa that could be the prM protein (Figure 2.8D – blue arrow).

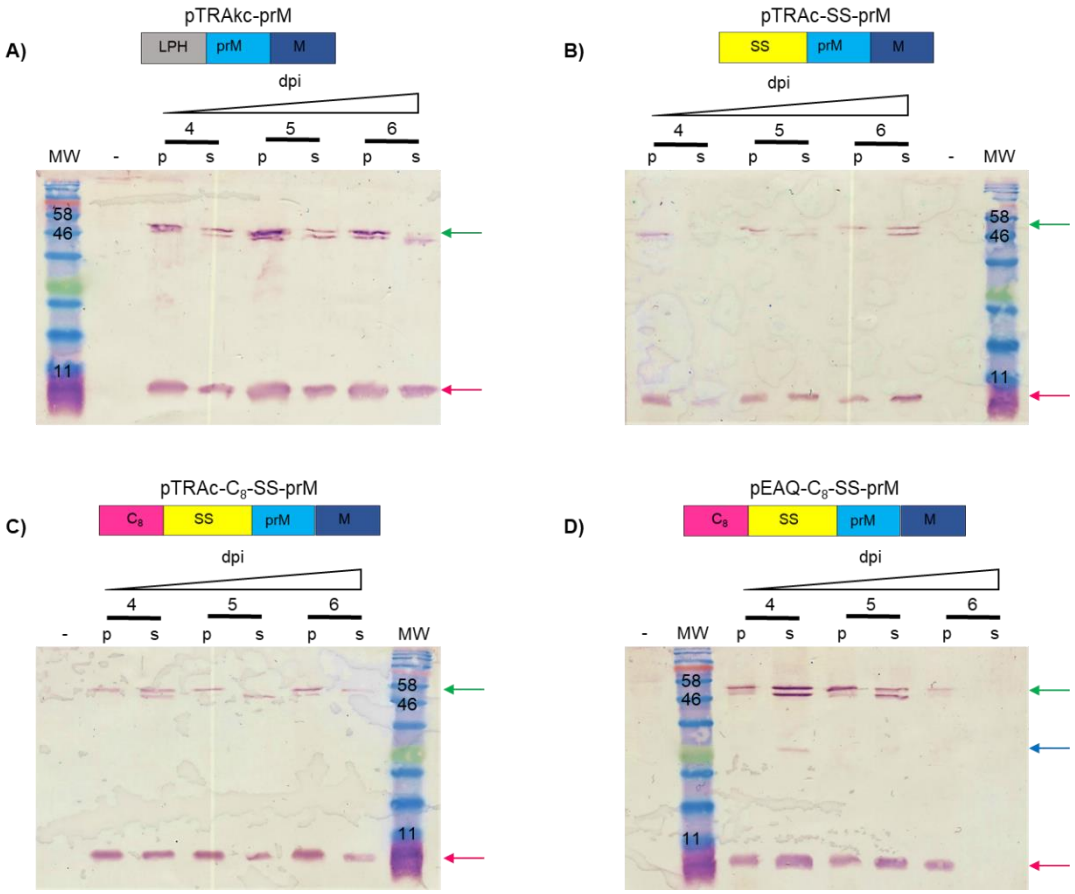

Figure 2.8. Co-expression of prM and E proteins over 6 days using different signal peptide permutations: **(A)** LPH, **(B)** SS, and **(C-D)** C_8-SS. Proteins were extracted as described in section 2.2.7.2 using 1x PBS (pH 6.0) and 25 µg TSP of pellet (p) and supernatant (s) crude extracts were loaded in each lane – green arrow indicates ~ 53 kDa E protein, pink arrow indicates ~ 10 kDa M protein and blue arrow indicates ~ 25 kDa putative prM protein. Proteins were detected with anti-WNV-EdIII combined with anti-WNV-M antisera (1:20 000 each). **(A)** pTRAkc-E + pTRAkc-prM, **(B)** pTRAkc-E + pTRAc-SS-prM, **(C)** pTRAkc-E + pTRAc-C_8-SS prM, **(D)** pTRAkc-E + pEAQ-C_8-SS-prM.The negative controls (-) are crude leaf extracts of plants infiltrated with pTRAkc-ERH empty vector. Label: dpi denotes 4, 5 and 6 days post infiltration. p represents the insoluble fraction; pellet. s represents the soluble fraction; supernatant. MW indicates the molecular weight marker.

Following the success of detectable yields of M protein from co-expression with the E protein, a triple co-expression with CNX was performed since co-expression with CNX improved the soluble yield of E (Figure 2.7). The three constructs (prM, E and CNX) were co-infiltrated at an OD_{600} of 0.3 each and leaves harvested and proteins extracted as described above (Figure 2.9). The M and E proteins were detected across all days sampled for each of the four co-expression permutations, but no prM was detected. The M protein was predominantly soluble (s) regardless of the construct expressed (Figure 2.9A-D: bottom panels). Similar band intensities were observed for both the soluble and insoluble fractions containing the E protein

(Figure 2.9A-D: top panels). Based on the soluble fractions, expression of both the M and E proteins was optimal at 4 dpi, with no observed increase in band intensities at 5 and 6 dpi.

When the *E* gene was co-infiltrated with either pEAQ-C_8-SS-prM or pTRAc-C_8-SS-prM, with the increase in dpi, a decrease in M protein expression was observed (Figure 2.9C-D: bottom panels). However, when the *E* gene was co-infiltrated with either pTRAkc-prM with the LPH signal peptide (Figure 2.9A) or pTRAc-SS-prM with just the native signal peptide (Figure 2.9B) the level of protein expression was consistent across all harvest days for both the M and E proteins.

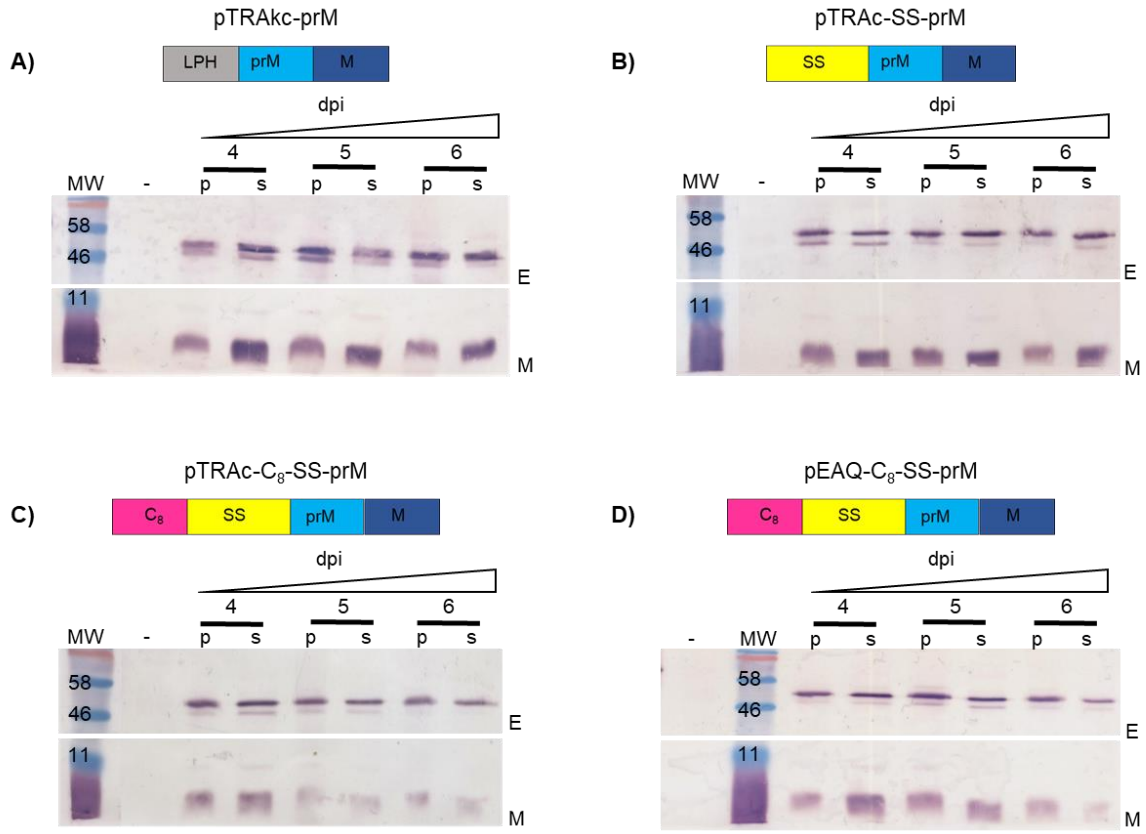

Figure 2.9. Co-expression of prM and E proteins with CNX over 6 days using different signal peptide permutations: **(A)** LPH, **(B)** SS, and **(C-D)** C_8-SS. The top panels represent the E protein and the bottom panels the M protein, detected with anti-WNV-EdIII and anti-WNV-M antiserum (1:20 000 each), respectively. 25 µg TSP **(A)** pTRAkc-E + pEAQ-CNX + pTRAkc-prM, **(B)** pTRAkc-E + pEAQ-CNX + pTRAc-SS-prM, **(C)** pTRAkc-E + pEAQ-CNX + pTRAc-C_8-SS prM, **(D)** pTRAkc-E + pEAQ-CNX + pEAQ-C_8-SS-prM was loaded in each lane. The negative controls (-) are crude leaf extracts of plants infiltrated with pTRAkc-ERH empty vector. Label: dpi denotes 4, 5 and 6 days post infiltration. p represents the insoluble fraction; pellet. s represents the soluble fraction; supernatant. MW indicates the molecular weight marker. E denotes detection with anti-WNV-EdIII antiserum. M denotes detection with anti-WNV-M antiserum.

2.4. Discussion

The use of plants as a production platform for recombinant proteins has become popular in recent years due to their safety, affordability, and ease of scalability (Rybicki, 2009; Rybicki, 2010; Schillberg *et al.*, 2019; Fischer & Buyel, 2020). Several studies have illustrated the success of producing VLPs in *N. benthamiana* by expression of heterologous proteins (van Zyl *et al.*, 2016; Dennis *et al.*, 2018a). Due to the success of these studies, it was proposed that WNV VLPs could be produced in *N. benthamiana* as a candidate vaccine.

We aimed at employing two strategies for the expression of the *prM* and *E* genes of a virulent South African WNV strain in *N. benthamiana* with a view to generating VLPs. The first strategy was focused on the expression of the prM-E polyprotein, however, sub-cloning of the *prM-E* polyprotein genes from pCC1 into pTRAkc-ERH was unsuccessful after several attempts. As an alternative, the *prM-E* genes were amplified from the pCC1 backbone to allow for subcloning into the pJET1.2/blunt vector to create a stable high copy number construct, as pCC1 is a low copy number vector. Amplification of the *prM-E* polyprotein gene was successful but after several failed attempts at ligation into pJET1.2/blunt, this strategy was discontinued and focus was shifted to the co-expression of the individual *prM* and *E* genes.

The E protein was successfully amplified with and without a 6x His tag fused to it and cloned into the commercial pJET1.2/blunt vector; this was followed by subcloning into the plant expression vector pTRAkc-ERH that contained the essential ER-targeting signal peptide for translocation of E to the ER. An additional prM construct was synthesised to include the native signal peptide and 8 amino acids of the C protein. This decision was based on evidence provided by Takahashi and colleagues who evaluated the effect additional amino acids of the C protein at the N terminus of the prM signal peptide had on protein expression in mammalian cells (Takahashi *et al.*, 2009). They found that the number of amino acids around the NS2B-3 cleavage site located 5' to the native SS, was important for the efficient processing and assembly of the E protein. These results further support the claims of the role that the prM protein plays as a chaperone for folding and assembly of the E protein (Lorenz *et al.*, 2002). Based on the observations made by Takahashi *et al*. it was decided to synthesize the *prM* gene to include 8 amino acids of the *C* gene in addition to the native SS to facilitate a similar evaluation of the effect of these residues on protein expression *in planta*. Consequently, we were able to compare the effect of the C_8-SS-prM and the SS-prM construct on E protein co-expression, which in mammalian cells resulted in an approximately 50-fold increase in E production by the SS-prM construct compared to co-expression with the C_8-SS-prM construct (Takahashi *et al.*, 2009).

When the E protein was expressed on its own, less protein was observed in the soluble than insoluble fraction of the crude extracts. However, when co-infiltrated with either human CNX or CRT, protein yields in the soluble fractions increased. This could be explained by the critical role that these chaperone proteins play in protein folding within the ER secretory pathway. CNX and CRT are ER lectin chaperones that interact with proteins that carry N-linked glycans, specifically binding monoglucosylated polymannose glycans (Caramelo & Parodi, 2008). By binding to these glycoproteins, CNX and CRT provide a protective folding environment, assist in inhibiting protein aggregation and finally prevent premature exit of proteins from the ER (Ellgaard & Helenius, 2003). In this way these chaperones prevent the accumulation of misfolded proteins in the ER which results in ER stress (Margolin *et al.*, 2018).

Co-expression of E with CNX resulted in greater band intensity in the soluble fraction than when co-expressed with CRT. This was expected as CNX preferentially interacts with nascent proteins associated with the ER membrane as it is a type I transmembrane protein (Ellgaard & Helenius, 2003) and the E glycoprotein has two transmembrane domains that embed within the ER membrane (Mukhopadhyay *et al.*, 2005) which explains protein insolubility. Therefore, the increase in soluble E protein observed from co-expression with CNX could be attributed to the decrease in misfolded and aggregated proteins that remain in the ER rather than being released from the ER for further processing in the TGN.

When the prM proteins were expressed on their own and extracted with 100 mM Tris.HCl (pH 7.4), the M protein could be detected using the pTRAc-SS-prM construct only and was present only in the insoluble fraction. A change in extraction buffer was introduced upon co-expression of the prM and E proteins. When extracted with 100 mM Tris.HCl (pH 7.4) the M protein was completely insoluble and the E protein was predominantly insoluble (Appendix F: Figure 3). The insolubility of the proteins was suspected to be a result of the maturation state of the proteins. During replication within the cell, the immature virions are transported to the TGN where the low pH of approximately 6.0 induces a conformational rearrangement of the prM-E proteins that drive the cleavage of the pr peptide from the M protein by furin (Mukhopadhyay *et al.*, 2005; Roby *et al.*, 2015). To mimic these conditions an extraction buffer of 1x PBS (pH 6.0) was used and improved solubilisation of both M and E proteins were observed.

Surprisingly, furin-like cleavage was observed upon the co-expression of the prM and E proteins. When in the immature state, the prM protein is approximately 19-25 kDa, however after maturation and the cleavage of the pr peptide by furin, the M protein is approximately 7-10 kDa (Lorenz *et al.*, 2002; Ohtaki *et al.*, 2010; Roby *et al.*, 2015). Western blotting of crude extracts of co-expressed prM and E proteins extracted with either extraction buffer revealed only a protein of ~8 kDa, with a single exception. When E was co-expressed with the

pEAQ-C_8-SS-prM construct and proteins extracted with 100 mM Tris.HCl (pH 7.4) a protein band of ~25 kDa was detected when developed with anti-WNV-M sera, which could represent the prM protein before cleavage (Appendix F: Figure 3). However, when extracted with 1x PBS (pH 6.0) only a ~8 kDa band was observed, suggesting cleavage had taken place. Chen and colleagues have also proposed furin-like cleavage taking place in *N. benthamiana* when processed M protein of the NY99 WNV strain was observed upon transient expression of the *prM* and *E* genes (Chen & Lai, 2013).

Interestingly, expression levels of the M protein decreased with an increase of dpi when the E protein was co-expressed with either pEAQ-C_8-SS-prM or pTRAc-C_8-SS-prM. The same trend was not observed when E was co-expressed with pTRAkc-prM or pTRAc-SS-prM, which suggests that the signal peptide might have played a role in this result. The reason for this assumption is that regardless of which plant expression vector was used, pEAQ-*HT* or pTRAc, in the presence of the 8 additional C terminal amino acids after 4 dpi a decrease in M protein levels could be observed. This might be due to the improper cleavage of the C_8-SS over time. In contrast to the results obtained by Takahashi *et al*. the expression of the E protein remained consistent regardless of the prM construct and only the M protein yield decreased. In their study, a significant decrease in the E protein was observed when the C_8-SS-prM-E polyprotein was expressed, in comparison to when the SS-prM-E polyprotein was expressed. They proposed that the E protein was not being properly cleaved which in turn resulted in a reduction in the release of VLPs (Takahashi *et al.*, 2009). However, as we did not observe a similar trend in E protein levels, we propose that the presence of the human chaperone CNX could augment the prM proteins' function as a chaperone for folding and assembly of the E protein (Lorenz *et al.*, 2002; Margolin *et al.*, 2018; Margolin *et al.*, 2020).

In conclusion, the prM and E proteins were successfully expressed in *N. benthamiana* suggesting that VLP assembly may be possible. Co-expression of prM and E with CNX and extraction in a low pH buffer improved protein yield in the soluble fraction.

Chapter 3:

Transient expression, characterisation and purification of putative WNV VLPs

3.1. Introduction

Plants have successfully been used as bioreactors for the production of VLPs for a number of viruses as candidate vaccines, and especially in our laboratory. Gunter and colleagues successfully produced porcine circovirus type 2 (PCV-2) VLPs in *N. benthamiana* by transiently expressing the PCV coat protein (Gunter *et al.*, 2019). Expression of this protein resulted in the formation of VLPs that were subsequently purified by density gradient ultracentrifugation. Additionally, the authors showed that these plant-produced PCV-2 VLPs elicited strong PCV-2 specific serum immune responses in mice. Similarly, human papillomavirus (HPV) VLPs can also be made from the expression of a single virus protein. Maclean and colleagues transiently expressed the HPV-16 L1 protein in *N. tabacum* and *N. benthamiana* plants and successfully purified HPV VLPs that induced both HPV-16 VLP-specific antibodies and NAbs in mice (Maclean *et al.*, 2007). Marsian *et al*. demonstrated the success of using plants for the production of Atlantic Cod nervous necrosis virus (ACNNV) VLPs as a candidate vaccine (Marsian *et al.*, 2019). The authors transiently expressed the coat protein of ACNNV in *N. benthamiana* and purified VLPs by density gradient ultracentrifugation with a yield of 10 mg/kg fresh weight. These VLPs were used to immunise sea bass, and in the absence of an adjuvant conferred moderate to strong protection in virus-challenged fish. Another example of using plants as bioreactors for the production of VLPs from the expression of a single protein is that of Rift Valley fever virus (RVFV). Transient expression of a chimaeric RVFV G*n* gene in *N. benthamiana* yielded VLPs at ~57 mg/kg fresh weight, that induced Gn-specific antibody responses in immunised mice (Mbewana *et al.*, 2018).

The above studies illustrate the success of using tobacco plants for the production of VLPs by transiently expressing a single protein. However, not all VLPs assemble from a single protein and typically several viral proteins are required for the formation of a particle. In the case of WNV, both the prM and E proteins need to be present for VLP formation, and this has been proven in both mammalian (Takahashi *et al.*, 2009; Ohtaki *et al.*, 2010; Ohtaki *et al.*, 2011) and insect cells (Qiao *et al.*, 2004; Rebollo *et al.*, 2018b). Chen and Lai reported in a review

focused on plant-produced VLPs as candidate vaccines, that WNV VLPs have been produced in *N. benthamiana* by transient expression of the prM and E proteins; however, these results were never published (Chen & Lai, 2013).

The production of VLPs from multiple proteins in plant expression systems has been illustrated in several studies. van Zyl and colleagues successfully assembled bluetongue virus serotype 8 (BTV-8) VLPs in *N. benthamiana* by transiently co-expressing the 4 proteins VP2, VP3, VP5 and VP7 (van Zyl *et al.*, 2016). Similarly, the transient co-expression of VP2, VP3, VP5 and VP7 of African horse sickness virus serotype 5 (AHSV-5) in *N. benthamiana* resulted in the assembly of VLPs that induced NAbs in both guinea pigs (Dennis *et al.*, 2018a) and horses (Dennis *et al.*, 2018b). In another study, Foot-and-mouth disease (FMDV) VLPs were produced in *N. benthamiana* by transient expression of the P1-2A protein that was proteolytically cleaved *in planta* into the three structural proteins (VP0, VP1 and VP3) required for particle assembly (Veerapen *et al.*, 2018). Interestingly, to achieve the same proteolytic cleavage in mammalian and insect cells the non-structural 3C protease needs to be co-expressed. Preliminary immunogenicity studies in mice of the plant-produced FMDV VLPs induced FMDV-specific antibodies. These examples of VLPs produced from the expression of single or multiple proteins and their ability to stimulate immune responses, illustrate the potential of using plants as biofactories for the production of particulate candidate vaccines.

In the previous chapter, I described the successful expression of the WNV *prM* and *E* genes and determined the optimal conditions for the expression of these genes. Work reported in this chapter investigated whether the expression of these genes *in planta* results in VLP assembly. Here, I describe the large scale expression of the WNV *prM* and *E* genes together with the human chaperone protein CNX in *N. benthamiana,* and the optimisation of VLP purification from infiltrated leaves by density gradient ultracentrifugation.

3.2. Materials and Methods

3.2.1. Large scale infiltration

Recombinant *A. tumefaciens* of pTRAkc-E, pTRAkc-prM, pTRAc-C_8-SS-prM, pTRAc-SS-prM, pEAQ-C_8-SS-prM and pEAQ-CNX were cultured as described in section 2.2.6. After cultivation, the cells were diluted to OD_{600} of 0.3 for each construct (Table 3.1, Appendix D: Table 5) in infiltration medium.

Fifteen to twenty six-week-old *N. benthamiana* plants were co-infiltrated as described in Table 3.1 (Appendix D: Table 5), by vacuum infiltration as described in section 2.2.6.

Table 3.1. Co-infiltration optical densities.

Co-infiltrations	OD_{600}	Combined OD_{600}
pTRAkc-E **pEAQ-CNX** **pTRAkc-prM**	0.3 each	0.9
pTRAkc-E **pEAQ-CNX** **pTRAc-SS-prM**	0.3 each	0.9
pTRAkc-E **pEAQ-CNX** **pTRAc-C_8-SS-prM**	0.3 each	0.9
pTRAkc-E **pEAQ-CNX** **pEAQ-C_8-SS-prM**	0.3 each	0.9

3.2.2. Optimisation of WNV VLP purification from *N. benthamiana*

Leaves co-infiltrated with pTRAkc-E, pEAQ-CNX and a prM construct (pTRAkc-prM, pEAQ-C_8-SS-prM, pTRAc-C_8-SS-prM or pTRAc-SS-prM) were harvested at 4 dpi and homogenised in 2 volumes PI buffer [1x PBS (pH 6.0), 1x cOmplete™ EDTA-free protease inhibitor (Roche)] using an IKA® T-25 ULTRA-TURRAX® (Sigma-Aldrich) homogeniser. Figure 3.1. illustrates the different strategies employed for VLP purification. Differences in the purification process can be observed at the maturation step (indicated in orange boxes). Following leaf homogenisation, the plant homogenate was either matured O/N at RT or 4°C (Figure 3.1C-D) or only incubated at 4°C for 30 min (Figure 3.1A-B, E) with gentle shaking. The plant homogenate was then filtered through 2 layers of MiraCloth™ (Merck) and clarified

by centrifugation at 15 000 *x* g for 10 min. The clarified extract was matured O/N at RT or 4°C with gentle shaking (Figure 3.1A-B, E) for particle maturation if not already matured in the plant homogenate state (Figure 3.1C-D). Particles were either concentrated through a 30% sucrose cushion (2 mL; Figure 3.1A-D) by ultracentrifugation at 174 586 *x* g for 1 h at 4°C in an SW32 Ti rotor (Beckman) or by precipitation during O/N maturation of the clarified extract with 9% polyethylene glycol 6000 (PEG 6000, Sigma-Aldrich) and 2.5% NaCl, followed by centrifugation at 10 000 *x* g for 30 min at 4°C (Figure 3.1E). Following the sucrose cushion or PEG precipitation, the pellet was resuspended in ~20 mL 1x PBS (pH 6.0) and layered over a 10- or 20-60% linear sucrose density gradient (3 mL each) and ultracentrifuged at either 174 586 *x* g for 1 h (Figure 3.1A, B and D) or 2 h 35 min (Figure 3.1C-E). The interface between the 30-40% (F1), 40-50% (F2) and 50-60% (F3) densities was extracted (~1 mL) using a 21 gauge needle and syringe.

Equal volumes of the collected samples were evaluated for the presence of the M, prM and E proteins by western blot as described in section 2.2.8. Polyclonal rabbit anti-WNV-EdIII and polyclonal rabbit anti-WNV-M antisera (1:20 000 dilution each) were used for primary detection and alkaline phosphatase-conjugated polyclonal goat anti-rabbit antibody (1:10 000 dilution) (Biocom Africa) was used for secondary detection.

Collected samples were evaluated for the presence of VLPs (25-30 nm) by TEM (as described in section 3.2.3).

3.2.3. Transmission electron microscopy

Carbon-coated copper grids (mesh size 200) were made hydrophilic by glow discharging at 25 mA for 30 s using a Model 900 SmartSet Cold Stage Controller (Electron Microscopy Sciences). The grids were floated on 20 µL of purified sample for 3 min and washed 5 times with sterile water. The samples were negatively stained for 1 min with 2% w/v uranyl acetate and viewed using a Technai G2 transmission electron microscope (FEI).

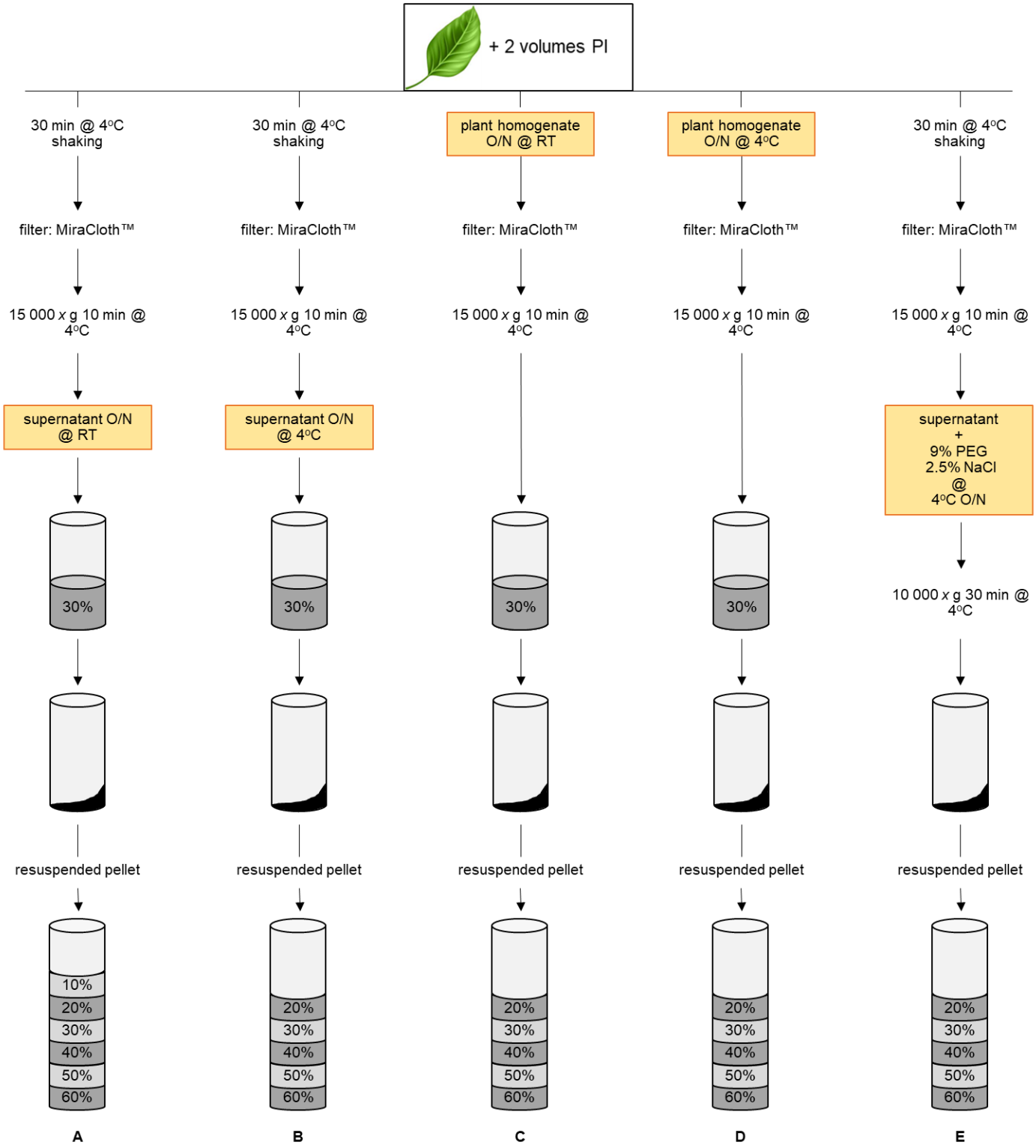

Figure 3.1. Schematic representation of strategies employed for WNV VLP purification. Sections highlighted in orange represent the particle maturation step performed at either RT or 4°C for either the clarified extract or plant homogenate or in combination with a PEG precipitation step. Infiltrated leaves were homogenised in 2 volumes PI buffer. **(A-B)** The plant homogenate was incubated at 4°C for 30 min and clarified by filtration and centrifugation. The clarified extract was incubated at RT (A) or 4°C (B) O/N for particle maturation, followed by concentration through a 30% sucrose cushion. The pellet was resuspended in 1x PBS (pH 6.0) and particles purified on a discontinuous sucrose density gradient. **(C-D)** The plant homogenate was incubated at RT (C) or 4°C (D) O/N for particle maturation and clarified by filtration and centrifugation. Particles were concentrated and purified as described for B. **(E)** The plant homogenate was treated as described for A and B. Following clarification, the clarified extract was incubated at 4°C O/N for particle maturation in the presence of 9% PEG-6000 and 2.5% NaCl for particle concentration. The extract was centrifuged and the pellet resuspended for purification of particles on a discontinuous sucrose density gradient as described for B.

3.3. Results

The results described in Chapter 2 illustrated that the WNV proteins involved in VLP formation could be successfully expressed in *N. benthamiana*. Here, I investigated whether these proteins assembled into VLPs and if so, how to optimally purify them from *N. benthamiana*.

3.3.1. Particle purification with maturation of clarified extract at RT

N. benthamiana plants were co-infiltrated with pTRAkc-E, pEAQ-CNX and any one of the 4 prM constructs pTRAkc-prM, pEAQ-C_8-SS-prM, pTRAc-C_8-SS-prM or pTRAc-SS-prM (Figure 2.3). Leaves were harvested at 4 dpi based on previous optimisation experiments carried out (section 2.3.4.2) and homogenised in 1x PI buffer. The plant homogenates were clarified and putative particles were matured O/N at RT, based on small scale purification of the M and E proteins (section 2.2.7), and subsequently concentrated through a 30% sucrose cushion, followed by purification on a 10-60% discontinuous sucrose density gradient (Figure 3.1A and 3.2). The 30/40%, 40/50% and 50/60% interfaces were collected (F1, F2 and F3 respectively), evaluated for the presence of WNV M (7-10 kDa – pink arrow), prM (19-25 kDa – blue arrow) and E (53 kDa – green arrow) proteins by western blot and VLPs (25-30 nm) by transmission electron microscopy (TEM, Figure 3.2).

Each of the 4 co-infiltration permutations resulted in similar density gradient profiles after ultracentrifugation (Figure 3.2 – Gradient), with white bands evident at the 30/40%, 40/50% and 50/60% interfaces. Based on the literature, WNV VLPs have an expected density of ~1.11-1.16 g/cm^3 (Qiao *et al.*, 2004; Takahashi *et al.*, 2009; Ohtaki *et al.*, 2010) which corresponds to ~25-40% sucrose; therefore, these interface-bands were collected. All three proteins (M, prM and E) were observed on western blots for the permutations where pEAQ-C_8-SS-prM (Figure 3.2B) or pTRAkc-prM (Figure 3.2F) were used. However, only the E protein was detected when co-infiltrating with pTRAc-C_8-SS-prM (Figure 3.2D) and faint prM and E proteins were detected when co-infiltrating with pTRAc-SS-prM (Figure 3.2E). Particles within the expected range of 25-30 nm were observed by TEM (Figure 3.2 – TEM) for all 4 co-infiltration permutations in at least one of the collected fractions within the expected 25-40% sucrose density range (F1 or F2). However, duplication of these results proved difficult as western blot and TEM results were inconsistent. The lack of reproducibility rendered this purification process ineffectual and a different approach was considered.

	Construct	Gradient	Western blot	TEM
A)	pEAQ-*HT* → empty vector control	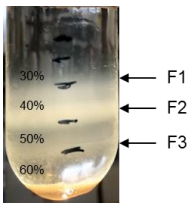		F1 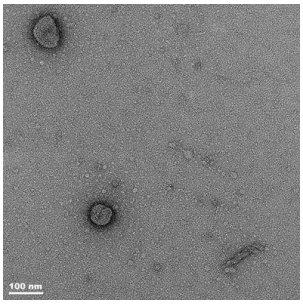
B)*	pEAQ-C_8-SS-prM C_8 SS prM M	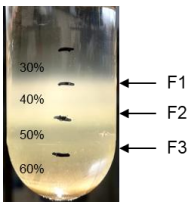	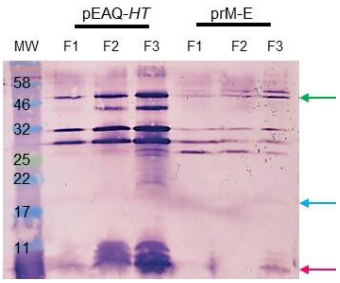	F1 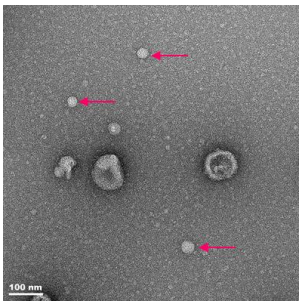
C)	pTRAkc-ERH → empty vector control	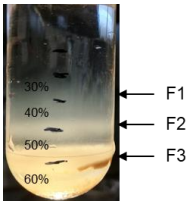		F1 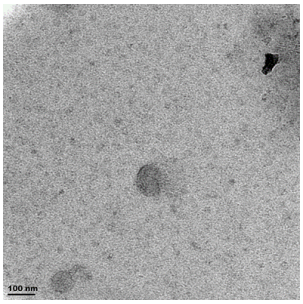
D)*	pTRAc-C_8-SS-prM C_8 SS prM M	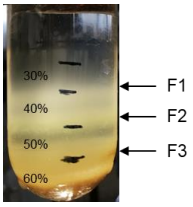	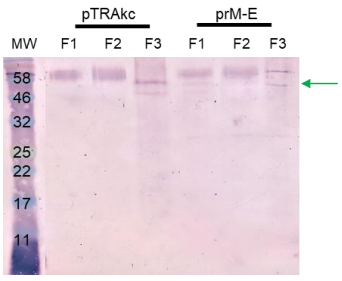	F2 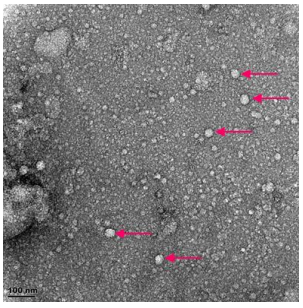
E)*	pTRAc-SS-prM SS prM M	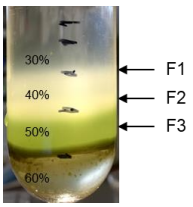	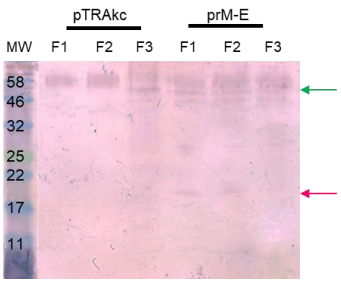	F2 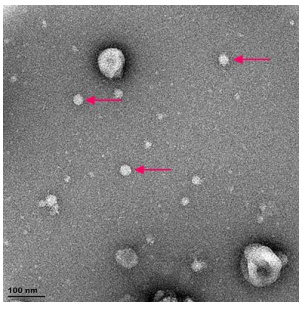
F)*	pTRAkc-prM LPH prM M	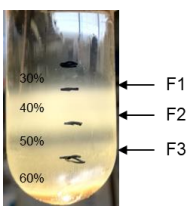	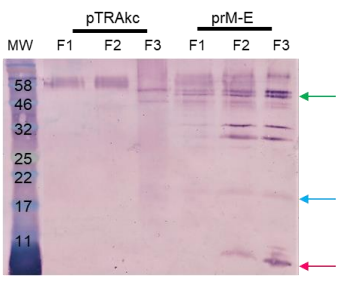	F1 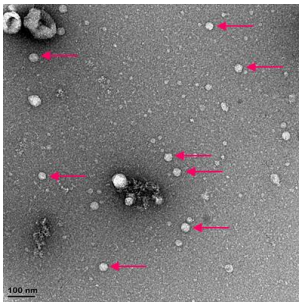

*Co-infiltrations were performed with pTRAkc-E, pEAQ-CNX and the prM construct as listed in the Construct column (B, D-F).

Figure 3.2. *From the previous page*. Putative WNV VLP purification from plants co-infiltrated with WNV E and prM (with different signal peptides) recombinant plasmids and the human chaperone CNX. Particles were purified as depicted in Figure 3.1A with maturation of the clarified extract at RT and the 30/40%, 40/50% and 50/60% interfaces were sampled (F1, F2 and F3 respectively). The presence of M (7-10 kDa -pink arrow), prM (19-25 kDa – blue arrow) and E (53 kDa – green arrow) proteins were evaluated by western blot using anti-WNV-EdIII combined with anti-WNV-M antiserum (1:20 000 each) and the presence of VLPs (25-30 nm – pink arrows) was determined by TEM (scale bar = 100 nm). MW, the molecular weight marker. The negative controls were purified extracts from leaves infiltrated with either empty pEAQ-*HT* or pTRAkc-ERH vector.

3.3.2. Particle purification with maturation of clarified extract at 4°C

It was considered that although an O/N incubation step is required for protein and particle maturation, performing this step at RT could potentially result in protein and/or particle degradation, which in turn could explain the inconsistency previously observed in the results for repeat experiments. Based on these postulations, I evaluated whether performing the maturation step at 4°C (Figure 3.1B) instead of RT might resolve this problem. To simplify this evaluation, only a single prM construct was selected for the continued optimisation of particle purification. The selection was based on the western blot and TEM results obtained from the purification as described and depicted in Figure 3.2. The construct selected for co-expression with the *E* gene and CNX was pTRAkc-prM (membrane protein with the LPH signal peptide) since the M, prM and E proteins were successfully detected at least once by western blot and several VLPs of the expected size were observed by TEM (Figure 3.2F).

N. benthamiana plants were co-infiltrated with pTRAkc-E, pEAQ-CNX and pTRAkc-prM, and leaves harvested at 4 dpi, homogenised in 1x PI buffer and clarified. Putative particles were matured O/N at 4°C and subsequently concentrated through a 30% sucrose cushion, the pellet resuspended and purified on a 20-60% discontinuous sucrose density gradient (Figure 3.1B). The 30/40%, 40/50% and 50/60% interfaces were collected (Figure 3.3A-B; F1, F2 and F3 respectively) and evaluated for the presence of WNV M, prM and E proteins by western blot (Figure 3.3C) and VLPs by TEM (Figure 3.3D-E).

Similar density gradient profiles, following ultracentrifugation, were observed for both the vector-only control (pTRAkc-ERH) and prM-E (Figure 3.3A-B) samples and were also comparable to those obtained when the clarified extract was matured at RT (Figure 3.2C and F). However, unlike these samples, western blot analysis resulted in the detection of only faint E protein bands and no M or prM proteins (Figure 3.3C). Electron microscopy analysis of collected fractions revealed several particles of 25-30 nm in size for F3 (Figure 3.3E), yet this was only observed for a single experiment. Once more, the lack of reproducibility led us to investigate another purification approach by reconsidering the maturation step of the purification process.

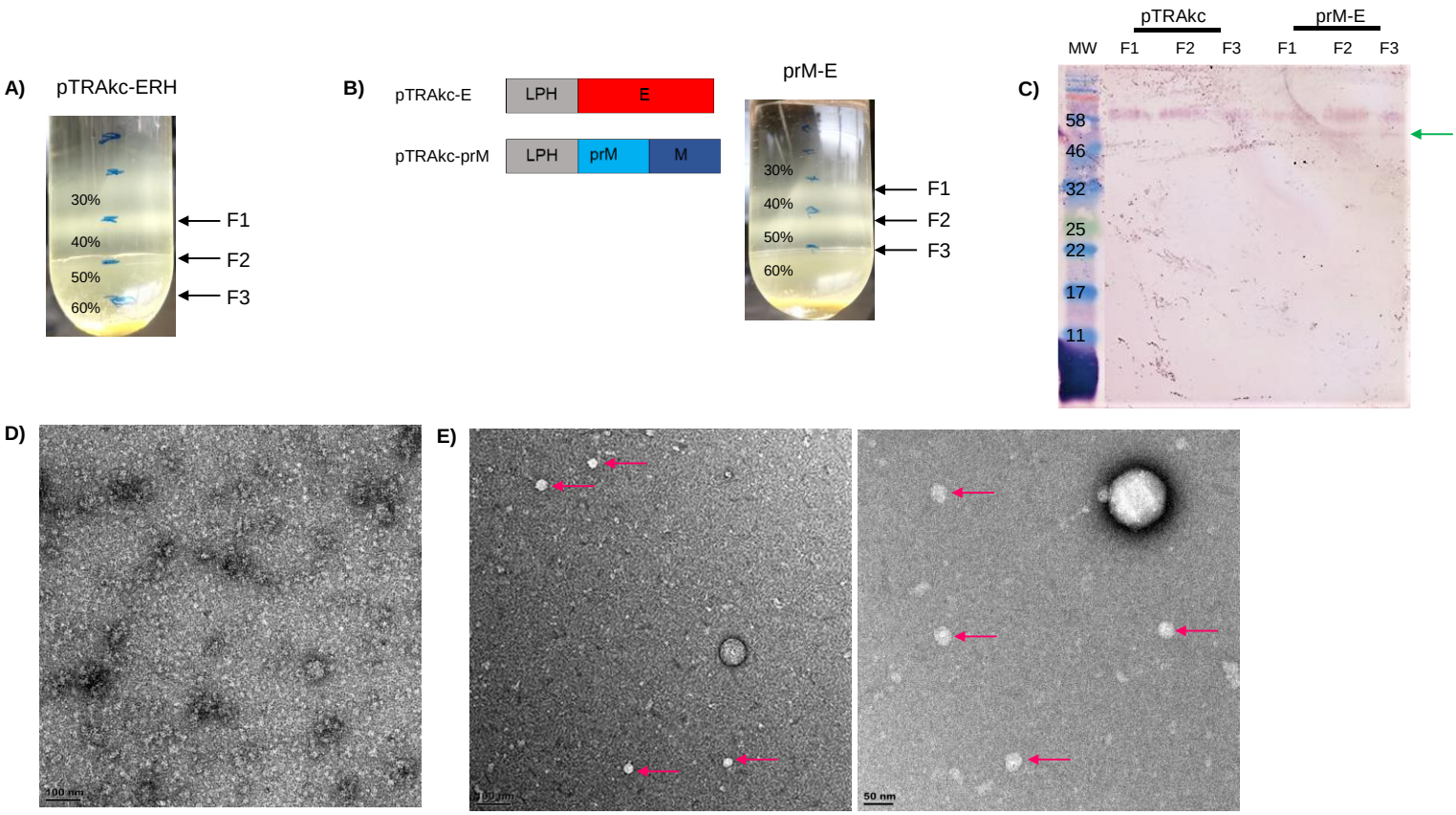

Figure 3.3. Putative WNV VLP purification from plants co-infiltrated with WNV E and prM (pTRAkc-prM) recombinant plasmids and the human chaperone CNX. Particles were purified as depicted in Figure 3.1B with maturation of the clarified extract at 4°C. **(A)** pTRAkc-ERH and **(B)** prM-E gradient profiles following ultracentrifugation. The 30/40%, 40/50% and 50/60% interfaces were collected (F1, F2 and F3 respectively). **(C)** Western blot analysis of collected fractions for the presence of M (7-10 kDa), prM (19-25 kDa) and E (53 kDa – green arrow) proteins using anti-WNV-EdIII combined with anti-WNV-M antiserum (1:20 000 each). Electron micrographs of F3 of **(D)** pTRAkc-ERH and **(E)** prM-E. VLPs of ~30 nm are indicated by pink arrows (scale bars = 100 nm or 50 nm). MW, the molecular weight marker.

3.3.3. Particle purification with maturation of plant homogenate at RT

Since performing the maturation of the clarified extract at 4°C did not improve on the results observed when the clarified extract was matured at RT, I speculated that besides temperature, the initial plant extract conditions might play a role in protein and/or particle yield and stability. Therefore, I investigated the effect of performing maturation of the plant homogenate instead of the clarified extract at both RT (Figure 3.1C) and 4°C (section 3.3.4, Figure 3.1D). Additionally, I increased the ultracentrifugation time to match what has previously been used for purification in other expression platforms (Ohtaki *et al.*, 2010).

N. benthamiana plants were co-infiltrated with pTRAkc-E, pEAQ-CNX and pTRAkc-prM, the leaves were harvested at 4 dpi and homogenised in 1x PI buffer. Putative particles were matured O/N at RT from the plant homogenate, clarified on the following day and subsequently concentrated through a 30% sucrose cushion. The pellet was resuspended followed by purification on a 20-60% discontinuous sucrose density gradient for 2 h 35 min (Figure 3.1C). The 30/40%, 40/50% and 50/60% interfaces were collected (Figure 3.4A-B; F1, F2 and F3 respectively) and evaluated for the presence of WNV M, prM and E proteins by western blot (Figure 3.4C) and VLPs by TEM.

Similar density gradient profiles were observed for both the vector-only control (pTRAkc-ERH) and prM-E (Figure 3.4A-B) samples, which were in contrast to the corresponding previous gradient profiles observed (Figure 3.2 and 3.3). A distinct green band at the 40/50% interface was observed whereas maturation of the clarified extract had a white band at this interface (specifically comparing pTRAkc-ERH and prM-E co-infiltrations with pTRAkc-prM). Evaluation of these fractions by western blot resulted in the detection of many non-specific bands in both the vector-only and the prM-E fractions (Figure 3.4C). However, no WNV-associated proteins were detected from the prM-E fractions, which was supported by the absence of particles visualised by TEM (data not shown). Based on this initial result, this purification process was not repeated. Simultaneously, however, I evaluated the effect of performing maturation of the plant homogenate instead of the clarified extract at 4°C (Figure 3.1D) and of which results were much more promising (section 3.3.4).

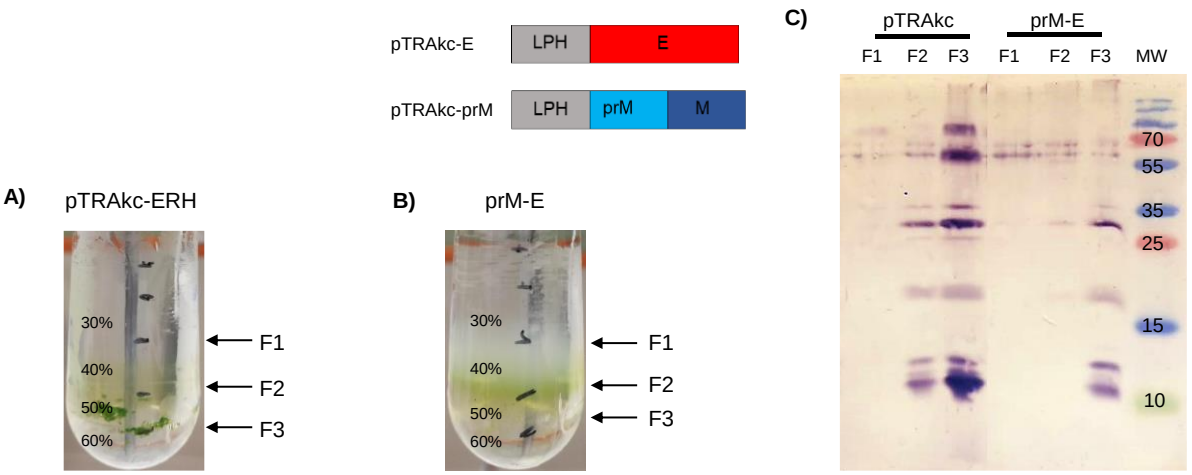

Figure 3.4. Putative WNV VLP purification from plants co-infiltrated with WNV E and prM recombinant plasmids and the human chaperone CNX. Particles were purified as depicted in Figure 3.1C with maturation of the plant homogenate at RT. **(A)** pTRAkc-ERH and **(B)** prM-E gradient profiles following ultracentrifugation. The 30/40%, 40/50% and 50/60% interfaces were collected (F1, F2 and F3 respectively). **(C)** Western blot analysis of collected fractions for the presence of M (7-10 kDa), prM (19-25 kDa) and E (53 kDa) proteins using anti-WNV-EdIII combined with anti-WNV-M antiserum (1:20 000 each). MW, the molecular weight marker.

3.3.4. Particle purification with maturation of plant homogenate at 4°C

As described previously, *N. benthamiana* plants were co-infiltrated with pTRAkc-E, pEAQ-CNX and pTRAkc-prM and the leaves were harvested at 4 dpi and homogenised in 1x PI buffer. Putative particles were matured O/N at 4°C in the plant homogenate, clarified on the following day and subsequently concentrated through a 30% sucrose cushion. The pellet was resuspended in a smaller volume and purified on a 20-60% discontinuous sucrose density gradient for 2 h 35 min (Figure 3.1D). The 30/40%, 40/50% and 50/60% interfaces were collected (Figure 3.5A-B; F1, F2 and F3 respectively), and evaluated for the presence of WNV M, prM and E proteins by western blot (Figure 3.5C) and VLPs by TEM (Figure 3.5D-E).

The density profiles for the vector-only control (pTRAkc-ERH) and prM-E differed in appearance (Figure 3.5A-B). As was observed in the purifications where the clarified extract was matured (Figure 3.2A and 3.3A), white bands were present at the gradient interfaces for the vector-only control (Figure 3.5A). In contrast, the prM-E interface bands were green with an increase in the intensity of the colour from F1 to F3 (Figure 3.5B). Western blot analysis of these fractions revealed dark E protein bands (Figure 3.5C – green arrow), faint prM protein bands (Figure 3.5C – blue arrow) and protein smears of the expected size for the M protein (Figure 3.5C – pink arrow). Electron microscopy of F1 revealed a mixture of pleomorphic particles of the expected size (~30 nm; Figure 3.5E – particles indicated by pink arrows) and

protein/particle aggregates. The western blot and TEM results were the most consistent between repeat purifications following this protocol. The E protein was consistently detected by western blot with variation in the detection of the prM and M proteins, and particles of ~30 nm, in the presence of protein/particle aggregates, were consistently visualised by TEM in F1 (30/40% interface).

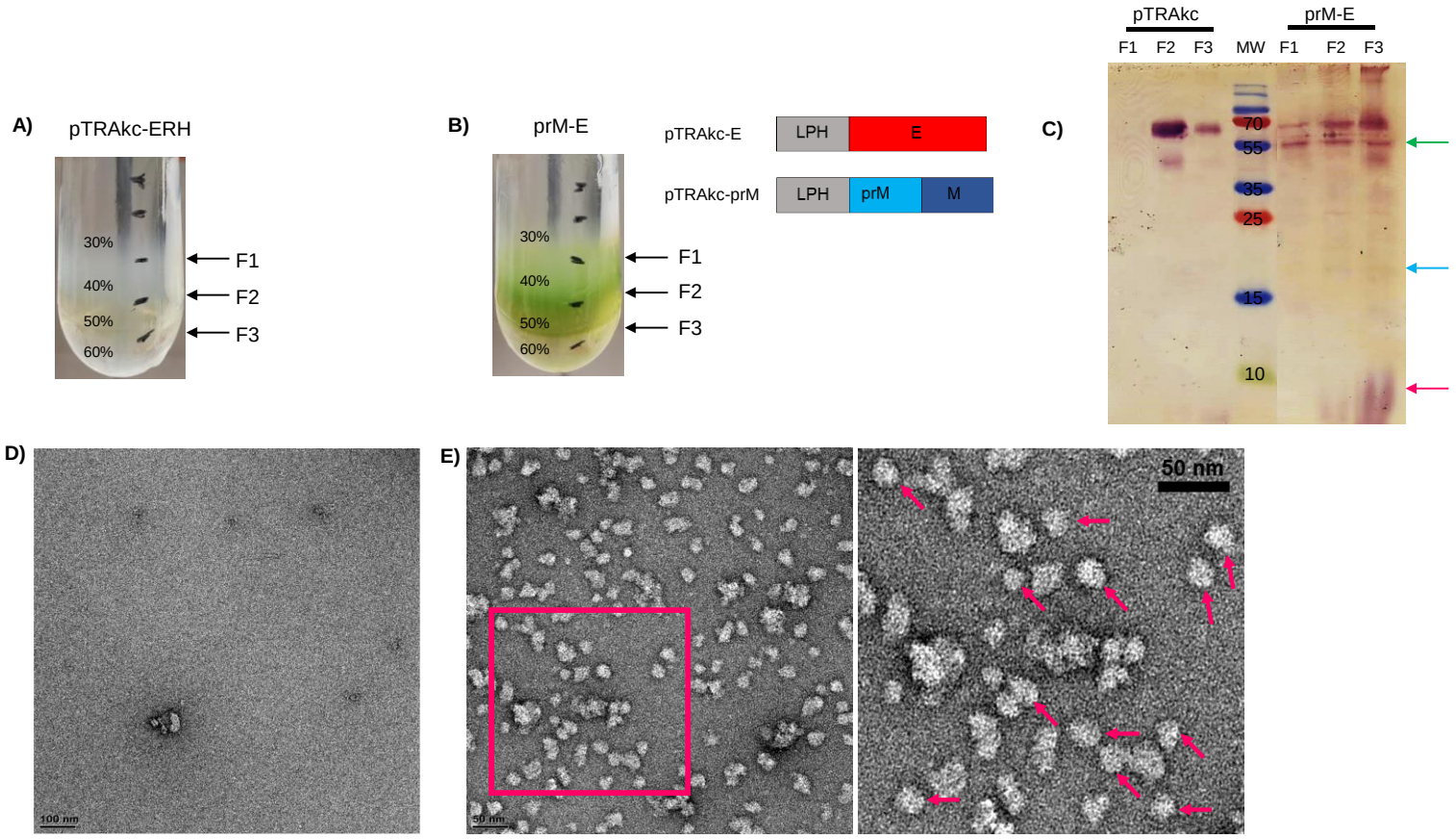

Figure 3.5. Representative results of putative WNV VLP purification from plants co-infiltrated with WNV E and prM recombinant plasmids and the human chaperone CNX. Particles were purified as depicted in Figure 3.1D with maturation of the plant homogenate at 4°C. **(A)** pTRAkc-ERH and **(B)** prM-E gradient profiles following ultracentrifugation. The 30/40%, 40/50% and 50/60% interfaces were collected (F1, F2 and F3 respectively). **(C)** Western blot analysis of collected fractions for the presence of M (7-10 kDa – pink arrow), prM (19-25 kDa – blue arrow) and E (53 kDa – green arrow) proteins using anti-WNV-EdIII combined with anti-WNV-M antiserum (1:20 000 each). Electron micrographs of F1 of **(D)** pTRAkc-ERH and **(E)** prM-E. VLPs of ~30 nm are indicated by pink arrows (scale bars = 100 nm or 50 nm). MW, the molecular weight marker.

3.3.5. Particle purification by PEG precipitation

I also investigated if it was possible to precipitate the particles using PEG (Figure 3.1E) for the removal of any free proteins prior to density gradient ultracentrifugation. I theorised that an additional PEG precipitation step could result in a cleaner preparation of VLPs, free of protein aggregates as seen when the plant homogenate was matured at 4°C (Figure 3.5C).

N. benthamiana plants were co-infiltrated with pTRAkc-E, pEAQ-CNX and pTRAkc-prM and the leaves were harvested at 4 dpi and homogenised in 1x PI buffer. The plant homogenate was clarified and PEG precipitated O/N at 4°C. The precipitate was collected by centrifugation, the pellet resuspended and subsequently purified on a 20-60% discontinuous sucrose density gradient for 2 h 35 min (Figure 3.1E). The 30/40%, 40/50% and 50/60% interfaces were collected (Figure 3.6A-B; F1, F2 and F3 respectively), and evaluated for the presence of WNV M, prM and E proteins by western blot (Figure 3.6C) and VLPs by TEM.

The vector-only control (pTRAkc-ERH) and prM-E samples had similar density profiles (Figure 3.6A-B) following ultracentrifugation. Faint white bands were visible for 30/40% and 40/50% interfaces. No WNV proteins were detected by western blot (Figure 3.6C) despite repeated purification using this method and no particles were observed by TEM (data not shown).

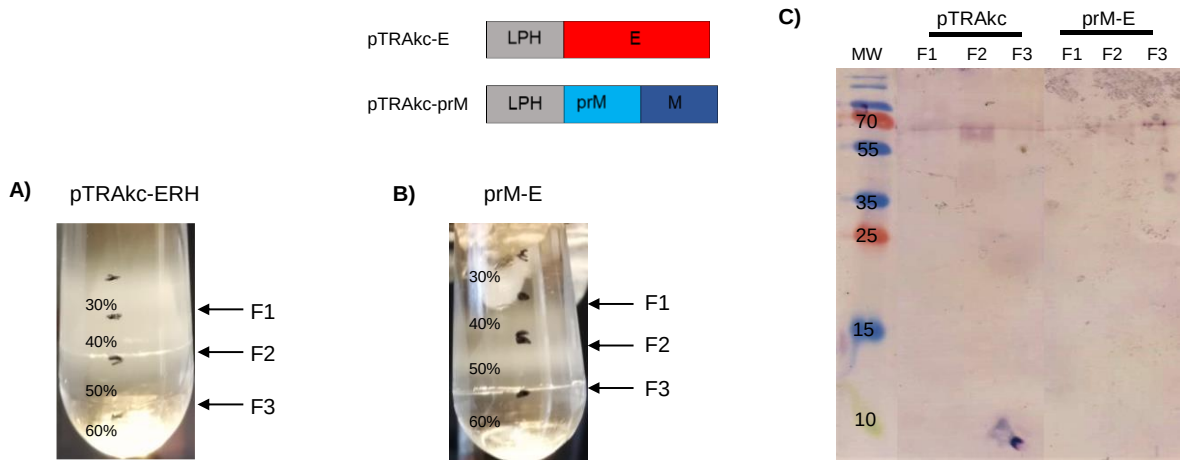

Figure 3.6. Putative WNV VLP purification from plants co-infiltrated with WNV E and prM recombinant plasmids and the human chaperone CNX. Particles were purified as depicted in Figure 3.1E by PEG precipitation. **(A)** pTRAkc-ERH and **(B)** prM-E gradient profiles following ultracentrifugation. The 30/40%, 40/50% and 50/60% interfaces were collected (F1, F2 and F3 respectively). **(C)** Western blot analysis of collected fractions for the presence of M (7-10 kDa), prM (19-25 kDa) and E (53 kDa) proteins using anti-WNV-EdIII combined with anti-WNV-M antiserum (1:20 000 each). MW, the molecular weight marker.

3.4. Discussion

West Nile VLPs are small non-infectious particles that assemble from the expression of the *prM* and *E* genes, and as such are highly favourable as vaccine candidates. These particles have been successfully produced in insect (Qiao *et al.*, 2004; Rebollo *et al.*, 2018b) and mammalian cells (Hanna *et al.*, 2005; Takahashi *et al.*, 2009; Ohtaki *et al.*, 2010; Ohtaki *et al.*, 2011; Taylor *et al.*, 2016). Additionally, the protective efficacy of WNV VLPs produced in insect cells has been demonstrated in immunised mice against WNV challenge (Qiao *et al.*, 2004) and VLPs produced in mammalian cells induced NAbs in immunised mice (Takahashi *et al.*, 2009) and protected them against lethal WNV infection (Ohtaki *et al.*, 2010). Although the immunogenicity results of these studies illustrate the potential of using these VLPs as candidate vaccines for WNV, they are not commercially available. However, the cost associated with the establishment, maintenance and running of cell-based expression systems does not make this a viable production option for LMIC. Plant production platforms are more favourable due to the lower cost involved in establishing facilities and their running costs, in addition to their safety and ease of scalability (Twyman *et al.*, 2003; Rybicki, 2009; Egelkrout *et al.*, 2012; Martinez *et al.*, 2012; Schillberg *et al.*, 2019; Fischer & Buyel, 2020). Several studies have illustrated the success of producing VLPs in *N. benthamiana* by expression of heterologous proteins (Maclean *et al.*, 2007; van Zyl *et al.*, 2016; Dennis *et al.*, 2018a; Mbewana *et al.*, 2018; Veerapen *et al.*, 2018; Gunter *et al.*, 2019; Marsian *et al.*, 2019) and due to the success of these studies, I proposed that the development of a method for the production of WNV VLPs in *N. benthamiana* could yield a potentially viable candidate vaccine.

The successful expression of the *prM* and *E* genes of a virulent South African WNV strain (components of WN VLPs) was demonstrated in chapter 2. Here, I investigated whether the co-expression of these genes led to the formation of VLPs *in planta*. Since all prM permutations expressed well on 4 dpi, I decided to evaluate all of them for VLP formation in case the potential structural difference between these permutations (SS or plant expression vector used) may influenced particle assembly.

As optimised in chapter 2, the pTRAkc-E, pEAQ-CNX and a prM construct (pTRAkc-prM, pEAQ-C_8-SS-prM, pTRAc-C_8-SS-prM or pTRAc-SS-prM) were co-infiltrated into *N. benthamiana* and leaves harvested and homogenised, the plant extract was clarified and the proteins/particles matured O/N at RT. VLPs produced in insect and mammalian cells were observed to have buoyant densities of ~1.11-1.16 g/cm^3 (Qiao *et al.*, 2004; Hanna *et al.*, 2005; Takahashi *et al.*, 2009; Ohtaki *et al.*, 2010) which corresponds to ~25-40% sucrose. Therefore, to concentrate the matured clarified extract I decided to pellet the particles through a 30% sucrose cushion followed by purification of the concentrated precipitate on a discontinuous

sucrose density gradient. Following ultracentrifugation, distinct bands at the 30/40%, 40/50% and 50/60% interfaces were observed, collected and evaluated for the presence of proteins and particles. Interestingly, protein detection for the different prM construct permutations used was not identical. All three proteins were observed for the permutations where pEAQ-C_8-SS-prM and pTRAkc-prM were used. Faint prM and E proteins were detected when co-infiltrated with pTRAc-SS-prM and only the E protein was detected when co-infiltrated with pTRAc-C_8-SS-prM. This could be as a result of the signal peptide used (LPH vs native SS with 8 amino acids of the C protein vs the native SS only) (Takahashi *et al.*, 2009), yet only the E protein was detected for the permutation where pTRAc-C_8-SS-prM was used and M, prM and E were detected when pEAQ-C_8-SS-prM was used, which suggests that the expression vector also plays a role in expression. A similar result was observed during optimisation (Chapter 2). A similar phenomenon was reported by Mbewana *et al*. who did not observe any RVFV chimaeric Gn protein when they infiltrated leaves with the chimaeric gene in the pTRAkc-ERH plant expression vector, but when they infiltrated the same chimaeric gene in the pEAQ-*HT* vector, protein expression was observed (Mbewana *et al.*, 2018).

Regardless of protein detection, fractions 1 and 2 of each co-infiltration permutation were evaluated for the presence of particles by TEM. VLPs of ~25-30 nm were observed for each of the permutations in at least one of these fractions, and were visually comparable to those produced in insect (Qiao *et al.*, 2004) and mammalian cells (Takahashi *et al.*, 2009; Ohtaki *et al.*, 2010). It has been suggested that the downstream translocation and topology of the prM-E polyprotein is affected by the signal domain in regulating the processing of the polyprotein and as such facilitating in the assembly, maturation and release of VLPs (Takahashi *et al.*, 2009). Takahashi and colleagues investigated the effect an extended or truncated signal sequence upstream or downstream of the NS2B-3 cleavage site would have on polyprotein processing (Takahashi *et al.*, 2009). The authors hypothesised that the construct containing the authentic signal sequence (in our study pTRAc-SS-prM) should result in the best yields regarding production, assembly, processing and secretion of VLPs. Interestingly, however, a mutant construct N-terminally truncated by three residues was the optimal producer of VLPs in mammalian cells. Similarly, based on our initial VLP purification the optimal producer of VLPs seemed to be the construct with the LPH signal peptide (pTRAkc-prM) and not the one with the native signal peptide (pTRAc-SS-prM). The LPH signal peptide is a plant-codon optimised murine mAB24 heavy chain signal sequence that targets proteins to the ER (Vaquero *et al.*, 1999), and has previously been shown to work well in plants (Maclean *et al.*, 2007; Margolin *et al.*, 2020). Reproducibility of the results for all co-infiltration permutations proved difficult, with inconsistent protein and particle observation.

Generally, structural viral proteins accumulate at modest levels when expressed in plants, however, viral glycoproteins express poorly and even below the threshold of detection in plants, for reasons not yet fully understood. Margolin and colleagues have hypothesised that one of the factors responsible for the poor expression could be the protein incompatibility with the endogenous plant chaperone proteins (Margolin *et al.*, 2018). To overcome this bottleneck, the authors have shown the effect that appropriate chaperones have on protein expression (Margolin *et al.*, 2020). No protein expression for several glycoproteins was observed from *N. benthamiana;* however, upon co-expression with either human chaperone CNX or CRT, detectable levels of proteins were observed by western blot. These results illustrate the importance of correct protein folding within the plant and the important role that these chaperones play in the secretory pathway. In conjunction with protein folding, correct protein glycosylation is also important. Hanna *et al.,* found that when they removed the glycosylation sites from either the prM or E proteins of WNV, there was a decrease in the release of VLPs in mammalian cells in comparison to when these proteins were glycosylated (Hanna *et al.*, 2005). In this study, the authors demonstrated the important impact N-linked carbohydrate structures have on particle assembly and release. Taking this into consideration, I believe that the poor reproducibility of our results may be due to poor protein stability. I established in chapter 2 that optimal protein expression for the E protein was in the presence of the human chaperone CNX. As I was co-infiltrating both these constructs with a membrane construct, I expected that the proteins were folding correctly; however, I do not know their glycosylation state.

In addition to protein folding and glycosylation, plant proteases also play a role in the stability of purified proteins. The recent annotation of *N. benthamiana's* core proteome has predicted that it contains 1243 putative proteases that include 165 aspartic proteases, 307 cysteine proteases, 498 serine proteases, 66 threonine proteases and 207 metalloproteases (Jutras *et al.*, 2020). Not all proteases are expressed in leaves but the most abundant leaf proteases are the papain-like cysteine proteases, subtilisins and pepsin-like aspartic proteases and these seem to affect recombinant proteins the most (Jutras *et al.*, 2020). Recombinant proteins expressed in plants are regularly targeted by these plant proteases and therefore result in complete or partial hydrolysis of recombinant proteins which affect their stability. To prevent further proteolytic activity following protein extraction from the leaf tissue I included 1x cOmplete™ EDTA-free protease inhibitor (Roche) in the extraction buffer. This protease inhibitor specifically inhibits serine and cysteine proteases; however, any proteases present in the leaf extract during maturation not inhibited by this protease inhibitor may still hydrolyse the WNV proteins, contributing to the instability of our purified product.

Given that I was performing the protein/particle maturation steps at room temperature, I considered that temperature could be responsible for protein and/or particle degradation and in turn, be responsible for the inconsistency in protein and particle detection due to their instability. Therefore, I theorised that performing the maturation step at 4°C instead of RT might resolve the problems I was facing regarding reproducibility specifically in increasing the life-span of the protease inhibitor activity. To simplify the process of optimising VLP purification, a single prM construct was selected for co-infiltration instead of continuing with four co-infiltration permutations. The pTRAkc-prM construct was selected based on the results observed for the first purification method, where western blot analysis showed the detection of the M, prM and E proteins and TEM revealed several VLPs. Although co-infiltration with pEAQ-C_8-SS-prM yielded similar results, more non-specific bands were detected by western blot and fewer particles were observed per frame of view than when co-infiltrated with pTRAkc-prM.

Purification of VLPs from plants co-infiltrated with pTRAkc-E, pEAQ-CNX and pTRAkc-prM was performed with the maturation step at 4°C instead of RT and following ultracentrifugation, the same fractions were collected as before. Once more, duplication of these results was inconsistent, with only the E protein being detected for one purification round and the M and prM proteins remained undetected for all purification repeats. Moreover, particles of the expected 25-30 nm size were only observed for a single purification experiment, once again rendering this purification process unreliable due to the lack of reproducibility.

Next, I considered whether the physiological conditions of the plant extract could be affecting the protein and/or particle stability since maturation of the clarified extract at 4°C did not improve VLP purification but rather seemed to be less effective than maturation of the clarified extract at RT. Consequently, I investigated the effect of performing the maturation on the plant homogenate instead of the clarified extract at both RT and 4°C and adjusted the discontinuous gradient ultracentrifugation time from 1 h to 2h 35 min to correspond with the conditions of Ohtaki *et al*. (2010).

The conditions between the clarified extract and plant homogenate are expected to be different: as all the plant material is removed for the clarified extract there should be fewer plant proteins and proteases present than in the plant homogenate, where the homogenised plant material is present. The disruption of the plant cells during homogenisation results in the release of the WNV target proteins, plant proteins and proteolytic enzymes from the different compartments of the host cell. During the clarification of the homogenised extract, most of these contaminants are removed; however, it has been shown that some proteases might co-purify with the target protein (Schiermeyer, 2020). However, the presence of the homogenised plant material in the plant homogenate extract could allow for the secretion of insoluble WNV

proteins from the plant material during the maturation step, while this is not possible for the clarified extract. A possible step to include for the reduction of the plant proteins and inactivation of proteases is a short heat treatment prior to the homogenisation of the leaf tissue (Schiermeyer, 2020), which I could explore in future purifications.

Apart from the centrifugation time, the maturation state (plant homogenate) and the maturation temperatures (RT vs 4°C), the purification process was performed as before. When the plant homogenate was matured at RT, no WNV proteins were detected by western blot and no VLPs were observed by TEM. The maturation of the plant homogenate at 4°C, however, had comparable results to when the clarified extract was matured at RT. Western blot analysis revealed the presence of the M, prM and E proteins and when the purification was repeated both the prM and E proteins were detected. Repeat purifications also presented similar TEM results of pleomorphic VLPs of 25-30 nm in F1 with the addition of protein/particle aggregates. With an increase in the fraction densities (F2 and F3) less individual particles were present with an increase in aggregates (data not shown). Takahashi and colleagues observed a similar effect when they purified WNV VLPs from mammalian cells (Takahashi *et al.*, 2009). Following density gradient ultracentrifugation, VLPs of ~30 nm were visualised at a density of 1.11 g/cm^3 and in a lower fraction with a density of 1.16 g/cm^3 they observed irregularly shaped particles (~20 nm) that also seemed to aggregate and they proposed that these consist of E protein aggregates. The authors stated that it is possible that the VLPs may be damaged during the purification process and as such convert into aggregates of the E protein, which is possibly what I observed. Interestingly, VLPs produced from maturation of the plant homogenate at 4°C more closely resembled those of DENV VLPs produced in *N. benthamiana* with their 'fuzzy' circular shape (Ponndorf *et al.*, 2020), than those produced in insect (Qiao *et al.*, 2004; Rebollo *et al.*, 2018b) and mammalian cells (Takahashi *et al.*, 2009; Ohtaki *et al.*, 2010; Ohtaki *et al.*, 2011) with their clear regular shape.

The purification of WNV VLPs from *N. benthamiana* was most consistent when matured in the plant homogenate at 4°C. Once a reproducible purification process was established where both WNV proteins and VLPs were regularly observed, I investigated whether I could refine the process for the removal of the protein/particle aggregates to obtain a purer VLP sample. A PEG precipitation step was performed followed by density gradient ultracentrifugation for further purification of the precipitate. Unexpectedly, the addition of the PEG precipitation step resulted in no protein or particle detection. Since the PEG precipitation was performed on the clarified extract overnight at 4°C, the lack of WNV proteins or particles could be because the maturation step was not performed in the plant homogenate first and subsequently followed by a PEG precipitation step. This is a strategy to investigate in future studies.

Various non-enveloped VLPs have been successfully produced in plants (Maclean *et al.*, 2007; Thuenemann *et al.*, 2013; Peyret *et al.*, 2015; van Zyl *et al.*, 2016; Dennis *et al.*, 2018a; Dennis *et al.*, 2018b; Veerapen *et al.*, 2018; Gunter *et al.*, 2019; Marsian *et al.*, 2019). In the case of enveloped VLPs, however, there is a limited number of plant-produced examples. These include Influenza virus (D'Aoust *et al.*, 2008; Lomonossoff & D'Aoust, 2016), Rift valley fever virus (Mbewana *et al.*, 2018) and most recently, dengue virus (Ponndorf *et al.*, 2020). The few published studies of enveloped VLPs produced *in planta* suggests that these are inherently more difficult to produce than non-enveloped VLPs, which could explain the difficulty I experienced in the purification of WNV VLPs.

In conclusion, I demonstrated that WNV VLPs can be produced in *N. benthamiana* from the co-expression of the WNV *prM* and *E* genes in the presence of the human chaperone protein calnexin, and determined a moderately reproducible purification process for the isolation of these particles. However, the difficulties experienced during the optimisation of this purification process and the extremely low VLP yields obtained could potentially lead to difficulties with scaling up for commercialisation purposes. I considered an alternative approach for the development of a candidate vaccine, based on antigen-display technology. This approach, which may be more amenable to yielding immunogenic WNV proteins in tobacco, is described in Chapter 4.

Chapter 4:

Design, transient expression and characterisation of Spy-VLPs

4.1. Introduction

The WNV envelope protein monomer consists of three structurally distinct domains: these are EdI, EdII and EdIII (Figure 1.3). EdI is the central unit that acts to stabilise the overall orientation of the E protein and plays a role in its conformational changes; EdII contains the fusion-loop peptide involved in virus-membrane fusion during virus entry, and EdIII is the immunodominant epitope that induces NAbs (Mukhopadhyay *et al.*, 2005; Zhang *et al.*, 2017; Campos *et al.*, 2018). Numerous studies have been performed on WNV NAbs that bind to different epitopes across EdI, EdII and EdIII (Beasley & Barrett, 2002; Nybakken *et al.*, 2005; Oliphant *et al.*, 2005; Oliphant *et al.*, 2006; Goo *et al.*, 2019), but data from murine mAbs suggests that EdIII is the best target for NAbs (Heinz & Stiasny, 2012). In addition, it has been shown that EdIII does not play a role in antibody-dependent enhancement (ADE) when inside cells expressing Fc γ receptors, in comparison to EdI and EdII, which do (Oliphant *et al.*, 2006; Brandler & Tangy, 2013). Consequently, EdIII is a favoured target domain for the development of recombinant vaccines (Martina *et al.*, 2008; Alonso-Padilla *et al.*, 2011).

He *et al*. produced WNV EdIII in *N. benthamiana* by transient expression (He *et al.*, 2014). They observed the highest levels of EdIII expression when it was targeted to the ER rather than when targeted to the cytosol or chloroplast, and they could easily purify EdIII by pH precipitation and nickel affinity chromatography, with an average accumulation of ~73 µg/g FLW. Immunogenicity studies in mice showed that plant-produced EdIII elicited an equivalent potency humoral response against WNV compared with *E. coli*-produced EdIII. In a follow-up study, the authors illustrated that plant-produced EdIII elicited potent neutralisation against WNV, with a 44-70% reduction in WNV infection in mice treated with serum from mice immunised with plant-produced EdIII. In addition to the plant-produced EdIII protecting mice against lethal challenge, no ADE was observed for ZIKV and DENV (Lai *et al.*, 2018).

Vaccines based on epitopes have the drawback that multiple injections and/or strong adjuvants are required for the induction of NAbs (Martina *et al.*, 2008; Alonso-Padilla *et al.*, 2011; He *et al.*, 2014; Lai *et al.*, 2018). Furthermore, the WNV EdIII antigen is a small polypeptide that is susceptible to proteolytic degradation, thus limiting the extent of the immune response stimulated (Thrane *et al.*, 2016). However, this could be resolved with the

use of antigen-display technology (section 1.4.3.5), by linking the EdIII antigen to VLPs, which are suited to stimulating a broad immune response due to the multiple arrays of antigen presented to the immune system. Chen and colleagues fused WNV EdIII to the 3' end of the hepatitis B surface antigen (HBcAg) gene and transiently expressed HBcAg VLPs displaying WNV EdIII in *N. benthamiana* (Chen *et al.*, 2011). Assembly of these chimaeric VLPs was confirmed, with high expression levels and they induced potent EdIII specific B and T cell responses in mice. Besides genetic linking, antigens can also be post-translationally linked to VLPs as demonstrated by Spon and colleagues who conjugated purified WNV EdIII protein to purified AP205 VLPs (Spohn *et al.*, 2010). Upon immunization, the EdIII-AP205 conjugate candidate vaccine induced virus NAbs and protected mice from WNV challenge.

The above examples demonstrate the direct linking of antigen to VLPs at either the genetic or protein level. Another approach to achieve conjugation is the use of peptides that have the affinity to form bonds with each other, such as the SpyTag/SpyCatcher (ST/SC) system (section 1.5). The ST/SC system is based on the affinity of the ST and SC peptides to spontaneously form an irreversible isopeptide bond (Figure 1.8). The coupling of ST and SC by the formation of an amide bond has been demonstrated to occur at a range of temperatures (4-37°C), pH values (5-8), buffers and in the presence of non-ionic detergents (Zakeri *et al.*, 2012), demonstrating the versatility of this system (Reddington & Howarth, 2015; Brune & Howarth, 2018).

Thrane *et al*. used the ST/SC technology to develop a Spy-VLP platform (section 1.5, Figure 1.9) (Thrane *et al.*, 2016). They fused the ST and SC peptides at the N terminus of the bacteriophage AP205 *C* gene which, upon expression, yields particles of ~ 36 nm and ~ 43nm, respectively, that display 180 ST/SC peptides on their surface. They successfully coupled 11 different antigens genetically fused to either ST or SC, to the Spy-VLPs *in vitro* that were produced in insect and bacterial cells and observed an average display capacity of 65%. This technology has also been used for the development of candidate vaccines for malaria (Brune *et al.*, 2016; Janitzek *et al.*, 2016; Singh *et al.*, 2017; Yenkoidiok-Douti *et al.*, 2019; Harmsen *et al.*, 2020) and breast cancer (Palladini *et al.*, 2018) predominantly produced in bacterial and insect cells. Janitzek *et al.* demonstrated the potential of this Spy-VLP system for the development of a combinatorial vaccine (Janitzek *et al.*, 2019). The authors genetically fused the *L2* gene of HPV and the SC peptide at the 5' and 3' ends of the AP205 *C* gene, respectively, and the ST peptide to the N terminus of the VAR2CSA *P. falciparum* protein. These constructs were expressed in *E. coli* and the purified products were coupled *in vitro* which resulted in the formation of VLPs that displayed both the HPV L2 and VAR2CSA antigens at high density. High levels of anti-L2 and anti-VAR2CSA IgGs were elicited in mice vaccinated with the combinatorial vaccines.

These studies illustrate the promise of this system for the development of VLP-based vaccines. This technology presents the possibility for quick candidate vaccine production in the instance of disease outbreaks as well as the opportunity for the development of multivalent vaccines. I propose that the Spy-VLP system is a promising platform for the production of candidate vaccines for flaviviruses such as WNV due to the potential of using EdIII as the display antigen.

This chapter describes the design, cloning, transient plant expression and coupling of WNV-EdIII to Spy-VLPs. Two SC-linked *EdIII* constructs were generated; one with the SC peptide at the N- and the other at the C-terminus of the *EdIII* gene in the plant expression vector pTRAkc-ERH. SC-linked EdIII protein expression was optimised by co-expression with human chaperones (CNX and CRT), and protein extraction with the evaluation of various extraction buffers. Finally, large scale protein purification was conducted as described by He *et al*. 2014. Spy-VLPs were produced from pEAQ-ST-AP205 as optimised by Dr Sue Dennis (BRU, UCT). Coupling of the ST-AP205 particles with SC-linked EdIII was tested using 3 different approaches.

4.2. Materials and Methods

4.2.1. In-Fusion® cloning of SC-linked *EdIII*

4.2.1.1. Fragment generation

The *E* gene was modified by amplification for: i) the isolation of the *EdIII* domain region, ii) the fusion of a 6x His tag and 15 bp overlap with the pTRAkc-ERH vector on the one terminus and, iii) the fusion of a GGGGS GGGGS flexible linker (Gly-linker) on the other terminus of *EdIII* (Figure 4.1).

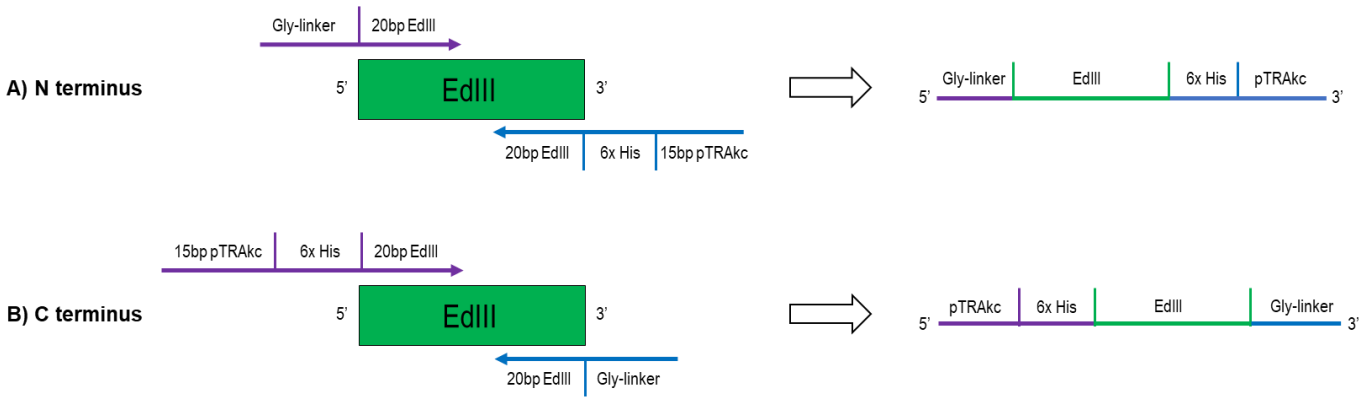

Figure 4.1. Schematic representation of In-fusion *EdIII* fragment generation by PCR amplification. **(A)** *EdIII* intermediate fragment for the attachment of the SC peptide to the N terminus. **(B)** *EdIII* intermediate fragment for the attachment of the SC peptide to the C terminus. Purple arrows represent forward primers and blue arrows represent reverse primers to be used. Generated fragments are illustrated after the black arrow.

The SC peptide was amplified from the pEAQ-SC-AP205 construct (available in BRU library) and then modified by amplification for i) the fusion of a 15 bp overlap with the pTRAkc-ERH vector or, ii) the fusion of a Gly-linker (Figure 4.2).

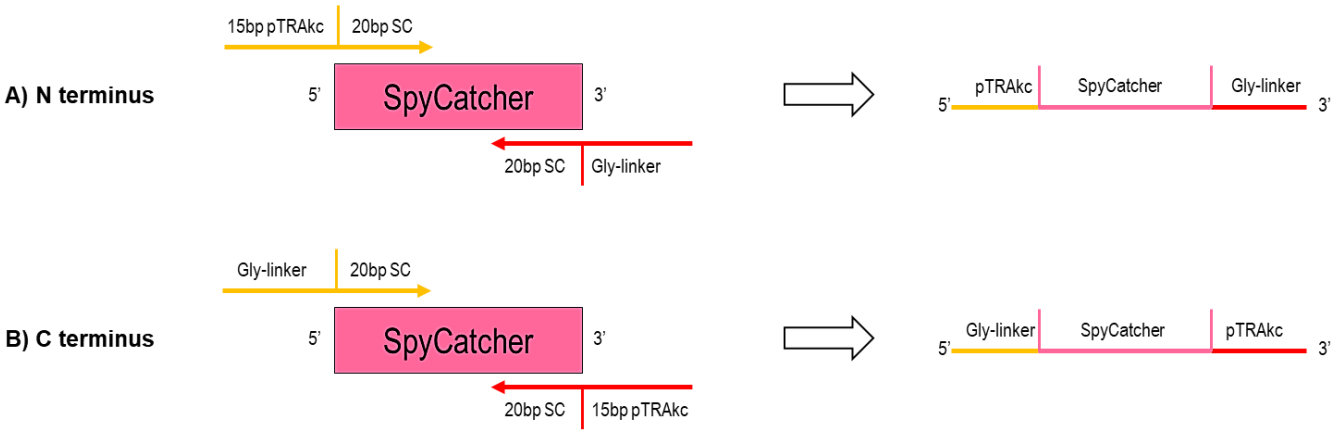

Figure 4.2. Schematic representation of In-fusion SC fragment generation by PCR amplification. **(A)** SC intermediate fragment for the attachment to the N terminus of *EdIII*. **(B)** SC intermediate fragment for the attachment to the C terminus of *EdIII*. Yellow arrows represent forward primers and red arrows represent reverse primers to be used. Generated fragments are illustrated after the black arrow.

Fragments illustrated in Figure 4.1 and 4.2 were generated by PCR amplification of 10 ng template DNA with primers specified in Table 4.1 (Appendix B: Table 3) using Phusion Hot Start II High-fidelity DNA Polymerase (Thermo Scientific) according to manufacturer's instructions. Amplified fragments were purified from agarose gels using the Macherey-Nagel™ NucleoSpin™ Gel and PCR Clean-up kit (Macherey-Nagel™) per manufacturer's instructions and stored at -20°C until further use.

Table 4.1. Primers used to generate *EdIII* and SC DNA fragments.

Gene	Primers	Ta (°C)	Size (bp)	5' addition	3' addition	Fragment
E	Fp1 Rp1	65	~360	pTRAkc-ERH 6x His	Gly-linker	pTRAkc-His-EdIII-Gly
SC	Fp2 Rp2	65	~400	Gly-linker	pTRAkc-ERH	Gly-SC-pTRAkc
E	Fp4 Rp4	65	~360	Gly-linker	pTRAkc-ERH 6x His	Gly-EdIII-His-pTRAkc
SC	Fp3 Rp3	65	~400	pTRAkc-ERH	Gly-linker	pTRAkc-SC-Gly

4.2.1.2. Fragment assembly

EdIII and SC DNA fragments generated (section 4.2.1.2) were assembled (Figure 4.3) for In-Fusion® cloning into the pTRAkc-ERH plant expression vector.

Fragments were assembled as detailed in Table 4.2 by PCR amplification and gel purification of generated fragments as described in section 4.2.1.1. Assembled fractions were stored at -20°C until further use.

Table 4.2. Primers used for fragment assembly of SC and *EdIII*.

SC terminus	Fragments	Primers	Ta (°C)	Size (bp)	Assembled Fragment
N	Gly-EdIII-His-pTRAkc pTRAkc-SC-Gly	Fp4 Rp3	65	~730	pTRAkc-SC-Gly-EdIII-His-pTRAkc
C	pTRAkc-His-EdIII-Gly Gly-SC-pTRAkc	Fp1 Rp2	65	~730	pTRAkc-His-EdIII-Gly-SC-pTRAkc

4.2.1.3. In-Fusion® reaction

Assembled fragments illustrated in Figure 4.3 and listed in Table 4.2 were ligated into linearised pTRAkc-ERH (section 2.2.4) and transformed in Stellar™ competent *E. coli* cells (Clontech) using the In-Fusion® HD Cloning kit (Separations) as per manufacturer's instructions (Figure 4.4).

E. coli colonies were screened for recombination by colony PCR using primers listed in Table 4.2 and recombinant plasmids were isolated as described in section 2.2.3 and all constructs verified by sequencing. Recombinant pTRAkc-ERH plasmids were electroporated into *A. tumefaciens* GV3101::pMP90RK cells and recombinant colonies screened as described in section 2.2.5.

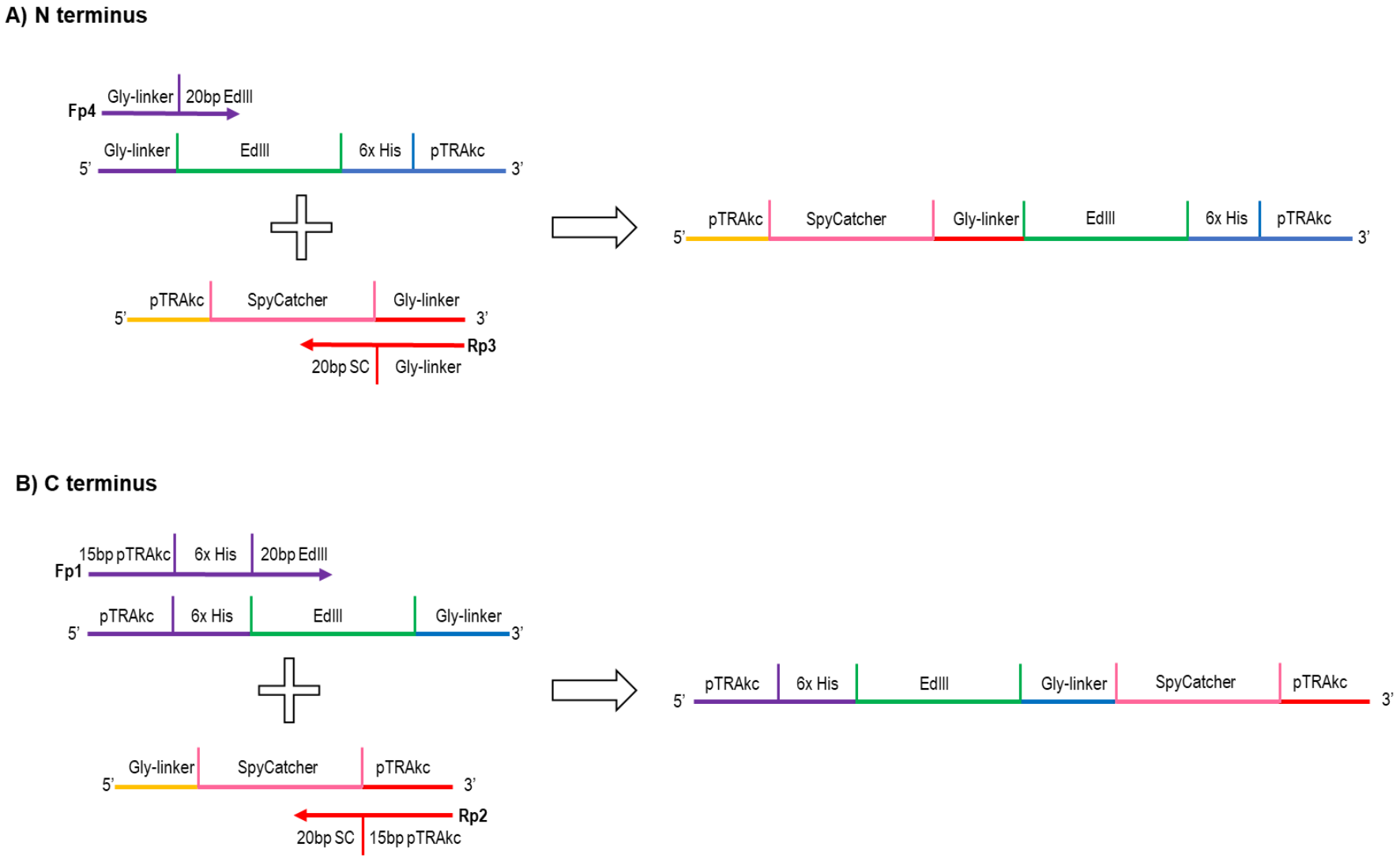

Figure 4.3. Schematic representation of In-fusion® fragment assembly by PCR amplification. **(A)** Assembly of SC and *EdIII* fragments to generate EdIII-SC N terminal fragment using primers; Fp4 and Rp3. **(B)** Assembly of SC and *EdIII* fragments to generate SC-EdIII C terminal fragment using primers; Fp1 and Rp2. Generated fragments are illustrated to the right of the black arrow

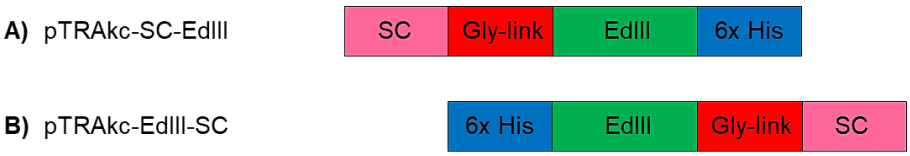

Figure 4.4. Schematic representation of SC-linked *EdIII* constructs in plant expression vector pTRAkc-ERH. **(A)** pTRAkc-SC-EdIII: *EdIII* with the SC peptide on the N terminus. **(B)** pTRAkc-EdIII-SC: *EdIII* with the SC peptide on the C terminus.

4.2.2. Small scale expression of SC-linked EdIII in *N. benthamiana*

A. tumefaciens-mediated transient small scale expression was performed as described in section 2.2.6 at optical densities as described in Appendix D: Table 5.

4.2.2.1. SC-linked EdIII expression

A. tumefaciens pTRAkc-SC-EdIII and pTRAkc-EdIII-SC constructs were each infiltrated at two OD_{600}: 0.25 and 0.5. Infiltrated leaves were harvested 4, 5 and 6 dpi and protein extracted as described in section 2.2.7.1 using 1x PBS (pH 7.4). Following maturation, pellet and supernatant crude extracts were evaluated for protein expression by western blot as described in section 2.2.8.

4.2.2.2. Co-expression of SC-EdIII with the human chaperone CNX

A. tumefaciens pTRAkc-SC-EdII was infiltrated with and without pEAQ-CNX at an OD_{600} 0.5 each. Infiltrated leaves were harvested 4, 5 and 6 dpi, and protein extracted and evaluated by western blot as described in section 4.2.2.1.

4.2.2.3. Optimal extraction buffer determination

A. tumefaciens pTRAkc-SC-EdIII and pTRAkc-EdIII-SC constructs were each co-infiltrated with pEAQ-CNX each at an OD_{600} 0.5. Infiltrated leaves were harvested at 4 dpi and protein extracted as described in section 2.2.7.1 comparing buffers: 1x PBS (pH 7.4), 1X PBS (pH 6.0) and Tris buffer [100 mM Tris.HCl (pH 8.0), 150 mM NaCl, 1x cOmplete™ EDTA-free protease inhibitor (Roche)]. Extracted protein was evaluated by western blot as described in section 2.2.8.

4.2.2.4. CNX vs CRT co-expression with SC-linked EdIII

A. tumefaciens pTRAkc-SC-EdIII and pTRAkc-EdIII-SC constructs were each co-infiltrated with pEAQ-CNX and pEAQ-CRT each at an OD_{600} 0.5. Infiltrated leaves were harvested at 4 dpi and protein extracted as described in section 2.2.7.1 using Tris buffer. Extracted protein was evaluated by western blot as described in section 2.2.8.

4.2.3. Large scale expression and purification of SC-linked EdIII from *N. benthamiana*

Large scale infiltration was performed as described in section 3.2.1. pTRAkc-SC-EdIII and pTRAkc-EdIII-SC were co-infiltrated with pEAQ-CRT each at an OD_{600} 0.5 and leaves harvested at 4 dpi. Proteins were purified as described by He *et al.* (2014) with modifications. Leaves were homogenised in 2 volumes of Tris buffer using an IKA® T-25 ULTRA-TURRAX® (Sigma-Aldrich) homogeniser. Crude extracts were matured O/N at 4°C with agitation and filtered through 2 layers of MiraCloth™ (Merck). The filtered extract was clarified by centrifugation at 18 000 *x* g for 30 min at 4°C. The pH of the clarified extract was adjusted to 5.0 and the extract centrifuged at 18 000 *x* g for 30 min at 4°C and the supernatant recovered. The pH of the recovered supernatant was adjusted back to 8.0 and subjected to another centrifugation. The supernatant was recovered, filtered through a 0.45 µM filter and then loaded on a 5 mL nickel affinity column (HisTrap™ HP, GE Healthcare) and purified with an automated fast protein liquid chromatography (FPLC) system (ÄKTA Explorer™, GE-Healthcare). The column was equilibrated with binding buffer [100 mM Tris.HCl (pH 8.0), 0.5 M NaCl] and SC-linked EdIII protein was eluted with elution buffer [100 mM Tris.HCl (pH 8.0), 0.5 M NaCl, 0.5 M imidazole). Five mililiter fractions were collected with a fraction collector and an absorbance reading at 280 nm determined for each fraction.

The purity of SC-linked EdIII proteins was determined and quantified by Coomassie blue-staining [0.1% Coomassie Brilliant Blue R-250, 50% methanol and 10% glacial acetic acid] of bands separated by SDS-PAGE. Quantification of SC-linked EdIII protein bands was performed using GeneTools software (Synoptics Inc.) as determined from a standard bovine serum albumin [(BSA) Separations] curve constructed from various concentrations (0.5 – 0.016 µg/µL). Purified fractions were stored at 4°C for further analysis.

4.2.4. ST-AP205 VLP purification from *N. benthamiana*

AP205 VLPs were generated and purified according to methods previously optimised by Dr Sue Dennis (BRU, UCT). pEAQ-ST-AP205 was infiltrated at an OD_{600} 0.25 and large scale infiltration was performed as described in section 3.2.1. Leaves were harvested at 4 dpi and homogenised in 2 volumes of 1x PBS (pH 7.4) using a Moulinex™ juice extractor. The leaf pulp was incubated with the extracted juice at 4°C for 30 min with agitation. The crude extract was filtered through 4 layers of MiraCloth™ (Merck) and clarified by centrifugation at 25 000 *x* g for 20 min at 4°C.

ST-AP205 VLPs were purified by ultracentrifugation through a discontinuous iodixanol (Optiprep™, Sigma Aldrich) density gradient. A 7 mL step gradient consisting of 23%, 29% and 35% iodixanol densities (2, 3 and 2 mL respectively) diluted in extraction buffer was layered under ~30 mL clarified plant extract and centrifuged at 174 586 *x* g for 2 h at 4°C in an SW32 Ti rotor (Beckman). Five-hundred microliter fractions were collected from the bottom of the tube and 30 µL of each was evaluated by western blot and Coomassie blue-stained SDS-PAGE. VLP proteins were quantified by gel densitometry and particles (~30 nm) visualised by TEM as described in section 3.2.3.

4.2.5. *In vitro* coupling of purified ST-AP205 VLPs and SC-linked EdIII

Purified ST-AP205 VLPs and SC-linked EdIII proteins stored at 4°C, were coupled at 1:1, 1:2, 1:5 and 1:10 molar ratios, respectively O/N at 4°C. ST-AP205 VLPs and SC-linked EdIII antigens were mixed with 1x cOmplete™ EDTA-free protease inhibitor (Roche) and coupling buffer [0.05 M MES, 0.05 M NaCl, 2.7 mM KCl, 10 mM NaH_2PO_4, 1.8 mM KH_2PO_4 (pH 6.4)]. Coupling controls included individual ST-AP205, SC-EdIII and EdIII-SC reactions. Reactions were evaluated for complex formation by Coomassie blue-stained SDS-PAGE.

Purified ST-AP205 VLPs and EdIII-SC proteins were coupled as described above with molar ratios of 1:1, 1.5:1, 2:1, 1:1.5 and 1:2 ST-AP205:EdIII-SC. Reactions were evaluated for complex formation by western blot with polyclonal rabbit anti-ST-AP205 and polyclonal rabbit anti-WNV-EdIII sera (Appendix E: Table 6).

4.2.6. ST-AP205 and EdIII-SC co-expression

pEAQ-ST-AP205, pTRAkc-EdIII-SC and pEAQ-CRT were co-infiltrated at OD_{600} 0.3 each as described in section 3.2.1. Leaves were harvested 5 dpi and VLPs purified as described in section 4.2.4 with a single modification. Homogenised leaf pulp and juice were incubated at

4°C for 1 h with agitation before clarification. Collected fractions were analysed by western blot with polyclonal rabbit anti-ST-AP205 and polyclonal rabbit anti-WNV-EdIII sera.

Total EdIII protein was quantified for fractions 6-9 by indirect ELISA. Ninety-six-well Maxisorp® microtitre plates (Nunc) were coated in triplicate with 100 µL/well 20 ng, 10 ng, 5 ng, 2.5 ng and 1.25 ng *E. coli*-produced WNV EdIII protein diluted in coating buffer [10 mM Tris (pH 8.5)] to generate a standard curve. The same was done for fractions 6-9 and the plate incubated O/N at 4°C. The plate was blocked with TBS blocking buffer [3% BSA in 1x TBS (50 mM Tris, 150 mM NaCl, pH 7.5)] for 1 h at 37°C after which it was washed four times with 1x TST [1x TBS (pH 7.5), 0.05% Tween®20]. Polyclonal rabbit anti-WNV-EdIII serum was diluted to 1:5000 in TBS blocking buffer and 100 µL added to each well and the plate incubated for 1 h at 37°C. Blank wells containing no antibody were included as a background control. The plate was washed as before and 100 µL of goat anti-rabbit IgG alkaline phosphatase conjugate (Sigma) diluted to 1:10 000 in blocking buffer was added to each well and incubated at 37°C for 1 h. Following incubation, the plate was washed four times with 1x TBS (pH 9) buffer and 200 µL SIGMAFAST™ p-Nitrophenyl phosphate (pNPP, Sigma) was added per well. The plate was developed in the dark for 30 min after which the absorbance was measured at 405 nm on a BIO-TEK® Powerwave XS microtitre plate reader.

Equal amounts of EdIII protein in fractions 6-9 was evaluated by western blot with polyclonal rabbit anti-ST-AP205 and polyclonal rabbit anti-WNV-EdIII sera.

4.2.7. ST-AP205 and EdIII-SC co-extraction

pEAQ-ST-AP205 and pTRAkc-EdIII-SC were infiltrated as described in sections 4.2.4 and 4.2.3, respectively. Leaves were harvested 5 dpi and a 1:1 ratio of FLW was combined for homogenisation, purification and quantification as described in section 4.2.6.

4.2.8. ST-AP205 and EdIII-SC co-extraction optimisation

4.2.8.1. Density gradient ultracentrifugation

pEAQ-ST-AP205 and pTRAkc-EdIII-SC were infiltrated as described in sections 4.2.4 and 4.2.3, respectively. Leaves were harvested 4 dpi and 1:2 FLW ST-AP205/EdIII-SC were homogenised in 2 volumes of 1x PBS (pH 7.4) using a Moulinex™ juice extractor. The leaf pulp was incubated with the extracted juice at 4°C O/N with agitation to allow for coupling to occur. The crude extract was filtered through 4 layers of MiraCloth™ (Merck) and clarified by centrifugation at 25 000 *x* g for 20 min at 4°C. Spy-VLPs were purified by ultracentrifugation

as described in section 4.2.4, the 29% fraction collected, diluted to 10 mL in 1x PBS (pH 7.4) and layered over a 10-40% linear iodixanol (Optiprep™, Sigma Aldrich) density gradient and centrifuged as before. One milliliter fractions were collected from the bottom of the tube and 25 µL of each was evaluated by western blot.

4.2.8.2. Extraction ratios

pEAQ-ST-AP205 and pTRAkc-EdIII-SC were infiltrated as described in sections 4.2.4 and 4.2.3, respectively. Leaves were harvested 4 dpi and 1:1, 1:2, 1:3 and 1:4 FLW ST-AP205/EdIII-SC were homogenised in 2 volumes of 1x PBS (pH 7.4) using a Moulinex™ juice extractor. The leaf pulp was incubated with the extracted juice at 4°C O/N with agitation to allow for coupling. Spy-VLPs were purified as described in section 4.2.4. and 1 mL fractions collected from the bottom of the tube. Total EdIII protein in fractions 3-5 was determined by indirect ELISA as described in section 4.2.6 and evaluated by western blot with polyclonal rabbit anti-ST-AP205 and polyclonal rabbit anti-WNV-EdIII sera; VLPs were visualised by TEM as described in 3.2.3.

The coupling efficiencies (percentage occupancy of a whole VLP's binding sites – assuming that coupling occurs at the same rate for every peptide-motif) were estimated by densitometric analysis of anti-ST-AP205 western blots using GeneTools software (Synoptics Inc.). The intensity value of the AP205:EdIII complex protein band (41.5 kDa) was divided by the intensity value of the ST-AP205 protein band (16.5 kDa) before isopeptide formation with EdIII-SC and multiplied by 100 to estimate the percentage coupling efficiency.

$$\%\ Coupling\ efficiency = \frac{AP205{:}\ EdIII\ intensity\ value}{ST\ AP205\ monomer\ intensity\ value\ before\ coupling} \times 100$$

The antigen-display capacity (number antigens/VLP) was estimated by multiplying the coupling efficiency with 180.

$$Antigen\ display\ capacity = coupling\ efficieny\ \times 180$$

The yield of coupled AP205:EdIII was determined by densitometric analysis of anti-WNV-EdIII western blots using GeneTools software (Synoptics Inc.) with an *E. coli* produced EdIII protein standard.

4.3. Results

4.3.1. Confirmation of SC-linked *EdIII* In-Fusion® constructs

The In-Fusion® cloning process was performed in three steps: i) generation of *EdIII* (Figure 4.1) and SC (Figure 4.2) fragments, ii) assembly of fragments to generate SC-linked *EdIII* fragments (Figure 4.3) and iii) In-Fusion® cloning of assembled fragments into linearised pTRAkc-ERH plant expression vector (Figure 4.4) to yield pTRAkc-SC-Gly-EdIII-His-pTRAkc and pTRAkc-His-EdIII-Gly-SC-pTRAkc.

The *EdIII* and SC fragments were successfully amplified with the primers listed in Table 4.1 for the incorporation of a 6x His tag, Gly-linker and 15 bp overlapping fragments of the pTRAkc-ERH vector (Figure 4.1 and 4.2) on the 5' or 3' termini. Amplification yielded the following fragments: pTRAkc-His-EdIII-Gly; ~360 bp, Gly-SC-pTRAkc; ~400 bp, pTRAkc-SC-Gly: ~400 bp, and Gly-EdIII-His-pTRAkc; ~360 bp (Figure 4.5A).

Following the *EdIII* and SC fragment generation, the fragments were assembled to allow for the construction of an N and C terminal SC-linked *EdIII* fragment (Figure 4.3). *EdIII* and SC fragments were successfully assembled by PCR amplification with primers listed in Table 4.2 to yield fragments of ~730 bp each (Figure 4.5B).

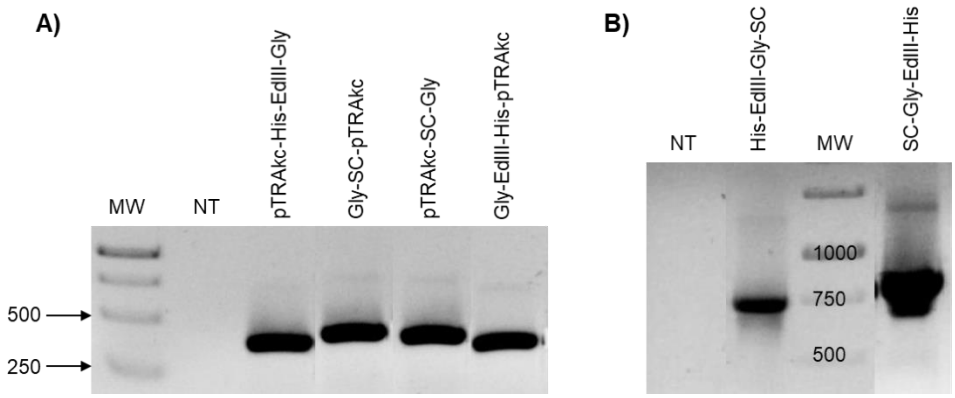

Figure 4.5. Generation of *EdIII* and SC fragments by PCR amplification and assembly of *EdIII* and SC fragments for In-Fusion® cloning visualised on agarose gels stained with ethidium bromide. **(A)** PCR amplification for isolation of *EdIII* and SC fragments for the addition of a 6x His tag, Gly-linker and 15 bp overlap of the pTRAkc-ERH vector to either terminus of *EdIII*, and the addition of a Gly-linker and 15 bp overlap of the pTRAkc-ERH vector to either terminus of SC. **(B)** Assembly of *EdIII* and SC fragments for the construction of SC-linked *EdIII* constructs. An N terminal SC-linked fragment: SC-Gly-EdIII-His, and a C terminal SC-linked fragment: His-EdIII-Gly-SC were generated. Both assembled fragments were flanked by 15 bp overlapping pTRAkc-ERH regions at the 5' and 3' termini to allow for In-Fusion® cloning. MW, the molecular weight marker. NT, no template control.

In-Fusion® cloning was performed following fragment assembly (Figure 4.5B) for the insertion of the assembled fragments into linearised pTRAkc-ERH (Figure 4.4) yielding pTRAkc-SC-EdIII and pTRAkc-EdIII-SC. Transformed *E. coli* cells were screened by colony PCR to yield products of ~730 bp (Figure 4.6A) as expected. The recombinant constructs were transformed into *A. tumefaciens* GV3101::pMP90RK. Successful transformation was confirmed by colony PCR using vector-specific primers (Appendix B: Table 1) to yield fragments of ~930 bp (Figure 4.6B).

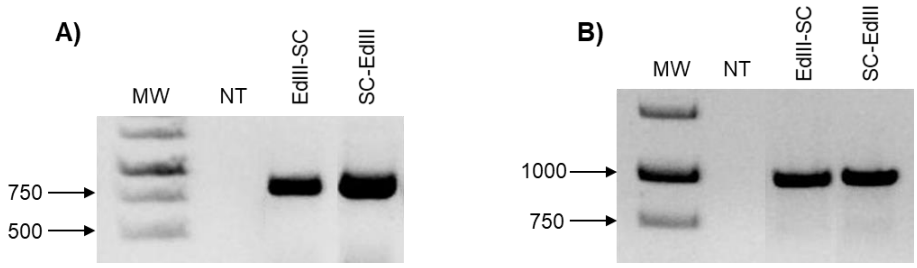

Figure 4.6. Verification of In-Fusion® clones by PCR amplification from transformed E. *coli* cells **(A)** and transformed *A. tumefaciens* GV3101::pMP90RK cells **(B)** visualised on agarose gels stained with ethidium bromide. Two pTRAkc-ERH constructs were generated resulting in SC being fused to *EdIII* on the N or the C terminus. MW, the molecular weight marker. NT, no template control.

4.3.2. Small scale expression of SC-linked EdIII in *N. benthamiana*

4.3.2.1. SC-linked EdIII expression

Two optical densities of *Agrobacterium* harbouring pTRAkc-SC-EdIII and pTRAkc-EdIII-SC were evaluated to determine the optimal OD_{600} for maximum SC-EdIII and EdIII-SC expression. TSP amounts were determined for the insoluble (pellet) and soluble (supernatant) fractions of crude extracts harvested from leaves at 4, 5 and 6 dpi for each infiltration permutation. Twenty-five micrograms of crude insoluble and soluble SC-linked EdIII protein extracts were evaluated by western blot using polyclonal rabbit anti-WNV-EdIII antiserum for the detection of SC-EdIII and EdIII-SC proteins of ~25 kDa in size.

No protein of the expected size was observed in either of the insoluble or soluble fractions for all harvest days for each infiltration permutation (OD_{600} 0.25 and 0.5) (Figure 4.7). However, a non-specific band of ~28 kDa was observed in the insoluble fractions (p), including the negative control for all infiltration permutations.

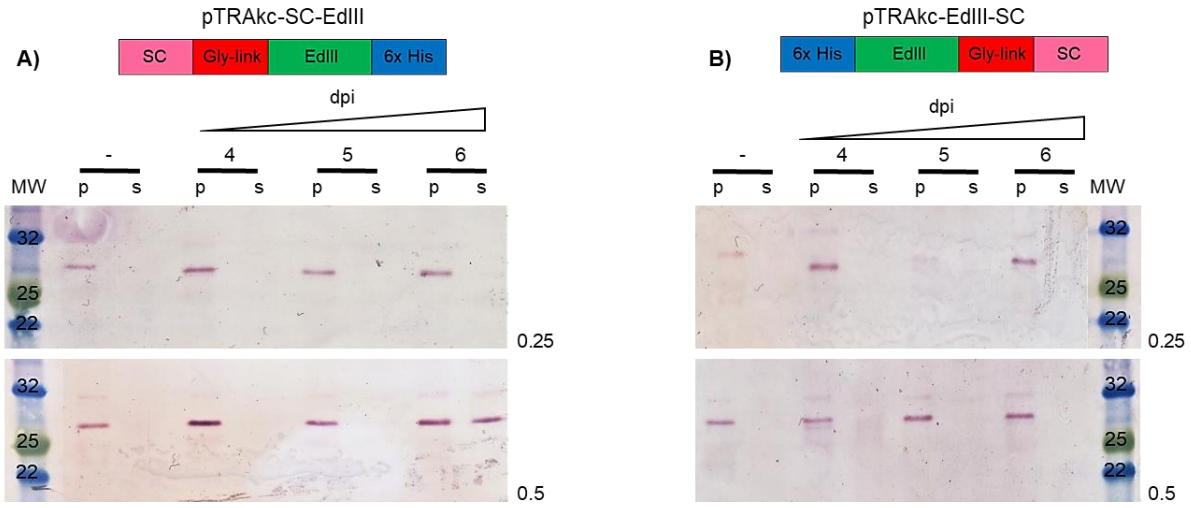

Figure 4.7. Expression of the SC-linked EdIII proteins at OD_{600} 0.25 and 0.5. Proteins were isolated 4, 5 and 6 dpi and 25 µg of TSP of pellet (p) and supernatant (s) were loaded into each lane. The negative controls (-) are crude leaf extracts of plants infiltrated with pTRAkc-ERH empty vector. Proteins were detected with anti-WNV-EdIII antiserum (1:20 000). MW, the molecular weight marker.

4.3.2.2. Co-expression of SC-EdIII with the human chaperone CNX

Since no SC-linked EdIII protein was detected when the constructs were expressed on their own, it was decided to co-express them with the human chaperone protein CNX due to the enhanced yields previously observed for E protein co-expression with CNX (Figure 2.7). Thus, pTRAkc-SC-EdIII was infiltrated with and without pEAQ-CNX at an OD_{600} 0.5 each and leaves harvested 4, 5 and 6 dpi. Equal amounts of TSP of the crude insoluble and soluble fractions was evaluated by western blot using polyclonal rabbit anti-WNV-EdIII antiserum for the detection of SC-EdIII protein; ~25 kDa (Figure 4.8).

When SC-EdIII was expressed on its own, no 25 kDa SC-EdIII protein was observed in both the insoluble and soluble fractions across all harvest days (Figure 4.8A) confirming previous observations (Figure 4.7). However, when SC-EdIII was co-expressed with CNX, a ~25 kDa band was observed in the soluble fractions across all harvest days (Figure 4.8B – indicated by the black arrow). The highest level of protein expression was observed at 4 dpi, based on band intensities. Two non-specific bands approximately 27 and 30 kDa were present in all fractions across all days with or without the co-expression of CNX, except for the soluble fractions where SC-EdIII protein was detected.

Based on these results I concluded that for SC-linked EdIII protein expression to be detected, co-expression with a human chaperone protein is necessary. When co-expressed with CNX the SC-EdIII protein was soluble and the highest protein yield was observed at 4 dpi.

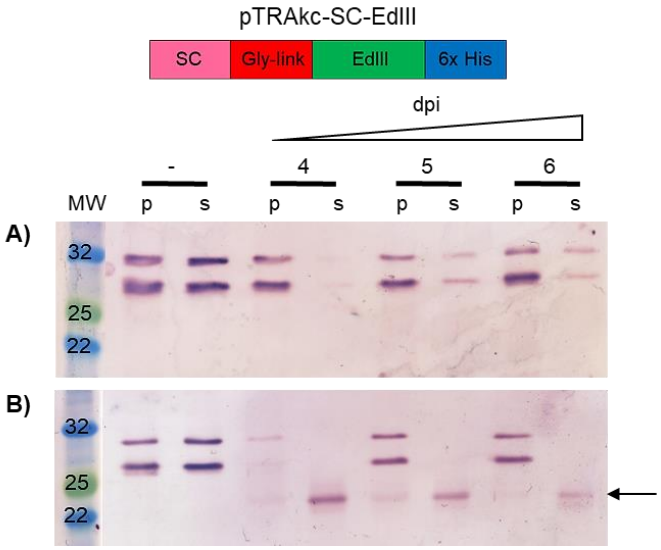

Figure 4.8. Expression of the SC-EdIII protein without **(A)** and with **(B)** CNX. Proteins were isolated 4, 5 and 6 dpi and 25 µg of TSP of pellet (p) and supernatant (s) was loaded into each lane. Proteins were detected with anti-WNV-EdIII antiserum (1:20 000). Black arrow indicates SC-EdIII protein (~25 kDa) **(A)** Expression of pTRAkc-SC-EdIII on its own. **(B)** Co-Expression of pTRAkc-SC-EdIII and pEAQ-CNX. The negative controls (-) are crude leaf extracts of plants infiltrated with pTRAkc-ERH empty vector. MW, the molecular weight marker.

4.3.2.3. Optimal extraction buffer determination

Since extraction buffer components can potentially influence protein yields, three extraction buffers were compared to determine the optimal buffer for extraction of maximum amounts of SC-EdIII and EdIII-SC. pTRAkc-SC-EdIII and pTRAkc-EdIII-SC were each co-infiltrated with pEAQ-CNX at an OD_{600} of 0.5 each. Leaves were harvested and protein extracted at 4 dpi. Protein was extracted using 1x PBS (pH 7.4); the standard buffer used for previous SC-linked extractions, 1x PBS (pH 6.0) selected based on the success observed previously when used for extraction of the prM and E proteins (Figure 2.9); and, Tris buffer described by He *et al.* (2014) who used this buffer for the extraction of EdIII protein from *N. benthamiana*. Equal amounts of TSP in insoluble and soluble fractions from crude extracts were evaluated by western blot using polyclonal rabbit anti-WNV-EdIII antiserum for the detection of SC-linked EdIII proteins; ~25 kDa (Figure 4.9).

Across all buffers tested, similar non-specific bands (~22, 24, 27 and 30 kDa) were observed for all samples including the negative control in the insoluble fractions (Figure 2.9A). SC-linked EdIII protein was detected in the insoluble fraction (pellet) for EdIII-SC, present in all buffer extracts, but no SC-EdIII was detected (Figure 2.9A – indicated by the red arrow). Both SC-EdIII and EdIII-SC proteins were detected in the soluble fraction (supernatant) for all

extraction buffers used (Figure 2.9B – indicated by the blue and red arrows respectively), however, SC-EdIII proteins were slightly smaller in size than EdIII-SC proteins but were expected to be the same size. Based on band intensity for both SC-linked EdIII proteins, more protein was isolated using the Tris extraction buffer in comparison to 1x PBS at pH 6.0 and pH 7.4 (Figure 2.9B). In the instance of EdIII-SC, when extracted with the Tris buffer no additional protein bands were detected in the soluble fraction compared to the other buffers. Overall, less non-specific protein bands were detected in the soluble fractions compared to the insoluble fractions.

Based on these observations I concluded that the SC-linked EdIII proteins are primarily soluble regardless of extraction buffer used. However, extraction with the Tris buffer resulted in higher SC-linked EdIII protein yields than when using 1x PBS regardless of the pH.

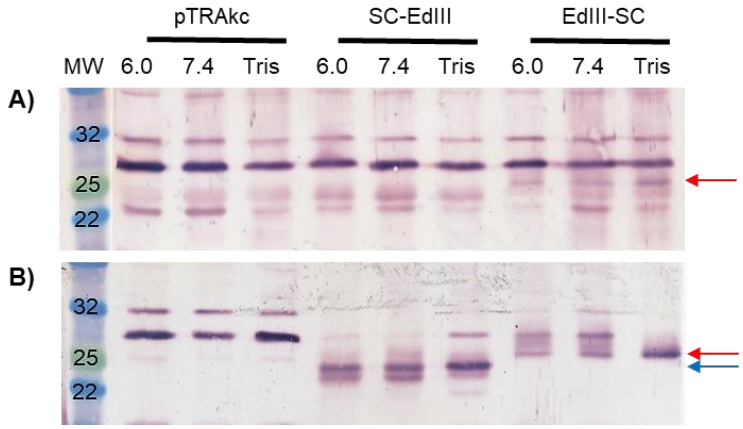

Figure 4.9. Extraction of SC-linked EdIII proteins with three buffers: 1x PBS (pH 6.0), 1x PBS (pH 7.4) and Tris buffer. Proteins were isolated 4 dpi and 25 µg of TSP of pellet **(A)** and supernatant **(B)** was loaded into each lane. Proteins were detected with anti-WNV-EdIII antiserum (1:20 000). The blue arrow indicates the SC-EdIII protein and the red arrows indicate EdIII-SC protein. **(A)** Insoluble fractions of crude protein extracts. **(B)** Soluble fractions of crude protein extracts. The negative controls are crude leaf extracts of plants infiltrated with pTRAkc-ERH empty vector. MW, the molecular weight marker. 6.0, 1x PBS (pH 6.0). 7.4, 1x PBS (pH 7.4). Tris, Tris buffer (pH 8.0).

4.3.2.4. CNX vs CRT co-expression with SC-linked EdIII

When the SC-linked EdIII proteins were co-expressed with CNX the proteins were primarily soluble. Therefore, co-expression with CNX and CRT were compared since these chaperones associate with insoluble and soluble proteins, respectively, to determine the best co-expression combination for each SC-linked EdIII protein.

pTRAkc-SC-EdIII and pTRAkc-EdIII-SC were each co-infiltrated with pEAQ-CNX and pEAQ-CRT at an OD_{600} 0.5 each. Leaves were harvested and protein extracted at 4 dpi using the Tris buffer. Equal amounts of TSP of crude extracts from insoluble and soluble fractions were evaluated by western blot using polyclonal rabbit anti-WNV-EdIII antiserum for the detection of SC-linked EdIII proteins; ~25 kDa (Figure 4.10).

As observed in Figure 4.9, only EdIII-SC protein was detected in the insoluble fraction (Figure 4.10A – indicated by the red arrow). No protein was observed for SC-EdIII in the insoluble fraction irrespective of the chaperone protein used for co-expression. However, both SC-linked EdIII proteins were observed in the soluble fraction for both co-expression permutations (Figure 4.10B), demonstrating that these proteins are highly soluble. For both EdIII-SC and SC-EdIII proteins, more protein was observed when co-expressed with CRT than CNX.

Based on these results, future co-expression was performed with CRT for optimal protein yields.

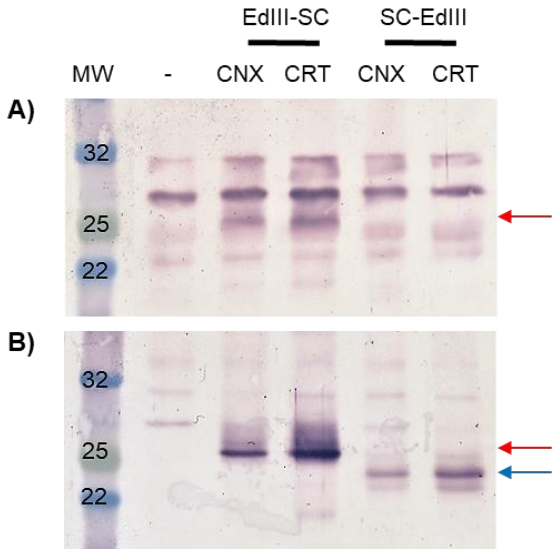

Figure 4.10. Co-expression of SC-linked EdIII proteins with human chaperone proteins, CNX and CRT. Proteins were isolated 4 dpi and 25 µg of TSP of pellet **(A)** and supernatant **(B)** was loaded into each lane. Proteins were detected with anti-WNV-EdIII antiserum (1:20 000). The blue arrow indicates the SC-EdIII protein and the red arrows indicate EdIII-SC protein. **(A)** Insoluble fractions of crude protein extracts. **(B)** Soluble fractions of crude protein extracts. The negative controls are crude leaf extracts of plants infiltrated with pTRAkc-ERH empty vector. MW, the molecular weight marker. CNX, co-expression with CNX. CRT, co-expression with CRT.

4.3.3. Large scale expression and purification of SC-linked EdIII from *N. benthamiana*

Approximately 70 g of leaves were homogenised for large scale purification of both SC-EdIII and EdIII-SC proteins. Following pH precipitation for the removal of plant proteins (Appendix F: Figure 4), the SC-linked EdIII proteins were further purified by nickel affinity chromatography (Appendix G: Figure 5). Protein elution fractions were evaluated for SC-linked EdIII proteins by western blot using polyclonal rabbit anti-WNV-EdIII antiserum; ~25 kDa (Figure 4.11A and C) and the purity of collected fractions was evaluated by Coomassie blue-stained SDS-PAGE (Figure 4.11B and D).

A protein elution peak was observed in F18-24 (Appendix G: Figure 5A) for SC-EdIII and subsequently, protein was detected in the crude (c) extract and F19-23 by western blot (Figure 4.11A), and F20-23 by Coomassie blue-stained gels (Figure 4.11B). The most intense protein bands were observed in F21-23 and these fractions had the least number of plant contaminating proteins.

For EdIII-SC, an elution peak was observed in F18-26 (Appendix G: Figure 5B) and protein was detected in the crude (c) extract and F18-25 by western blot (Figure 4.11C) and Coomassie Blue-stained gels (Figure 4.11D); ~25 kDa. The EdIII-SC protein band in F25 was the most intense of all the evaluated fractions, with no contaminating plant proteins.

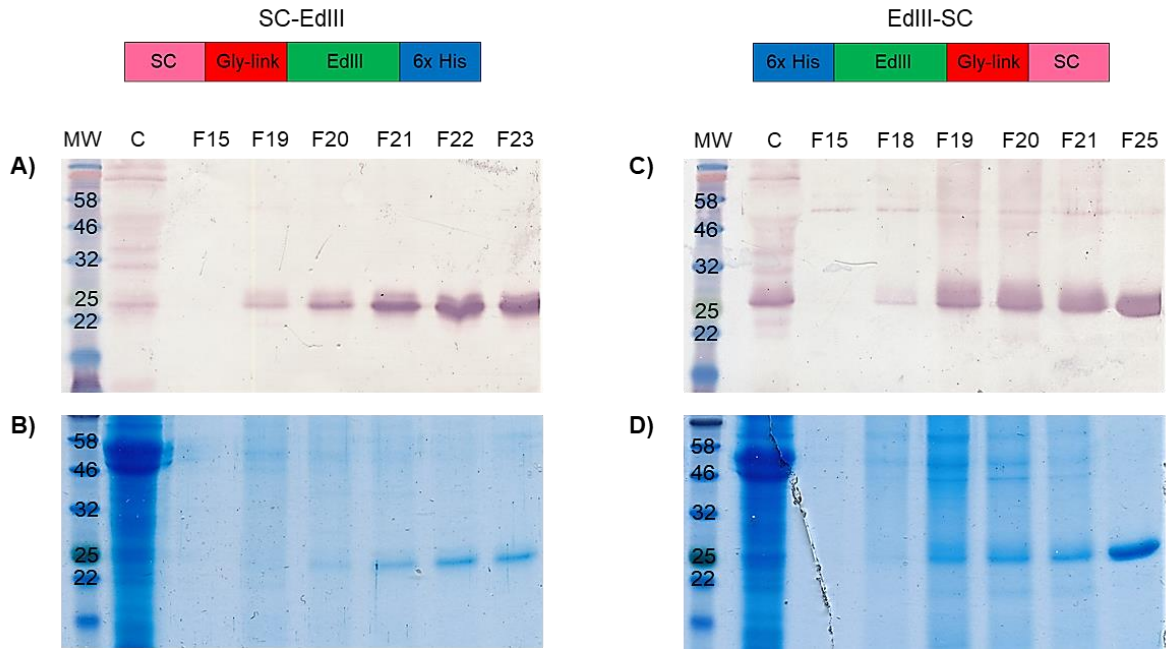

Figure 4.11. Purification of SC-linked EdIII proteins using nickel affinity chromatography following pH precipitation. Equal volumes of clarified crude plant extract and elution fractions were loaded in each lane. F15 represented an unbound fraction. Proteins were detected with anti-WNV-EdIII antiserum (1:20 000) for western blots. **(A)** SC-EdIII fractions analysed by western blot and **(B)** Coomassie blue-stained gel. **(C)** EdIII-SC fractions analysed by western blot and **(D)** Coomassie blue-stained gel. MW, the molecular weight marker. C, clarified crude plant extract. F, fraction collected.

Based on the intensity of the protein bands observed in F23 and F25 of SC-EdIII and EdIII-SC, respectively, and that the elution peaks spanned F18-24 (Appendix G: Figure 5) it was concluded that these fractions contained most of the desired protein. Therefore, F23 and F24 of SC-EdIII and F24 and F25 of EdIII-SC were quantified by gel densitometry (Figure 4.12). F23 and F24 of SC-EdIII had similar protein concentrations of 0.013 µg/µL and 0.011 µg/µL respectively (Figure 4.12A). Higher concentrations were observed for EdIII-SC with ~0.1 µg/µL for F24 and 0.15 µg/µL for F25 (Figure 4.12B).

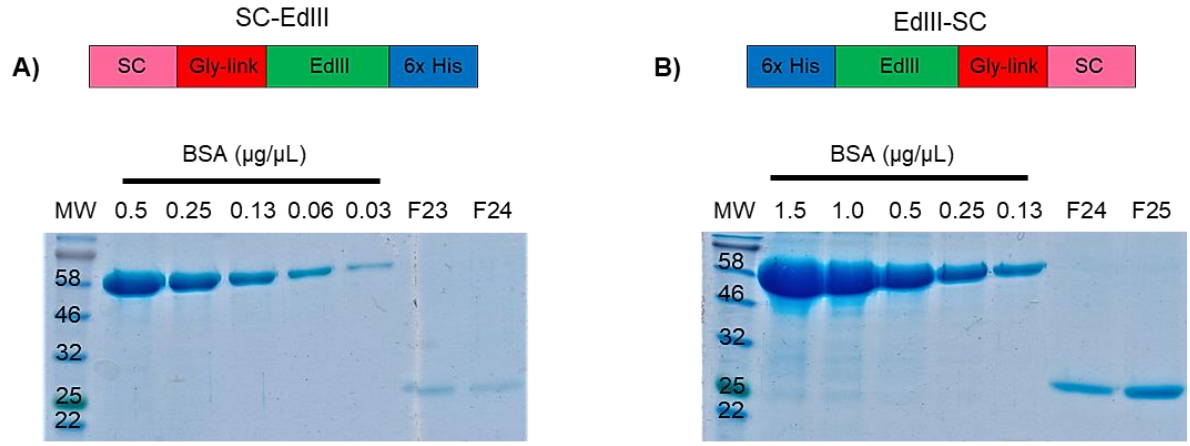

Figure 4.12. Quantification of purified SC-linked EdIII proteins by gel densitometry using a BSA standard. **(A)** Quantification of SC-EdIII protein fractions collected after purification by nickel affinity chromatography. F23 = 0.013 µg/µL and F24 = 0.011 µg/µL. **(B)** Quantification of EdIII-SC protein fractions collected after purification by nickel affinity chromatography. F24 ≈ 0.1 µg/µL and F25 = 0.15 µg/µL. MW, the molecular weight marker.

4.3.4. ST-AP205 VLP purification from *N. benthamiana*

The Spy-VLP system (ST-AP205) developed by Thrane *et al.* (2016) was selected as the VLP core for the display of the EdIII protein of WNV. This system was selected due to the successful expression and purification of the ST-AP205 VLPs in high yields from *N. benthamiana* as demonstrated previously by Dr Sue Dennis (BRU, UCT).

The pEAQ-ST-AP205 construct was infiltrated at an OD_{600} of 0.25 and leaves harvested at 4 dpi. ST-AP205 VLPs were purified by discontinuous iodixanol density gradient ultracentrifugation and 30 µL of collected fractions were evaluated for ST-AP205 protein (Figure 4.13A) and quantified (Figure 4.13B) by Coomassie blue-stained SDS-PAGE and VLPs (~30 nm) visualised by TEM (Figure 4.13C and D).

ST-AP205 protein was observed in fractions 1-6 (Figure 4.13A). In all fractions, a monomer of 16.5 kDa, a dimer of 33 kDa and a tetramer of ~66 kDa was present (as previously shown by Dr Sue Dennis during her PhD) with an increase in band intensity corresponding with a decrease in iodixanol density (F5-6). A band of approximately 55 kDa in size representing the RuBisCO large subunit was also visible in the negative control and all purified fractions.

Purified fractions were stored at 4°C for several days before protein quantification was performed. Upon protein quantification, a faint monomeric ST-AP205 coat protein band was observed for fraction 4 and 5 (Figure 4.13B) as a result of protein degradation occurring during

storage. Protein concentrations were determined from a BSA standard as F4 = 0.027 µg/µL and F5 = 0.044 µg/µL.

Electron micrographs of fraction 6 showed numerous particles with a diameter of approximately 30 nm, indicating that the ST-AP205 protein purified from plants forms VLPs (Figure 4.13C and D).

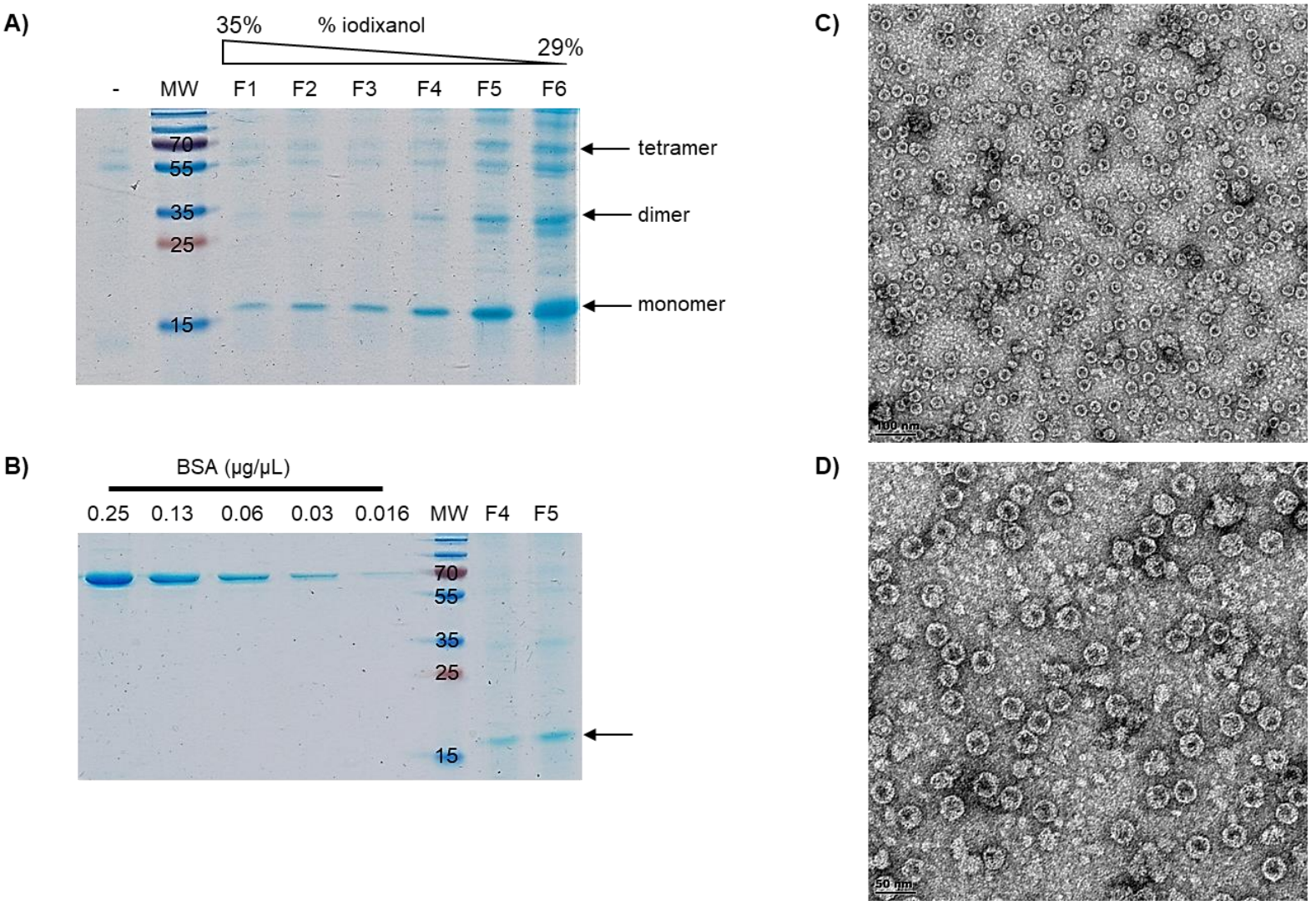

Figure 4.13. Purification of ST-AP205 VLPs from *N. benthamiana*. **(A)** Coomassie blue-stained SDS-PAGE of collected fractions following ultracentrifugation through a discontinuous iodixanol density gradient. Arrows indicate a ST-AP205 protein monomer (16.5 kDa), dimer (33 kDa) and tetramer (66 kDa). The negative control is crude leaf extracts of plants infiltrated with pTRAkc-ERH empty vector. MW, molecular weight marker. **(B)** Quantification of purified ST-AP205 protein fractions 4 and 5 by gel densitometry using a BSA standard. Arrow indicates the quantified bands: F4 = 0.027 µg/µL and F5 = 0.044 µg/µL. MW, molecular weight marker. **(C-D)** Electron micrograph of purified ST-AP205 VLPs (~30 nm) from fraction 6. Scale bars (C) 100 nm and (D) 50 nm.

4.3.5. *In vitro* coupling of purified ST-AP205 VLPs and SC-linked EdIII

The purified ST-AP205 VLPs (section 4.3.4) were coupled *in vitro* with purified SC-linked EdIII proteins (section 4.3.3). Complex formation between ST-AP205 and the SC-linked EdIII proteins is confirmed by a molecular weight shift (Figure 4.14). Since I showed that the AP205 coat protein can exist in multimeric forms, it is possible that at least 2 different-sized complexes may be detected: 16.5 kDa ST-AP205 monomer + 25 kDa SC-linked EdIII = 41.5 kDa AP205:EdIII monomeric product; and 33 kDa ST-AP205 dimer + 25 kDa SC-linked EdIII = 58 kDa AP205:EdIII dimeric product.

Purified ST-AP205 VLPs and SC-linked EdIII proteins were coupled at various molar ratios O/N at 4°C and evaluated for complex formation by Coomassie blue-stained SDS-PAGE or by western blot (Figure 4.15).

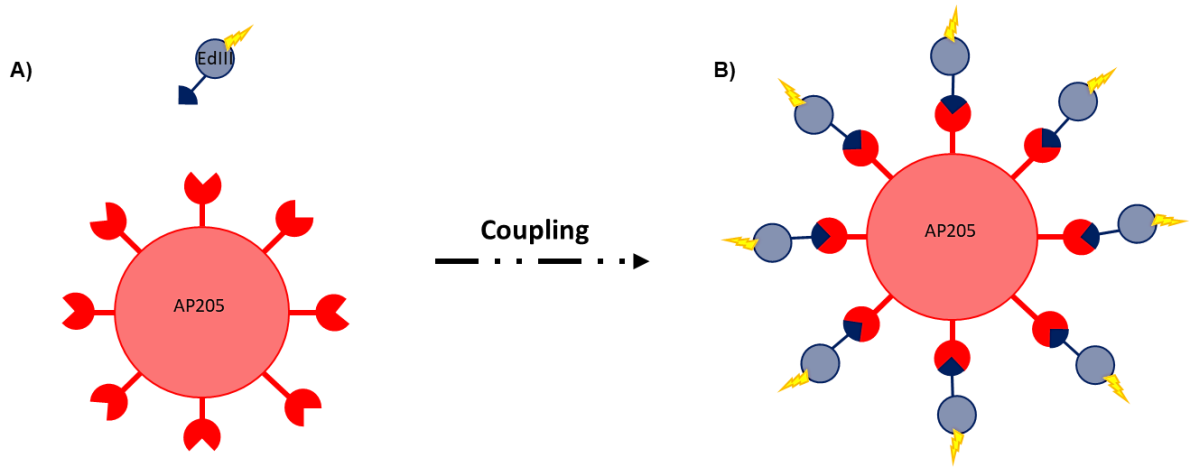

Figure 4.14. Schematic representation of ST-AP205 VLP and SC-linked EdIII coupling. **(A)** SC-linked EdIII protein (yellow lightning bolt represents the 6x His tag) and ST-AP205 VLPs with 180 binding motifs (as each AP205 VLP is composed of 180 coat protein subunits) are added together to allow for isopeptide bond formation between the ST and SC peptides located on the EdIII antigen and AP205 VLP, respectively. **(B)** Following incubation of the coupling reaction an AP205:EdIII complex forms, where the EdIII antigen is displayed on the AP205 VLP surface. This complex formation is detected by a molecular weight shift from the two single components' size in kDa to the sum of them.

Coupling reactions with ST-AP205 and SC-EdIII did not result in any detectable molecular weight shifts for any of the coupling ratios tested (Figure 4.15A). Only monomeric ST-AP205 protein (red arrow) and SC-EdII protein (blue arrow) were visualised in the Coomassie blue-stained SDS polyacrylamide gel. However, complex formation was observed when EdIII-SC was coupled with ST-AP205 (Figure 4.15B). In addition to the 16.5 kDa (red arrow) and

25 kDa (blue arrow) sized bands of ST-AP205 and EdIII-SC, respectively, a protein band of ~41.5 kDa (black arrow) representing a ST-AP205 monomer coupled to EdIII-SC was visualised in all 4 coupling reactions carried out. However, no corresponding increase in coupled product yield (black arrow) with an increase in the amount of EdIII-SC included in the coupling reaction was observed.

The influence of different molar ratios of ST-AP205 and EdIII-SC on AP205:EdIII coupled product yield was investigated by varying both ST-AP205 and EdIII-SC ratios (Figure 4.15C). In this case, both monomeric and dimeric AP205:EdIII coupled products (black arrows) were observed for all 5 coupling molar ratios tested with similar yields regardless of the molar ratios (black arrows).

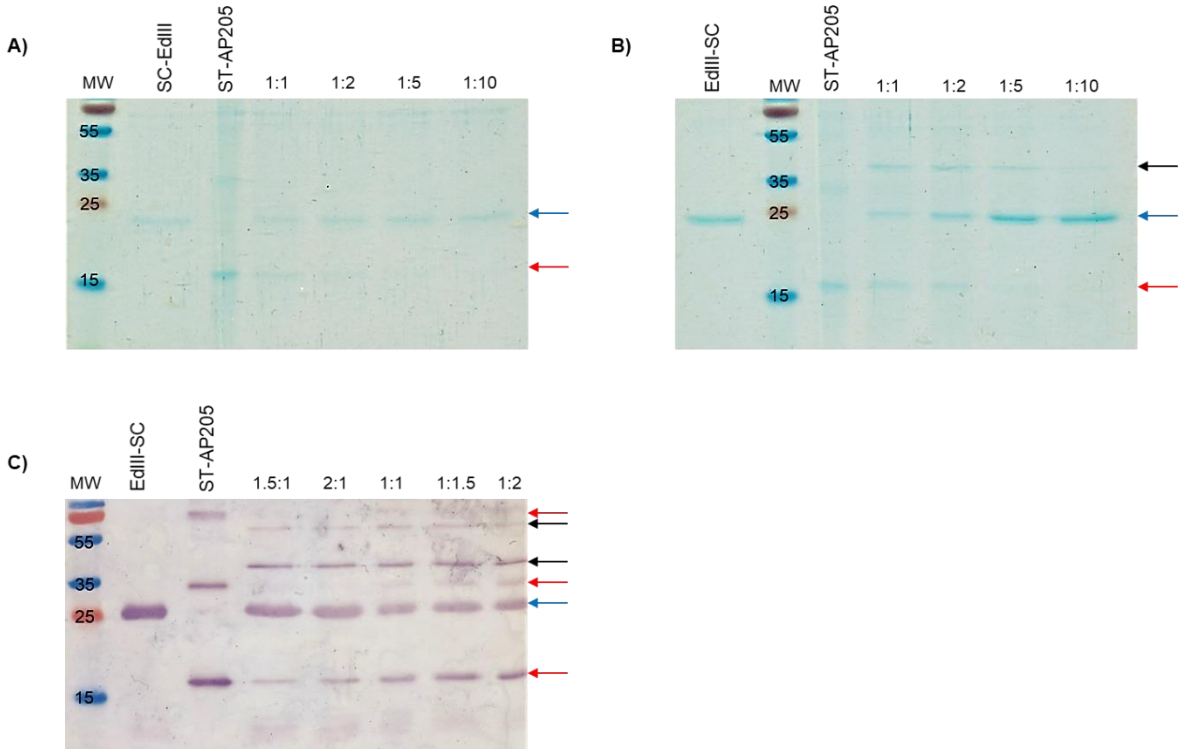

Figure 4.15. Analysis of ST-AP205 and SC-linked EdIII complex formation by Coomassie blue-stained SDS-PAGE **(A-B)** and by western blot using anti-ST-AP205 combined with anti-WNV-EdIII sera (1:20 000 each) **(C)**. Coupling reactions were performed at molar ratios of 1:1, 1:2, 1:5 and 1:10 ST-AP205:SC-linked EdIII **(A-B)** and 1:1, 1.5:1, 2:1, 1:1.5 and 1:2 ST-AP205:EdIII-SC **(C)**. Red arrows indicate ST-AP205 proteins (monomer = 16.5 kDa, dimer = 33 kDa, tetramer = 66 kDa), blue arrows indicated the SC-linked EdIII proteins (~25 kDa) and black arrows indicate the complex formation (AP205:EdIII) revealed by a molecular weight shift to 41.5 kDa (16.5 kDa + 25 kDa) as a monomer and 58 kDa (33 kDa + 25 kDa) as a dimer. **(A)** Coupling analysis of ST-AP205 and SC-EdIII. **(B-C)** Coupling analysis of ST-AP205 and EdIII-SC. MW, molecular weight marker. SC-EdIII, SC-EdIII protein only control. ST-AP205, ST-AP205 only control. EdIII-SC, EdIII-SC protein only control.

4.3.6. ST-AP205 and EdIII-SC co-expression vs co-extraction

Following the success of *in vitro* coupling of purified ST-AP205 VLPs and purified EdIII-SC proteins, I investigated whether coupling could occur *in vivo* by the co-expression of pEAQ-ST-AP205 and pTRAkc-EdIII-SC in *N. benthamiana*. The ST-AP205 proteins were targeted to the cytosol while the EdIII-SC proteins were targeted to the ER followed by secretion to the cytosol, thus if coupling should take place it would be in the plant cytosol. I also investigated if co-extraction of leaves separately infiltrated with each of these constructs would result in coupling. Spy-VLPs from co-expression and co-extraction experiments were purified by discontinuous iodixanol density gradient ultracentrifugation and fractions collected from the bottom of the tube were analysed by western blot using anti-ST-AP205 and anti-WNV-EdIII sera.

Coupled AP205:EdIII products (41.5 kDa and 58 kDa) were observed both when ST-AP205 and EdIII-SC were co-expressed *in vivo* (Figure 4.16A black arrows) and when leaves individually infiltrated with ST-AP205 and EdIII-SC were co-extracted (Figure 4.16B black arrows). ST-AP205 proteins as different subunits; monomeric, dimeric and tetrameric were detected for both co-expression (Figure 4.16A red arrows) and co-extraction (Figure 4.16B red arrows) of ST-AP205/EdIII-SC, but no uncoupled EdIII-SC protein was observed. In fractions 6-9 (29% iodixanol) for both co-expression and co-extraction; protein doublets were detected for ST-AP205 protein subunits which could be as a result of protein degradation or loss of the ST peptide by enzymatic cleavage during purification (AP205 coat protein only ~14 kDa).

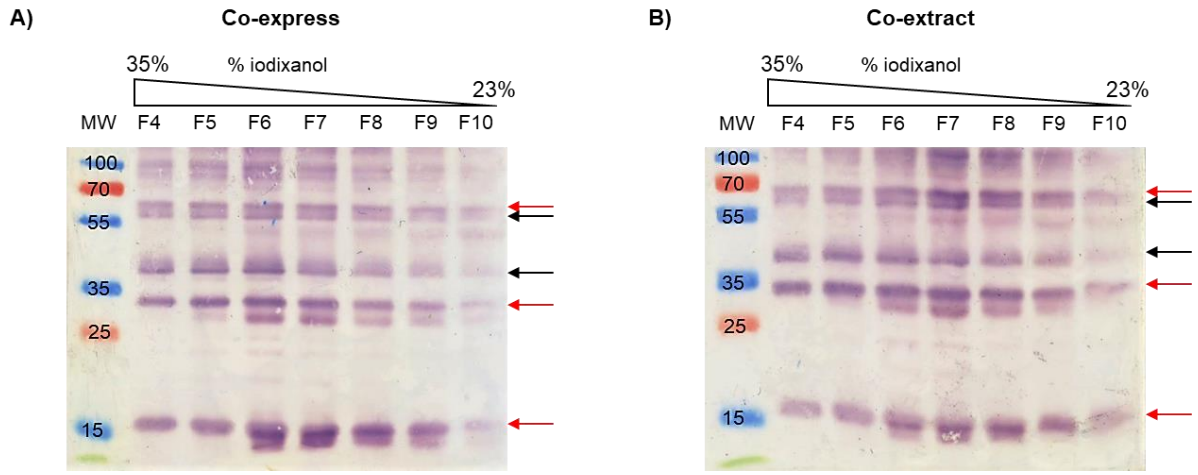

Figure 4.16. Analysis of ST-AP205 and EdIII-SC complex formation by western blot using anti-ST-AP205 and anti-WNV-EdIII sera (1:20 000 each). Red arrows indicate ST-AP205 proteins (monomer = 16.5 kDa, dimer = 33 kDa, tetramer = 66 kDa) and black arrows indicate the complex formation revealed by a molecular weight shift to 41.5 kDa (16.5 kDa + 25 kDa) as a monomer and 58 kDa (33 kDa + 25 kDa) as a dimer. **(A)** Coupling analysis of ST-AP205 and EdIII-SC co-expressed in *N. benthamiana*. **(B)** Coupling analysis of ST-AP205 and EdIII-SC from leaves co-extracted from individual infiltrations. MW, molecular weight marker.

Since both ST-AP205/EdIII-SC co-expression and co-extraction resulted in AP205:EdIII complex formation (Figure 4.16), it was determined which of the two methods – co-expression or co-extraction – resulted in the highest yield of AP205:EdIII complexes. Total protein concentrations of EdIII were determined by indirect ELISA in fractions 6-9 (29% iodixanol). For each quantified fraction of the co-expressed and co-extracted ST-AP205/EdIII-SC, 12 ng of EdIII protein was subsequently evaluated for complex formation by western blot using anti-WNV-EdIII (Figure 4.17A) and anti-ST-AP205 (Figure 4.17B) sera.

In both fractions 7 and 8 from co-extracted ST-AP205/EdIII-SC, a monomer and dimer of AP205:EdIII was detected (Figure 4.17A black arrows). Whereas from samples of co-expressed of ST-AP205/EdIII-SC, monomeric and dimeric AP205:EdIII complexes were only detected in fraction 7. The protein bands observed in the co-extraction fractions were more intense than those observed in the co-expression fraction when detected with anti-EdIII sera.

When anti-ST-AP205 serum was used for protein detection, monomeric AP205:EdIII was faintly detected in fractions 7 and 8 of co-extracted ST-AP205/EdIII-SC (Figure 4.17B black arrow). No other AP205:EdIII complexes were detected, but multimeric uncoupled ST-AP205 proteins (Figure 4.17B red arrows) were detected across all lanes. As observed in Figure 4.16, multiple bands for ST-AP205 were detected specifically in the monomeric form (Figure 4.17B)

which could be as a result of protein degradation and/or proteolytic cleavage of the ST peptide from AP205 during either or both the purification process and storage at 4°C.

Based on band intensities, since equal EdIII protein was loaded, I concluded that co-extraction of ST-AP205/EdIII-SC resulted in the highest yield of AP205:EdIII complexes.

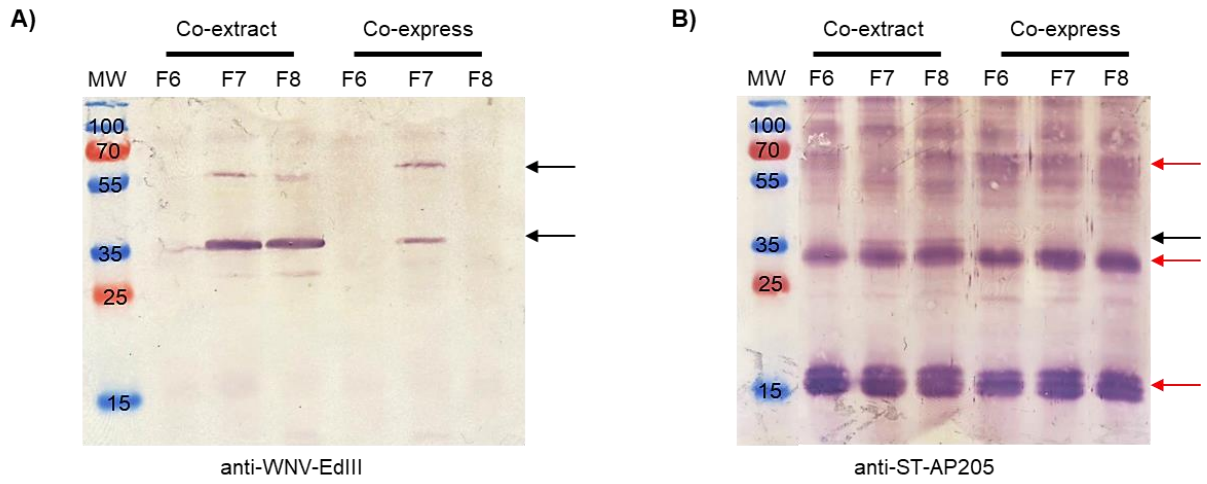

Figure 4.17. Analysis of ST-AP205 and EdIII-SC complex formation by western blot. Equal EdIII protein (12 ng) was loaded in each lane for fraction 6-9 of co-expressed and co-extracted ST-AP205/EdIII-SC. Red arrows indicate ST-AP205 proteins (monomer = 16.5 kDa, dimer = 33 kDa, tetramer = 66 kDa) and black arrows indicate the complex formation revealed by a molecular weight shift to 41.5 kDa (16.5 kDa + 25 kDa) as a monomer and 58 kDa (33 kDa + 25 kDa) as a dimer. **(A)** EdIII protein detection of fractions 6-9 of ST-AP205/EdIII-SC co-expressed vs. co-extracted using anti-WNV-EdIII serum (1:20 000). **(B)** ST-AP205 protein detection of fractions 6-9 of ST-AP205/EdIII-SC co-expressed vs co-extracted using anti-ST-AP205 serum (1:20 000). MW, molecular weight marker.

4.3.7. ST-AP205 and EdIII-SC co-extraction optimisation

The purification of the AP205:EdIII complexes was further investigated to remove uncoupled proteins, specifically ST-AP205 due to its abundance (Figure 4.17B red arrows). The first approach was to evaluate if the AP205:EdIII complexes could be separated from uncoupled ST-AP205 proteins with a two-step density gradient ultracentrifugation purification protocol (section 4.3.7.1). The second approach was to vary the FLW ratio of ST-AP205 to EdIII-SC to determine whether I could reduce the presence of uncoupled ST-AP205 proteins and at the same time increase the AP205:EdIII coupled product yield by increasing the amount of EdIII-SC FLW (section 4.3.7.2).

4.3.7.1. Density gradient ultracentrifugation

To determine whether I could purify the AP205:EdIII complex from the uncoupled ST-AP205 proteins, a second density gradient ultracentrifugation step was performed. Following discontinuous density gradient ultracentrifugation; the 29% fraction was collected, diluted and loaded onto a 10-40% linear iodixanol density gradient and ultracentrifuged for the separation of the AP205:EdIII complexes from all the uncoupled ST-AP205 protein subunits (16.5, 33 and 66 kDa). The collected fractions were evaluated by western blot using anti-ST-AP205 and anti-WNV-EdIII sera.

Further separation of uncoupled ST-AP205 protein subunits and AP205:EdIII complexes were not observed with the additional density gradient ultracentrifugation step (Figure 4.18). Protein bands for both coupled and uncoupled products were detected in the same fractions (F15-26). Instead, a dilution of the AP205:EdIII complex across several fractions was observed rather than a separation from uncoupled ST-AP205, when compared to the 29% input load.

Based on these observations I concluded that a second density gradient ultracentrifugation purification does not result in the separation of AP205:EdIII complexes from uncoupled ST-AP205 protein subunits.

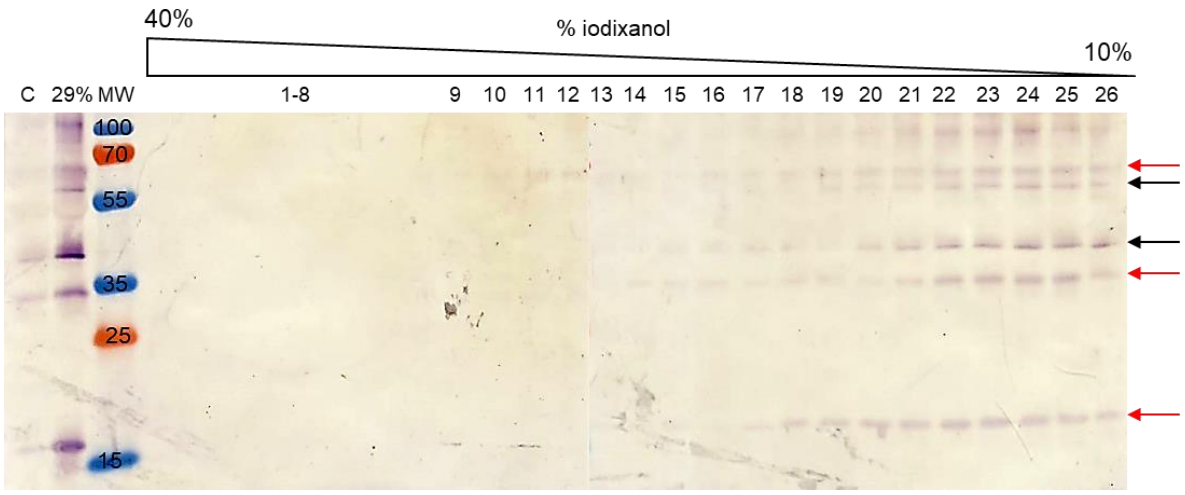

Figure 4.18. Western blot analysis of ST-AP205 subunits and AP205:EdIII complexes following a two-step density gradient ultracentrifugation purification. Proteins were detected using anti-ST-AP205 combined with anti-WNV-EdIII antisera (1:20 000 each). Red arrows indicate ST-AP205 proteins (monomer = 16.5 kDa, dimer = 33 kDa, tetramer = 66 kDa) and black arrows indicate the AP205:EdIII complex revealed by a molecular weight shift to 41.5 kDa (monomer) and 58 kDa (dimer). **(A)** C, crude plant homogenate. 29%, diluted 29% fraction diluted that was loaded onto the linear density gradient. MW, molecular weight marker.

4.3.7.2. Extraction ratios

Since a second density gradient ultracentrifugation purification step did not result in the separation of the AP205:EdIII complexes from uncoupled ST-AP205 protein subunits (Figure 4.18), the focus was shifted towards decreasing the amount of uncoupled ST-AP205 protein subunits while at the same time increasing the yield of AP205:EdIII complexes by varying FLW extraction ratios. Infiltrated leaves were extracted at FLW ratios of 1:1, 1:2, 1:3 and 1:4 of ST-AP205 to EdIII-SC. Spy-VLPs were purified by ultracentrifugation through a discontinuous iodixanol density gradient and total EdIII protein in fractions 3-5 (29% iodixanol) was determined by indirect ELISA. Equal EdIII quantities of 6 ng for each extraction ratio permutation was evaluated by western blot using anti-WNV-EdIII (Figure 4.19A) and anti-ST-AP205 (Figure 4.19B) sera.

Figure 4.19A presents equal amounts of EdIII protein detected by anti-WNV-EdIII serum for each of the extraction ratios. AP205:EdIII monomeric and dimeric complexes were detected for extraction ratios 1:1, 1:2 and of 1:3, with only monomeric AP205:EdIII detected for the 1:4 extraction ratio (black arrows). Based on protein band intensities of the AP205:EdIII monomer complex, the highest yield of coupled product was observed in fractions 3 and 4 at an extraction ratio of 1:2 and the lowest yield was observed when extracted at a 1:4 ratio (ST-AP205 to EdIII-SC).

When considering the presence of uncoupled ST-AP205, more uncoupled ST-AP205 protein subunits could be observed than coupled AP205:EdIII complexes when leaves were extracted at a 1:1 FLW ratio (Figure 4.19B red arrows). As expected, with an increase in the FLW of EdIII-SC to ST-AP205, a decrease in uncoupled ST-AP205 protein subunits was observed. However, unexpectedly a decrease in coupled AP205:EdIII complexes was also observed when extracted at a 1:4 FLW ratio. Similarly to the observation in Figure 4.19A, the highest yield of AP205:EdIII was observed when leaves were extracted at a 1:2 FLW ratio of ST-AP205 to EdIII-SC.

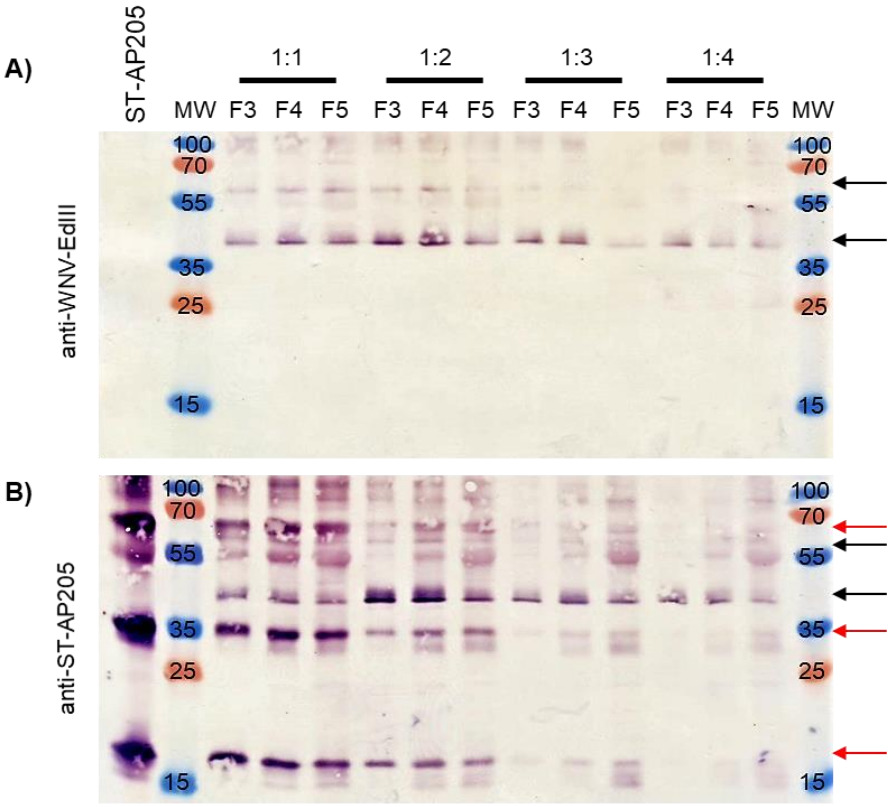

Figure 4.19. Western blot analysis of ST-AP205/EdIII-SC FLW extraction ratios. Infiltrated leaves were extracted at ratios of 1:1, 1:2, 1:3 and 1:4 ST-AP205/EdIII-SC. Equal EdIII protein (6 ng) was loaded in each lane for fractions 3-5 of each extraction ratio. Red arrows indicate ST-AP205 proteins (monomer = 16.5 kDa, dimer = 33 kDa, tetramer = 66 kDa) and black arrows indicate the AP205:EdIII complex revealed by a molecular weight shift to 41.5 kDa (monomer) and 58 kDa (dimer). **(A)** EdIII protein detection of fractions 3-5 of each extraction ratio using anti-WNV-EdIII serum (1:20 000). **(B)** ST-AP205 protein detection of fractions 3-5 of each extraction ratio using anti-ST-AP205 serum (1:20 000). ST-AP205, purification of ST-AP205 leaves only. MW, molecular weight marker.

Biological repeats of these extraction ratios consistently resulted in the highest yield of AP205:EdIII complexes when extracted at a 1:2 FLW ratio, with an average coupling efficiency of 51% for F3-5 which correlates to an antigen-display capacity of 92 EdIII/VLP.

4.3.7.3. TEM of purified AP205:EdIII VLPs

The presence of Spy-VLPs was confirmed by TEM (Figure 4.20) for F3 of the 1:2 extraction ratio. VLPs of the expected diameter size of ~30 nm was observed with an average of 27 particles per field of view at a magnification of X80 000 (Figure 4.20B).

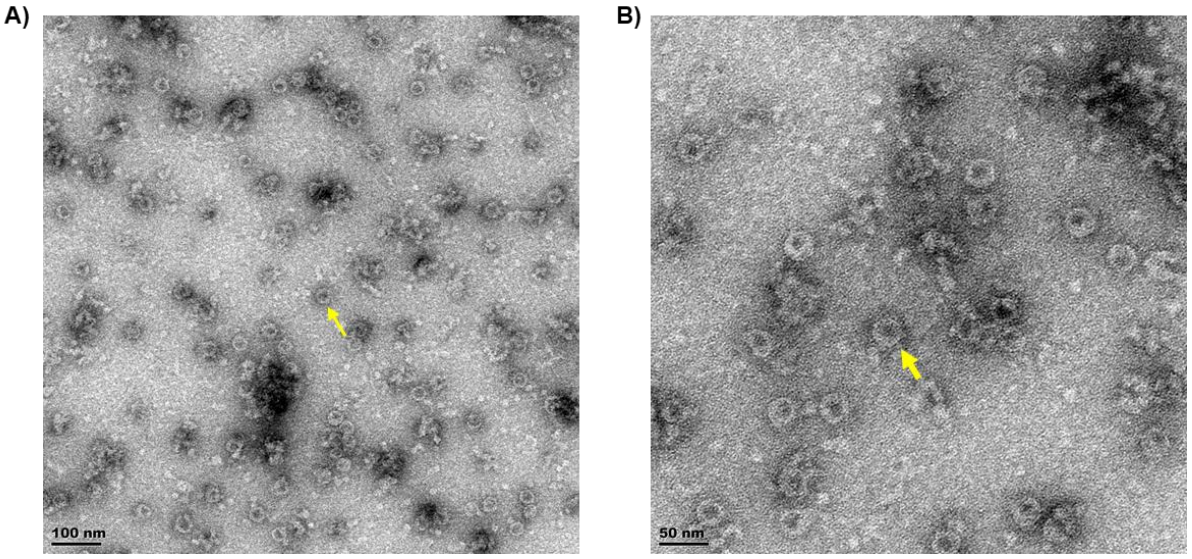

Figure 4.20. Electron micrograph of 1:2 extraction ratio purified AP205:EdIII VLPs (25-30 nm) from fraction 3. Yellow arrows indicate VLPs. Scale bars (A) 100 nm (X40 000 magnification) and (B) 50 nm (X80 000 magnification).

4.4. Discussion

The use of antigen-display technology for the production of particulate candidate vaccines has become popular in the past couple of years (Spohn *et al.*, 2010; Chen *et al.*, 2011; Brune *et al.*, 2016; Janitzek *et al.*, 2016; Singh *et al.*, 2017; Palladini *et al.*, 2018; Yenkoidiok-Douti *et al.*, 2019; Harmsen *et al.*, 2020). The advantages of using VLPs instead of singular antigens as vaccines are in large part due to their size (20-200 nm) that allow for optimal uptake by antigen-presenting cells as well as their dense repetitive surface structures that enable complement fixation and B cell receptor clustering, which are responsible for the activation of the innate immune system and antibody production (Chen & Lai, 2013; Thrane *et al.*, 2016). Due to the difficulty experienced in producing a native WNV candidate vaccine based on the expression of the *prM* and *E* genes (Chapter 3), it was proposed to develop an antigen-display based vaccine using the ST/SC technology to present the immunodominant WNV EdIII protein on the surface of AP205 VLPs.

DNA constructs were generated with the SC peptide fused to the N or C terminus of the EdIII region. The SC peptide rather than the ST peptide was selected for genetic fusion to the *EdIII* gene due to the increased expression yields observed for several *E. coli* produced proteins when fused to the SC rather than the ST peptide (Thrane *et al.*, 2016). Additionally, our lab has demonstrated that a higher yield of AP205 protein is obtained from infiltrated plants when fused to the ST peptide than when fused to the SC peptide. Expression of the SC-linked EdIII constructs in *N. benthamiana* resulted in no detectable SC-linked EdIII proteins. Subsequently, I co-expressed SC-EdIII with the human chaperone protein CNX, as Margolin *et al.* found that protein expression could only be detected for certain glycoproteins when co-expressed with a human chaperone protein to ensure correct protein folding (Margolin *et al.*, 2020). Upon the co-expression of SC-EdIII with CNX, SC-EdIII protein was detected. Since the SC-EdIII proteins were soluble, I investigated which human chaperone protein (CNX vs CRT) resulted in the best protein expression. A higher yield of protein was obtained when SC-linked EdIII was co-expressed with CRT, which was expected as CRT is a soluble luminal protein situated within the ER that is known to associate with soluble proteins, whereas CNX is known to associate with membrane-bound proteins (Ellgaard & Helenius, 2003). From this point onwards, CRT was always co-expressed with SC-linked EdIII constructs when infiltrating *N. benthamiana*.

Next, the influence of different extraction buffers on protein yield was evaluated as this can influence protein yields (Martínez *et al.*, 2010; Buyel *et al.*, 2015). The original buffer used for protein extraction was a neutral buffer: 1x PBS (pH 7.4); the use of this was compared to that of an acidic buffer: 1x PBS (pH 6.0). The acidic buffer was tested due to the success previously

observed when used for extracting WNV prM and E proteins from plants (Chapter 3). The final buffer selected for comparison was a Tris buffer (pH 8.0) used by He *et al.* (2014) for the purification of plant produced WNV EdIII protein. SC-linked EdIII proteins were successfully isolated using all three buffers with the highest protein yield and least non-specific bands obtained using the Tris buffer (pH 8.0). Based on this result, the SC-linked EdIII proteins were further purified using this buffer and the protocol described by He *et al.* (2014), making use of pH precipitation followed by nickel affinity chromatography. This resulted in high concentrations of purified proteins similar to what they obtained (~73µg/g FLW) specifically for EdIII-SC of approximately 69 mg/kg FLW, with a much lower yield observed for SC-EdIII of approximately 9 mg/kg FLW.

In vitro coupling of the purified SC-linked EdIII proteins to purified ST-AP205 VLPs at various molar ratios was successful when the SC peptide was located on the C terminus of the EdIII protein. However, when the SC peptide was located on the N terminus of EdIII, no coupling was observed. I suspect that this could be as a result of proteolytic cleavage taking place near or within the SC peptide during protein processing given that the SC-EdIII protein was observed to be several kilodaltons smaller than the EdIII-SC protein, when in fact they should be the same size. If a piece of the SC peptide gets cleaved off the SC-EdIII protein it almost certainly would render the peptide incapable of forming the covalent bond with the ST peptide on the AP205 particle and as a result, would explain the lack of coupling.

The various processes required to produce coupled AP205:EdIII consisted of; infiltration, purification by density gradient ultracentrifugation and quantification of the Spy-VLP proteins as well as infiltration, purification by pH precipitation and nickel affinity chromatography followed by quantification of the EdIII-SC protein. Once the concentrations of the two components were known, the molar ratios for *in vitro* coupling could be calculated, and only then could the coupling reaction be performed. This lengthy process does not lend itself well to commercialisation because of the time it takes to obtain the final product and the cost associated with each purification step especially when considering large-scale production. Therefore, I wanted to investigate if there was a way in which I could achieve the same result of a coupled AP205:EdIII complex, avoiding unnecessary purification steps.

Peyret *et al.* demonstrated the successful coupling of GFP-ST and the HIV capsid protein P24-ST with tHBcAg-SC *in vivo*, by co-infiltrating each of the Spytagged constructs with the tHBcAg-SC construct in *N. benthamiana*. tHBcAg VLPs were purified by density gradient ultracentrifugation and coupling between the VLP and either GFP or P24 was confirmed by western blot (Peyret *et al.*, 2020). Furthermore, Röder *et al.* successfully coupled endoglucanase Cel12A fused to the SC peptide to Spytagged Potato virus X (PVX-ST) particles by simply homogenising PVX-ST systemically infected *N. benthamiana* leaves

together with leaves infiltrated with the Cel12A-SC construct and purifying the coupled PVX particles further by layered bead chromatography (Röder *et al.*, 2017). Based on these successes, I investigated if I could purify coupled AP205:EdIII by co-infiltration of the ST-AP205 and EdIII-SC/CRT constructs and/or if I co-extracted leaves from plants infiltrated separately with these constructs. Both approaches resulted in the purification of coupled AP205:EdIII by a single density gradient ultracentrifugation purification step. These results, together with those obtained by Peyret and colleagues and Röder *et al*., illustrate that coupled products can be obtained without the need for several and lengthy purification processes, thereby making the downstream processing less time consuming and possibly more economically viable (Röder *et al.*, 2017; Peyret *et al.*, 2020).

I found that co-extraction of leaves from plants infiltrated separately with ST-AP205 and EdIII-SC/CRT resulted in a higher yield of AP205:EdIII complexes in comparison to when these constructs were co-infiltrated. Co-extraction involved the modification of the assembled AP205 VLPs however the co-expression of ST-AP205 and EdIII-SC would involve the modification of the AP205 coat protein prior to the incorporation into VLPs, which could explain the difference in coupling yields. Similar to the *in vitro* coupling experiment, co-infiltration and co-extraction of the ST-AP205 and EdIII-SC proteins yielded uncoupled products. However, in the instance of co-infiltration and co-extraction, there was only uncoupled ST-AP205 protein subunits detected, whereas for the *in vitro* coupling both uncoupled ST-AP205 protein subunits, as well as uncoupled EdIII-SC protein, was detected. Since the co-infiltrated and co-extracted proteins were purified by density gradient ultracentrifugation specifically for particle isolation, it was possible to remove all uncoupled EdIII-SC proteins as their density allowed them to accumulate in the supernatant above the 23% iodixanol density step. This is in contrast to Peyret *et al*. who after a two-step cushion ultracentrifugation purification of their co-infiltrated leaf extracts had both uncoupled GFP-ST and P24-ST proteins in addition to the uncoupled tHBcAg-SC proteins in their 70% purified fraction (Peyret *et al.*, 2020). Röder *et al.* also observed both uncoupled Cel12A-SC and PVX-ST proteins after co-extraction, but layered bead chromatography successfully removed all uncoupled Cel12A-SC and similar to this study they only observed uncoupled PVX-ST proteins together with their coupled product (Röder *et al.*, 2017).

The presence of uncoupled proteins appears to be a typical by-product of this technology regardless of the production platform and purification process used (Zakeri *et al.*, 2012; Brune *et al.*, 2016; Janitzek *et al.*, 2016; Thrane *et al.*, 2016; Singh *et al.*, 2017; Palladini *et al.*, 2018; Janitzek *et al.*, 2019; Harmsen *et al.*, 2020). Importantly, what needs to be noted is that the VLP cores (in most cases) consist of multiple copies of a single protein; in the instance of AP205 VLPs, this is 180 coat protein subunits. Therefore, each VLP core has different display

capacities: e.g. ST-AP205 has 180 (Thrane *et al.*, 2016), PVX-ST has ~1200 (Röder *et al.*, 2017) and tHBcAg-SC has either 90 or 120 (Peyret *et al.*, 2015; Peyret *et al.*, 2020). Considering this, logically it makes sense that most particles would have the target protein (antigen, enzyme etc.) coupled to at least one peptide-motif displayed on its surface, rather than having particles with 100% occupancy and some with 0%. Therefore, I need to consider that what I refer to as uncoupled VLP proteins represent only some of the protein subunits within a particle that are not coupled, rather than an entire 'uncoupled' particle. Nonetheless, the final goal is to reach the highest coupling density possible since it is an important factor in B cell activation (Thrane *et al.*, 2016).

Due to the ease of coupling by co-extraction and the absence of uncoupled EdIII-SC protein after purification, this strategy was selected for further optimisation instead of co-infiltration and *in vitro* coupling after ST-AP205 and EdIII-SC protein purification. Further purification to remove the uncoupled ST-AP205 protein subunits was investigated for the co-extracted ST-AP205 and EdIII-SC infiltrated leaves. Due to the presence of a His-tag on the N terminus of EdIII, the next obvious step was to purify the fractions containing AP205:EdIII by nickel affinity chromatography. However, the AP205:EdIII complex did not bind to the nickel column and was present in the flow-through (data not shown). It is possible that the His-tag was hidden due to how the proteins have folded and as a result could not bind to the nickel resin (Egelkrout *et al.*, 2012). This could be resolved by the addition of a linker sequence (e.g. Gly-linker) between the *EdIII* gene and the His-tag as was done for the genetic fusion of the SC peptide (Chen *et al.*, 2013).

The next approach was directed towards separating the AP205:EdIII complex from any uncoupled ST-AP205 protein subunits based on their density. I hypothesized that due to the display of EdIII on the surface of AP205, a particle with high EdIII occupancy might have a slightly greater density than a ST-AP205 particle that has little to no coupled EdIII and that these might be separated by a linear density gradient. Consequently, the 29% density fraction from the discontinuous iodixanol density gradient was diluted following ultracentrifugation and subject to a second ultracentrifugation through a linear iodixanol density gradient. No separation between the uncoupled ST-AP205 protein subunits and AP205:EdIII complexes was observed. Instead, the AP205:EdIII product was diluted across several fractions.

Consequently, the third approach rather focused on decreasing the amount of uncoupled ST-AP205 protein subunits and/or increasing the amount of AP205:EdIII complexes at the same time, basically aiming to increase the VLP occupancy by EdIII. This was investigated by varying the FLW extraction ratios, specifically looking at whether if I increased the FLW of EdIII-SC I would see an increase in coupling and as a result a decrease in uncoupled ST-AP205. Four FLW extractions ratios were evaluated; namely a 1:1, 1:2, 1:3 and 1:4 ST-AP205

to EdIII-SC and as expected an increase in AP205:EdIII and a decrease in uncoupled ST-AP205 were observed. Interestingly, however, at an extraction ration of 1:4 little to no uncoupled ST-AP205 was detected with a similar quantity of AP205:EdIII as for the 1:1 extraction ratio. Thrane and colleagues observed that there was a correlation between antigen size and the density of antigen display on the particles which suggests that steric hindrance plays a role in coupling (Thrane *et al.*, 2016). I propose that in the presence of too much protein, steric hindrance could also affect the coupling process and as such explain why I see similar coupling densities when co-extracting at a 1:1 and 1:4 FLW ratio, with coupling efficiencies of 9% and 8% respectively.

Similar coupling densities were observed for the 1:2 and 1:3 FLW co-extraction ratios, with average coupling efficiencies of 51% and 48% respectively. These are similar to previously reported results obtained when using the ST/SC technology (Janitzek *et al.*, 2016; Thrane *et al.*, 2016; Röder *et al.*, 2017; Palladini *et al.*, 2018). Both of these extraction ratios resulted in a larger quantity of coupled product than the 1:1 and 1:4 extraction ratios. As expected a decrease in the uncoupled ST-AP205 protein subunits was achieved with the increase in the EdIII-SC FLW ratio, representing an increase in VLP occupancy with EdIII. Consistently, the 1:2 FLW extraction ratio had higher coupling efficiencies and better coupling densities based on western blot band intensity and as such was selected as the optimal expression ratio to use with a yield of approximately 36 mg/kg AP205:EdIII per FLW. The presence of particles was also confirmed by TEM and VLPs of ~30 nm in diameter were observed at an amount of approximately 27 particles per field of view at a magnification of X80 000.

The work reported in this chapter illustrates the ease and diversity with which this Spy-VLP system can be used. I could readily produce pure ST-AP205 VLPs at high yields in plants of approximately 50 mg/kg FLW. Although the production of pure SC-linked EdIII proteins was more time consuming than for ST-AP205, I could produce EdIII-SC which successfully coupled to ST-AP205 at a yield of approximately 69 mg/kg FLW. Alternatively, I demonstrated that coupled AP205:EdIII could be produced by co-infiltration of these constructs as well as co-extraction of leaves individually infiltrated with these constructs, with a yield of ~36 mg/kg AP205:EdIII per FLW for the latter.

The ease of production of these coupled products and the yields at which I could produce them, in comparison to the difficulty with the production of native WNV VLPs (Chapter 3), illuminates the potential of this platform for the production of VLP-based vaccines for WNV. Additionally, this work represents the potential of using plants as biofactories for the production of recombinant proteins.

Chapter 5:

Conclusion

Since the first isolation of WNV in Uganda in 1937 (Smithburn *et al.*, 1940), the virus has spread and become endemic in countries across Africa, America, the Middle East, West Asia and Australia (Castro-Jorge *et al.*, 2019). The rapid and continuous spread of WNV and its continuous disease outbreaks in human, horse and bird populations (David & Abraham, 2016; Venter *et al.*, 2017; Aberle *et al.*, 2018; Kolodziejek *et al.*, 2018; López-Ruiz *et al.*, 2018; Silva *et al.*, 2019; Sinigaglia *et al.*, 2019; Papagiannis *et al.*, 2020; Zana *et al.*, 2020) are of great concern since there is no specific antiviral treatment available and little to no surveillance of the virus.

WNV can be prevented by vaccination, with several equine vaccines licensed and produced in America (Castro-Jorge *et al.*, 2019) and Europe (Rebollo *et al.*, 2018a); however, no human vaccine has been licensed. Even though there are equine vaccines available these can be difficult to obtain in LMIC due to the costs associated with the importation of the vaccines, the administrative challenges of procuring import permits, the cost of the vaccines themselves and the need for annual vaccination. Therefore, there is a desperate need for the development of a safe, effective and affordable vaccine that could be readily produced in LMIC to resolve these issues.

The development of plant-based production platforms is favourable in LMIC due to the lower cost involved for the establishment and running of the facilities as well as their safety and ease of scalability (Twyman *et al.*, 2003; Rybicki, 2009; Egelkrout *et al.*, 2012; Martinez *et al.*, 2012; Schillberg *et al.*, 2019; Fischer & Buyel, 2020). The use of plants as biofactories for the production of VLPs, specifically in *N. benthamiana*, has been illustrated for many viruses (Maclean *et al.*, 2007; D'Aoust *et al.*, 2008; Peyret *et al.*, 2015; van Zyl *et al.*, 2016; Dennis *et al.*, 2018a; Mbewana *et al.*, 2018; Veerapen *et al.*, 2018; Gunter *et al.*, 2019; Marsian *et al.*, 2019; Ponndorf *et al.*, 2020), demonstrating the promise of this technology for the development of particulate candidate vaccines. The main aim of this study was to develop a particulate candidate vaccine for WNV using *N. benthamiana* as the production platform. Our approach was two-fold; firstly to determine whether I could produce a native VLP candidate vaccine by expressing the WNV *prM* and *E* genes; and secondly, to investigate the production of a display-based candidate vaccine using the ST/SC technology to display the WNV EdIII protein on the bacteriophage AP205 particle surface.

I successfully demonstrated the production of both of these candidate vaccines. The production of the native WNV VLP proved difficult due to poor reproducibility and low VLP yield. Regardless, I demonstrated that VLPs assembled by co-expressing any of the four WNV *prM* gene permutations (based on signal sequences or plant expression vector) with the WNV *E* gene together with the human chaperone CNX *in planta*. Protein expression time-trials of the E protein illustrated a significant increase in soluble protein when expressed in the presence of the human chaperone protein CNX. Similarly, SC-linked EdIII proteins were undetectable by western blot until expressed with either human CNX or CRT, highlighting the impact chaperones have on protein production *in planta* and that glycoproteins might be incompatible with the plant endogenous chaperones (Margolin *et al.*, 2018; Margolin *et al.*, 2020).

The optimisation of native WNV VLP purification was performed using a single prM construct which contained the LPH signal peptide. It would, however, be interesting to see what the results would yield when the E protein is co-expressed with the other 3 prM constructs generated in this study and whether this would influence the VLP assembly or yield when purified using the optimised protocol. Additionally, it would be interesting to investigate whether any of these plant-produced VLPs induce an immune response in mice.

The antigen-display based candidate vaccine proved much easier to produce than the native VLP vaccine. In this study, I demonstrated the successful coupling of the WNV EdIII protein on the AP205 VLP surface applying the ST/SC technology coupling reaction using three different approaches: 1) *in vitro* coupling following purification of each Spy-linked component, 2) *in vitro* coupling by co-extracting leaves infiltrated individually with each Spy-linked component, and 3) *in vivo* coupling by co-expressing the Spy-linked components. The successful coupling of EdIII-SC to ST-AP205 using each of these techniques illustrates the robustness of this technology with its application *in planta*. In future, I would like to conduct immunogenicity studies in mice, to investigate whether this candidate vaccine elicits an immune response, specifically neutralising antibodies. The induction of an immune response can be investigated by indirect ELISAs with the immunised mice serum for the detection of anti-WNV-EdIII antibodies and presence of neutralising antibodies can be detected by neutralisation assays. Additionally, I hope to translate this strategy to other flaviviruses as proof of concept of the technology's plug-and-play capability, as has been exemplified in recent publications.

With the recent Coronavirus outbreak (COVID-19), several studies have been published using the ST/SC technology for the development of candidate vaccines. COVID-19 disease is caused by the severe acute respiratory syndrome coronavirus 2 (SARS-CoV-2), which was first reported in Wuhan, China in December 2019 (Zhu *et al.*, 2020). Since then the virus has

spread across the globe and was declared a pandemic by the World Health Organisation (WHO) in March 2020. As of October 2020, there have been over 44 million confirmed COVID-19 cases worldwide with approximately 1.1 million recorded deaths (WHO, 2020). To date, there is no vaccine or specific antiviral treatment for COVID-19, however, since August 2020 several vaccine candidates are in clinical evaluation.

Tan and colleagues developed a SARS-CoV-2 candidate vaccine focused on displaying the spike receptor-binding domain (RBD) on the surface of the mi3 VLP using the ST/SC technology (Tan *et al.*, 2020). The authors conjugated purified ST-RBD from mammalian cells to the SC-mi3 VLP to generate the RBD:mi3 immunogen with a coupling efficiency of ~64% that translated to ~38 RBD/VLP. The immunogen was shown to be stable at -80°C, -20°C, 4°C and 25°C for two weeks, demonstrating the high resilience of the RBD:mi3. Immunogenicity of RBS:mi3 induced high neutralising antibody titres in two mice strains from relatively low doses of the immunogen. In comparison, when mice were immunised with RBD only at the same doses as RBD:mi3 the antibody responses were negligible.

In another study, Zhang *et al*. displayed the SARS-CoV-2 spike trimer on the *Aquifex aeolicus* lumazine synthase (LuS) 60-mer nanoparticle scaffold also employing the ST/SC technology with a coupling efficiency of ~91% (Zhang *et al.*, 2020). Mice immunised with 0.08 µg of the LuS:CoV-2 spike nanoparticle elicited a higher neutralising response than mice immunised with 2 µg of the trimeric spike protein. Both these studies illustrate that a significantly lower dose of immunogen is required to elicit a potent neutralising response when the antigen is displayed on the surface of a particle compared to when it's used as an immunogen on its own. Since glycoproteins are generally difficult to produce in plants and are usually only produced at low yields, the display of these proteins on a particle may circumvent the need of high yields for immunising as described above. I was able to produce EdIII-SC at a yield of 69 mg/kg which is comparable to that produced by He and colleagues of 73 mg/kg (He *et al.*, 2014). The authors evaluated the immunogenicity of their plant-produced WNV EdIII antigen in mice at a dose of 5 µg and 25 µg. An immune response was detected after the first dose of 25 µg in mice, however, for the mice immunised with 5 µg, a response was only detectable after the third immunisation. Based on the findings by both Tan *et al*. (2020) and Zhang *et al*. (2020), I expect to get a similar or even better response of our AP205:EdIII candidate vaccine at the same or lower dose as when I immunise with EdIII-SC alone.

The establishment of a particle core for the display of proteins, whether it is the coat protein of the AP205 bacteriophage (Thrane *et al.*, 2016) or PVX (Röder *et al.*, 2017), the LuS of *A. aeolicus* (Zhang *et al.*, 2020), the mi3 VLP computationally engineered *Thermotoga maritima*

(Bruun *et al.*, 2018; Tan *et al.*, 2020) or the core protein of tHBcAg (Peyret *et al.*, 2020) for use with the ST/SC technology, allows for relatively easy plug-and-play applications.

The above studies, together with the work presented in this study illustrates the potential of the ST/SC technology as a fast and effective approach for the development of candidate vaccines in the midst of disease outbreak. The combination of this technology with that of plant molecular farming creates the opportunity for LMIC to locally produce their own pharmaceuticals which work towards fulfilling the goals of the 'One Health' Initiative.

In this study, I illustrated the promise of using plants as biofactories for the production of VLP-based candidate vaccines. Although I experienced difficulty with producing WNV native VLPs as a candidate vaccine, VLPs were assembled but at yields which were insufficient for preparing doses for testing in animals. Alternatively, using the ST/SC technology allowed us to produce a particle display-based WNV candidate vaccine in *N. benthamiana* that could easily be purified at yields which are sufficiently high to use for vaccine doses, thereby fulfilling the aim of my study.

Appendix

Appendix A: Amino acid alignment of *prM* and *E* genes of South African WNV strains.

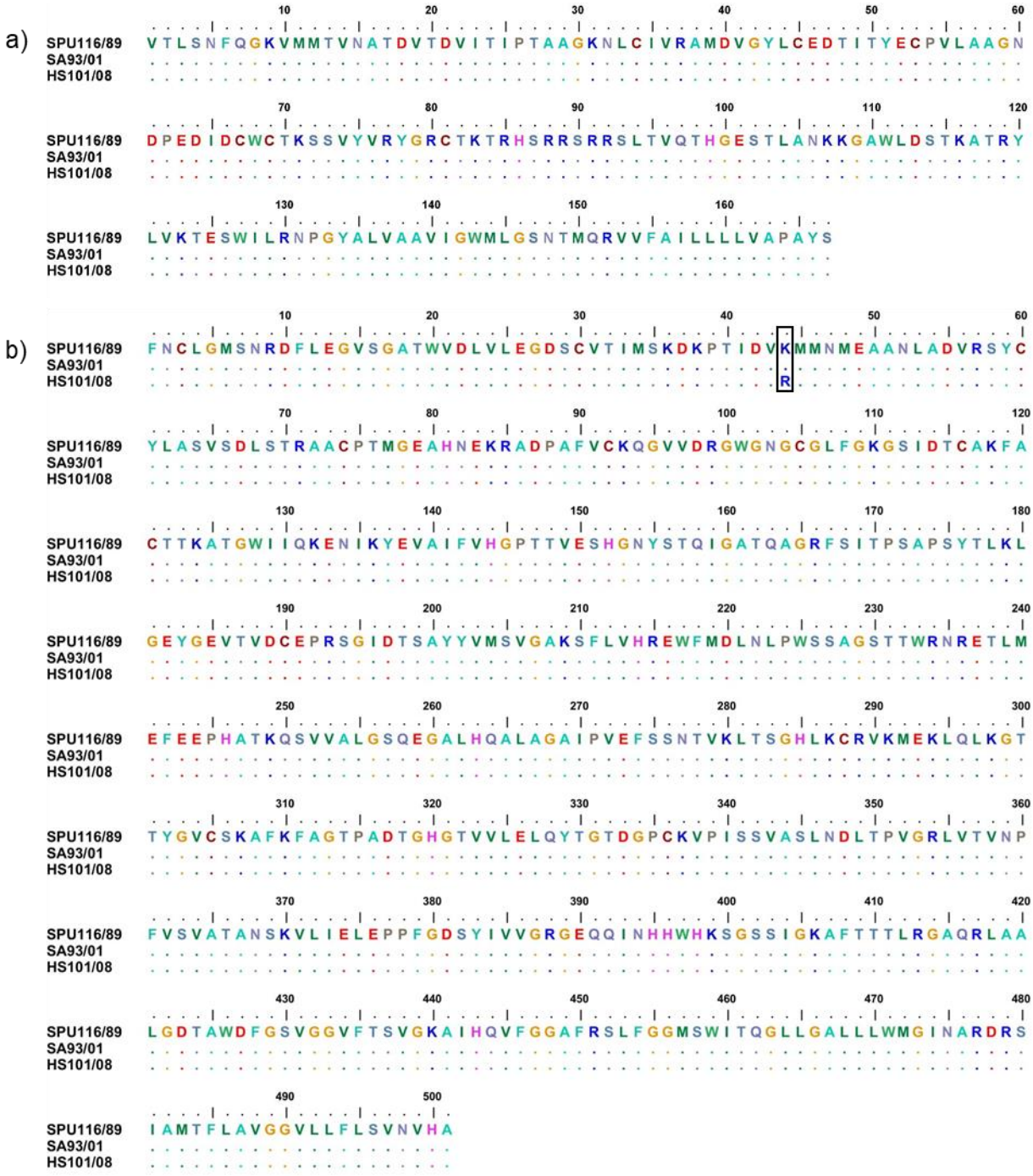

Figure 1. ClustalW alignment of the prM and E amino acid sequences of three South African WNV strains. **(A)** Alignment of prM amino acid sequences with complete homology observed. **(B)** Alignment of E amino acid sequences with complete homology between the human strains; SPU116/89 and SA93/01. A single difference was observed for the horse strain, HS101/08, at the Lys44 residue of SPU116/89 and SA93/01, with an Arg44 for HS101/08. GenBank accessions: SPU116/89; EF429197, SA93/01; EF429198, HS101/08; JN393308.

Appendix B: Polymerase chain reaction primer sequences.

Table 1. Vector-specific primer sequences.

Primer name	5'-3' sequence	Tm (°C)	Base pairs
pTRA-F	CAT TTC ATT TGG AGA GGA CAC G	58	22
pTRA-R	GAA CTA CTC ACA CAT TAT TCT GG	56	23
pEAQ-F	TTC TTC TTC TTG CTG ATT GG	55	20
pEAQ-R	CAC AGA AAA CCG CTC ACC	57	18

Table 2. Gene-specific and gene-alteration primer sequences.

Primer name	5'-3' sequence	Tm (°C)	Base pairs	Enzyme site
LPH-AgeI-F	**ACC GGT** ATG GAG TGG AGC TGG AT	66	23	*Age*I
E-NcoI-F32	AT**C CAT GG**T TAA TTG TTT GGG AAT GTC TAA TA	62	32	*Nco*I
E-XhoI-R	AT**C TCG AG**C GTG CAC ATT CAC AGA TA	65	25	*Xho*I
E-HIS-XhoI-R	AT**C TCG AG**T TA**G TGA TGG TGA TGG TGA TG**A GCG TGC ACA TTC ACA GAT AA	51	50	*Xho*I 6x His
AgeI-NcoI-prM-F	**ACC GGT CCA TGG** CCA GGT CTA CTA AGC AGA	72	30	*Age*I *Nco*I
Age-NcoI-SS-F	**ACC GGT CCA TGG** GAG GAA CAG CAG GTT T	72	28	*Age*I *Nco*I
XhoI-prM-R	**CTC GAG** TTA ACT GTA AGC AGG AGC CAC TA	65	29	*Xho*I

Table 3. In-fusion cloning primer sequences.

Primer name	5'-3' sequence	Tm (°C)	Base pairs	Enzyme site
Fp1	GGT GTT CAC TCC ATG CAT CAC CAT CAC CAT CAC ATG GGA GTT TGC TCA AAG GC	60	53	6x His
Rp1	AGA ACC TCC TCC TCC AGA TCC ACC TCC TCC TGA CTT ATG CCA ATG ATG AT	54	50	-
Fp2	GGA GGA GGT GGA TCT GGA GGA GGA GGT TCT ATG GGT GCT ATG GTT GAT AC	58	50	-
Rp2	**GGA TCC** GAG **CTC GAG** TTA AAT ATG AGC ATC TCC CTT AG	56	38	*Xho*I *BamH*I
Fp3	GGT GTT CAC TCC ATG GGT GCT ATG GTT GAT ACT CT	58	35	-
Rp3	AGA ACC TCC TCC TCC AGA TCC ACC TCC TCC AAT ATG AGC ATC TCC CTT AG	56	50	-
Fp4	GGA GGA GGT GGA TCT GGA GGA GGA GGT TCT ATG GGA GTT TGC TCA AAG GC	60	50	-
Rp4	GGA TCC GAG CTC GAG TTA GTG ATG GTG ATG GTG ATG TGA CTT ATG CCA ATG ATG AT	54	56	*Xho*I *BamH*I

Appendix C: Agrobacterium strains used and their respective antibiotics.

Table 4. *A. tumefaciens* strains' relevant antibiotics and concentrations.

Antibiotics	***Agrobacterium tumefaciens* strain**		
	LBA4404	**GV3101::pMP90RK**	**AGL1**
Carbenicillin	-	100 µg/mL	25 µg/mL
Kanamycin	30 µg/mL	30 µg/mL	50 µg/mL
Rifampicin	50 µg/mL	50 µg/mL	-

Appendix D: Infiltration optical densities.

Table 5. Optical densities at which constructs were co-infiltrated.

Co-infiltrations	OD_{600}	Combined OD_{600}
pTRAkc-E-HIS **pEAQ-CNX/CRT**	0.5 each	1/1.5
pTRAkc-E-HIS **pBIN-NSs**	0.5 0.25	0.75
pTRAkc-E-HIS **pEAQ-CNX/CRT** **pBIN-NSs**	0.5 0.5 0.25	1.25
pTRAkc-E **pEAQ-CNX** **pTRAkc-prM**	0.3 each	0.9
pTRAkc-E **pEAQ-CNX** **pEAQ-C_8-SS-prM**	0.3 each	0.9
pTRAkc-E **pEAQ-CNX** **pTRAc-C_8-SS-prM**	0.3 each	0.9
pTRAkc-E **pEAQ-CNX** **pTRAc-SS-prM**	0.3 each	0.9
pTRAkc-SC-EdIII	0.25/0.5	0.25/0.5
pTRAkc-EdIII-SC	0.25/0.5	0.25/0.5
pTRAkc-SC-EdIII **pEAQ-CNX/CRT**	0.5 each	1
pTRAkc-EdIII-SC **pEAQ-CNX/CRT**	0.5 each	1
pEAQ-ST-AP205	0.25	0.25
pEAQ-ST-AP205 **pTRAkc-EdIII-SC** **pEAQ-CRT**	0.3 each	0.9

Appendix E: Antiserum used for protein detection.

Table 6. Antiserum and dilutions used for the detection of proteins expressed in this study.

Antiserum*	Proteins detected			
	E	**prM**	**EdIII-SC**	**ST-AP205**
Polyclonal rabbit anti-WNV-EdIII	1:20 000	-	1:20 000	-
Polyclonal rabbit anti-WNV-M	-	1:20 000	-	
Polyclonal rabbit anti-ST-AP205	-	-	-	1:20 000

* All three antisera were produced in-house.

Appendix F: Supplementary western blots and Coomassie-stained gels

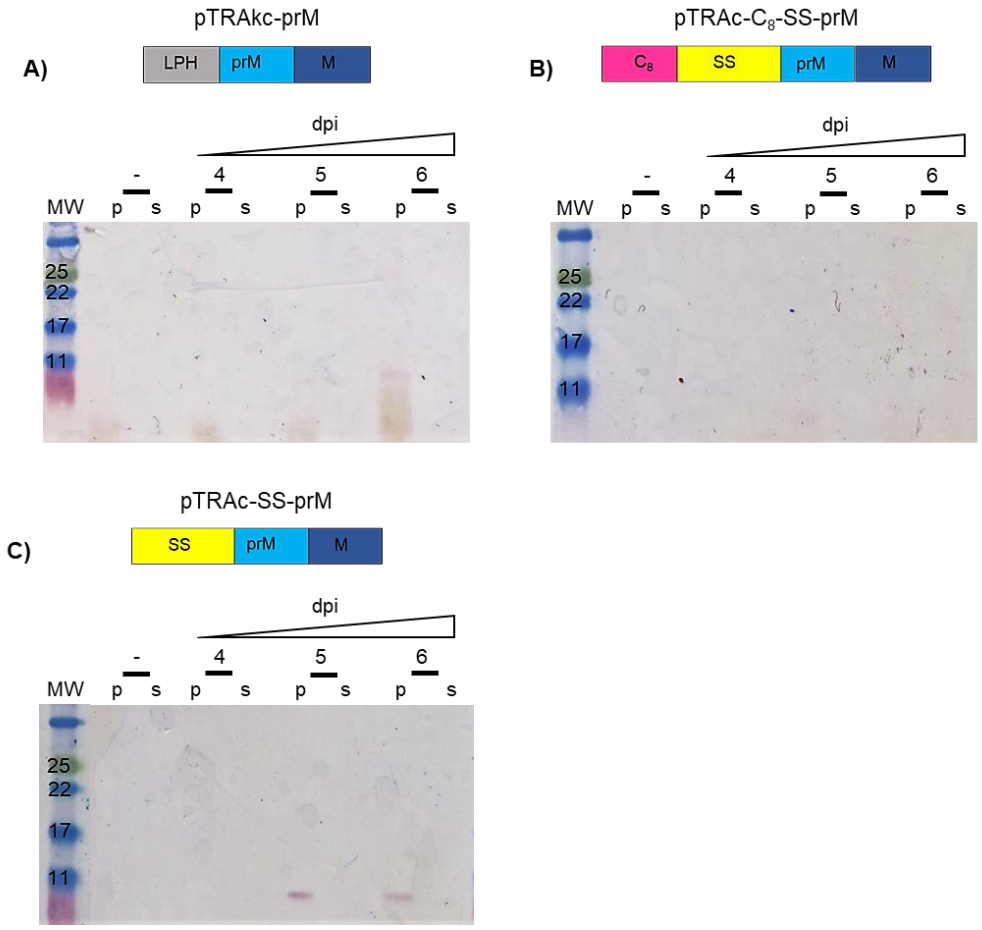

Figure 2. Expression of prM proteins over 6 days using different signal peptide permutations **(A)** LPH, **(B)** C_8-SS, and **(C)** SS. Proteins were extracted as described in section 2.2.7.1 using 100 mM Tris.HCl (pH 7.4) and 30 µg TSP of pellet (p) and supernatant (s) crude extracts were loaded in each lane. Proteins were detected with anti-WNV-M antiserum (1:20 000). **(A)** pTRAkc-prM, **(B)** pTRAc- C_8-SS-prM, and **(C)** pTRAc-SS-prM. The negative controls (-) are crude leaf extracts of plants infiltrated with pTRAkc-ERH empty vector. Label: dpi denotes 4, 5 and 6 days post infiltration. p represents the insoluble fraction; pellet. s represents the soluble fraction; supernatant. MW indicates the molecular weight marker.

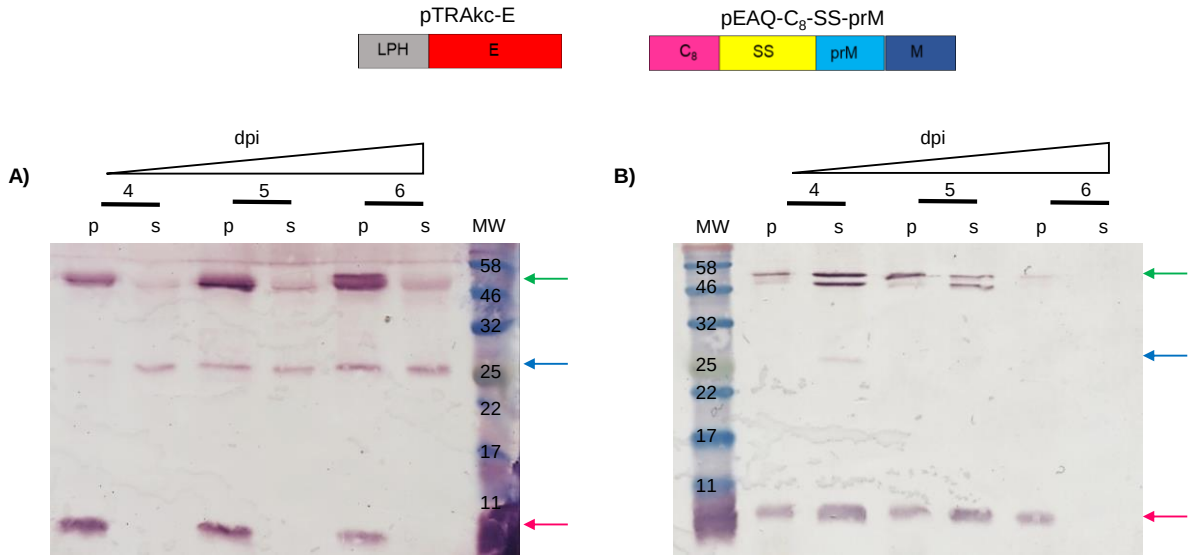

Figure 3. Co-expression of pTRAkc-E and pEAQ-C_8-SS-prM over 6 days extracting with different buffers. Proteins were extracted as described in section 2.2.7.1 using 100 mM Tris.HCl (pH 7.4) and loading 30 µg TSP **(A)** or as described in section 2.2.7.2 using 1x PBS (pH 6.0) and loading 25 µg TSP of pellet (p) and supernatant (s) crude extracts in each lane. Proteins were detected with anti-WNV-EdIII combined with anti-WNV-M antisera (1:20 000 each); E – green arrow, prM – blue arrow, M – pink arrow. Label: dpi denotes 4, 5 and 6 days post infiltration. p represents the insoluble fraction; pellet. s represents the soluble fraction; supernatant. MW indicates the molecular weight marker.

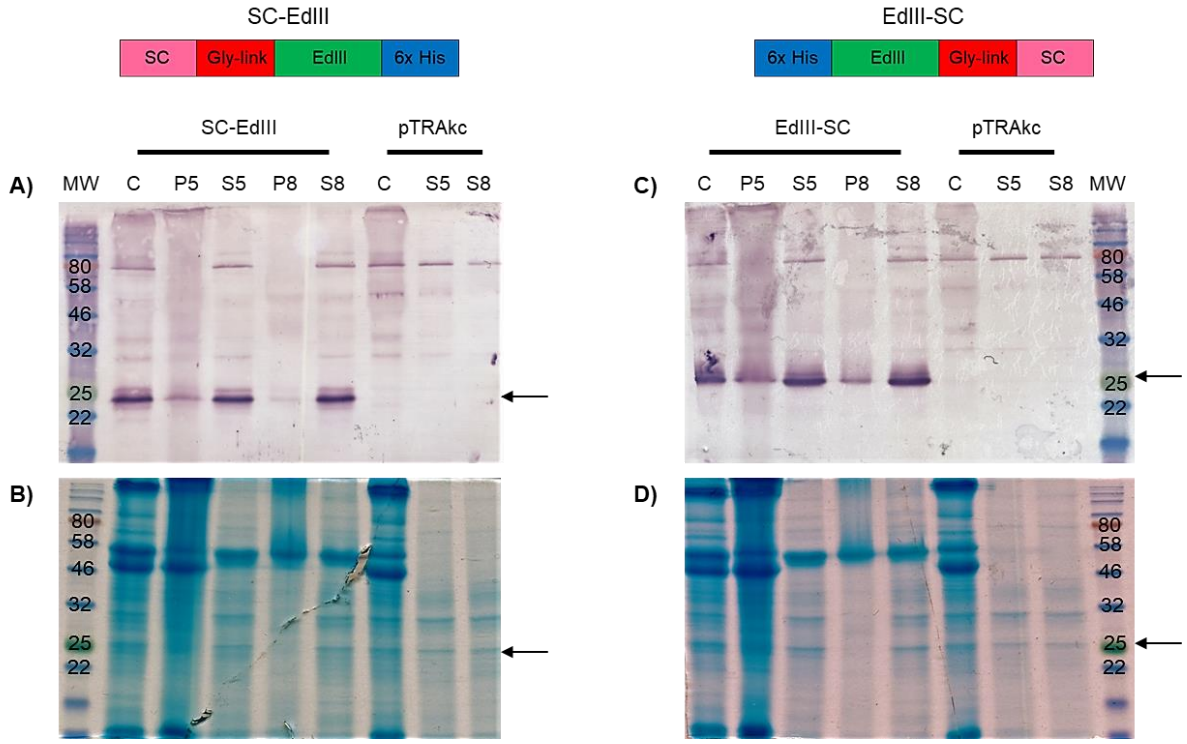

Figure 4. Purification of SC-linked EdIII protein by pH precipitation. The pH of clarified crude plant extracts was dropped to 5, centrifuged and the supernatant readjusted to pH 8.0, centrifuged and the supernatant subject to nickel affinity chromatography. Equal volumes of clarified crude plant extract and samples at each step during pH precipitation was loaded in each lane. SC-linked EdIII proteins were detected using anti-WNV-EdIII antiserum (1:20 000). Arrows indicate SC-linked EdIII proteins **(A)** SC-EdIII samples analysed by western blot and **(B)** Coomassie blue-stained gel. **(C)** EdIII-SC samples analysed by western blot and **(D)** Coomassie blue-stained gel. MW, the molecular weight marker. C, clarified crude plant extract. P, pellet. S, supernatant. 5, pH 5.0. 8, pH 8.0.

Appendix G: Nickel affinity chromatograms

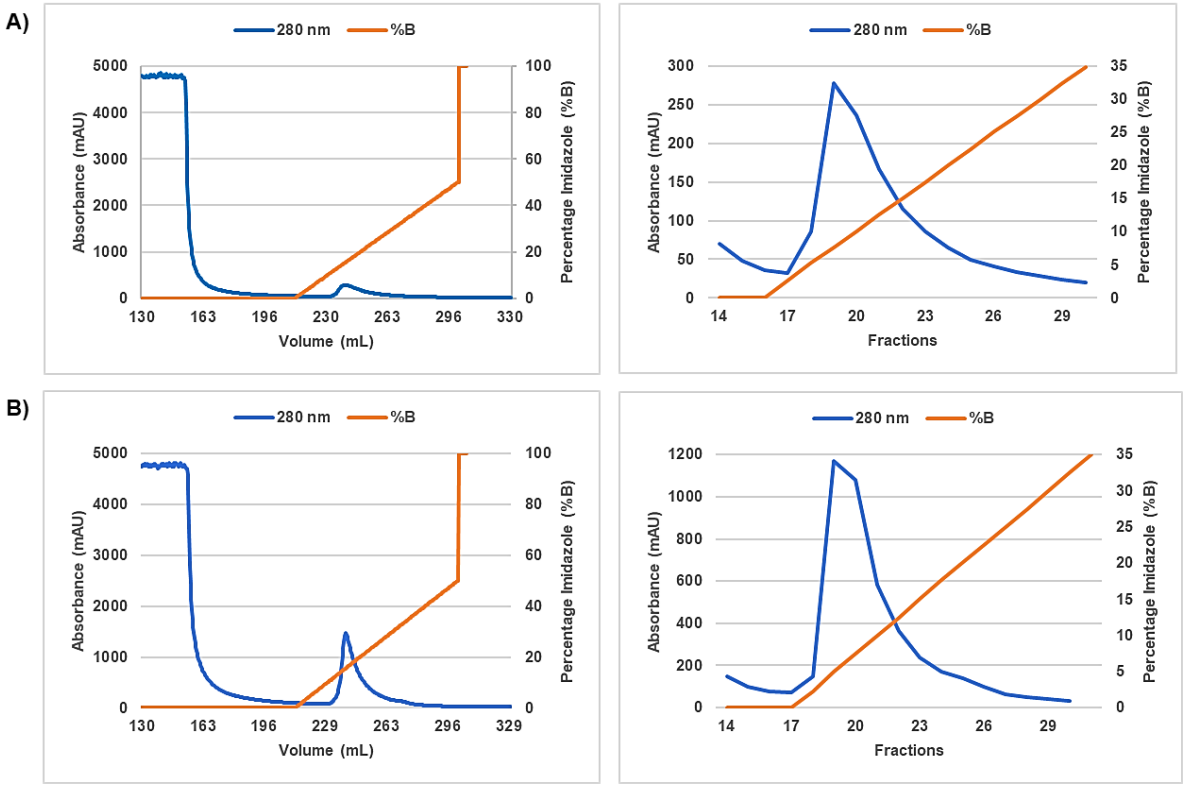

Figure 5. Purification of SC-linked EdIII proteins using nickel affinity chromatography. Chromatographic elution profiles showing **(A)** SC-EdIII and **(B)** EdIII-SC proteins eluted from nickel columns with increasing imidazole concentrations (orange line).

Bibliography

Aberle, S. W., Kolodziejek, J., Jungbauer, C., Stiasny, K., Aberle, J. H., Zoufaly, A., Hourfar, M. K., Weidner, L. & Nowotny, N. (2018) Increase in human West Nile and Usutu virus infections, Austria, 2018. *Eurosurveillance*, 23(43).

Agrawal, A. G. & Petersen, L. R. (2003) Human Immunoglobulin as a Treatment for West Nile Virus Infection. *The Journal of Infectious Diseases*, 188(1), 1-4.

Alam, A., Jiang, L., Kittleson, G. A., Steadman III, K. D., Nandi, S., Fuqua, J. L., Palmer, K. E., Tusé, D. & McDonald, K. A. (2018) Technoeconomic Modeling of Plant-Based Griffithsin Manufacturing. *Frontiers in bioengineering and biotechnology*, 6, 102.

Alonso-Padilla, J., de Oya, N. J., Blazquez, A. B., Escribano-Romero, E., Escribano, J. M. & Saiz, J. C. (2011) Recombinant West Nile virus envelope protein E and domain III expressed in insect larvae protects mice against West Nile disease. *Vaccine*, 29(9), 1830-5.

American Veterinary Medical Association *Intervet/Schering-Plough recalls PreveNile vaccine* (Updated: 2010). Available online: https://www.avma.org/javma-news/2010-06-15/intervetschering-plough-recalls-prevenile-vaccine [Accessed: 14 April 2020].

Anderson, J. F. & Rahal, J. J. (2002) Efficacy of interferon α-2b and ribavirin against West Nile virus in vitro. *Emerging infectious diseases*, 8(1), 107.

Antoniadis, A., Alexiou-Daniel, S., Malissiovas, N., Doutsos, J., Polyzoni, T., LeDue, J., Peters, C. & Saviolakis, G. (1990) Seroepidemiological survey for antibodies to arboviruses in Greece, *Hemorrhagic Fever with Renal Syndrome, Tick-and Mosquito-Borne Viruses*Springer, 277-285.

Arroyo, J., Miller, C., Catalan, J., Myers, G. A., Ratterree, M. S., Trent, D. W. & Monath, T. P. (2004) ChimeriVax-West Nile virus live-attenuated vaccine: preclinical evaluation of safety, immunogenicity, and efficacy. *Journal of virology*, 78(22), 12497-12507.

Assaid, N., Mousson, L., Moutailler, S., Arich, S., Akarid, K., Monier, M., Beck, C., Lecollinet, S., Failloux, A. & Sarih, M. (2020) Evidence of circulation of West Nile virus in Culex pipiens mosquitoes and horses in Morocco. *Acta Tropica*, 205, 105414.

Baba, M., Logue, C. H., Oderinde, B., Abdulmaleek, H., Williams, J., Lewis, J., Laws, T. R., Hewson, R., Marcello, A. & D'Agaro, P. (2013) Evidence of arbovirus co-infection in suspected febrile malaria and typhoid patients in Nigeria. *The Journal of Infection in Developing Countries*, 7(01), 051-059.

Bagnarelli, P., Marinelli, K., Trotta, D., Monachetti, A., Tavio, M., Del Gobbo, R., Capobianchi, M., Menzo, S., Nicoletti, L. & Magurano, F. (2011) Human case of autochthonous West Nile virus lineage 2 infection in Italy, September 2011. *Eurosurveillance*, 16(43), 20002.

Bakonyi, T., Ferenczi, E., Erdélyi, K., Kutasi, O., Csörgő, T., Seidel, B., Weissenböck, H., Brugger, K., Bán, E. & Nowotny, N. (2013) Explosive spread of a neuroinvasive lineage 2 West Nile virus in Central Europe, 2008/2009. *Veterinary microbiology*, 165(1-2), 61-70.

Bakonyi, T., Hubálek, Z., Rudolf, I. & Nowotny, N. (2005) Novel flavivirus or new lineage of West Nile virus, central Europe. *Emerging infectious diseases*, 11(2), 225.

Bakonyi, T., Ivanics, É., Erdélyi, K., Ursu, K., Ferenczi, E., Weissenböck, H. & Nowotny, N. (2006) Lineage 1 and 2 strains of encephalitic West Nile virus, central Europe. *Emerging infectious diseases*, 12(4), 618.

Barzon, L., Squarzon, L., Cattai, M., Franchin, E., Pagni, S., Cusinato, R. & Palu, G. (2009) West Nile virus infection in Veneto region, Italy, 2008-2009. *Eurosurveillance*, 14(31), 19289.

Beasley, D. W. & Barrett, A. D. (2002) Identification of neutralizing epitopes within structural domain III of the West Nile virus envelope protein. *Journal of virology*, 76(24), 13097-13100.

Bernkopf, H., Levine, S. & Nerson, R. (1953) Isolation of West Nile virus in Israel. *The Journal of infectious diseases*, 207-218.

Best, S. M. (2017) The many faces of the flavivirus NS5 protein in antagonism of type I interferon signaling. *Journal of virology*, 91(3), e01970-16.

Biedenbender, R., Bevilacqua, J., Gregg, A. M., Watson, M. & Dayan, G. (2011) Phase II, randomized, double-blind, placebo-controlled, multicenter study to investigate the immunogenicity and safety of a West Nile virus vaccine in healthy adults. *Journal of Infectious Diseases*, 203(1), 75-84.

Bin, H., Grossman, Z., Pokamunski, S., Malkinson, M., Weiss, L., Duvdevani, P., Banet, C., Weisman, Y., Annis, E. & Gandaku, D. (2001) West Nile Fever in Israel 1999-2000: From Geese to Humans. *Annals of the New York Academy of Sciences*, 951(1), 127-142.

Boehringer Ingelheim *Vetera WNV* (Updated: 2019). Available online: https://www.bi-vetmedica.com/species/equine/products/vetera_vaccines/Vetera_WNV.html [Accessed: 14 April 2020].

Bofill, D., Domingo, C., Cardeñosa, N., Zaragoza, J., de Ory, F., Minguell, S., Sánchez-Seco, M. P., Domínguez, A. & Tenorio, A. (2006) Human West Nile virus infection, Catalonia, Spain. *Emerging infectious diseases*, 12(7), 1163.

Bondre, V. P., Jadi, R., Mishra, A., Yergolkar, P. & Arankalle, V. (2007) West Nile virus isolates from India: evidence for a distinct genetic lineage. *Journal of General Virology*, 88(3), 875-884.

Borisevich, V., Seregin, A., Nistler, R., Mutabazi, D. & Yamshchikov, V. (2006) Biological properties of chimeric West Nile viruses. *Virology*, 349(2), 371-381.

Brandler, S. & Tangy, F. (2013) Vaccines in development against West Nile virus. *Viruses*, 5(10), 2384-2409.

Brinton, M. A. (2002) The molecular biology of West Nile Virus: a new invader of the western hemisphere. *Annual Reviews in Microbiology*, 56(1), 371-402.

Brune, K. D. & Howarth, M. (2018) New Routes and Opportunities for Modular Construction of Particulate Vaccines: Stick, Click, and Glue. *Frontiers in Immunology*, 9(1432).

Brune, K. D., Leneghan, D. B., Brian, I. J., Ishizuka, A. S., Bachmann, M. F., Draper, S. J., Biswas, S. & Howarth, M. (2016) Plug-and-Display: decoration of Virus-Like Particles via isopeptide bonds for modular immunization. *Scientific reports*, 6, 19234.

Bruun, T. U. J., Andersson, A.-M. C., Draper, S. J. & Howarth, M. (2018) Engineering a Rugged Nanoscaffold To Enhance Plug-and-Display Vaccination. *ACS nano*, 12(9), 8855-8866.

Burt, F. J., Grobbelaar, A. A., Leman, P. A., Anthony, F. S., Gibson, G. & Swanepoel, R. (2002) Phylogenetic relationships of southern African West Nile virus isolates. *Emerging infectious diseases*, 8(8), 820-826.

Buyel, J., Twyman, R. & Fischer, R. (2015) Extraction and downstream processing of plant-derived recombinant proteins. *Biotechnology advances*, 33(6), 902-913.

Campos, J. L. S., Mongkolsapaya, J. & Screaton, G. R. (2018) The immune response against flaviviruses. *Nature Immunology*, 19(11), 1189-1198.

Caramelo, J. J. & Parodi, A. J. (2008) Getting in and out from calnexin/calreticulin cycles. *Journal of Biological Chemistry*, 283(16), 10221-10225.

Cardona-Ospina, J. A., Sepúlveda-Arias, J. C., Mancilla, L. & Gutierrez-López, L. G. (2016) Plant expression systems, a budding way to confront chikungunya and Zika in developing countries? *F1000Research*, 5.

Castro-Jorge, L. A. d., Siconelli, M. J. L., Ribeiro, B., Moraes, F. M. d., Moraes, J. B. d., Agostinho, M. R., Klein, T. M., Floriano, V. G. & Fonseca, B. (2019) West Nile virus infections are here! Are we prepared to face another flavivirus epidemic? *Revista da Sociedade Brasileira de Medicina Tropical*, 52, e20190089-e20190089.

Centers for Disease Control and Prevention (2001) *Human West Nile virus surveillance-Connecticut, New Jersey, and New York, 2000*.

Chambers, T. J., Hahn, C. S., Galler, R. & Rice, C. M. (1990) Flavivirus genome organization, expression, and replication. *Annual Reviews in Microbiology*, 44(1), 649-688.

Chancey, C., Grinev, A., Volkova, E. & Rios, M. (2015) The global ecology and epidemiology of West Nile virus. *BioMed research international*, 2015.

Chen, Q. (2015) Plant-made vaccines against West Nile virus are potent, safe, and economically feasible. *Biotechnology journal*, 10(5), 671-680.

Chen, Q., He, J., Phoolcharoen, W. & Mason, H. S. (2011) Geminiviral vectors based on bean yellow dwarf virus for production of vaccine antigens and monoclonal antibodies in plants. *Human vaccines*, 7(3), 331-338.

Chen, Q. & Lai, H. (2013) Plant-derived virus-like particles as vaccines. *Human vaccines & immunotherapeutics*, 9(1), 26-49.

Chen, X., Zaro, J. L. & Shen, W.-C. (2013) Fusion protein linkers: property, design and functionality. *Advanced drug delivery reviews*, 65(10), 1357-1369.

Chisenhall, D. M. & Mores, C. N. (2009) Diversification of West Nile virus in a subtropical region. *Virology journal*, 6, 106-106.

Chu, J. & Ng, M. (2004) Infectious entry of West Nile virus occurs through a clathrin-mediated endocytic pathway. *Journal of virology*, 78(19), 10543-10555.

Chu, X., Li, Y., Long, Q., Xia, Y., Yao, Y., Sun, W., Huang, W., Yang, X., Liu, C. & Ma, Y. (2016) Chimeric HBcAg virus-like particles presenting a HPV 16 E7 epitope significantly suppressed tumor progression through preventive or therapeutic immunization in a TC-1-grafted mouse model. *International journal of nanomedicine*, 11, 2417.

Cielens, I., Jackevica, L., Strods, A., Kazaks, A., Ose, V., Bogans, J., Pumpens, P. & Renhofa, R. (2014) Mosaic RNA Phage VLPs Carrying Domain III of the West Nile Virus E Protein. *Molecular Biotechnology*, 56(5), 459-469.

Ciota, A. T. & Kramer, L. D. (2013) Vector-virus interactions and transmission dynamics of West Nile virus. *Viruses*, 5(12), 3021-3047.

D'Aoust, M.-A., Lavoie, P.-O., Couture, M. M.-J., Trépanier, S., Guay, J.-M., Dargis, M., Mongrand, S., Landry, N., Ward, B. J. & Vézina, L.-P. (2008) Influenza virus-like particles produced by transient expression in Nicotiana benthamiana induce a protective immune response against a lethal viral challenge in mice. *Plant Biotechnology Journal*, 6(9), 930-940.

Danis, K., Papa, A., Theocharopoulos, G., Dougas, G., Athanasiou, M., Detsis, M., Baka, A., Lytras, T., Mellou, K. & Bonovas, S. (2011) Outbreak of West Nile virus infection in Greece, 2010. *Emerging infectious diseases*, 17(10), 1868.

David, S. & Abraham, A. M. (2016) Epidemiological and clinical aspects on West Nile virus, a globally emerging pathogen. *Infectious Diseases*, 48(8), 571-586.

Davis, B. S., Chang, G.-J. J., Cropp, B., Roehrig, J. T., Martin, D. A., Mitchell, C. J., Bowen, R. & Bunning, M. L. (2001) West Nile virus recombinant DNA vaccine protects mouse and horse from virus challenge and expresses in vitro a noninfectious recombinant antigen that can be used in enzyme-linked immunosorbent assays. *Journal of virology*, 75(9), 4040-4047.

Davis, C. T., Ebel, G. D., Lanciotti, R. S., Brault, A. C., Guzman, H., Siirin, M., Lambert, A., Parsons, R. E., Beasley, D. W. C., Novak, R. J., Elizondo-Quiroga, D., Green, E. N., Young, D. S., Stark, L. M., Drebot, M. A., Artsob, H., Tesh, R. B., Kramer, L. D. & Barrett, A. D. T. (2005) Phylogenetic analysis of North American West Nile virus isolates, 2001–2004: Evidence for the emergence of a dominant genotype. *Virology*, 342(2), 252-265.

Dayan, G. H., Bevilacqua, J., Coleman, D., Buldo, A. & Risi, G. (2012) Phase II, dose ranging study of the safety and immunogenicity of single dose West Nile vaccine in healthy adults≥ 50 years of age. *Vaccine*, 30(47), 6656-6664.

Dayan, G. H., Pugachev, K., Bevilacqua, J., Lang, J. & Monath, T. P. (2013) Preclinical and clinical development of a YFV 17 D-based chimeric vaccine against West Nile virus. *Viruses*, 5(12), 3048-3070.

De Filette, M., Ulbert, S., Diamond, M. S. & Sanders, N. N. (2012) Recent progress in West Nile virus diagnosis and vaccination. *Veterinary research*, 43.

Dennis, S. J., Meyers, A. E., Guthrie, A. J., Hitzeroth, I. I. & Rybicki, E. P. (2018a) Immunogenicity of plant-produced African horse sickness virus-like particles: implications for a novel vaccine. *Plant biotechnology journal*, 16(2), 442-450.

Dennis, S. J., O'Kennedy, M. M., Rutkowska, D., Tsekoa, T., Lourens, C. W., Hitzeroth, I. I., Meyers, A. E. & Rybicki, E. P. (2018b) Safety and immunogenicity of plant-produced African horse sickness virus-like particles in horses. *Veterinary research*, 49(1), 105.

Diaz, L. A., Komar, N., Visintin, A., Juri, M. J. D., Stein, M., Allende, R. L., Spinsanti, L., Konigheim, B., Aguilar, J. & Laurito, M. (2008) West Nile virus in birds, Argentina. *Emerging Infectious Diseases*, 14(4), 689.

Ding, F. X., Wang, F., Lu, Y. M., Li, K., Wang, K. H., He, X. W. & Sun, S. H. (2009) Multiepitope peptide-loaded virus-like particles as a vaccine against hepatitis B virus–related hepatocellular carcinoma. *Hepatology*, 49(5), 1492-1502.

Dinu, S., Cotar, A., Pănculescu-Gătej, I., Fălcuţă, E., Prioteasa, F., Sîrbu, A., Oprişan, G., Bădescu, D., Reiter, P. & Ceianu, C. (2015) West Nile virus circulation in south-eastern Romania, 2011 to 2013. *Eurosurveillance*, 20(20), 21130.

Durbin, A. P., Wright, P. F., Cox, A., Kagucia, W., Elwood, D., Henderson, S., Wanionek, K., Speicher, J., Whitehead, S. S. & Pletnev, A. G. (2013) The live attenuated chimeric vaccine rWN/DEN4Δ30 is well-tolerated and immunogenic in healthy flavivirus-naïve adult volunteers. *Vaccine*, 31(48), 5772-5777.

Egelkrout, E., Rajan, V. & Howard, J. A. (2012) Overproduction of recombinant proteins in plants. *Plant science*, 184, 83-101.

El Garch, H., Minke, J., Rehder, J., Richard, S., Toulemonde, C. E., Dinic, S., Andreoni, C., Audonnet, J., Nordgren, R. & Juillard, V. (2008) A West Nile virus (WNV) recombinant canarypox virus vaccine elicits WNV-specific neutralizing antibodies and cell-mediated immune responses in the horse. *Veterinary immunology and immunopathology*, 123(3), 230-239.

El Rhaffouli, H., Lahlou-Amine, I., Loutfi, C., Laraqui, A., Bajjou, T., Fassi-Fihri, O. & El Harrak, M. (2013) Serological evidence of West Nile Virus infection among humans in the southern Provinces of Morocco. *The Journal of Infection in Developing Countries*, 7(12), 999-1002.

Ellgaard, L. & Helenius, A. (2003) A Chaperone System for Glycoprotein Folding: The Calnexin/Calreticulin Cycle, in Eggleton, P. & Michalak, M. (eds), *Calreticulin. Molecular Biology Intelligence Unit*, 2nd edition. Boston, MA: Springer, 19-29.

Farajollahi, A., Fonseca, D. M., Kramer, L. D. & Kilpatrick, A. M. (2011) ‘‘Bird biting’’mosquitoes and human disease: A review of the role of Culex pipiens complex mosquitoes in epidemiology. *Infection, Genetics and Evolution*, 11, 1577-1585.

Figuerola, J., Soriguer, R., Rojo, G., Tejedor, C. G. & Jimenez-Clavero, M. A. (2007) Seroconversion in wild birds and local circulation of West Nile virus, Spain. *Emerging infectious diseases*, 13(12), 1915.

Fischer, R. & Buyel, J. F. (2020) Molecular farming – The slope of enlightenment. *Biotechnology Advances*, 40, 107519.

Fischer, R., Stoger, E., Schillberg, S., Christou, P. & Twyman, R. M. (2004) Plant-based production of biopharmaceuticals. *Current opinion in plant biology*, 7(2), 152-158.

García-Bocanegra, I., Jaén-Téllez, J. A., Napp, S., Arenas-Montes, A., Fernández-Morente, M., Fernández-Molera, V. & Arenas, A. (2011) West Nile fever outbreak in horses and humans, Spain, 2010. *Emerging infectious diseases*, 17(12), 2397.

Garg, H., Mehmetoglu-Gurbuz, T. & Joshi, A. (2020) Virus Like Particles (VLP) as multivalent vaccine candidate against Chikungunya, Japanese Encephalitis, Yellow Fever and Zika Virus. *Scientific Reports*, 10(1), 1-13.

George, S., Gourie-Devi, M., Rao, J., Prasad, S. & Pavri, K. (1984) Isolation of West Nile virus from the brains of children who had died of encephalitis. *Bulletin of the World Health Organization*, 62(6), 879-882.

Geser, A., Henderson, B. E. & Christensen, S. (1970) A multipurpose serological survey in Kenya: 2. Results of arbovirus serological tests. *Bulletin of the World Health Organization*, 43(4), 539.

Góez-Rivillas, Y., Taborda, N., Díaz, F. J., Góngora, A., Rodas, J. D., Ruiz-Sáenz, J. & Osorio, J. E. (2010) Antibodies to West Nile virus in equines of Antioquia and Meta, Colombia, 2005-2008. *Revista Colombiana de Ciencias Pecuarias*, 23(4), 462-470.

Gollins, S. W. & Porterfield, J. S. (1986) pH-dependent fusion between the flavivirus West Nile and liposomal model membranes. *Journal of General Virology*, 67(1), 157-166.

Goo, L., Debbink, K., Kose, N., Sapparapu, G., Doyle, M. P., Wessel, A. W., Richner, J. M., Burgomaster, K. E., Larman, B. C. & Dowd, K. A. (2019) A potently neutralizing human monoclonal antibody targeting an epitope in the West Nile virus E protein preferentially recognizes mature virions. *Nature microbiology*, 4(1), 71.

Goverment of Canada *Surveillance of West Nile virus* (Updated: 18 November 2019). Available online: https://www.canada.ca/en/public-health/services/diseases/west-nile-virus/surveillance-west-nile-virus.html [Accessed: 17 March 2020].

Gray, T. J. & Webb, C. E. (2014) A review of the epidemiological and clinical aspects of West Nile virus. *International journal of general medicine*, 7, 193.

Gregson, A. L., Oliveira, G., Othoro, C., Calvo-Calle, J. M., Thorton, G. B., Nardin, E. & Edelman, R. (2008) Phase I trial of an alhydrogel adjuvanted hepatitis B core virus-like particle containing epitopes of Plasmodium falciparum circumsporozoite protein. *PloS one*, 3(2).

Gresikova, M., Thiel, W., Batikova, M., Stünzner, D., Sekeyova, M. & Sixl, W. (1973) Haemagglutination-inhibiting antibodies against arboviruses in human sera from different regions in Steiermark (Austria). I. *Zentralblatt fur Bakteriologie, Parasitenkunde, Infektionskrankheiten und Hygiene*, 224(3), 298-302.

Gunter, C. J., Regnard, G. L., Rybicki, E. P. & Hitzeroth, I. I. (2019) Immunogenicity of plant-produced porcine circovirus-like particles in mice. *Plant biotechnology journal*, 17(9), 1751-1759.

Hall, R. A., Scherret, J. H. & Mackenzie, J. S. (2001) Kunjin virus: an Australian variant of West Nile? *Annals of the New York Academy of Sciences*, 951(1), 153-160.

Hall, T. A. (1999) BioEdit: a user-friendly biological sequence alignment editor and analysis program for Windows 95/98/NT, *Nucleic acids symposium series*. [London]: Information Retrieval Ltd., c1979-c2000.

Hanna, S. L., Pierson, T. C., Sanchez, M. D., Ahmed, A. A., Murtadha, M. M. & Doms, R. W. (2005) N-linked glycosylation of west nile virus envelope proteins influences particle assembly and infectivity. *Journal of virology*, 79(21), 13262-13274.

Harmsen, C., Turner, L., Thrane, S., Sander, A. F., Theander, T. G. & Lavstsen, T. (2020) Immunization with virus-like particles conjugated to CIDRα1 domain of Plasmodium falciparum erythrocyte membrane protein 1 induces inhibitory antibodies. *Malaria Journal*, 19, 1-11.

Hayes, C. G. (1989a) West nile fever, in Monath, T. P. (ed), *The arboviruses: epidemiology and ecology*. Boca Raton, FL.: CRC Press, Inc., 59-88.

Hayes, C. G. (1989b) West nile fever. *The arboviruses: epidemiology and ecology*, 5, 59-88.

Hayes, E. B. (2005) Epidemiology and transmission dynamics of West Nile virus disease.

Hayes, E. B., Sejvar, J. J., t Sherif, R. Z., Bode, A. V. & Campbell, G. L. (2005) Virology, Pathology, and Clinical Manifestations of West Nile Virus Disease. *Emerging Infectious Disease journal*, 11(8), 1174-1179.

He, J., Peng, L., Lai, H., Hurtado, J., Stahnke, J. & Chen, Q. (2014) A plant-produced antigen elicits potent immune responses against West Nile virus in mice. *BioMed Research International*, 2014, https://doi.org/10.1155/2014/952865.

Hefferon, K. (2013) Plant-derived pharmaceuticals for the developing world. *Biotechnology journal*, 8(10), 1193-1202.

Heinz, F. X. & Stiasny, K. (2012) Flaviviruses and flavivirus vaccines. *Vaccine*, 30(29), 4301-4306.

Hu, X., Deng, Y., Chen, X., Zhou, Y., Zhang, H., Wu, H., Yang, S., Chen, F., Zhou, Z. & Wang, M. (2017) Immune response of a novel ATR-AP205-001 conjugate anti-hypertensive vaccine. *Scientific reports*, 7(1), 1-13.

Hubalek, Z. & Halouzka, J. (1999) West Nile fever--a reemerging mosquito-borne viral disease in Europe. *Emerging infectious diseases*, 5(5), 643.

Inziani, M., Adungo, F., Awando, J., Kihoro, R., Inoue, S., Morita, K., Obimbo, E., Onyango, F. & Mwau, M. (2020) Seroprevalence of yellow fever, dengue, West Nile and chikungunya viruses in children in Teso South Sub-County, Western Kenya. *International Journal of Infectious Diseases*, 91, 104-110.

Janitzek, C. M., Matondo, S., Thrane, S., Nielsen, M. A., Kavishe, R., Mwakalinga, S. B., Theander, T. G., Salanti, A. & Sander, A. F. (2016) Bacterial superglue generates a full-length circumsporozoite protein virus-like particle vaccine capable of inducing high and durable antibody responses. *Malaria journal*, 15(1), 545.

Janitzek, C. M., Peabody, J., Thrane, S., H. R. Carlsen, P., G. Theander, T., Salanti, A., Chackerian, B., A. Nielsen, M. & Sander, A. F. (2019) A proof-of-concept study for the design of a VLP-based combinatorial HPV and placental malaria vaccine. *Scientific Reports*, 9(1), 5260.

Jentes, E. S., Robinson, J., Johnson, B. W., Conde, I., Sakouvougui, Y., Iverson, J., Beecher, S., Diakite, F., Coulibaly, M. & Bausch, D. G. (2010) Acute arboviral infections in Guinea, west Africa, 2006. *The American journal of tropical medicine and hygiene*, 83(2), 388-394.

Jiménez-Clavero, M., Gómez, T., Rojo, G., Soriguer, R. & Figuerola, J. (2007) Serosurvey of West Nile virus in equids and bovids in Spain. *Veterinary Record*, 161(6).

Jordan, I., Briese, T., Fischer, N., Lau, J. Y.-N. & Lipkin, W. I. (2000) Ribavirin inhibits West Nile virus replication and cytopathic effect in neural cells. *The Journal of infectious diseases*, 182(4), 1214-1217.

Jupp, P. G., McIntosh, B. M. & Blackburn, N. K. (1986) Experimental assessment of the vector competence of Culex (Culex) neavei Theobald with West Nile and Sindbis viruses in South Africa. *Transactions of the Royal Society of Tropical Medicine and Hygiene*, 80(2), 226-230.

Jutras, P. V., Dodds, I. & van der Hoorn, R. A. (2020) Proteases of Nicotiana benthamiana: an emerging battle for molecular farming. *Current opinion in biotechnology*, 61, 60-65.

Kaiser, J. A. & Barrett, A. D. (2019) Twenty Years of Progress Toward West Nile Virus Vaccine Development. *Viruses*, 11(9), 823.

Kalil, A. C., Devetten, M. P., Singh, S., Lesiak, B., Poage, D. P., Bargenquast, K., Fayad, P. & Freifeld, A. G. (2005) Use of interferon-α in patients with West Nile encephalitis: report of 2 cases. *Clinical infectious diseases*, 40(5), 764-766.

Kanai, R., Kar, K., Anthony, K., Gould, L. H., Ledizet, M., Fikrig, E., Marasco, W. A., Koski, R. A. & Modis, Y. (2006) Crystal structure of West Nile virus envelope glycoprotein reveals viral surface epitopes. *Journal of virology*, 80(22), 11000-11008.

Kaptoul, D., Viladrich, P. F., Domingo, C., Niubó, J., Martínez-Yélamos, S., De Ory, F. & Tenorio, A. (2007) West Nile virus in Spain: report of the first diagnosed case (in Spain) in a human with aseptic meningitis. *Scandinavian journal of infectious diseases*, 39(1), 70-71.

Karaca, K., Bowen, R., Austgen, L., Teehee, M., Siger, L., Grosenbaugh, D., Loosemore, L., Audonnet, J.-C., Nordgren, R. & Minke, J. (2005) Recombinant canarypox vectored West Nile virus (WNV) vaccine protects dogs and cats against a mosquito WNV challenge. *Vaccine*, 23(29), 3808-3813.

Kokernot, R., Smithburn, K. & Weinbren, M. (1956) Neutralizing antibodies to arthropod-borne viruses in human beings and animals in the Union of South Africa. *The journal of immunology*, 77(5), 313-323.

Kolodziejek, J., Jungbauer, C., Aberle, S. W., Allerberger, F., Bagó, Z., Camp, J. V., Dimmel, K., de Heus, P., Kolodziejek, M., Schiefer, P., Seidel, B., Stiasny, K. & Nowotny, N. (2018) Integrated analysis of human-animal-vector surveillance: West Nile virus infections in Austria, 2015–2016. *Emerging Microbes & Infections*, 7(1), 1-15.

Komar, N. (2001) West Nile virus surveillance using sentinel birds. *Annals of the New York Academy of Sciences*, 951(1), 58-73.

Komar, N., Panella, N. A., Burns, J. E., Dusza, S. W., Mascarenhas, T. M. & Talbot, T. O. (2001) Serologic evidence for West Nile virus infection in birds in the New York City vicinity during an outbreak in 1999. *Emerging Infectious Diseases*, 7(4), 621.

Krisztalovics, K., Ferenczi, E., Molnar, Z., Csohan, A., Ban, E., Zöldi, V. & Kaszas, K. (2008) West Nile virus infections in Hungary, August–September 2008. *Eurosurveillance*, 13(45), 19030.

Krol, E., Brzuska, G. & Szewczyk, B. (2019) Production and biomedical application of flavivirus-like particles. *Trends in biotechnology*.

Kuno, G., Chang, G.-J. J., Tsuchiya, K. R., Karabatsos, N. & Cropp, C. B. (1998) Phylogeny of the genus Flavivirus. *Journal of virology*, 72(1), 73-83.

Kutasi, O., Bakonyi, T., Lecollinet, S., Biksi, I., Ferenczi, E., Bahuon, C., Sardi, S., Zientara, S. & Szenci, O. (2011) Equine encephalomyelitis outbreak caused by a genetic lineage 2 West Nile virus in Hungary. *Journal of veterinary internal medicine*, 25(3), 586-591.

LaBeaud, A. D., Sutherland, L. J., Muiruri, S., Muchiri, E. M., Gray, L. R., Zimmerman, P. A., Hise, A. G. & King, C. H. (2011) Arbovirus prevalence in mosquitoes, Kenya. *Emerging infectious diseases*, 17(2), 233.

Lafri, I., Hachid, A. & Bitam, I. (2019) West Nile virus in Algeria: a comprehensive overview. *New microbes and new infections*, 27, 9-13.

Lai, H., Engleb, M., Fuchsb, A., Kellera, T., Johnsonc, S., Gorlatovc, S., Diamondb, M. S. & Chena, Q. (2010) Monoclonal antibody produced in plants efficiently treats West Nile virus infection in mice. *PNAS*, 107(6), 2419-2424.

Lai, H., Paul, A. M., Sun, H., He, J., Yang, M., Bai, F. & Chen, Q. (2018) A plant-produced vaccine protects mice against lethal West Nile virus infection without enhancing Zika or dengue virus infectivity. *Vaccine*, 36(14), 1846-1852.

Le Guenno, B., Bougermouh, A., Azzam, T. & Bouakaz, R. (1996) West Nile: a deadly virus? *The Lancet*, 348(9037), 1315.

Ledgerwood, J. E., Pierson, T. C., Hubka, S. A., Desai, N., Rucker, S., Gordon, I. J., Enama, M. E., Nelson, S., Nason, M. & Gu, W. (2011) A West Nile virus DNA vaccine utilizing a modified promoter induces neutralizing antibody in younger and older healthy adults in a phase I clinical trial. *Journal of Infectious Diseases*, 203(10), 1396-1404.

Ledizet, M., Kar, K., Foellmer, H. G., Wang, T., Bushmich, S. L., Anderson, J. F., Fikrig, E. & Koski, R. A. (2005) A recombinant envelope protein vaccine against West Nile virus. *Vaccine*, 23(30), 3915-3924.

Lieberman, M. M., Nerurkar, V. R., Luo, H., Cropp, B., Carrion, R., de la Garza, M., Coller, B.-A., Clements, D., Ogata, S. & Wong, T. (2009) Immunogenicity and protective efficacy of a recombinant subunit West Nile virus vaccine in rhesus monkeys. *Clinical and Vaccine Immunology*, 16(9), 1332-1337.

Lindenbach, B. D. & Rice, C. M. (2003) Molecular biology of flaviviruses. *Advances in virus research*, 59, 23-62.

Lindenbach, B. D., Thiel, H.-J. & Rice, C. M. (2007) *Flaviviridae*: The viruses and their replication, in Knipe, D. M. & Howley, P. M. (eds), *Fields Virology*, 5th edition. Philadelphia: Lippincott-Raven Publishers, 1101-1152.

Liu, F., Wu, X., Li, L., Ge, S., Liu, Z. & Wang, Z. (2013) Virus-like particles: promising platforms with characteristics of DIVA for veterinary vaccine design. *Comparative immunology, microbiology and infectious diseases*, 36(4), 343-352.

Liu, Z., Zhou, H., Wang, W., Tan, W., Fu, Y.-X. & Zhu, M. (2014) A novel method for synthetic vaccine construction based on protein assembly. *Scientific reports*, 4, 7266.

Loh, H.-S., Green, B. J. & Yusibov, V. (2017) Using transgenic plants and modified plant viruses for the development of treatments for human diseases. *Current Opinion in Virology*, 26, 81-89.

Lomonossoff, G. P. & D'Aoust, M.-A. (2016) Plant-produced biopharmaceuticals: A case of technical developments driving clinical deployment. *Science*, 353(6305), 1237-1240.

López-Ruiz, N., del Carmen Montaño-Remacha, M., Durán-Pla, E., Pérez-Ruiz, M., Navarro-Marí, J. M., Salamanca-Rivera, C., Miranda, B., Oyonarte-Gómez, S. & Ruiz-Fernández, J. (2018) West Nile virus outbreak in humans and epidemiological surveillance, west Andalusia, Spain, 2016. *Eurosurveillance*, 23(14).

Lorenz, I. C., Allison, S. L., Heinz, F. X. & Helenius, A. (2002) Folding and dimerization of tick-borne encephalitis virus envelope proteins prM and E in the endoplasmic reticulum. *Journal of virology*, 76(11), 5480-5491.

Ma, J. K., Drake, P. M. & Christou, P. (2003) The production of recombinant pharmaceutical proteins in plants. *Nature Reviews Genetics*, 4(10), 794-805.

Macini, P., Squintani, G., Finarelli, A., Angelini, P., Martini, E., Tamba, M., Dottori, M., Bellini, R., Santi, A. & Piccolomini, L. L. (2008) Detection of West Nile virus infection in horses, Italy, September 2008. *Eurosurveillance*, 13(39), 18990.

Mackenzie, J. S., Gubler, D. J. & Petersen, L. R. (2004) Emerging flaviviruses: the spread and resurgence of Japanese encephalitis, West Nile and dengue viruses. *Nature medicine*, 10(12), S98-S109.

Maclean, J., Koekemoer, M., Olivier, A., Stewart, D., Hitzeroth, I., Rademacher, T., Fischer, R., Williamson, A.-L. & Rybicki, E. (2007) Optimization of human papillomavirus type 16 (HPV-16) L1 expression in plants: comparison of the suitability of different HPV-16 L1 gene variants and different cell-compartment localization. *Journal of General Virology*, 88, 1460-1469.

Magnusson, S. E., Karlsson, K. H., Reimer, J. M., Corbach-Söhle, S., Patel, S., Richner, J. M., Nowotny, N., Barzon, L., Bengtsson, K. L. & Ulbert, S. (2014) Matrix-M™ adjuvanted envelope protein vaccine protects against lethal lineage 1 and 2 West Nile virus infection in mice. *Vaccine*, 32(7), 800-808.

Magurano, F., Remoli, M., Baggieri, M., Fortuna, C., Marchi, A., Fiorentini, C., Bucci, P., Benedetti, E., Ciufolini, M. & Rizzo, C. (2012) Circulation of West Nile virus lineage 1 and 2 during an outbreak in Italy. *Clinical Microbiology and Infection*, 18(12), E545-E547.

Mandji, J. L., Mounguengui, D., Ondounda, M., Nguema, B. E., Vandji, J. & Tchoua, R. (2009) A case of meningo-encephalitis due to West Nile virus in Libreville, Gabon. *Medecine tropicale: revue du Corps de sante colonial*, 69(5), 501-502.

Marberg, K., Goldbltjm, N., Sterk, V. V., Jasinska-Klingbehg, W. & Klingberg, M. A. (1956) The natural history of West Nile Fever. I. Clinical observations during an epidemic in Israel. *American journal of hygiene*, 64(3), 259-69.

Marfin, A. A., Petersen, L. R., Eidson, M., Miller, J., Hadler, J., Farello, C., Werner, B., Campbell, G. L., Layton, M. & Smith, P. (2001) Widespread West Nile virus activity, eastern United States, 2000. *Emerging infectious diseases*, 7(4), 730.

Margolin, E., Chapman, R., Williamson, A. L., Rybicki, E. P. & Meyers, A. E. (2018) Production of complex viral glycoproteins in plants as vaccine immunogens. *Plant Biotechnology Journal*, 16(9), 1531-1545.

Margolin, E., Oh, Y. J., Verbeek, M., Naude, J., Ponndorf, D., Meyers, A. E., Lomonossoff, G. P., Matoba, N., Williamson, A.-L. & Rybicki, E. P. (2020) Co-expression of human calreticulin significantly improves the production of HIV gp140 and other viral glycoproteins in plants. *Plant Biotechnology Journal*, 1-9.

Marques, L. É. C., Silva, B. B., Dutra, R. A. F., Florean, E. O. P. T., Menassa, R. & Guedes, M. I. F. (2019) Transient expression of dengue virus NS1 antigen in Nicotiana benthamiana for use as a diagnostic antigen. *Frontiers in Plant Science*, 10, 1674.

Marsian, J., Hurdiss, D. L., Ranson, N. A., Ritala, A., Paley, R., Cano, I. & Lomonossoff, G. P. (2019) Plant-Made Nervous Necrosis Virus-Like Particles Protect Fish Against Disease. *Frontiers in Plant Science*, 10(880).

Marsian, J. & Lomonossoff, G. P. (2016) Molecular pharming—VLPs made in plants. *Current opinion in biotechnology*, 37, 201-206.

Martin, J. E., Pierson, T. C., Hubka, S., Rucker, S., Gordon, I. J., Enama, M. E., Andrews, C. A., Xu, Q., Davis, B. S. & Nason, M. C. (2007) A West Nile Virus DNA Vaccine Induces Neutralizing Antibody in Healthy Adults during a Phase 1 Clinical Trial. *J Infect Dis*, 196(12), 1732-1740.

Martina, B. E., Koraka, P., van Den Doel, P., van Amerongen, G., Rimmelzwaan, G. F. & Osterhaus, A. D. (2008) Immunization with West Nile virus envelope domain III protects mice against lethal infection with homologous and heterologous virus. *Vaccine*, 26(2), 153-157.

Martinez, C., Giulietti, A. & Talou, J. R. (2012) Research advances in plant-made flavivirus antigens. *Biotechnology advances*, 30(6), 1493-1505.

Martínez, C. A., Topal, E., Giulietti, A. M., Talou, J. R. & Mason, H. (2010) Exploring different strategies to express Dengue virus envelope protein in a plant system. *Biotechnology letters*, 32(6), 867-875.

Mattar, S., Edwards, E., Laguado, J., González, M., Alvarez, J. & Komar, N. (2005) West Nile virus antibodies in Colombian horses. *Emerging infectious diseases*, 11(9), 1497-1498.

May, F. J., Davis, C. T., Tesh, R. B. & Barrett, A. D. (2011) Phylogeography of West Nile Virus: from the Cradle of Evolution in Africa to Eurasia, Australia, and the Americas. *JOURNAL OF VIROLOGY*, 2964-2974.

Mbewana, S., Meyers, A. E. & Rybicki, E. P. (2018) Chimaeric Rift Valley fever virus-like particle vaccine candidate production in Nicotiana benthamiana. *Biotechnology journal*, 1800238.

McIntosh, B., Jupp, P., Dos Santos, I. & Meenehan, G. (1976) Epidemics of West Nile and Sindbis viruses in South Africa with Culex (Culex) univittatus Theobald as vector. *South African Journal of Science*, 72(10), 295-300.

McNulty, M. J., Gleba, Y., Tusé, D., Hahn-Löbmann, S., Giritch, A., Nandi, S. & McDonald, K. A. (2019) Techno-economic analysis of a plant-based platform for manufacturing antimicrobial proteins for food safety. *Biotechnology progress*, e2896.

Mease, L. E., Coldren, R. L., Musila, L. A., Prosser, T., Ogolla, F., Ofula, V. O., Schoepp, R. J., Rossi, C. A. & Adungo, N. (2011) Seroprevalence and distribution of arboviral infections among rural Kenyan adults: a cross-sectional study. *Virology journal*, 8(1), 371.

Medrouh, B., Lafri, I., Beck, C., Leulmi, H., Akkou, M., Abbad, L., Lafri, M., Bitam, I. & Lecollinet, S. (2020) First serological evidence of West Nile virus infection in wild birds in Northern Algeria. *Comparative Immunology, Microbiology and Infectious Diseases*, 101415.

Melnick, J. L., Paul, J. R., Riordan, J. T., Barnett, V. H., Goldblum, N. & Zabin, E. (1951) Isolation from human sera in Egypt of a virus apparently identical to West Nile virus. *Proceedings of the Society for Experimental Biology and Medicine*, 77(4), 661-665.

Merck *Prestige WNV* (Updated: 2019). Available online: https://www.merck-animal-health-usa.com/species/equine/product/PRESTIGE_WNV [Accessed: 14 April 2020].

Merial *Equilis West Nile* (Updated: 2020). Available online: https://www.msd-tiergesundheit.at/produkt/equilis-west-nile/ [Accessed: 14 April 2020].

Miller, B. R., Nasci, R. S., Godsey, M. S., Savage, H. M., Lutwama, J. J., Lanciotti, R. S. & Peters, C. J. (2000) First field evidence for natural vertical transmission of West Nile virus in Culex univittatus complex mosquitoes from Rift Valley Province, Kenya. *The American journal of tropical medicine and hygiene*, 62(2), 240-246.

Minke, J., Siger, L., Cupillard, L., Powers, B., Bakonyi, T., Boyum, S., Nowotny, N. & Bowen, R. (2011) Protection provided by a recombinant ALVAC®-WNV vaccine expressing the prM/E genes of a lineage 1 strain of WNV against a virulent challenge with a lineage 2 strain. *Vaccine*, 29(28), 4608-4612.

Minke, J., Siger, L., Karaca, K., Austgen, L., Gordy, P., Bowen, R., Renshaw, R., Loosmore, S., Audonnet, J. & Nordgren, B. (2004) Recombinant canarypoxvirus vaccine carrying the prM/E genes of West Nile virus protects horses against a West Nile virus-mosquito challenge, in Calisher, C. & Griffin, D. (eds), *Emergence and Control of Zoonotic Viral Encephalitides*. Vienna: Springer, 221-230.

Mir-Artigues, P., Twyman, R. M., Alvarez, D., Cerda Bennasser, P., Balcells, M., Christou, P. & Capell, T. (2019) A simplified techno-economic model for the molecular pharming of antibodies. *Biotechnology and bioengineering*, 116(10), 2526-2539.

Monath, T. P., Liu, J., Kanesa-Thasan, N., Myers, G. A., Nichols, R., Deary, A., McCarthy, K., Johnson, C., Ermak, T. & Shin, S. (2006) A live, attenuated recombinant West Nile virus vaccine. *PNAS*, 103(17).

Morales, M. A., Barrandeguy, M., Fabbri, C., Garcia, J. B., Vissani, A., Trono, K., Gutierrez, G., Pigretti, S., Menchaca, H. & Garrido, N. (2006) West Nile virus isolation from equines in Argentina, 2006. *Emerging infectious diseases*, 12(10), 1559.

Morrey, J. D., Day, C. W., Julander, J. G., Blatt, L. M., Smee, D. F. & Sidwell, R. W. (2004) Effect of interferon-alpha and interferon-inducers on West Nile virus in mouse and hamster animal models. *Antiviral Chemistry and Chemotherapy*, 15(2), 67-75.

Mostashari, F., Bunning, M. L., Kitsutani, P. T., Singer, D. A., Nash, D., Cooper, M. J., Katz, N., Liljebjelke, K. A., Biggerstaff, B. J. & Fine, A. D. (2001) Epidemic West Nile encephalitis, New York, 1999: results of a household-based seroepidemiological survey. *The lancet*, 358(9278), 261-264.

Moustafa, K., Makhzoum, A. & Trémouillaux-Guiller, J. (2016) Molecular farming on rescue of pharma industry for next generations. *Critical reviews in biotechnology*, 36(5), 840-850.

Mukhopadhyay, S., Kim, B.-S., Chipman, P. R., Rossmann, M. G. & Kuhn, R. J. (2003) Structure of west nile virus. *Science*, 302(5643), 248-248.

Mukhopadhyay, S., Kuhn, R. J. & Rossmann, M. G. (2005) A structural perspective of the flavivirus life cycle. *Nature Reviews Microbiology*, 3(1), 13.

Murai, N. (2013) Plant Binary Vectors of Ti Plasmid in Agrobacterium tumefaciens with a Broad Host-Range Replicon of pRK2, pRi, pSa or pVS1. *American Journal of Plant Sciences*, 4, 932-939.

Murgue, B., Murri, S., Triki, H., Deubel, V. & Zeller, H. (2001) West Nile in the Mediterranean Basin: 1950-2000. *Annals of the New York Academy of Sciences*, 951(1), 117-126.

Mweene-Ndumba, I., Siziya, S., Monze, M., Mazaba, M. L., Masaninga, F., Songolo, P., Mwaba, P. & Babaniyi, O. A. (2015) Seroprevalence of West Nile virus specific IgG and IgM antibodies in North-Western and Western provinces of Zambia. *African health sciences*, 15(3), 803-809.

Nada, R. M. (2016) Novel recombinant binary vectors harbouring Basta (bar) gene as a plant selectable marker for genetic transformation of plants. *Physiology and Molecular Biology of Plants*, 22(2), 241-251.

Nakamura, S., Mano, S., Tanaka, Y., Ohnishi, M., Nakamori, C., Araki, M., Niwa, T., Nishimura, M., Kaminaka, H. & Nakagawa, T. (2010) Gateway binary vectors with the bialaphos resistance gene, bar, as a selection marker for plant transformation. *Bioscience, biotechnology, and biochemistry*, 74(6), 1315-1319.

Nandi, S., Kwong, A. T., Holtz, B. R., Erwin, R. L., Marcel, S. & McDonald, K. A. (2016) Techno-economic analysis of a transient plant-based platform for monoclonal antibody production, *MAbs*. Taylor & Francis.

National Institute of Allergy and Infectious Diseases, N. *NIAID Emerging Infectious Diseases/ Pathogens* (Updated: 26 July 2018). Available online: https://www.niaid.nih.gov/research/emerging-infectious-diseases-pathogens [Accessed: 7 May 2020].

Nybakken, G. E., Oliphant, T., Johnson, S., Burke, S., Diamond, M. S. & Fremont, D. H. (2005) Structural basis of West Nile virus neutralization by a therapeutic antibody. *Nature*, 437(7059), 764-769.

Ohtaki, N., Takahashi, H., Kaneko, K., Gomi, Y., Ishikawa, T., Higashi, Y., Kurata, T., Sata, T. & Kojima, A. (2010) Immunogenicity and efficacy of two types of West Nile virus-like particles different in size and maturation as a second-generation vaccine candidate. *Vaccine*, 28(40), 6588-6596.

Ohtaki, N., Takahashi, H., Kaneko, K., Gomi, Y., Ishikawa, T., Higashi, Y., Todokoro, M., Kurata, T., Sata, T. & Kojima, A. (2011) Purification and concentration of non-infectious West Nile virus-like particles and infectious virions using a pseudo-affinity Cellufine Sulfate column. *Journal of Virological Methods*, 174(1), 131-135.

Oliphant, T., Engle, M., Nybakken, G. E., Doane, C., Johnson, S., Huang, L., Gorlatov, S., Mehlhop, E., Marri, A. & Chung, K. M. (2005) Development of a Humanized Monoclonal Antibody with Therapeutic Potential against West Nile Virus. *Nat Med*, 11(5), 522-530.

Oliphant, T., Nybakken, G. E., Engle, M., Xu, Q., Nelson, C. A., Sukupolvi-Petty, S., Marri, A., Lachmi, B.-E., Olshevsky, U. & Fremont, D. H. (2006) Antibody recognition and neutralization determinants on domains I and II of West Nile Virus envelope protein. *Journal of virology*, 80(24), 12149-12159.

Omilabu, S., Olaleye, O., Aina, Y. & Fagbami, A. (1990) West Nile Complement Fixing antibodies in Nigerian domestic animals and humans. *Journal of hygiene, epidemiology, microbiology, and immunology*, 34(4), 357-363.

Orba, Y., Hang'ombe, B., Mweene, A., Wada, Y., Anindita, P., Phongphaew, W., Qiu, Y., Kajihara, M., Mori-Kajihara, A. & Eto, Y. (2018) First isolation of West Nile virus in Zambia from mosquitoes. *Transboundary and emerging diseases*.

Osorio, J. E., Ciuoderis, K. A., Lopera, J. G., Piedrahita, L. D., Murphy, D., LeVasseur, J., Carrillo, L., Ocampo, M. C. & Hofmeister, E. (2012) Characterization of West Nile Viruses Isolated from Captive American Flamingoes (Phoenicopterus ruber) in Medellin, Colombia. *Am. J. Trop. Med. Hyg*, 87(3), 565-572.

Palladini, A., Thrane, S., Janitzek, C. M., Pihl, J., Clemmensen, S. B., de Jongh, W. A., Clausen, T. M., Nicoletti, G., Landuzzi, L. & Penichet, M. L. (2018) Virus-like particle display of HER2 induces potent anti-cancer responses. *Oncoimmunology*, 7(3), e1408749.

Papa, A., Bakonyi, T., Xanthopoulou, K., Vázquez, A., Tenorio, A. & Nowotny, N. (2011) Genetic characterization of West Nile virus lineage 2, Greece, 2010. *Emerging infectious diseases*, 17(5), 920.

Papa, A., Danis, K., Baka, A., Bakas, A., Dougas, G., Lytras, T., Theocharopoulos, G., Chrysagis, D., Vassiliadou, E. & Kamaria, F. (2010a) Ongoing outbreak of West Nile virus infections in humans in Greece, July–August 2010. *Eurosurveillance*, 15(34), 19644.

Papa, A., Perperidou, P., Tzouli, A. & Castilletti, C. (2010b) West Nile virus–neutralizing antibodies in humans in Greece. *Vector-Borne and Zoonotic Diseases*, 10(7), 655-658.

Papagiannis, I., Tsolaki, M., Kiryttopoulos, A., Antoniadi, E., Kyriakogianni, C., Fotiou, D., Notas, K., Liougka, E., Myrou, A. & Hatzitolios, A. (2020) West Nile neuroinvasive disease. Report of 4 cases in Northern Greece, 2018. *Journal of Medical Virology*, 1-4.

Pasin, F., Bedoya, L. C., Bernabé-Orts, J. M., Gallo, A., Simón-Mateo, C., Orzaez, D. & García, J. A. (2017) Multiple T-DNA delivery to plants using novel mini binary vectors with compatible replication origins. *ACS synthetic biology*, 6(10), 1962-1968.

Pauvolid-Corrêa, A., Morales, M. A., Levis, S., Figueiredo, L. T. M., Couto-Lima, D., Campos, Z., Nogueira, M. F., Silva, E. E. d., Nogueira, R. M. R. & Schatzmayr, H. G. (2011) Neutralising antibodies for West Nile virus in horses from Brazilian Pantanal. *Memórias do Instituto Oswaldo Cruz*, 106(4), 467-474.

Pereira, E. O., Kolotilin, I., Conley, A. J. & Menassa, R. (2014) Production and characterization of in planta transiently produced polygalacturanase from Aspergillus niger and its fusions with hydrophobin or ELP tags. *BMC biotechnology*, 14(1), 59.

Perera, R. & Kuhn, R. J. (2008) Structural proteomics of dengue virus. *Current Opinion in Microbiology*, 11(4), 369-377.

Petersen, L. R., Brault, A. C. & Nasci, R. S. (2013) West Nile virus: review of the literature. *Jama*, 310(3), 308-315.

Peyret, H., Brown, J. K. & Lomonossoff, G. P. (2019) Improving plant transient expression through the rational design of synthetic 5′ and 3′ untranslated regions. *Plant methods*, 15(1), 108.

Peyret, H., Gehin, A., Thuenemann, E. C., Blond, D., El Turabi, A., Beales, L., Clarke, D., Gilbert, R. J. C., Fry, E. E., Stuart, D. I., Holmes, K., Stonehouse, N. J., Whelan, M., Rosenberg, W., Lomonossoff, G. P. & Rowlands, D. J. (2015) Tandem Fusion of Hepatitis B Core Antigen Allows Assembly of Virus-Like Particles in Bacteria and Plants with Enhanced Capacity to Accommodate Foreign Proteins. *PLOS ONE*, 10(4), e0120751.

Peyret, H., Ponndorf, D., Meshcheriakova, Y., Richardson, J. & Lomonossoff, G. P. (2020) Covalent protein display on Hepatitis B core-like particles in plants through the in vivo use of the SpyTag/SpyCatcher system. *Scientific Reports*, 10(1), 17095.

Pierce, K. K., Whitehead, S. S., Kirkpatrick, B. D., Grier, P. L., Jarvis, A., Kenney, H., Carmolli, M. P., Reynolds, C., Tibery, C. M., Lovchik, J., Janiak, A., Luke, C. J., Durbin, A. P. & Pletnev, A. G. (2016) A Live Attenuated Chimeric West Nile Virus Vaccine, rWN/DEN4Δ30, Is Well Tolerated and Immunogenic in Flavivirus-Naive Older Adult Volunteers. *The Journal of Infectious Diseases*, 215(1), 52-55.

Platonov, A. E., Shipulin, G. A., Shipulina, O. Y., Tyutyunnik, E. N., Frolochkina, T. I., Lanciotti, R. S., Yazyshina, S., Platonova, O. V., Obukhov, I. L. & Zhukov, A. N. (2001) Outbreak of West Nile virus infection, Volgograd Region, Russia, 1999. *Emerging infectious diseases*, 7(1), 128.

Pletnev, A. G., Claire, M. S., Elkins, R., Speicher, J., Murphy, B. R. & Chanock, R. M. (2003) Molecularly engineered live-attenuated chimeric West Nile/dengue virus vaccines protect rhesus monkeys from West Nile virus. *Virology*, 314(1), 190-195.

Pletnev, A. G., Putnak, R., Speicher, J., Wagar, E. J. & Vaughn, D. W. (2002) West Nile virus dengue type 4 virus chimeras that are reduced in neurovirulence and peripheral virulence without loss of immunogenicity or protective efficacy. *PNAS*, 99(5).

Pletnev, A. G., Swayne, D. E., Speicher, J., Rumyantsev, A. A. & Murphy, B. R. (2006) Chimeric West Nile/dengue virus vaccine candidate: Preclinical evaluation in mice, geese and monkeys for safety and immunogenicity. *Vaccine*, 24, 6392-6404.

Ponndorf, D., Meshcheriakova, Y., Thuenemann, E., Alonso, A. D., Overman, R., Holton, N., Dowall, S., Kennedy, E., Stocks, M., Lomonossoff, G. & Peyret, H. (2020) Plant-made dengue virus-like particles produced by co-expression of structural and non-structural proteins induce a humoral immune response in mice. *Plant Biotechnology Journal*.

Qiao, M., Ashok, M., Bernard, K. A., Palacios, G., Zhou, Z. H., Lipkin, W. I. & Liang, T. J. (2004) Induction of sterilizing immunity against West Nile Virus (WNV), by immunization with WNV-like particles produced in insect cells. *Journal of infectious diseases*, 190(12), 2104-2108.

Quintel, B. K., Thomas, A., DeRaad, D. E. P., Slifka, M. K. & Amanna, I. J. (2019) Advanced oxidation technology for the development of a next-generation inactivated West Nile virus vaccine. *Vaccine*, 37(30), 4214-4221.

Rao, T. R. (1971) Immunological surveys of arbovirus infections in South-East Asia, with special reference to dengue, chikungunya, and Kyasanur Forest disease. *Bulletin of the World Health Organization*, 44(5), 585.

Rebollo, B., Sarraseca, J., Lecollinet, S., Abouchoaib, N., Alonso, J., García-Bocanegra, I., Sanz, A. J., Venteo, Á. & Jiménez-Clavero, M. A. (2018a) Monitoring Anti-NS1 Antibodies in West Nile Virus-Infected and Vaccinated Horses. *BioMed Research International*, 2018.

Rebollo, B., Sarraseca, J., Rodríguez, M. J., Sanz, A., Jiménez-Clavero, M. Á. & Venteo, Á. (2018b) Diagnostic aptitude of West Nile virus-like particles expressed in insect cells. *Diagnostic microbiology and infectious disease*, 91(3), 233-238.

Reddington, S. C. & Howarth, M. (2015) Secrets of a covalent interaction for biomaterials and biotechnology: SpyTag and SpyCatcher. *Current Opinion in Chemical Biology*, 29, 94-99.

Regnard, G. L., Halley-Stott, R. P., Tanzer, F. L., Hitzeroth, I. I. & Rybicki, E. P. (2010) High level protein expression in plants through the use of a novel autonomously replicating geminivirus shuttle vector. *Plant biotechnology journal*, 8(1), 38-46.

Reiter, P. (2010) West Nile virus in Europe: understanding the present to gauge the future. *Eurosurveillance*, 15(10), 19508.

Rizzo, C., Vescio, F., Declich, S., Finarelli, A., Macini, P., Mattivi, A., Rossini, G., Piovesan, C., Barzon, L. & Palù, G. (2009) West Nile virus transmission with human cases in Italy, August-September 2009. *Eurosurveillance*, 14(40), 19353.

Roby, J. A., Setoh, Y. X., Hall, R. A. & Khromykh, A. A. (2015) Post-translational regulation and modifications of flavivirus structural proteins. *Journal of General Virology*, 96(7), 1551-1569.

Röder, J., Fischer, R. & Commandeur, U. (2017) Engineering potato virus X particles for a covalent protein based attachment of enzymes. *Small*, 13(48), 1702151.

Rossini, G., Cavrini, F., Pierro, A., Macini, P., Finarelli, A. C., Po, C., Peroni, G., Di Caro, A., Capobianchi, M. R. & Nicoletti, L. (2008) First human case of West Nile virus neuroinvasive infection in Italy, September 2008–case report. *Eurosurveillance*, 13(41), 19002.

Rybicki, E. P. (2009) Plant-produced vaccines: promise and reality. *Drug discovery today*, 14(1-2), 16-24.

Rybicki, E. P. (2010) Plant-made vaccines for humans and animals. *Plant biotechnology journal*, 8(5), 620-637.

Rybicki, E. P., Hitzeroth, I., Meyers, A., Jose Dus Santos, M. & Wigdorovitz, A. (2013) Developing country applications of molecular farming: case studies in South Africa and Argentina. *Current pharmaceutical design*, 19(31), 5612-5621.

Sainsbury, F. & Lomonossoff, G. P. (2014) Transient expressions of synthetic biology in plants. *Current Opinion in Plant Biology*, 19, 1-7.

Sainsbury, F., Thuenemann, E. C. & Lomonossoff, G. P. (2009) pEAQ: versatile expression vectors for easy and quick transient expression of heterologous proteins in plants. *Plant biotechnology journal*, 7(7), 682-693.

Schepp-Berglind, J., Luo, M., Wang, D., Wicker, J. A., Raja, N. U., Hoel, B. D., Holman, D. H., Barrett, A. D. T. & Dong, J. Y. (2007) Complex Adenovirus-Mediated Expression of West Nile Virus C, PreM, E, and NS1 Proteins Induces both Humoral and Cellular Immune Responses. *Clinical and Vaccine Immunology*, 14(9), 1117-1126.

Schiermeyer, A. (2020) Optimizing product quality in molecular farming. *Current opinion in biotechnology*, 61, 15-20.

Schillberg, S., Raven, N., Spiegel, H., Rasche, S. & Buntru, M. (2019) Critical Analysis of the Commercial Potential of Plants for the Production of Recombinant Proteins. *Frontiers in Plant Science*, 10(720).

Seino, K., Long, M., Gibbs, E., Bowen, R., Beachboard, S., Humphrey, P., Dixon, M. & Bourgeois, M. (2007) Comparative Efficacies of Three Commercially Available Vaccines against West Nile Virus (WNV) in a Short-Duration Challenge Trial Involving an Equine WNV Encephalitis Model. *Clinical and Vaccine Immunology: CVI*, 14(11), 1465.

Sejvar, J. J. (2014) Clinical manifestations and outcomes of West Nile virus infection. *Viruses*, 6(2), 606-623.

Shen, W.-J. & Forde, B. G. (1989) Efficient transformation of Agrobacterium spp. by high voltage electroporation. *Nucleic acids research*, 17(20), 8385.

Silva, A. S. G., Matos, A. C. D., da Cunha, M. A. C. R., Rehfeld, I. S., Galinari, G. C. F., Marcelino, S. A. C., Saraiva, L. H. G., Martins, N. R. d. S., Maranhão, R. d. P. A. & Lobato, Z. I. P. (2019) West Nile virus associated with equid encephalitis in Brazil, 2018. *Transboundary and emerging diseases*, 66(1), 445-453.

Silva, J. R., de Medeiros, L. C., dos Reis, V. P., Chávez, J. H., Munhoz, T. D., Borges, G. P., Soares, O. A. B., de Campos, C. H. C., Machado, R. Z. & Baldani, C. D. (2013) Serologic survey of West Nile virus in horses from Central-West, Northeast and Southeast Brazil. *Mem Inst Oswaldo Cruz, Rio de Janeiro*, 108(6), 000-000.

Simmonds, P., Becher, P., Bukh, J., Gould, E. A., Meyers, G., Monath, T., Muerhoff, S., Pletnev, A., Rico-Hesse, R. & Smith, D. B. (2017) ICTV virus taxonomy profile: Flaviviridae. *The Journal of general virology*, 98(1), 2.

Singh, S. K., Thrane, S., Janitzek, C. M., Nielsen, M. A., Theander, T. G., Theisen, M., Salanti, A. & Sander, A. F. (2017) Improving the malaria transmission-blocking activity of a Plasmodium falciparum 48/45 based vaccine antigen by SpyTag/SpyCatcher mediated virus-like display. *Vaccine*, 35(30), 3726-3732.

Sinigaglia, A., Pacenti, M., Martello, T., Pagni, S., Franchin, E. & Barzon, L. (2019) West Nile virus infection in individuals with pre-existing Usutu virus immunity, northern Italy, 2018. *Eurosurveillance*, 24(21).

Sirbu, A., Ceianu, C., Panculescu-Gatej, R., Vazquez, A., Tenorio, A., Rebreanu, R., Niedrig, M., Nicolescu, G. & Pistol, A. (2011) Outbreak of West Nile virus infection in humans, Romania, July to October 2010.

Smithburn, K., Hughes, T., Burke, A. & Paul, J. (1940) A Neurotropic Virus Isolated from the Blood of a Native of Uganda 1. *Am J Trop Med Hyg*, 1(4).

Sockett, P. *The Incursion and Expansion of West Nile Virus into Canada* (Updated: 2005). Available online: https://webbertraining.com/files/library/docs/26.pdf [Accessed: 17 March 2020].

Spohn, G., Jennings, G. T., Martina, B. E., Keller, I., Beck, M., Pumpens, P., Osterhaus, A. D. & Bachmann, M. F. (2010) A VLP-based vaccine targeting domain III of the West Nile virus E protein protects from lethal infection in mice. *Virology journal*, 7(1), 146.

Sterner, F. J., Goovaerts, D. G. E., Lum, M. A. & Mellencamp, M. W. (2012) *Inactivated chimeric vaccines and related methods of use* (United States Patent US 8,133,712 B2).

Stiasny, K., Aberle, S. W. & Heinz, F. X. (2013) Retrospective identification of human cases of West Nile virus infection in Austria (2009 to 2010) by serological differentiation from Usutu and other flavivirus infections. *Eurosurveillance*, 18(43), 20614.

Sule, W. F., Oluwayelu, D. O., Adedokun, R. A. M., Rufai, N., McCracken, F., Mansfield, K. L. & Johnson, N. (2015) High seroprevelance of West Nile Virus antibodies observed in horses from Southwestern Nigeria. *Vector-borne and Zoonotic Diseases*, 15(3), 218-220.

Sule, W. F., Oluwayelu, D. O., Hernández-Triana, L. M., Fooks, A. R., Venter, M. & Johnson, N. (2018) Epidemiology and ecology of West Nile virus in sub-Saharan Africa. *Parasites & Vectors*, 11(1), 414.

Sutherland, L. J., Cash, A. A., Huang, Y.-J. S., Sang, R. C., Malhotra, I., Moormann, A. M., King, C. L., Weaver, S. C., King, C. H. & LaBeaud, A. D. (2011) Serologic evidence of arboviral infections among humans in Kenya. *The American journal of tropical medicine and hygiene*, 85(1), 158-161.

Takahashi, H., Ohtaki, N., Maeda-Sato, M., Tanaka, M., Tanaka, K., Sawa, H., Ishikawa, T., Takamizawa, A., Takasaki, T. & Hasegawa, H. (2009) Effects of the number of amino acid residues in the signal segment upstream or downstream of the NS2B-3 cleavage site on production and secretion of prM/ME virus-like particles of West Nile virus. *Microbes and infection*, 11(13), 1019-1028.

Takeda, A., Sugiyama, K., Nagano, H., Mori, M., Kaido, M., Mise, K., Tsuda, S. & Okuno, T. (2002) Identification of a novel RNA silencing suppressor, NSs protein of Tomato spotted wilt virus. *FEBS letters*, 532(1-2), 75-79.

Tan, T. K., Rijal, P., Rahikainen, R., Keeble, A., Schimanski, L., Hussain, S., Harvey, R., Hayes, J., Edwards, J. & McLean, R. (2020) A COVID-19 vaccine candidate using SpyCatcher multimerization of the SARS-CoV-2 spike protein receptor-binding domain induces potent neutralising antibody responses. *bioRxiv*.

Taylor, T. J., Diaz, F., Colgrove, R. C., Bernard, K. A., DeLuca, N. A., Whelan, S. P. & Knipe, D. M. (2016) Production of immunogenic West Nile virus-like particles using a herpes simplex virus 1 recombinant vector. *Virology*, 496, 186-193.

Thrane, S., Janitzek, C. M., Matondo, S., Resende, M., Gustavsson, T., Jongh, W. A., Clemmensen, S., Roeffen, W., Vegte-Bolmer, M. & Gemert, G. J. (2016) Bacterial superglue enables easy development of efficient virus-like particle based vaccines. *Journal of nanobiotechnology*, 14(1), 30.

Thuenemann, E., Lenzi, P., Love, A., Taliansky, M., Bécares, M., Zuñiga, S., Enjuanes, L., Zahmanova, G., Minkov, I. & Matic, S. (2013) The use of transient expression systems for the rapid production of virus-like particles in plants. *Current pharmaceutical design*, 19(31), 5564-5573.

Tigoi, C., Lwande, O., Orindi, B., Irura, Z., Ongus, J. & Sang, R. (2015) Seroepidemiology of selected arboviruses in febrile patients visiting selected health facilities in the lake/river basin areas of Lake Baringo, Lake Naivasha, and Tana River, Kenya. *Vector-Borne and Zoonotic Diseases*, 15(2), 124-132.

Tirado, S. M. C. & Yoon, K.-J. (2003) Antibody-dependent enhancement of virus infection and disease. *Viral immunology*, 16(1), 69-86.

Tissot, A. C., Renhofa, R., Schmitz, N., Cielens, I., Meijerink, E., Ose, V., Jennings, G. T., Saudan, P., Pumpens, P. & Bachmann, M. F. (2010) Versatile virus-like particle carrier for epitope based vaccines. *PloS one*, 5(3).

Tsai, T., Popovici, F., Cernescu, C., Campbell, G. & Nedelcu, N. (1998) West Nile encephalitis epidemic in southeastern Romania. *The Lancet*, 352(9130), 767-771.

Tschofen, M., Knopp, D., Hood, E. & Stöger, E. (2016) Plant molecular farming: much more than medicines. *Annual Review of Analytical Chemistry*, 9, 271-294.

Tsekoa, T. L., Singh, A. A. & Buthelezi, S. G. (2020) Molecular farming for therapies and vaccines in Africa. *Current Opinion in Biotechnology*, 61, 89-95.

Twyman, R. M., Stoger, E., Schillberg, S., Christou, P. & Fischer, R. (2003) Molecular farming in plants: host systems and expression technology. *TRENDS in Biotechnology*, 21(12), 570-578.

Tzfira, T. & Citovsky, V. (2006) Agrobacterium-mediated genetic transformation of plants: biology and biotechnology. *Current opinion in biotechnology*, 17(2), 147-154.

Valiakos, G., Athanasiou, L. V., Touloudi, A., Papatsiros, V., Spyrou, V., Petrovska, L. & Billinis, C. (2013) West Nile Virus: Basic Principles, Replication Mechanism, Immune Response and Important Genetic Determinants of Virulence, *Viral Replication* German Rosas-Acosta, IntechOpen, 43-68.

van Eeden, C., Swanepoel, R. & Venter, M. (2014) Antibodies against West Nile and Shuni Viruses in Veterinarians, South Africa. *Emerging infectious diseases*, 20(8), 1409.

van Zyl, A. R., Meyers, A. E. & Rybicki, E. P. (2016) Transient Bluetongue virus serotype 8 capsid protein expression in Nicotiana benthamiana. *Biotechnology Reports*, 9, 15-24.

Vaquero, C., Sack, M., Chandler, J., Drossard, J., Schuster, F., Monecke, M., Schillberg, S. & Fischer, R. (1999) Transient expression of a tumor-specific single-chain fragment and a chimeric antibody in tobacco leaves. *Proceedings of the National Academy of Sciences*, 96(20), 11128-11133.

Veerapen, V. P., van Zyl, A. R., Wigdorovitz, A., Rybicki, E. P. & Meyers, A. E. (2018) Novel expression of immunogenic foot-and-mouth disease virus-like particles in Nicotiana benthamiana. *Virus Research*, 244, 213-217.

Venter, M., Human, S., Van Niekerk, S., Williams, J., Van Eeden, C. & Freeman, F. (2011) Fatal neurologic disease and abortion in mare infected with lineage 1 West Nile virus, South Africa. *Emerging infectious diseases*, 17(8), 1534.

Venter, M., Pretorius, M., Fuller, J. A., Botha, E., Rakgotho, M., Stivaktas, V., Weyer, C., Romito, M. & Williams, J. (2017) West Nile Virus Lineage 2 in Horses and Other Animals with Neurologic Disease, South Africa, 2008–2015. *Emerging infectious diseases*, 23(12), 2060.

Vieira, M. A., Romano, A. P., Borba, A. S., Silva, E. V., Chiang, J. O., Eulálio, K. D., Azevedo, R. S., Rodrigues, S. G., Almeida-Neto, W. S. & Vasconcelos, P. F. (2015) West Nile virus encephalitis: the first human case recorded in Brazil. *The American journal of tropical medicine and hygiene*, 93(2), 377-379.

Wang, T., Anderson, J. F., Magnarelli, L. A., Wong, S. J., Koski, R. A. & Fikrig, E. (2001) Immunization of mice against West Nile virus with recombinant envelope protein. *The Journal of Immunology*, 167(9), 5273-5277.

Wang, W., Sarkodie, F., Danso, K., Addo-Yobo, E., Owusu-Ofori, S., Allain, J.-P. & Li, C. (2009) Seroprevalence of West Nile virus in Ghana. *Viral Immunology*, 22(1), 17-22.

Ward, M. P., Schuermann, J. A., Highfield, L. D. & Murray, K. O. (2006) Characteristics of an outbreak of West Nile virus encephalomyelitis in a previously uninfected population of horses. *Veterinary Microbiology*, 118, 255-259.

Watts, D. M., Tesh, R. B., Siirin, M., da Rosa, A. T., Newman, P. C., Clements, D. E., Ogata, S., Coller, B.-A., Weeks-Levy, C. & Lieberman, M. M. (2007) Efficacy and durability of a recombinant subunit West Nile vaccine candidate in protecting hamsters from West Nile encephalitis. *Vaccine*, 25(15), 2913-2918.

WHO *Weekly operational Update on COVID-19* (Updated: 30 October 2020). Available online: https://www.who.int/publications/m/item/weekly-operational-update---30-october-2020 [Accessed: 6 November 2020].

Widman, D. G., Ishikawa, T., Fayzulin, R., Bourne, N. & Mason, P. W. (2008) Construction and characterization of a second-generation pseudoinfectious West Nile virus vaccine propagated using a new cultivation system. *Vaccine*, 26(22), 2762-2771.

Widman, D. G., Ishikawa, T., Giavedoni, L. D., Hodara, V. L., De La Garza, M., Montalbo, J. A., Da Rosa, A. P. T., Tesh, R. B., Patterson, J. L. & Carrion Jr, R. (2010) Evaluation of RepliVAX WN, a single-cycle flavivirus vaccine, in a non-human primate model of West Nile virus infection. *The American journal of tropical medicine and hygiene*, 82(6), 1160-1167.

Widman, D. G., Ishikawa, T., Winkelmann, E. R., Infante, E., Bourne, N. & Mason, P. W. (2009) RepliVAX WN, a single-cycle flavivirus vaccine to prevent West Nile disease, elicits durable protective immunity in hamsters. *Vaccine*, 27(41), 5550-5553.

Wodak, E., Richter, S., Bagó, Z., Revilla-Fernández, S., Weissenböck, H., Nowotny, N. & Winter, P. (2011) Detection and molecular analysis of West Nile virus infections in birds of prey in the eastern part of Austria in 2008 and 2009. *Veterinary microbiology*, 149(3-4), 358-366.

Wong, S. H., Jassey, A., Wang, J. Y., Wang, W.-C., Liu, C.-H. & Lin, L.-T. (2019) Virus-Like Particle Systems for Vaccine Development against Viruses in the Flaviviridae Family. *Vaccines*, 7(4), 123.

Xu, J., Dolan, M. C., Medrano, G., Cramer, C. L. & Weathers, P. J. (2012) Green factory: plants as bioproduction platforms for recombinant proteins. *Biotechnology advances*, 30(5), 1171-1184.

Yamshchikov, V. (2015) Development of a human live attenuated West Nile infectious DNA vaccine: conceptual design of the vaccine candidate. *Virology*, 484, 59-68.

Yamshchikov, V., Manuvakhova, M. & Rodriguez, E. (2016) Development of a human live attenuated West Nile infectious DNA vaccine: Suitability of attenuating mutations found in SA14-14-2 for WN vaccine design. *Virology*, 487, 198-206.

Yamshchikov, V., Manuvakhova, M., Rodriguez, E. & Hébert, C. (2017) Development of a human live attenuated West Nile infectious DNA vaccine: Identification of a minimal mutation set conferring the attenuation level acceptable for a human vaccine. *Virology*, 500, 122-129.

Yang, M., Lai, H., Sun, H. & Chen, Q. (2017) Virus-like particles that display Zika virus envelope protein domain III induce potent neutralizing immune responses in mice. *Scientific reports*, 7(1), 1-12.

Yenkoidiok-Douti, L., Williams, A. E., Canepa, G. E., Molina-Cruz, A. & Barillas-Mury, C. (2019) engineering a Virus-Like particle as an Antigenic Platform for a Pfs47-targeted Malaria transmission-Blocking Vaccine. *Scientific reports*, 9(1), 1-9.

Zaayman, D. & Venter, M. (2012) West Nile virus neurologic disease in humans, South Africa, September 2008–May 2009. *Emerging infectious diseases*, 18(12), 2051.

Zakeri, B., Fierer, J. O., Celik, E., Chittock, E. C., Schwarz-Linek, U., Moy, V. T. & Howarth, M. (2012) Peptide tag forming a rapid covalent bond to a protein, through engineering a bacterial adhesin. *Proceedings of the National Academy of Sciences*, 109(12), E690-E697.

Zana, B., Erdélyi, K., Nagy, A., Mezei, E., Nagy, O., Takács, M., Bakonyi, T., Forgách, P., Korbacska-Kutasi, O. & Fehér, O. (2020) Multi-Approach Investigation Regarding the West Nile Virus Situation in Hungary, 2018. *Viruses*, 12(1), 123.

Zhang, B., Chao, C. W., Tsybovsky, Y., Abiona, O. M., Hutchinson, G. B., Moliva, J. I., Olia, A. S., Pegu, A., Phung, E., Stewart-Jones, G. B. E., Verardi, R., Wang, L., Wang, S., Werner, A., Yang, E. S., Yap, C., Zhou, T., Mascola, J. R., Sullivan, N. J., Graham, B. S., Corbett, K. S. & Kwong, P. D. (2020) A platform incorporating trimeric antigens into self-assembling nanoparticles reveals SARS-CoV-2-spike nanoparticles to elicit substantially higher neutralizing responses than spike alone. *Scientific Reports*, 10(1), 18149.

Zhang, X., Jia, R., Shen, H., Wang, M., Yin, Z. & Cheng, A. (2017) Structures and Functions of the Envelope Glycoprotein in Flavivirus Infections. *Viruses*, 9(11), 338.

Zhu, N., Zhang, D., Wang, W., Li, X., Yang, B., Song, J., Zhao, X., Huang, B., Shi, W. & Lu, R. (2020) A novel coronavirus from patients with pneumonia in China, 2019. *New England Journal of Medicine*.

Zoetis *Duvaxyn WNV* (Updated: 2020a). Available online: https://www.zoetis.co.za/products/horses/duvaxyn-wnv.aspx [Accessed: 14 April 2020].

Zoetis *Equip WNV* (Updated: 2020b). Available online: https://www.zoetis.hu/termekek/lovas-termekek/equip-wnv.aspx [Accessed: 14 April 2020].

Zoetis *West Nile-Innovator* (Updated: 2020c). Available online: https://www.zoetisus.com/products/horses/west-nile-equine-vaccine-for-horses.aspx [Accessed: 14 April 2020].